This meeting will be co-sponsored by The Electrochemical Society

BRNO UNIVERSITY OF TECHNOLOGY
FACULTY OF ELECTRICAL ENGINEERING AND COMMUNICATION

Institute of Inorganic Chemistry AS CR

11th ABAF

BRNO 2010

Advanced Batteries, Accumulators and Fuel Cells

INTERNATIONAL CONFERENCE

September 19th - September 22th 2010

Organised by:

Department of Electrotechnology,
Faculty of Electrical Engineering and Communication,
Brno University of Technology

Institute of Inorganic Chemistry,
Academy of Science of Czech Republic, Řež near Prague

Organizing committee:
Jiří Vondrák
Marie Sedlaříková

ISBN 978-80-214-4148-4

Conference is sponsored by:

Parners:

Medial partners:

This meeting will be co-sponsored by The Electrochemical Society

We would like to express our thanks to the Brno University of Technology, Faculty of Electrical Engineering and Communication and to the Institute of Inorganic Chemistry AS CR for support and help with organising 11th ABAF conference.

Honourary Scientific Committee:

Arnaldo Visitin
Germano Ferrara
Jaromír Kadlec
Stefan Koller
Doron Aurbach
Mladen Mladenov
Raisa Apostolova
Petr Vanýsek
Libuše Trnková
Jana Bludská
Jiří Kazelle
Josef Jirák
Jiří Vondrák
Marie Sedlaříková

Organisation Committee:

Jiří Vondrák
Marie Sedlaříková
Vítězslav Novák
Tibor Jirák
Miroslav Zatloukal
Kristýna Jandová
Tomáš Knotek

Program Committee:

Jiří Vondrák
Marie Sedlaříková
Jiří Kazelle
Stefan Koller
Arnaldo Visitin
Vítězslav Novák
Petr Bača
Jiří Špinka
Helena Polsterová
Zdenka Rozsívalová
Edita Hejátková
Miroslav Zatloukal
Ondřej Čech

Contents

Materials for Lithium Systems

L. Bohne, T. Pirk, W. Jaegermann
CRYSTALLINE STRUCTURE OF SPUTTERED $LiCoO_2$ FOR THIN FILM LITHIUM ION BATTERIES 13

O. Cech, J.E. Thomas, A. Visintin, M. Sedlarikova, J. Vondrak
SYNTHESIS OF $LiFePO_4$/C COMPOSITE CATHODE FOR LITHIUM-ION BATTERIES 17

A. Fedorková, R. Oriňáková, A. Oriňák, A. Heile, H. D. Wiemhöfer, H. F. Arlinghaus
ELECTROCHEMICAL AND TOF-SIMS INVESTIGATION ON PPy/PEG-$LiFePO_4$ CATHODE MATERIAL FOR Li-ION BATTERIES 21

T. Jirák, J. Vondrák, M. Sedlaříková
ELECTROCHEMICAL CHARACTERISTICS OF MANUFACTURED MATERIAL $Li_4Ti_5O_{12}$ 22

P. Vorel, D. Červinka, I. Pazdera
PRACTICAL EXPERIENCES WITH LI-ION TRACTION ACCUMULATOR IN AN ELECTRIC BIKE 26

M. Filkusová, A. Fedorková, R. Oriňáková, M. Kupková
STRUCTURAL AND CHEMICAL STUDIES OF THE $LiFePO_4$ MWCNTs CATHODE MATERIAL FOR Li-ION BATTERIES 32

Milos Dusek, Jaromir Pytel Jan, M. Macak
ELECTROSPUN METAL OXIDES FOR ENERGY STORAGE 35

C. God, O. Moser, C. Bayer, C. Stangl, S. Koller, K.W. Leitner, M. Schulz-Dobrick
INVESTIGATION OF THE OXIDATIVE STABILITY OF ELECTROLYTE SYSTEMS ON 5 V CATHODE MATERIALS BY INSITU MASS SPECTROMETRY 36

H. Kren, M. Scharfegger, A. Droisner, C. God, S. Koller
NEW MATERIALS FOR ADVANCED LITHIUM ION BATTERIES 38

Electrolytes

R. Kořínek, J. Vondrák, K. Bartušek, M. Mrnka
STUDY OF GEL ELECTROLYTES PROPERTIES BY MR METHODS 43

A. Tron, I. Maksuta, E. Shembel
AMORPHOUS SOLID INORGANIC ELECTROLYTE ON BASIS OF Li_2O-LiF-Li_2WO_4-B_2O_3 FOR LITHIUM POWER SOURCES 48

J. Vondrák, M. Sedlaříková, M. Zatloukal, P. Dvořák
SULFOLANE AS A SOLVENT FOR APROTIC ELECTROLYTES 52

J. Vondrák, M. Sedlaříková, J. Velická , M. Macalík
RECENT DEVELOPMENTS IN THE RESEARCH OF GEL POLYMER ELECTROLYTES 57

New Materials

M. O. Danilov, N. D Ivanova., E. I. Boldirev, O. A. Stadnik, A. V. Filatov
NANOSTRUCTURAL COMPOSITES FOR POWER CELLS BASED ON MOLYBDENUM-MODIFIED CARBON NANOTUBES.....63

G. Ferrara, F. Vergottini, R. Inguanta, S. Piazza, C. Sunseri
NANOSTRUCTURED BINARY TIN ALLOY FABRICATION.....68

V.I. Barbashov, G.G. Levchenko, E.V. Nesova, N.E. Pismenova
LOW-TEMPERATURE ANOMALY IN IONIC CONDUCTIVITY OF SCANDIA-STABILIZED ZIRCONIA.....72

J. Vondrák, M. Sedlaříková, M. Macalík,M. Zatloukal, J. Mohelníková
COUNTER ELECTRODES FOR ELECTROCHROMIC DEVICES.....76

J. Vondrák, M. Macalík, J. Kazelle, J. Mohelníková
ELECTROCHROMIC LAYERS.....79

J. Vondrák, P. Špičák, J. Kazelle
SODIUM INSERTION INTO THIN LAYER V_2O_5 ELECTRODES.....82

J. Jirák, J. Runštuk, J. Špinka
PROBLEMS OF "IN SITU" SPECIMEN OBSERVATION IN ESEM.....85

J. Špinka
SPECIMENS OBSERVATION IN ESEM.....87

Supercapacitors

R. Apostolova, O. Kolomoyets, U.Tkachenko, E. Shembel
ELECTROLYTIC NICKEL SULFIDE FILMS IN ELECTROCHEMICAL CAPACITOR.....91

M. Mladenov, N. Petrov, T. Budinova, B. Tsyntsarski, T. Petrov, D. Kovacheva, R. Raicheff
SYNTHESIS, CHARACTERIZATION AND ELECTROCHEMICAL PROPETIES OF NANOSTRUCTURED ELECTRODE MATERIALS FOR SUPERCAPACITORS.....95

Fuel Cells

L. Chladil, V. Novák, P. Barath
NEW TYPE OF CARBON MATERIALS FOR CATALYTIC LAYER OF MEA STRUCTURES FOR PEM FUEL CELLS.....103

P. Procházka, V. Minárik
NEXA FUEL CELL CHARACTERISTIC.....107

D. Pléha, V. Novák
STUDY OF MANGANEESE OXIDES PROPERTIES BY THE EQCM METHOD.....113

Electrolysis

R. Inguanta, G. Ferrara, S. Piazza, C. Sunseri
ONE-DIMENSIONAL NANOSTRUCTURES AS ELECTRODE MATERIALS FOR WATER ELECTROLYSIS 119

T. Knotek, J. Vondrák
RESEARCH OF MATERIAL FOR ELECTROLYZER 124

M. Kunovjánek, J. Vondrák, M. Sedlaříková
USE OF NONWOVEN TEXTILES AS MEMBRANES FOR ELECTROLYSER 128

P. Barath, L. Trnkova, F. Jelen
THE INFLUENCE OF PURINES ON REDOX PROPERTIES OF COPPER 132

Aqueous batteries

T.Máca, L.Nezgoda, V. Špachman, J.Vondrák, M.Sedlaříková
INFLUENCE OF DISCHARGING DEPTH AND OVERCHARGING ON PERFORMANCE OF ALPHA NICKEL HYDROXIDE 137

D. Becker, G. Garaventta, F. Rodríguez Nieto, A. Visintin, P. Barath, M. Sedlaříková, J. Vondrak
CHEMICAL AND ELECTROCHEMICAL SYNTHESIS OF NICKEL HYDROXIDE 142

J.Vrbický, J. Vondrák, M. Sedlaříková
THE INFLUENCE OF SURFACTANTS ON ALPHA NICKEL HYDROXIDE 147

P. Křivík
DETERMINATION OF LEAD ACID BATTERY STATE OF CHARGE (SOC) II 149

J. Neoral, P.Bača, P. Abraham
THERMAL PHENOMENA IN LEAD ACID BATTERIES, INFLUENCE OF DIFFERENT SEPARATORS 153

Solar Cells

J. Dolenský, J. Vaněk, A. Veselý, L. Winkler
ANALYSIS BACKSIDES OF SOLAR CELLS 159

J. Hofman, J. Vanek
ACTIVE LOAD FOR THE TESTING OF SOLAR MODULES 163

R. Stojan, J. Vanek
SYSTEM OF VERY LOW TEMPERATURE CONTROLLING DURING THE DEFECT DETECTION OF SOLAR CELLS 167

A. Vesely, J. Vanek, J. Dolenský, F. Kucera
NEW CONTROL SOFTWARE FOR LBIC WORKPLACE 171

Electric Vehicles

M. Patočka, P. Huták, D. Červinka, P. Vorel
E-CAR ENERGY MANAGEMENT SIMULATION 177

M. Patočka, D. Červinka, P. Huták, P. Vorel
ULTRACAPACITORS IN E-CARS, YES OR NOT? 183

J. Marušinec
BATTERY ELECTRIC CAR CONVERSION OF SKODA SUPERB 189

Sponsors

THE ELECTROCHEMICAL SOCIETY 193

BOCHEMIE S.R.O. 195

ENVINET A.S. 197

H TEST. 199

SIGMA ALDRICH 201

SPECION 203

Nominal

Abraham P. 153
Apostolova R. 91
Arlinghaus H. F. 21
Bača P. 153
Barath P. 103, 132, 142
Barbashov V.I. 72
Bartušek K. 43
Bayer C. 36
Becker D. 142
Bohne L. 13
Boldirev E. I. 63
Budinova T. 95
Cech O. 17
Červinka D. 26, 177, 183
D Ivanova N. 63
Danilov M. O. 63
Dolenský J. 159, 171
Droisner A. 38
Dusek Milos 35
Dvořák P. 52
Fedorková A. 21, 32
Ferrara G. 68, 119
Filatov A. V. 63
Filkusová M. 32
Garaventta G. 142
God C. 36, 38
Heile A. 21
Hofman J. 163
Huták P. 177, 183
Chladil L. 103
Inguanta R. 68, 119
Jaegermann W. 13
Jelen F. 132
Jirák J. 85
Jirák T. 22
Kazelle J. 79, 82
Knotek T. 124
Koller S. 36, 38
Kolomoyets O. 91
Kořínek R. 43
Kovacheva D. 95
Kren H. 38
Křivík P. 149
Kucera F. 171
Kunovjánek M. 128
Kupková M. 32
Leitner K. W. 36
Levchenko G. G. 72
Máca T. 137
Macak M. 35
Macalík M. 57, 76, 79
Maksuta I. 48
Marušinec J. 189
Minárik V. 107
Mladenov M. 95
Mohelníková J. 76, 79
Moser O. 36
Mrnka M. 43
Neoral J. 153
Nesova E. V. 72
Nezgoda L. 137
Novák V. 103, 113
Oriňák A. 21
Oriňáková R. 21, 32
Patočka M. 177, 183
Pazdera I. 26
Petrov N. 95
Petrov T. 95
Piazza S. 68, 119
Pirk T. 13
Pismenova N. E. 72
Pléha D. 113
Procházka P. 107
Pytel Jan Jaromir 35
Raicheff R. 95
Rodríguez Nieto F. 142
Runštuk J. 85
Sedlaříková M. 17, 22, 52, 57, 76, 128, 137, 142, 147
Shembel E. 48, 91
Scharfegger M. 38
Schulz-Dobrick M. 36
Stadnik O. A. 63
Stangl C. 36
Stojan R. 167
Sunseri C. 68, 119
Špachman V. 137

Špičák P.	82
Špinka J.	85, 87
Thomas J.E.	17
Tkachenko U.	91
Trnkova L.	132
Tron A.	48
Tsyntsarski B.	95
Vaněk J.	159, 163, 167, 171
Velická J.	57
Vergottini F.	68
Veselý A.	159, 171
Visintin A.	17, 142
Vondrák J.	17, 22, 43, 52, 57, 76, 79, 82, 124, 128, 137, 142, 147
Vorel P.	26, 177, 183
Vrbický J.	147
Wiemhöfer H. D.	21
Winkler L.	159
Zatloukal M.	52, 76

11th ABAF

BRNO 2010

Advanced Batteries, Accumulators and Fuel Cells

Materials for Lithium Systems

CRYSTALLINE STRUCTURE OF SPUTTERED $LiCoO_2$ FOR THIN FILM LITHIUM ION BATTERIES

L. Bohne[1], T. Pirk[1], W. Jaegermann[2]

[1] Robert Bosch GmbH, Research and Advance Engineering, Gerlingen-Schillerhoehe, Germany
[2] Fachbereich Material- und Geowissenschaften, Fachgebiet Oberflaechenforschung, Technische Universitaet Darmstadt, Darmstadt, Germany

Corresponding author: Laura Bohne (Laura.Bohne@de.bosch.com)
Phone: +49 711 811 38192, Fax: +49 711 811 5183357

Introduction

Lithium cobalt oxide ($LiCoO_2$) is the most common cathode material in rechargeable all solid-state thin film batteries [[1]-[3]]. It has several advantages like its high working voltage, high specific capacity and energy density as well as a low self-discharge and excellent cycle life [[4]-[6]]. A typical assembly is shown in Fig. 1. The battery consists of a Pt current collector, a $LiCoO_2$ cathode, a solid state electrolyte LiPON, and an Al anode, deposited on a Si substrate. A silicon oxide layer serves as diffusion barrier underneath the platinum.

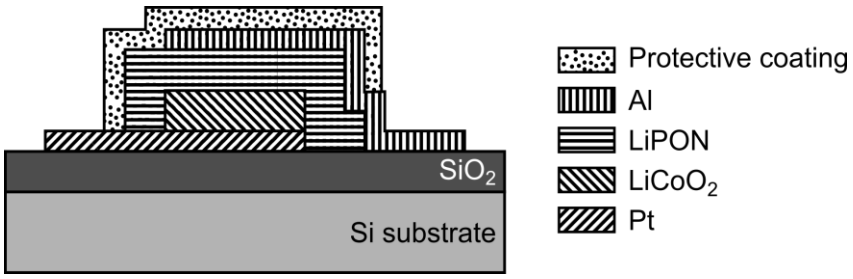

Fig. 1 *Schematic cross-section of a typical assembly of an all solid-state microbattery*

$LiCoO_2$ thin films deposited by RF magnetron sputtering and subsequent annealing at 700°C in O_2 atmosphere have a hexagonal layered crystal structure, providing fast Li^+ intercalation and deintercalation during charge-discharge cycling [[7]]. If the film additionally exhibits a preferential (101) or (104) texture as shown in Fig. 2, high power rates are achieved [[5]]. Thus it would be advantageous to control that orientation.

According to [[8]-[10]], the percentage of (003) oriented grains decreases with increasing thickness in $LiCoO_2$ thin films, independent of the deposition method and conditions. Yet the preparation of a thin film battery as shown in Fig. 1 yielded the unfavored (003) orientation and not the preferred (101)/(104) orientation, despite a 1.2 µm thick $LiCoO_2$ cathode film.

In the present work the $LiCoO_2$ crystalline structure is thus discussed as a function of the subjacent layer.

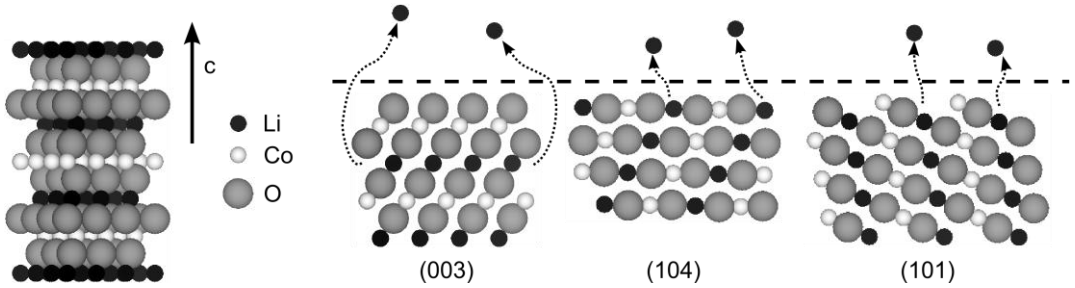

Fig. 2 *Hexagonal layered structure of $LiCoO_2$ with different preferential crystal orientations with respect to the direction of Li^+ ion extraction and insertion*

Experimental

All $LiCoO_2$ thin films were deposited by RF magnetron sputtering from a $LiCoO_2$ target with 200 mm diameter in argon and oxygen atmosphere with a total flow rate of 12 sccm and an Ar to O_2 ratio of 2:1 to 3:1. The RF power was varied between 200 and 500 W. The $LiCoO_2$ films were deposited for 4 to 12 hours at a working pressure of 1e-2 mbar without an active substrate heating.

To determine the influence of the uppermost substrate layer on the crystalline orientation of $LiCoO_2$ thin films, different substrates were used: 1) Si wafer, 2) Si wafer / SiO_2 (2.5 µm), and 3) Si wafer / SiO_2 (2.5 µm) / Pt (0.2 µm, current collector).

The Si wafers used have a (100) orientation and a diameter of 150 mm. The SiO_2 was thermally grown and serves as a diffusion barrier as well as an electrical isolation between the battery cells on the wafer. The Pt current collector was deposited by DC sputtering. Because the as-deposited $LiCoO_2$ films are amorphous, the samples were treated with a subsequent annealing step at 700°C for 2 h in an oxygen atmosphere to obtain the desired hexagonal layered crystal phase.

The thickness of $LiCoO_2$ films was determined with a Tencor P10 surface profiler. The crystalline structure and orientation of the deposited and annealed $LiCoO_2$ films was determined by X-ray diffraction (XRD) and Raman spectroscopy. The XRD measurements were carried out on a Bruker AXS D8 ADVANCE diffractometer using Cu K alpha radiation (wavelength 0.154 nm) and Bragg-Brentano optics. Raman spectroscopy was carried out at room temperature and in air on a LabRAM ARAMIS spectrometer by HORIBA Jobin Yvon with a He-Ne laser (wavelength 633 nm) in backscattering geometry.

Results and Discussion

The XRD patterns of $LiCoO_2$ films sputtered on Si substrates with various thicknesses are shown in Fig. 3 a). A preferential (101)/(012) out of plane orientation is found for every thickness, only the thinnest film with 0.4 µm thickness exhibits a low percentage of (003) oriented grains. According to [[8]-[10]] this is due to a film thickness less than 0.5 µm. The corresponding Raman spectra are shown in Fig. 3 d). The peaks at 486 cm^{-1} and 596 cm^{-1} correspond to the E_g and A_{1g} modes, respectively. These are an evidence for the preferred hexagonal high temperature phase of $LiCoO_2$. The peak at 521 cm^{-1} is attributed to the

Si substrate. Due to increasing $LiCoO_2$ film thickness, the depth of penetration of the laser radiation in the silicon substrate decreases and thus the intensity of this Si peak, too.

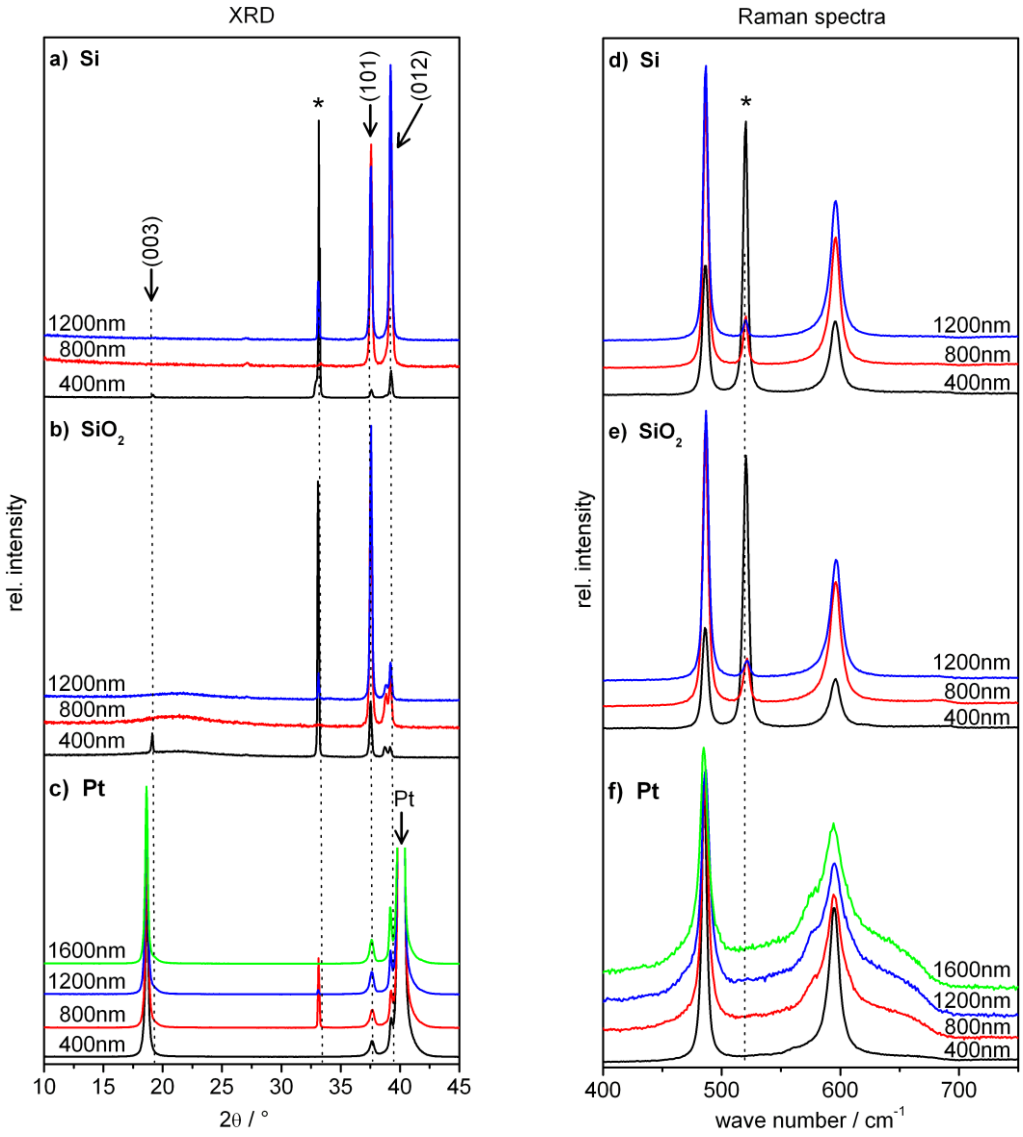

Fig. 3 *XRD patterns (a–c) and corresponding Raman spectra (d–f) of LiCoO2 of different thicknesses deposited on various substrates: a)+d) on Si wafer, b)+e) on oxidized Si wafer, c)+f) on Pt on oxidized Si wafer. Peaks marked by an asterisk (*) correspond to the Si substrate.*

As the Raman spectrum in Fig. 3 e) shows, $LiCoO_2$ films sputtered on a SiO_2 coated Si wafer exhibit the same crystal structure as $LiCoO_2$ sputtered on Si. But the corresponding XRD pattern in Fig. 3 b) shows that, compared to $LiCoO_2$ deposited on Si, the percentage of grains with (101) orientation exceeds the percentage of the (012) oriented grains. The broad peak observed at 21.5° is attributed to silicon dioxide. The small (003) peak for the 0.4 µm thick film is due to the small film thickness as described above.

Sputtering $LiCoO_2$ films with the same thicknesses as before (0.4, 0.8, 1.2, and 1.6 µm, respectively) on a platinum coated substrate results in a strong preferential (003) out of plane orientation for all these films, independent of their thickness (see Fig. 3 c). The peak observed at 40° is attributed to platinum. Compared to the results obtained for $LiCoO_2$ sputtered on Si and SiO_2, even a 1.6 µm thick $LiCoO_2$ film exhibits a high (003) texture, whereas $LiCoO_2$ films deposited on Si and SiO_2 are completely (101)/(012) oriented as

soon as their thickness exceeds 0.4 µm. Furthermore, the intensity of the (003) diffraction peak in Fig. 3 c) increases with increasing film thickness. This is a clear constriction of the results obtained from Xia et. al [[11]], who reported a gradual decrease of (003) and increase of preferred (101)/(104) oriented grains when the $LiCoO_2$ film thickness exceeds 0.5 µm. In contrast to Raman spectra of $LiCoO_2$ deposited on Si and SiO_2, no Si peak is obtained in the case of $LiCoO_2$ sputtered on Pt, because the Pt film reflects the whole laser radiation (see Fig. 3 f). Moreover, the peaks of the E_g and A_{1g} are broadened with increasing film thickness, maybe due to increasing structural disorder or scattering of the laser radiation in the $LiCoO_2$ film.

Conclusions

Sputtering $LiCoO_2$ on different substrates with various film thicknesses shows, that not only the film thickness has a strong influence on the crystal structure of $LiCoO_2$ as reported before, but also the choice of the substrate and subjacent layer. The threshold of about 0.5 µm film thickness reported in literature for a change from (003) to (101)/(104) out of plane orientation could not be verified in the conducted experiments. Rather, a preferred (101) orientation is already found for 0.4 µm thick $LiCoO_2$ films sputtered on pure and oxidized silicon wafers. Depositing $LiCoO_2$ on a Pt current collector with a barrier layer underneath, even a 1.6 µm thick film exhibits a preferential (003) crystal orientation. These results show that the determination of $LiCoO_2$'s crystalline structure should be carried out with the intended current collector material underneath the cathode to ensure that the actual crystal orientation within the battery assembly is known.

Acknowledgements

The authors would like to thank Dr. T. Koehler and M. Wessling for their support with the implementation of the XRD measurements and Raman spectroscopy.

References

[1] J.B. Bates et al.: Solid State Ionics **135** (2000) 33
[2] J. Song et al.: J. Micromech. Microeng. **19** (2009) 045004
[3] W.C. West et al.: J. Micromech. Microeng. **12** (2002) 58
[4] K. Edström et al.: Electrochimica Acta **50** (2004) 397
[5] G.G. Amatucci et al.: J. Electrochem. Soc. **143** (1996) 1114
[6] E. Antolini: Solid State Ionics **170** (2004) 159
[7] H. Gabrisch et al.: Electrochimica Acta **52** (2006) 1499
[8] J.B. Bates et al.: J. Electrochem. Soc. **147** (2000) 59
[9] P.J. Bouwman: PhD thesis, Twente, University (2002)
[10] Y. Iriyama et al.: J. Power Sources **94** (2001) 175
[11] H. Xia et al.: URL *http://dspace.mit.edu/bitstream/handle/1721.1/35827/AMMNS001.pdf?sequence=1*

SYNTHESIS OF $LiFePO_4$/C COMPOSITE CATHODE FOR LITHIUM-ION BATTERIES

O. Cech[1], J.E. Thomas[2], A. Visintin[2], M. Sedlarikova[1], J. Vondrak[3]

[1] Faculty of Electrical Engineering and Communication, Department of Electrotechnology, Údolní 53, 602 00 Brno, Czech Republic
[2] Instituto de Investigaciones Fisicoquímicas Teóricas y Aplicadas (INIFTA), Facultad de Ciencias Exactas, UNLP, CCT La Plata-CONICET, La Plata, Argentina
[3]Department of Inorganic Chemistry, Academy of Science, Husinec, Řež near Praque,Czech Republic

Corresponding author: O. Cech (xcecho01@phd.feec.vutbr.cz)
Phone: +420777699932

Introduction

All conventional electrode materials used for lithium-ion cell cathode suffer from poor electronic conductivity, which is in range of 10^{-2} – 10^{-9} S/cm. Because electrode system of a lithium ion battery has to allow flowing of both lithium ions and electrons it is necessary to add some conductive agents to the mass of electrode active material. Many researchers have discovered different conductive materials for cathode electronic conductivity enhancement. Not only electronic conductivity but also ionic conductivity influences electrochemical performance of the composite cathode. This can be improved mostly by increasing electrode porosity and thus contact surface between electrolyte solution and active material. This is best way to shorten ion diffusion lengths. Higher specific capacity and especially better high rate performance are achieved by template-synthesized hollow-sphere thin wall particles or nanotubes.

Nowadays, olivine $LiFePO_4$ is going to be the leading material for high-power li-ion rechargeable batteries because of its thermal stability, cost and environmental harmlessness. $LiFePO_4$ unfortunately suffers from much poorer electronic conductivity than widely used layered $LiCoO_2$ material. Improved electrochemical performance can be achieved by obtaining nanostructured active material particles together with highly conductive material – usually carbon black. Electronic conductivity is affected by carbon support and ionic conductivity rises due to higher porosity.

In our experiment, sintering of lithium, iron and phosphate sources together with organic carbon precursor and little amount of Super P, was used. Organic precursor is carbonized during heating and is believed to be used for particle coating. The presence of Super P carbon in the base reaction mixture can prevent oxidation of Fe^{2+} to Fe^{3+} during synthesis [2].

Experimental

The synthesis was carried out by combustion method with glycine. Reaction precursors used were lithium nitrate, iron oxalate, ammonium dihydrogenphosphate, glycine and Super P. Reagents in stechiometric amounts were dispersed in a hot aqueous solution, dried with constant stirring until smooth paste was obtained. Amount of 2% of Super P carbon black was then added to the hot solution. This mixture was then dried under Ar flowing atmosphere at 300°C for 5h and sintered at 750°C for 6h. After cooling down the product was milled and prepared for the physical and electrochemical characterization. The physical characterisation was made by SEM, XRD, TEM and EDS. Electrochemical characterizations evolved were cyclic voltammetry, charge-discharge and electrochemical impedance spectroscopy.

Cyclic voltammetry was performed in Ar atmosphere Glovebox using glass 3 electrode cell. Charge-discharge measurements along with electrochemical impedance spectroscopy data were collected with EL-Cell two electrode testing titanium stack.

Results and Discussion

SEM pictures show conglomerates from 5 to 60 micrometers in diameter. It is possible to see two differently colored phases on the grains. On TEM pictures we can see the inside composition of this conglomerates. They are made by nanosized core-shell structured round shaped particles fixed in transparent matrix.

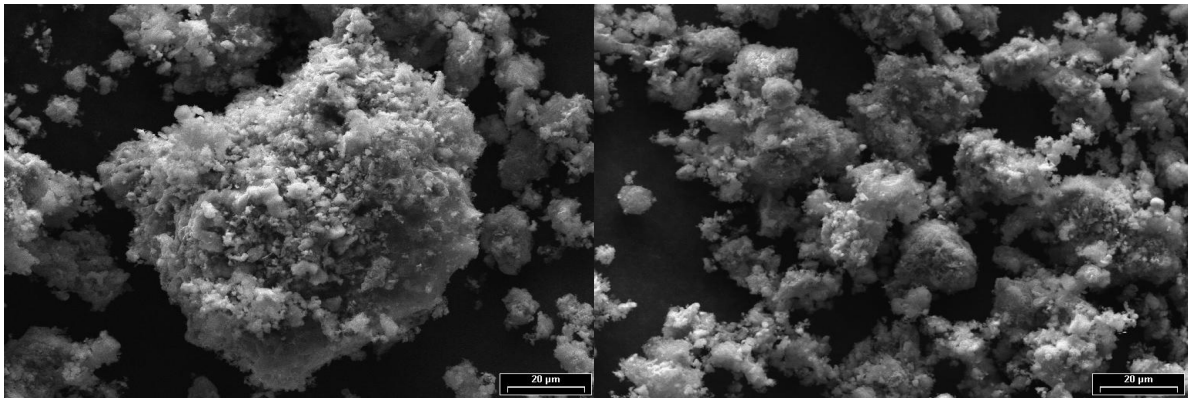

Fig. 1: *SEM images of $LiFePO_4$/C composite*

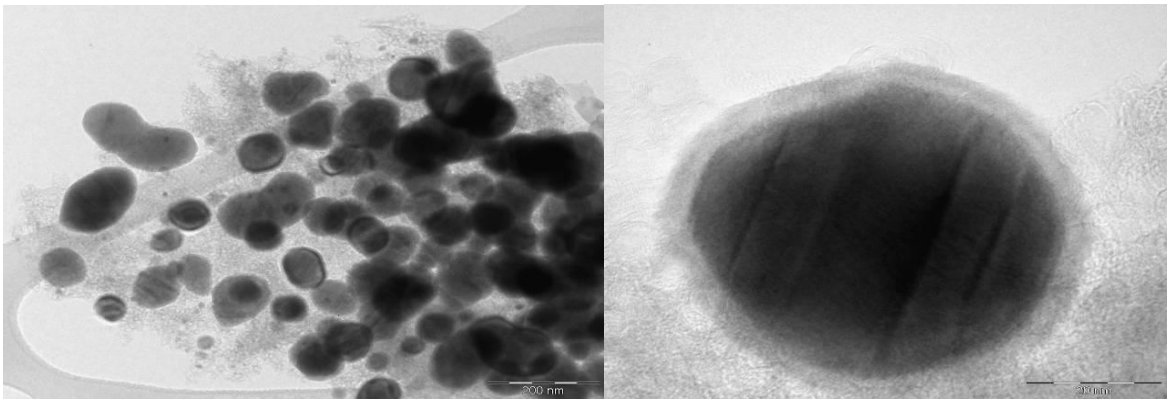

Fig. 2: *TEM pictures of $LiFePO_4$ nanosized core-shell structured particles inside macro grains*

The XRD measurements show that we obtained $LiFePO_4$ in triphylite form with Pnma orthorhombic space group.

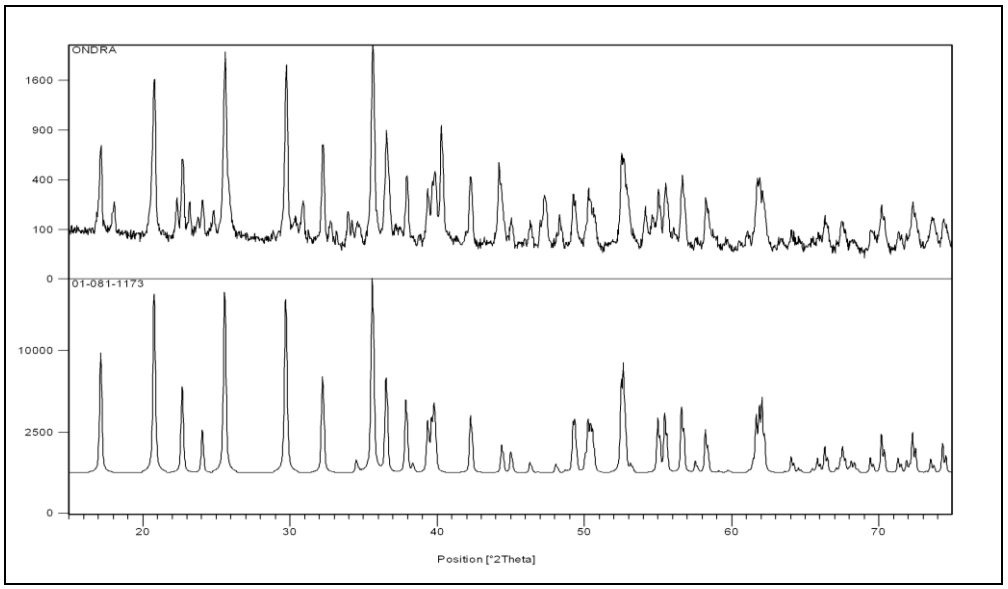

Fig. 3: *a) measured XRD pattern of composite LiFePO4 b) simulated pattern of LiFePO4*

Tab. 1: *Elements proportions by EDS*

Element	*Wt %*	*At %*
C	29.58	54.86
O	12.29	17.11
P	15.14	10.89
Fe	42.99	17.14

EDS measurements were performed by SEM microscope at different grains of the sample. Via this method, we can obtain information about amount of the residual carbon in sample volume for further electrochemical performance measurements.

Figure 4a. shows cyclic voltammogram obtained by sweep rate 0.1 mVs^{-1}. Apearence of single cathodic and anodic peak proves the one electron reaction $LiFePO_4$ to $FePO_4$. Figure 4b. is Nyquist plot of impedance spectroscopy measurement with 10mV sinus excitation voltage and frequency 1mHz to 1 Mhz.

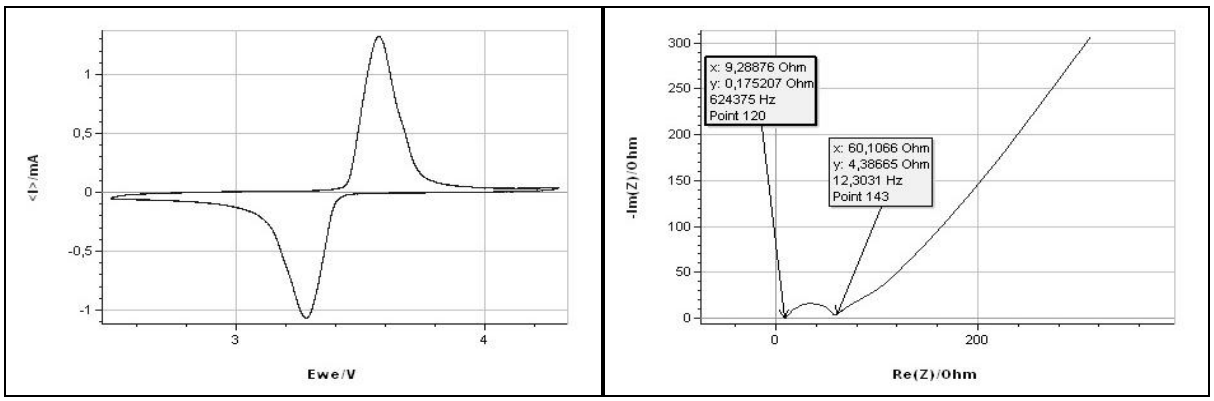

Fig. 4 : *a) CV of $LiFePO_4$/C* *b) PEIS of $LiFePO_4$ cathode*

Conclusions

Nanostructured $LiFePO_4$ was obtained by combustion method with using glycine as carbon source. XRD shows, that clear one phase synthetic tripthylite-like ortorhombic space group material was made. Electrochemical measurements show that obtained material is suitable for using as cathode for lithium-ion batteries.

Acknowledgements

This work at Brno University of Technology was supported by Ministry of Education of Czech Republic, Project MSM 0021630516, the Academy of Sciences, Grant No.P102/10/2091 and FEKT-S-10-14.

Moreover, the work at the Institute of Inorganic chemistry was supported by the Academy of Sciences, Research Plan AV/ 0Z403 0502.

The authors acknowledge financial support from Consejo Nacional de Investigaciones Científicas y Técnicas (CONICET), the Agencia Nacional de Promoción Científica y Tecnológica, and the Universidad Nacional de La Plata.

References

[1] N. Kalaiselvi, A. Manthiram: Journal of Power Sources 195 (2010) 2894–2899
[2] G.T.K. Fey, T.L. Lu, J. Power Sources 178 (2008) 807
[3] D. Wang, H. Li, L.Q. Chen, Electrochim. Acta 50 (2005) 2955

ELECTROCHEMICAL AND TOF-SIMS INVESTIGATION ON PPy/PEG-$LiFePO_4$ CATHODE MATERIAL FOR Li-ION BATTERIES

A. Fedorková[1], R. Oriňáková[2], A. Oriňák[2], A. Heile[3], H.-D. Wiemhöfer[4], H. F. Arlinghaus[3]

[1]Department of Analytical Chemistry, Faculty of Science, Comenius University, Mlynská Dolina, SK-842 15 Bratislava 4, Slovak Republic
[2]Institute of Chemistry, Faculty of Science, P.J. Šafárik University, Moyzesova 11, SK-04154 Košice, Slovak Republic
[3]Physikalisches Institut, Westfälische Wilhelms Universität, Wilhelm-Klemm-Str. 10, D-481 49 Münster, Germany
[4]Department of Inorganic and Analytical Chemistry, Westfälische Wilhelms Universität, Correnstrasse 30, D-481 49 Münster, Germany

Corresponding author: Andrea Fedorková (fedorkova@fns.uniba.sk)
Phone: +421-55-2342327, Fax: +421-55-6222124

Abstract

The role of polyethyleneglycole (PEG) in mixed polypyrrole (PPy) polymer blend for new cathode material development has been studied. The films of PPy containing PEG were prepared by chemical oxidative polymerization of Py monomer. PEG has been applied as an additive during polymerization process to improve mechanical and structural properties of PPy in final PPy/PEG-$LiFePO_4$ cathode material aiming also better electronic conductivity. The electrochemical behaviour of the samples was examined by galvanostatic charge/discharge technique, cyclic voltammetry (CV) and electrochemical impedance spectroscopy (EIS). It was found that PPy/PEG blend polymer decreases the contact resistance and improves the Li^+ insertion/extraction during cycling. Charge/discharge measurements confirmed the increase in capacity when applying PEG in PPy. Impedance measurements showed that the PPy/PEG coating decreases the charge transfer resistance of the corresponding $LiFePO_4$ cathode material. Time of flight secondary ion mass spectrometry (TOF-SIMS) analysis confirmed supporting effect of PEG in PPy predominantly for mixed polymer mechanical stability (important at charging cycles). Distribution of PPy, PEG and Li^+ fragments within blended polymer films were monitored by measuring the intensities of different secondary ions, applying SIMS. The lateral morphology of the system was studied with optical microscopy revealing strong similarities to the bulk system.

ELECTROCHEMICAL CHARACTERISTICS OF MANUFACTURED MATERIAL $Li_4Ti_5O_{12}$

T. Jirák[1], J. Vondrák[2], M. Sedlaříková[1]

[1] Department of Electrical and Electronic Technology, Brno University of Technology, Údolní 53, Brno 60200, Czech Republic
[2] Institute of Inorganic Chemistry, Academy of Sciences of the Czech Republic, Řež near Prague 25068, Czech Republic

Corresponding author: Tibor Jirák (tibor.jirak@phd.feec.vutbr.cz)
Phone: 00420 541 146 112, Fax: 00420 541 146 147

Introduction

The article deals with manufactured electrode materials for lithium secondary batteries - nanostructured $Li_4Ti_5O_{12}$. Material was chosen for research by virtue of very good intercalation / insertion characteristics, possibility utilization high charge and discharge rate and for his environmental safety.

In Czech Republic, there is the manufacturer of nanosized $Li_4Ti_5O_{12}$ suitable for battery industry as material with good electrochemical properties and high stability in the electrochemical processes.

Experimental

The material of composition $Li_4Ti_5O_{12}$ was taken from industrial production of the company ELMARCO, Liberec, Czech Republic, and it was annealed to 750^{o}C in air for ca. 3 hours as it had been confirmed by DTA-GTA curves. Microscope photographs were taken before electrochemical measurements.

The sample for research was assembled with pure material and conductive Ni mesh of area 1 cm^2 was used as carrier (PTFE served as binder in quantities max. 5%). Aprotic electrolyte consisted of lithium salt ($LiPF_6$) dissolved in EC-DMC (1:1).

All measurements were executed in glove box Mbraun Labmaster with argon atmosphere. Purity values were checked and were hold at rates 0.1 ppm for H_2O and 0.1 ppm for O_2.

Results and Discussion

The electrochemical properties were tested in a three-electrode cell containing Li counter and reference electrodes. Potentiostat AUTOLAB (ECOCHEMIE, The Netherland) was assessed for setting up standard electrochemical techniques (cyclic voltammetry) and recording achieving results.

HRTEM and SEM photographs were taken in special laboratory of Academy of Sciences of Czech Republic.

Obtained results are clearly presented via figures and tables thereinafter.

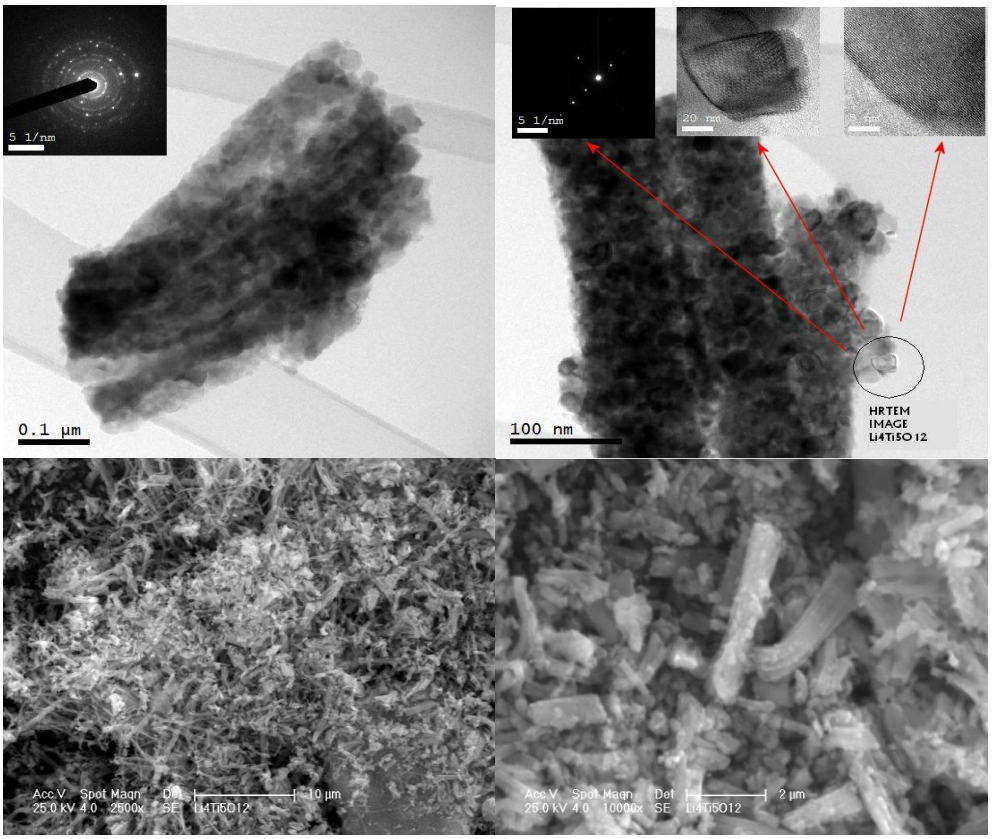

Fig. 1: *HRTEM and SEM photographs of $Li_4Ti_5O_{12}$*
HRTEM photographs - nanoparticles $Li_4Ti_5O_{12}$ are deposited on binders (dark pipes).
SEM photographs – magnification 2500x (left), 10 000x (right)

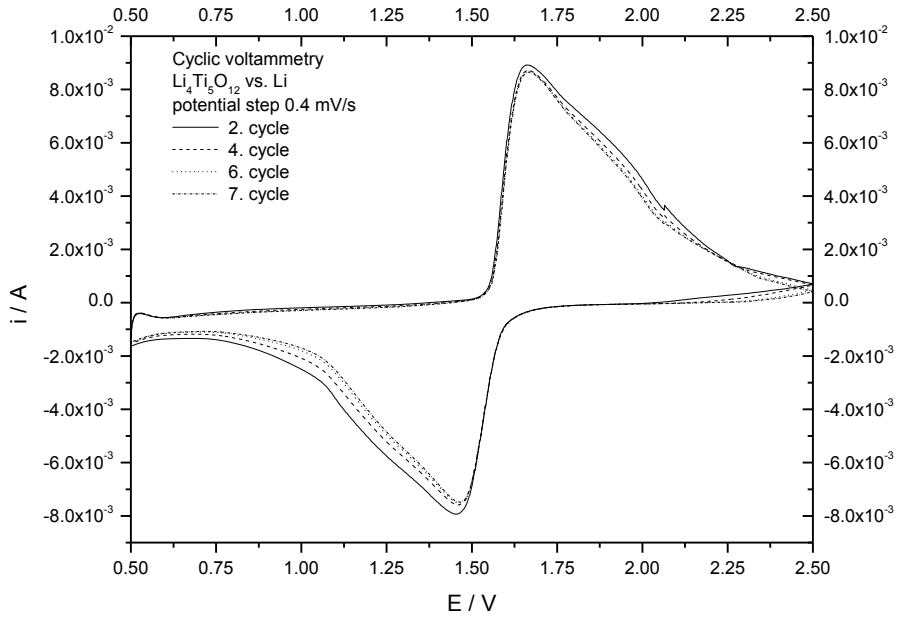

Fig. 2: *Cyclic voltammogram of $Li_4Ti_5O_{12}$ – electrolyte 1M $LiPF_6$ in EC-DMC (50:50 wt. %), parameters CV (0.4 mV.s^{-1} scan rate, 0.5 ÷ 2.5 V potential window), weight of electrode 18.5 mg.*

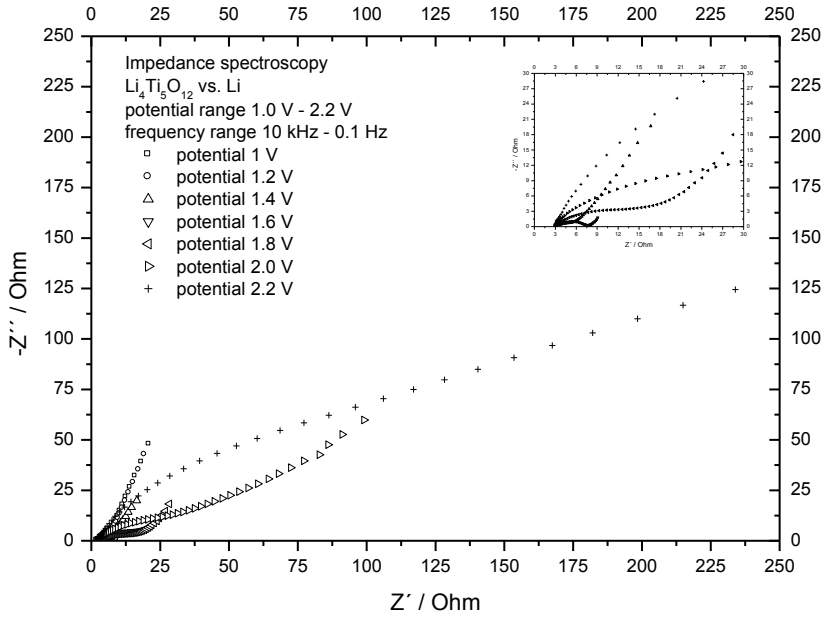

Fig. 3: *Impedance spectroscopy of $Li_4Ti_5O_{12}$ – electrolyte 1M $LiPF_6$ in EC-DMC (50:50 wt. %), parameters (potential range 1.0 V ÷ 2.2 V, frequency range 10 kHz ÷ 0.1 Hz), weight of electrode 26.8 mg.*

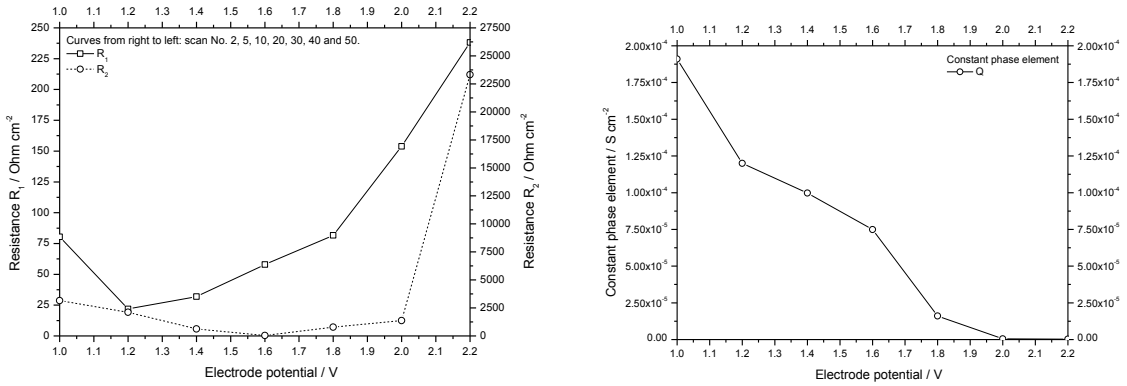

Fig. 4: *Impedance spectroscopy of $Li_4Ti_5O_{12}$ – electrolyte 1M $LiPF_6$ in EC-DMC (50:50 wt. %), parameters (potential range 1.0 V ÷ 2.2 V, frequency range 10 kHz ÷ 0.1 Hz), weight of electrode 26.8 mg – resistances (left), constant phase element (right).*

Conclusions

The material is rather active and it can be exposed to long cycling. The insertion of lithium is fast and it originates from its nanosized structure on one hand and by the massive increase of conductivity due to inserted lithium on other hand.

The results show electrode material with good behaviour in the field of reversibility reaction and electrochemical efficiency and also point to usage of investigated electrode material in high charge/discharge systems.

Acknowledgements

The investigations were supported by:
Ministry of Education of Czech Republic, Project MSM002130516,
Czech Science Foundation, Grant No. P102/10/2091.

References

[1] L. Kavan, J. Procházka, T. M. Spitler, M. Kalbáč, M. Zukalová, T. Drezen, M. Gratzel: Li insertion into $Li_4Ti_5O_{12}$ (Spinel). Charge capability vs. particle size in thin-film electrodes, in: Journal of The Electrochemical society, 150, p. 1000-1007. June 2003.

[2] D. Djian, F. Alloin, S. Martinet, H. Lignier, J. Y. Sanchez: Lithium-ion batteries with high charge rate capacity: Influence of the porous separator, in: Journal of power sources, 172, p. 416-421. July 2007.

[3] H. Ge, N. Li, D. Li, C. Dai, D. Wang: Electrochemical characteristics of spinel $Li_4Ti_5O_{12}$ discharged to 0.01 V, in: Electrochemistry communications, 10, p. 719-722. February 2008.

[4] H. F. Xiang, Q. Y. Jin, R. Wang, C. H. Chen, X. W. Ge: Nonflammable electrolyte for 3-V lithium-ion battery with spinel materials $LiNi_{0.5}Mn_{1.5}O_4$ and $Li_4Ti_5O_{12}$. Journal of Power Sources, 2008, 179, p. 351 – 356.

PRACTICAL EXPERIENCES WITH Li-ion TRACTION ACCUMULATOR IN AN ELECTRIC BIKE

P. Vorel[1], D. Červinka[1], I. Pazdera[1]

[1] UVEE FEKT, Brno University of Technology, Technická 8, 616 00 Brno, Czech republic

Corresponding author: Ivo Pazdera (xpazde05@stud.feec.vutbr.cz)
Phone: +420 5 4114 2536, fax: +420 5 4114 2464

Introduction

An electric bike (1kW) with a Li-Ion accumulator 28V/42A was constructed and tested in the Department of power electrical and electronic engineering (UVEE). Small Panasonic cells CGR18650C (ca 2Ah) are used in the accumulator. The battery is completed with 7 serial-connected blocks. Each block is a set of 21 parallel-connected cells.

Fig. 1: *Li-ion battery pack constructed for the bike.*

The accumulator was tested in the vehicle since 2005 till now. During the tests a distance of approx. 12000km was driven. Some theoretical know-how about the used charging and discharging strategy and about the battery management system is proposed in this contribution. Practical results regarding the lifetime, capacity decreasing, charging problems, temperature dependencies and cell voltage balancing are visible from the long-time experiment described in this contribution too.

Fig. 2: *Complete view of the constructed electric bike.*

The DC link (accumulator) voltage of the electric vehicle is 28V and the maximum accumulator current taken with the traction inverter is ca 50A. More detailed technical parameters of the accumulator are in Tab.1.

Tab. 1: *Electric parameters of the accumulator.*

Nominal voltage (3.6V per 1 cell)	25.2V
Chosen minimum voltage (3.1V per cell)	21.7V
Chosen maximum voltage (4.1V per cell)	28.7V
Maximum steady discharging current (2A per cell)	42A
Maximum charging current (1.4A per cell)	29.4A
Usable Ah capacity (ca 1.9Ah per cell)	40Ah
Internal resistance (120mΩ per cell)	40mΩ

The existence of 21 parallel cells in each block improves statistically the regularity of the capacity and internal leakage of the blocks each other. However voltage monitoring circuits (for each serial block) were used to check the voltage of each cell separately.

Battery management system

The electronic circuits of the used battery management system are in Fig.3. Comparators monitoring the over-voltage and under-voltage of each cell create the core of the system. These comparators are included in the modules marked “BLOK1” to “BLOK7”.

The internal schema of these comparator modules (“BLOK1” to “BLOK7”) is in Fig.4. These blocks are continuously supplied from the corresponding cells. Two logic signals are in the output of the blocks, see Fig.4. These signals are galvanically separated from the monitored cell. One common over-voltage signal “prepeti” and one common under-voltage signal “podpeti” are created from these separate block output signals.

If an over-voltage appears in one ore more cells then the signal over-voltage is zero. If no cell has the over-voltage then this signal is one.

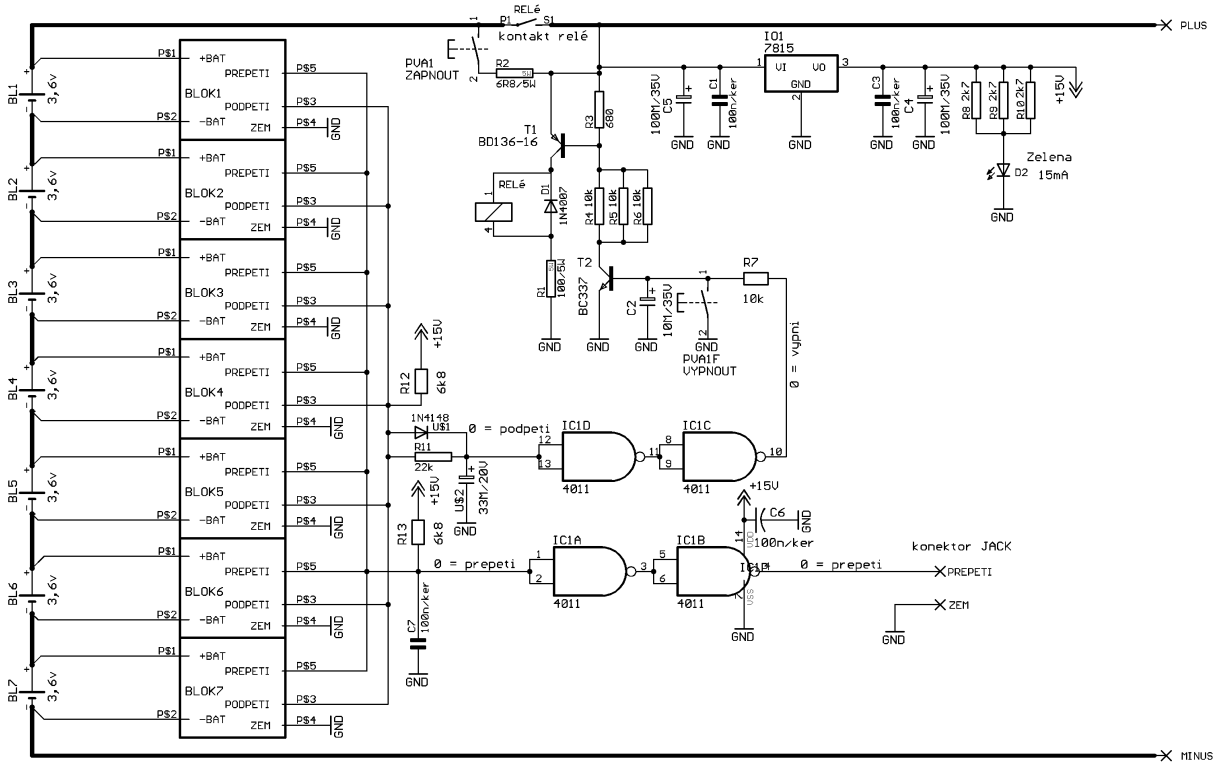

Fig. 3: *Used simple battery management system*

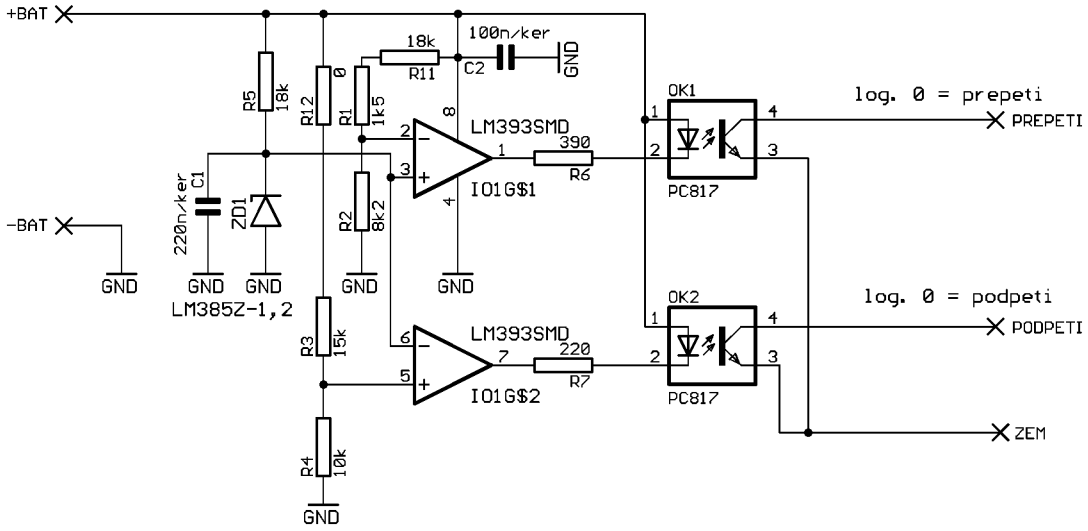

Fig. 4: *Comparator module (BLOK1 to BLOK7 in Fig.1)*

If an under-voltage appears in one ore more cells then the signal under-voltage is zero. If no cell has the under-voltage then this signal is one. The logical zero of this signal (under-voltage at any cell) appears then the relay turns off the power terminal of the accumulator (no further discharging is possible).

If an over-voltage appears in any cell then the over-voltage signal does not turn off the output terminals but this signal leads to the traction inverter where the regenerative

braking starts to be limited. Moreover this signal leads to the charger to be used there as the control feedback, see below.

Charger control strategy

A single-acting buck converter with transformer is used in the charger. Its basic parameters are in Tab.2.

Tab. 2: *Charger basic parameters.*

Input	1x230V/50Hz
Power	600W
Maximum output current	20A
Frequency	200kHz
Mass	1.5kg
Dimensions	60x120x170

A cascade control strategy is used in principle. A slave current loop is used. The demanded current value is obtained from a simple non-traditional master voltage controller which ensures that no cell can be over-charged. The control structure is in Fig. 5.

The over-voltage logic signal from the management system is filtered by a low-pass filter with a high time constant. If any cell is already near to the full voltage then the over-voltage signal oscillates between 0 and 1. Then the average value of this pulse signal serves as the demanded current.

Using this charger control strategy and described battery management system a perfect accumulator behaviour (regular cell voltage distribution, high lifetime) was achieved with no additional balancing! This was verified by 5years operation in a real traffic, see below.

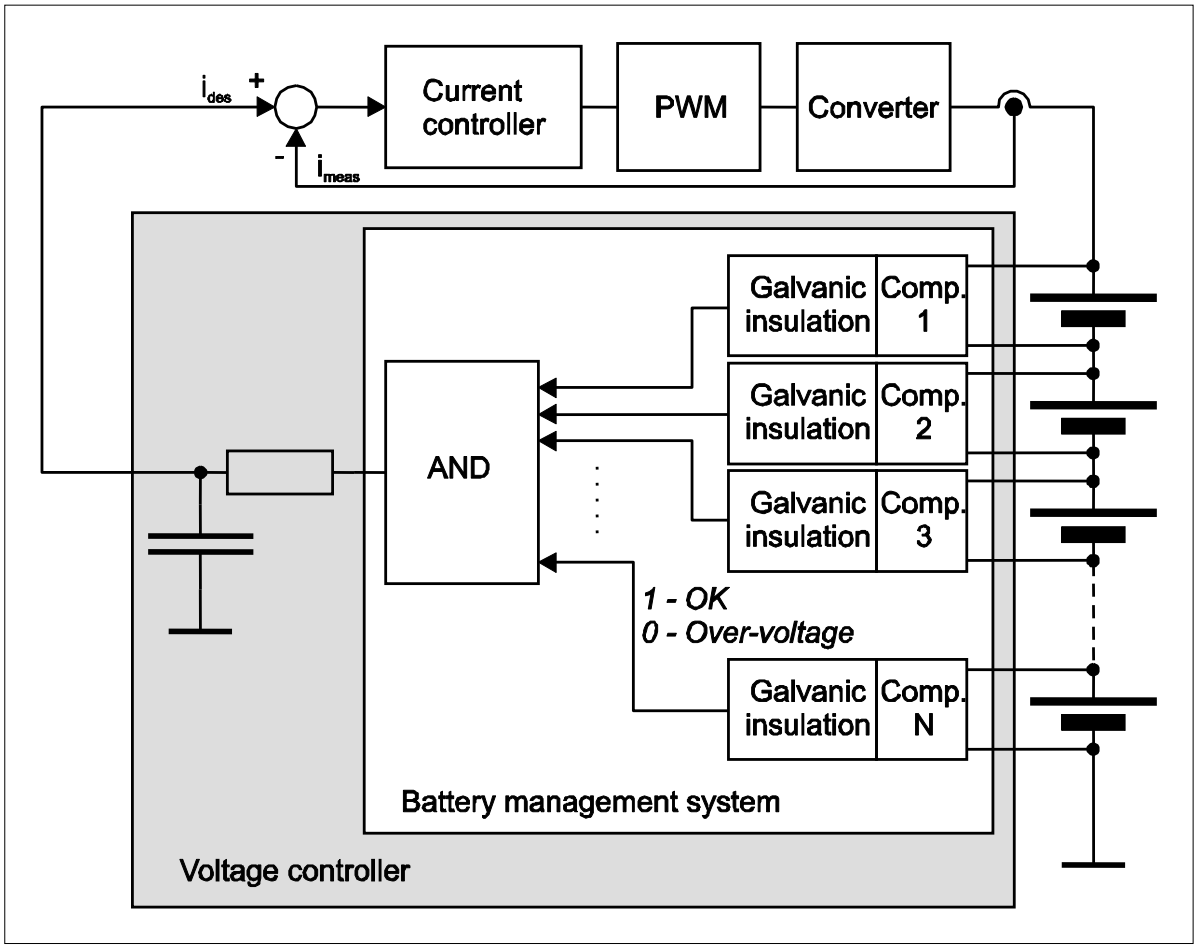

Fig. 5: *Charger control strategy*

Practical traffic load experiences

The action radius of the bike is 60km per one battery full-charging cycle (ca 1kWh). From 2005 till now (2010) a discharging measurement of the capacity and internal resistance was done periodically. The measurement results are in Tab.3.

Tab. 3: *Periodical capacity and internal resistance measurement.*

Date:	Total km:	Ah capacity:	Internal res. [mΩ]
10.8.2005	540	39.2	40
26.7.2006	1666	37.7	40
30.1.2008	4667	35.0	40
21.10.2008	9192	35.0	40
7.7.2009	10847	34.3	40
7.5.2010	12074	33.0	40

Conclusions

The full-charging voltage of the accumulator remains always 28.7V and the capacity decreases due to the battery age. No charging unbalance among the cells appeared during the 5 years although no additional balancing circuits are used.

If the battery was discharged fully to the minimum voltage and again fully recharged then the number of charging cycles corresponding to the whole 12074km would be 200. However in the real traffic the battery was charged in each nearest occasion - not after it is fully discharged. This way the lifetime is prolonged certainly. The number of partial charging cycles is approx. 600.

It is visible from Tab.3 that the internal resistance does not grow yet, what is interesting.

The manufacturer of used cells recommends the maximum voltage 4,2V and minimum voltage ca 3V (to reach the full capacity). We chose 4,1V instead of 4,2V and 3,1V instead of 3V (stricter criterion limits). Due to this the usable capacity was reduced about ca 10% but the lifetime was probably prolonged strongly.

Acknowledgements

This research has been supported by the European Commission under the ENIAC CA-E3Car-2008-120001 E3CAR - Nanoelectronics for an Energy Efficient Electrical Car project. Further this was supported by the project MSM0021630516 “Zdroje, akumulace a optimalizace využití energie v podmínkách trvale udržitelného rozvoje”.

References

[1] VOREL, P. ŽIVOTNOST LITHIUM-IONTOVÉHO TRAKČNÍHO AKUMULÁTORU 28V/40Ah. In Sborník celostátní konference EPVE 2008. Brno: CERM, 2008. s. 100-105. ISBN: 978-80-7204-603-4.

[2] HEJKRLÍK, J.; VONDRUŠ, J.; CIPÍN, R.; VOREL, P. Monitorovací systém akumulátorů Li- FePo elektromobilu Jawa Chic. In ELEKTRICKÉ POHONY A VÝKONOVÁ ELEKTRONIKA - SBORNÍK KONFERENCE. Brno: 2009. ISBN: 978-80-214-3974- 0.

[3] PROCHÁZKA, P.; VOREL, P.; PAZDERA, I. ELEKTROMOBIL S VODÍKOVÝM PALIVOVÝM ČLÁNKEM A AKUMULÁTOREM. In MODERNÍ SMĚRY VÝUKY ELEKTROTECHNIKY A ELEKTRONIKY. Brno: Univerzita obrany, 2008. s. 169-172. ISBN: 978-80-7231-554-3.

STRUCTURAL AND CHEMICAL STUDIES OF THE $LiFePO_4$-MWCNTs CATHODE MATERIAL FOR Li-ion BATTERIES

M. Filkusová[1], A. Fedorková[2], R. Oriňáková[3], M. Kupková[4]

[1] Department of Physical and Theoretical Chemistry, Faculty of Science, Comenius University, Mlynská Dolina, SK–842 15 Bratislava 4, Slovak Republic
[2] Department of Analytical Chemistry, Faculty of Science, Comenius University, Mlynská Dolina, SK–842 15 Bratislava 4, Slovak Republic
[3] Department of Physical Chemistry, Faculty of Science, P.J. Šafárik University, Moyzesova 11, SK–04154 Košice, Slovak Republic
[4] Institute of Material Research, Slovak Academy of Science, Watsonova 47, SK-04353 Košice, Slovak Republic

Corresponding author: Mária Filkusová (maria.filkusova@gmail.com)
Phone: +421–55–2342328, Fax: +421–55–6222124

Introduction

Carbon nanotubes (CNTs) have recently attracted considerable interest in consequence of their potential applications in field emitters, nanoelectronic devices, probe tips for scanning probe microscopies and nanotube-based composites due to their excellent structural, mechanical and electronic properties [1]. Therefore, the combination of conducting polymer with CNTs was a good idea and in reality it was proven to have enhanced charge density, electrical conductivity and electrocatalytic activity compared with each pure component [2–4]. Among known conducting polymers, polypyrrole (PPy) is most frequently used in the commercial applications due to the high conductivity, long-term stability of its conductivity and the possibility to form homopolymers or composites with optimal mechanical properties. PPy offers potential applications in the domain of composite materials, tissue engineering, actuators, supercapacitors, electronic and electro optic devices [5].

Experimental

Carbon-free $LiFePO_4$ sample was prepared by solvothermal method. 1.5 g of pyrrole monomer (Aldrich Chemicals Co.) and 1 g of $LiFePO_4$ were placed in a 100 ml round-bottom flask. 1.42 g of $FeCl_3$ (99.9% Aldrich), used as oxidation agent, was dispersed in an aqueous solution of 0.1 mol/l HCl (50 ml) and added to the flask with $LiFePO_4$ powder. For preparation of PPy/PEG-$LiFePO_4$ sample polyethylene glycol was used at the beginning of polymerization. Three different samples of $LiFePO_4$ (LFP) with polymer coating were prepared as reported in [6]. Multi-walled carbon nanotubes (MWCNTs) were purified in H_2SO_4+HNO_3 (for 24 h) and than dispersed on LFP particles in ultrasonic bath. Morphology of the samples was characterized ex situ using a TESLA BS 340 scanning electron microscope (SEM).

Results and Discussion

Morphologies of LFP-MWCNTs, LFP-PPy-MWCNTs, LFP-PPy-PEG-MWCNTs are presented in Fig. 1. The morphology is made up of many tubular structures joined to one another. The nanotubes and LFP are associated together what should improve the ionic and electronic conductivity of resulting materials. The surface of MWCNs-LFP (Fig. 1) is rough and porous, with average diameter between 50-100 nm. The most homogeneous structure was observed for LFP-PPy-PEG-MWCNTs sample.

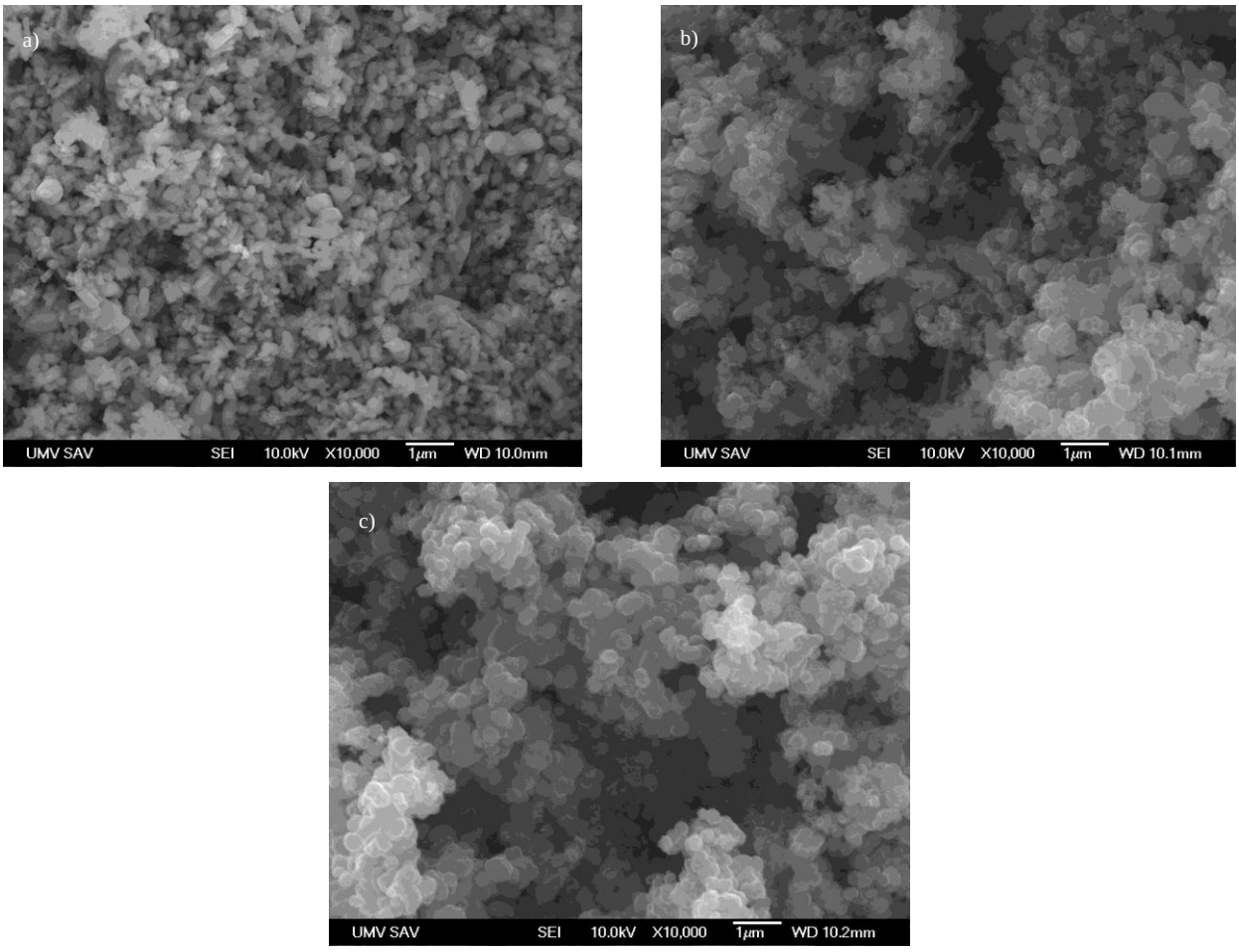

Fig. 1: *SEM images showing the surface morphology of a) LFP-MWCNTs, b) LFP-PPy-MWCNTs, c) LFP-PPy-PEG-MWCNTs*

Conclusions

The homogeneous structure and tight alignment of LFP-PPy-PEG-MWCNTs particles are the best assumptions for improving the ionic and electronic conductivity, capacity and performance of cathode material.

Acknowledgement

The authors thank for the financial support of the research by the Grant VEGA 1/0043/08 of the Slovak Grant Agency.

References

[1] T.M. Wu, H.L. Chang, Y.W Lin, Composites Science and Technology **69** (2009) 639-644.
[2] C. Peng, J. Jin, G.Z. Chen, Electrochim. Acta **53** (2007) 525–537.
[3] J.Y. Kim, K.H. Kim, K.B. Kim, J. Power Sources **176** (2008) 396–402.
[4] J.C.C. Yu, E.P.C. Lai, React. Funct. Polym. **66** (2006) 702–711.
[5] T.T.N. Liena, T. D. Lamb, V. T. H. Ana, T. V. Hoanga, D. T. Quangc,D. Q. Khieuc, T. Tsukaharad, Y. H. Leee, J. S. Kime, Talanta **80** (2010) 1164–1169.
[6] A. Fedorková , A. Nacher-Alejos , P. Gómez-Romero , R. Oriňáková , D. Kaniansky, Electrochim. Acta, **37** (2010) 943-947.

ELECTROSPUN METAL OXIDES FOR ENERGY STORAGE

Milos Dusek, Jaromir Pytel Jan, M. Macak

ELMARCO Ltd., Nano Divison
Svárovská 621, 460 10 Liberec, Czech Republic

Corresponding author: Milos Dusek (milos.dusek@elmarco.com)

The electrospinning is a progressive method for production of fibrous structured materials with fiber diameter in the range of hundreds of nanometers. The Nanospider^{TM} technology followed by subseqent calcination treatment has been used for the large-scale production of lithium titanate $Li_4Ti_5O_{12}$ (LTO). With this technology we achieved high specific surface area, highly crystalline spinel LTO nanofibers. In addition, recently also other materials appropriate for cathodes have been successfully electrospun.

The synthesis and properties of the nanofibers, as well as critical usability issues of these materials in the Li-ion battteries will be discussed.

INVESTIGATION OF THE OXIDATIVE STABILITY OF ELECTROLYTE SYSTEMS ON 5 V CATHODE MATERIALS BY *INSITU* MASS SPECTROMETRY

C. God[1], O. Moser[1], C. Bayer[1], C. Stangl[1], S. Koller[1], K.W. Leitner[2], M. Schulz-Dobrick[3]

[1] Institute for Chemistry and Technology of Materials, Graz University of Technology, Stremayrgasse 16, 8010 Graz, Austria
[2] BASF SE, GCI/E – M311, 67056 Ludwigshafen, Germany,
[3] BASF SE, GCC/PS – M300, 67056 Ludwigshafen, Germany

Corresponding author: Colin God (colin.god@TUGraz.at)

Abstract

Lithium-ion batteries are outstanding within all electric energy storage technologies due to their high energy density and excellent cycling stability. They are the most promising system as energy source for hybrid electric- (HEV) and electric-vehicles (EV). However, improvements of these systems are still necessary to meet the high energy demand of HEV & EV) applications. One strategy to increase the battery energy density is the use of new cathode materials with 5 V working voltage. Many investigations concerning these so called “5 V cathode materials” have been done already. An auspicious cathode material represents a modification of the spinel-structured $LiMn_2O_4$ with the general composition $LiM_xMn_{2-x}O_4$ [1]. This modification increases the average discharge voltage to 4.7 V, whereby in combination with a common graphite anode a theoretical specific energy of ~470 $Wh \cdot kg^{-1}$ could be achieved.

Due to the high working potential of this material the oxidation stability of the electrolyte plays an important role. In this work the anodic stability of carbonate based electrolyte systems are investigated. To achieve knowledge not only on the decomposition potential but also on the reaction mechanism cyclic voltammetry (figure 1) was combined with “*insitu*” mass spectrometry (figure 2) [2, 3]. Unfortunately, this method is not sensitive enough to provide information on the small quantities of gas that are formed at the working potential of the material. For quantification the pressure gain in a Swagelok T-cell during cycling was tested, which sheds also a light on the amount of decomposed electrolyte.

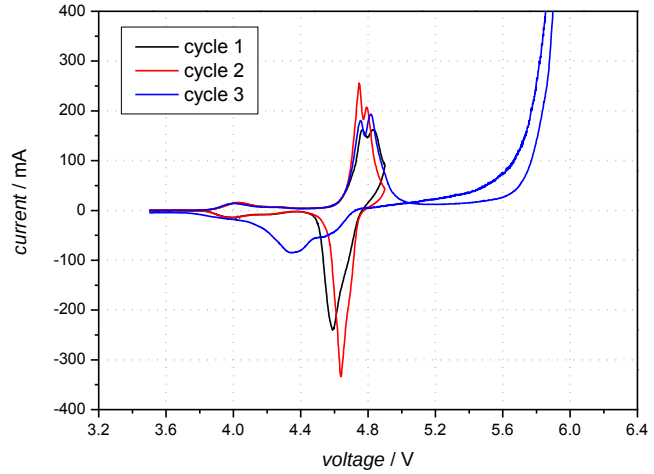

Fig. 1: *Cyclic voltammogram of a BASF-LiM$_x$Mn$_{2-x}$O$_4$-cathode with the electrolyte EC/PC (1:1, v:v), 1M LiPF$_6$.*

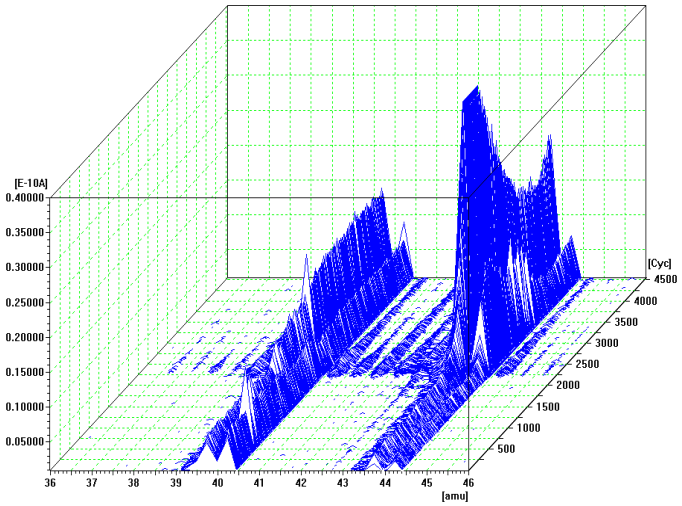

Fig. 2: *In situ mass spectrometry for the mass points of propane of the 3rd CV-cycle, which is shown in figure 1.*

References

[1] S. Patoux, L. Sannier, H. Lignier, Y. Reynier, C. Bourbon, S. Jouanneau, F. Le Cras, S. Martinet, *Electrochimica Acta 53,* ***2008****, 4137-4145*.

[2] Jee.Sun Shin, Chi-Hwan, Un-Ho Jung, Shunk-Ik Lee, Hyeong-Jin Kim, Keon Kim, *Journal of Power Sources 109,* ***2002****, 47-52*.

[3] M. Holzapfel, A. Würsig, W. Scheifele, J. Vetter, P. Novák, *Journal of Power Sources 174,* ***2007****, 1156-1160*.

NEW MATERIALS FOR ADVANCED LITHIUM ION BATTERIES

H. Kren[1], M. Scharfegger[1], A. Droisner[1], C. God[2], S. Koller[1]

[1]Varta Micro Innovation, Stremayrgasse 9, 8010 Graz
[2]Graz University of Technology

Corresponding Author: Stefan Koller (s.koller@vartamicroinnivation.com)
WWW: www.vartamicroinnovation.com

Introduction

Since the large automotive companies go ahead with the electrification of the power train, also the demand for more powerful electrochemical energy storage systems is growing. However not only the automotive industry requires more powerful accumulators. In the area of mobile consumer electronics the proceedings of the last years are compensated by the rising energy demand of the devices., Accordingly the doubling of the energy density of lithium ion batteries, since they were commercialized by Sony in 1991, increased only imperceptibly the operating time.

Experimental

The key to enter new application fields like the storage of solar energy, or wind power is the development of new materials. The specific energy of a lithium ion battery is given by the product of specific charge - more precisely the lithium storage ability per mass and the voltage difference of negative and positive electrode. As far as the negative electrode is concerned lithium and lithium compounds already represent the most reductive species of the electrochemical series. However carbonaceous materials that are used in state of the art lithium ion batteries are only able to store up to 1 lithium ion per 6 carbon atoms [1] in the case of fully crystalline graphite, which results in a quite low specific charge of 372 $Ah \cdot kg^{-1}$. The application of metals or semi metalloids, which are able to store lithium under formation of an intermetallic phase represents a very promising alternative, whereat especially silicon is able to store up to 4.4 [2] lithium ions per silicon atom. Unfortunately the high capacity of the Si/Li-intermetallic phases is accompanied by large volume changes during lithium insertion and deinsertion, which leads to cracking and disintegration of particles and a fast capacity decay [3]. This, and of course also the mechanical instability of the SEI during the volume changes are problems that need to be solved for a successful implementation of this materials. An overview on possible strategies and approaches to overcome these problems will be given.

Transition metal oxides based on an insertion-type mechanism are today's state of the art materials for the positive electrode. Due to the high molecular weight of the used transition metals (Co, Ni, Mn, Fe) the accessible specific charges are very limited. To achieve the same improvements such as by the replacement of graphite through silicon, a change of the reaction mechanism of the cathode material is necessary. Unfortunately reaction type cathode materials like sulfur still show large disadvantages in terms of cycleability and rate capability and need large improvements to enter an applicable development level. On a

short term cathode materials that offer a higher working potential like the spinell-type $LiNi_{0.5}Mn_{1.5}O_4$ show a better probability for realization. Therefore the stability of the electrolyte system has to be improved to potentials up to 5 V vs. Li/Li^+. An overview on the problems caused by the high voltage cathode materials and possible solution strategies will be given.

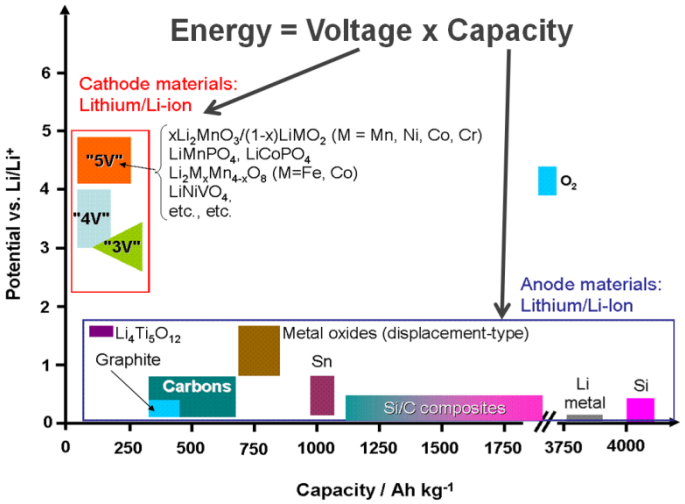

Fig. 1: *State of the art and future materials for Lithium ion batteries*

References

[1] Martin Winter, Jürgen O. Besenhard,* Michael E. Spahr, and Petr Novák, *Advanced Materials*, **1998**, 10, No. 10

[2] B.A. Boukamp, G.C. Lesh, R.A. Huggins, J. *Electrochem. Soc*. Vol.128 No. 4, **1981**, 725-729

[3] J.O. Besenhard et.al., *Journal of Power Sources*, **1997**, 68, 87-90

11th ABAF

BRNO 2010

Advanced Batteries, Accumulators and Fuel Cells

Electrolytes

STUDY OF GEL ELECTROLYTES PROPERTIES BY MR METHODS

R. Kořínek[1], J. Vondrák[2,3], K. Bartušek[4], M. Mrnka[1]

[1] Department of theoretical and experimental electrical engineering FEEC BUT, Kolejní 4, 612 00 Brno, CZE, e-mail: radim.korinek@centrum.cz
[2] Department of Electrotechnology FEEC BUT, Údolní 53, 602 00 Brno, CZE
[3] Institute of Inorganic Chemistry of the ASCR, v.v.i., 250 68 Řež, CZE
[4] Institute of Scientific Instruments of the ASCR, v.v.i., Královopolská 147, 612 64 Brno, CZE

Introduction

In this paper are introduced basic methods for measuring the properties of the gel structure during polymerization, particularly relaxation times T_1, T_2 spin density and diffusion coefficients. We can obtain these parameters using the MR pulse sequences. To measure of relaxation time T_1 are used SR techniques (Saturation Recovery) and IR techniques (Inversion Recovery) usually. To measure of relaxation time T_2 can be used SE (Spin Echo) technique. To measure diffusion coefficinets are used PFG-SE and PFG-SSE methods (Pulsed Field Gradient Spin Echo a Pulsed Field Gradient Stimulated Echo) and of course their modification. Experiment itself is described sample preparation of gel electrolytes and to measure their relaxation times.

Measurement of diffusion

Measuring the diffusion NMR experiment is a decisive introduction diffusion gradient of spin echo, referred to in the work of Stejskal and Tanner [1]. The resulting signal is proportional to size of the movement of molecules. The basic form of PFG-SE sequence is shown in Fig.1. This sequence is often named to as "6 interval method". Shape of the gradient corresponds to the b-factor for the square wave gradient is given by:

$$b = \gamma^2 G^2 \delta^2 \left(\Delta - \frac{\delta}{3} \right).$$

If there are leading edges, so *b* – factor is:

$$b = \gamma^2 G^2 \left[\delta^2 \left(\Delta - \frac{\delta}{3} \right) + \frac{\varepsilon^3}{30} - \frac{\delta \varepsilon^3}{6} \right].$$

For the round shape of the gradient is *b* - factor:

$$b = 4\pi^{-2} \gamma^2 G^2 \delta^2 \left(\Delta - \frac{\delta}{3} \right).$$

Diffusion coefficient is then expressed by:

$$D = -\frac{\ln\left(\frac{M}{M_{G_D=0}}\right)}{b}.$$

Where $M_{G_D=0}$ = 0 is signal intensity without diffusion influence (measured sequence without diffusion gradients).

Magnetic susceptibility distorts of the static magnetic field and the diffusion measurement is subject to significant errors. To eliminate this influence is suitable compensation, using a dual polarity gradient [3]. Measurement of diffusion of sodium nuclei in liquid electrolytes is limited by the short relaxation times and low sensitivity of MRI measurements.

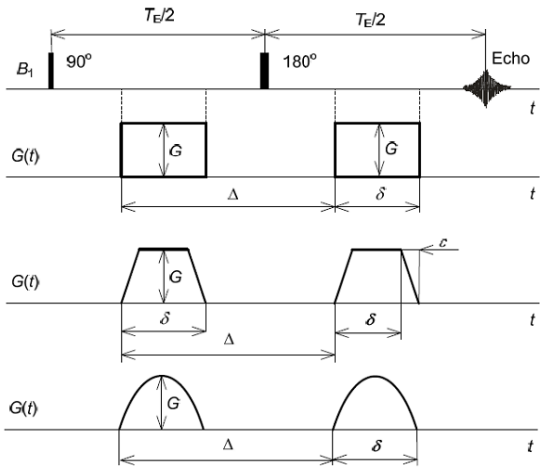

Fig. 1: *Arrangement PFG-SE sequence and different shapes of diffusion gradients, taken from [2].*

Gel polymer electrolytes

Currently, research is focused on 3 generation of polymer electrolytes with high chemical stability and exploitable potential of 3.5 to 4.5 V. In [4] are experimentally measured times T_1 and T_2 and their changes during polymerization of the gel. Polymerization was carried out by heating the gel at a temperature of 80°C for 10 minutes and measurements were repeated after 30 minutes. Figures 2, 3 and 4 taken from [5].

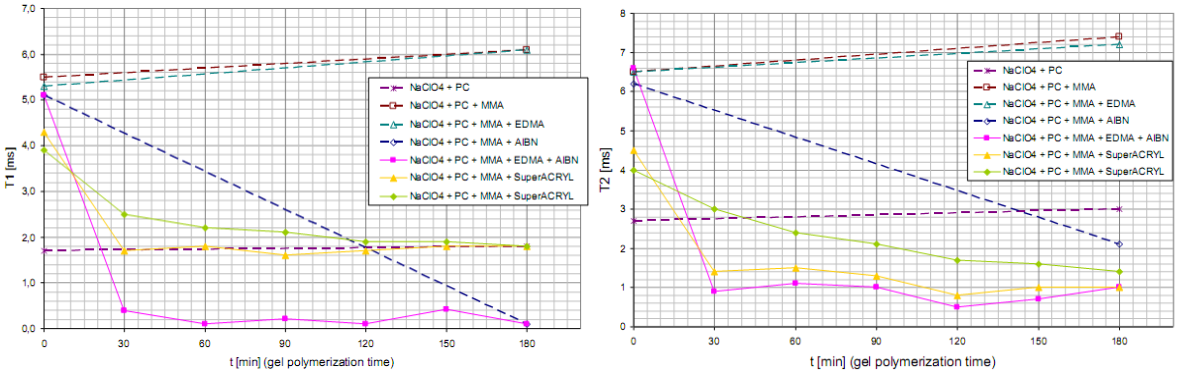

Fig. 2: *(left) T1 relaxation (Inversion Recovery) as a function of aging gel.*
Fig. 3: *(right) T2 relaxation (Hahn echo) as a function of aging gel.*

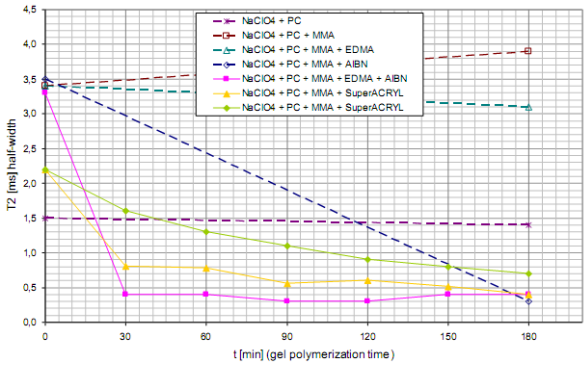

Fig. 4: *T_2 relaxation (Half-width spectral line) as a function of aging gel.*

Experimental

We are selected for the experiment, gel electrolytes with conductivity based on sodium ions Na+ (NaClO4 solution in PC (propylene)), and polymerization was induced by an auxiliary UV (initiator BEE). The aim was to determine the relaxation times T_1 and T_2 during the polymerization of gels and determining the influence of salt concentration on the values of relaxation times. Measurement of diffusion constants was not possible for very short relaxation times. Measurements were carried out on the MR system 200MHz/70mm (4.7T/70mm) in the ISI. The relaxation times T_1 and T_2 and their changes during polymerization were experimentally measured. For the T_1 measurement was used the Inversion Recovery method and for the T_2 measurement the spin echo method and the determination of the half-width of spectral lines FID signal from the relation

$$T_2 = \frac{1}{\pi.\Delta f'},$$

where $\Delta f'$ is half-width of spectral line.

NaClO4 in PC (propylene) make a liquid electrolyte. After mixing with MMA (methyl methacrylic acid, 99%), EDMA (networking factor) and BEE (UV polymerization Initiator) is created by UV radiation (total time of polymerization for several hours), gradually gel electrolyte. Composition is summarized in Table 1.

Table 1: *The composition of the measured samples*

	1.sample	2.sample	3.sample	4.sample
Concentration	1M	0,5M	1M	1,5M
NaClO4 [g]	0,980	0,245	0,490	0,735
PC [ml]	8	4	4	4
MMA [ml]		4	4	4
EDMA [g]		0,040	0,040	0,040
BEE [g]		0,062	0,062	0,062

For the polymerization the two UV 15W tubes power and 45 cm long was used. Tubes emit light with wavelengths 320-400nm and 290-320nm. Light intensity was 160 mW/cm^2 and a glass wall attenuation vials of 25%. The dependence of relaxation times T_1 and T_2 on the polymerization time are shows on Fig.5., and Fig.6. On Fig. 7. are shown the

measured dependence of relaxation times T_1 and T_2 on the size of the sample concentrations.

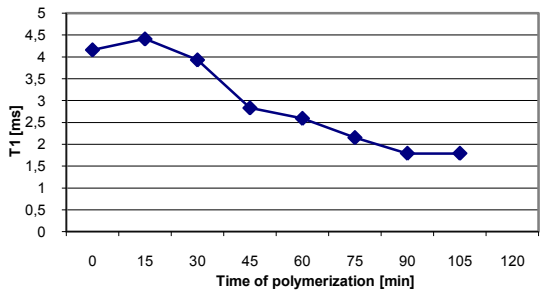

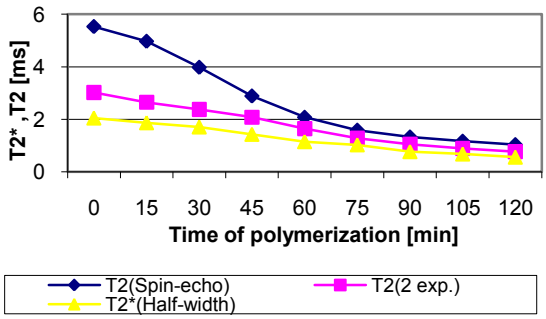

Fig. 5: *(left) T1 relaxation time depending on the time of polymerization of the sample with a concentration of 0.5 M.*
Fig. 6: *(right) Comparison of T2 (SE) and T2* relaxation times in dependence on the polymerization with concentration 0,5 M.*

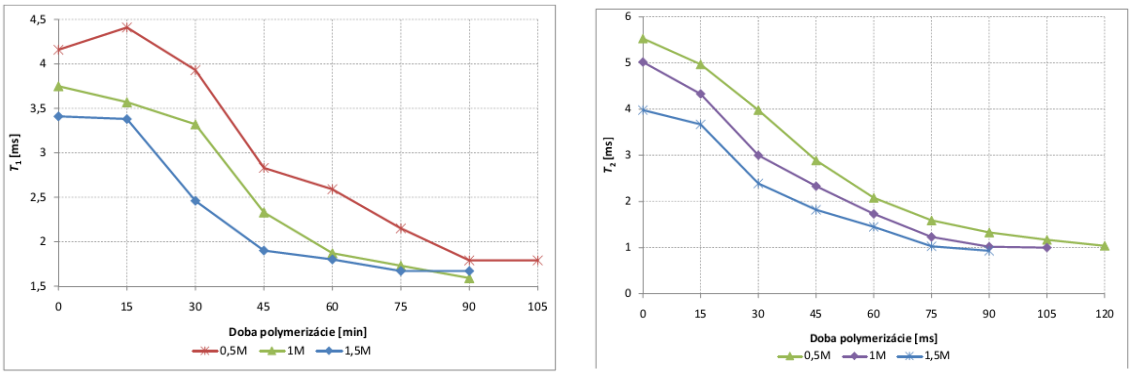

Fig. 7: *Comparison of T1 and T2 relaxation times for various concentrations of the samples in dependence on the time of polymerization.*

Result and discussion

During the measurements there was a gradual reduction of relaxation times. An exception was the sample with a concentration of 0.5 M, where after 15 minutes of UV illumination was observed increase in time T_1. Such a result could be due to a slower onset of polymerization of this sample. Such a result could be due to a slower onset of polymerization of this sample. This gel most often stiffens between 15 and 45 minutes, where it recorded the most significant decrease of relaxation times. Decreased relaxation times in the course of polymerization indicate a change in the internal structure of the gels and the change of chemical bonds.

Acknowledgements

The work described in the paper was financially supported by the research project of Czech Science Foundation, Grant No. P102/10/2091, the Grant Agency of the Czech Republic GA102/09/0314 and research plan MSM0021630516.

References

[1] STEJSKAL, E.O., Tanner, J. E. Spin diffusion measurements: spin echoes in presence of a time-dependent field gradient. J. Chem. Phys. 42, s. 288.
[2] BARTUŠEK, K. Speciální metody měření difúzních koeficientu metodami nukleární rezonance. VUTIUM, 2007, 21 s. ISBN 978-80-214-3379-3.
[3] BARTUŠEK, K., GESCHEIDTOVÁ, E. Kompenzace vlivu statického magnetického pole při MR měření difúze. Elektrorevue 2008/29, 6 s.
[4] REITER, J., VONDRÁK, J., VELICKÁ J., MIČKA, Z. Nové elektrolyty nejen pro chemické zdroje elektrické energie. Chem. Listy 2006/100, s. 133-139.
[5] VOGNAR, J.,MACALÍK, M., ŠPIČÁK, P., VONDRÁK J., NOVÁK, V., KREJZA, O., BARTUŠEK, K. A study of PMMA based gel electrolytes containing Na+ ions by nuclear magnetic resonance. In 9th ABA Brno 2008. Brno, BUT in Brno. 2008. p. 66 – 70.

AMORPHOUS SOLID INORGANIC ELECTROLYTE ON BASIS OF Li_2O-LiF-Li_2WO_4-B_2O_3 FOR LITHIUM POWER SOURCES

A. Tron[2], I. Maksuta[2], E. Shembel[1,2]

[1] Research laboratory of chemical power sources (NILhit), Ukrainian State Chemical-Technology Universality, 49005, 8, Gagarin Ave., Dnipropetrovs'k, Ukraine
[2] Enerize Corporation, Coral Springs, Fl, USA

Corresponding author: Elena Shembel (shembel@onil.dp.ua)
Phone, fax: +38 (0562) 47-03-91

Introduction

From the point of view of the use as solid electrolytes of chemical power sources (CPS) large interest is been of by the borate solid electrolytes Li_2O-B_2O_3, modified by the oxides of metals with a large ionic radius, for example, WO_3. It is related to that "loosening" of structural net of solid electrolyte (SE), consisting of groups [BO_3] and [BO_4], large polyhedrons [WO_4] will result in the substantial increase of the free volume SE and, as a result, to the increase of their conductivity on the ions of lithium. However in literature the information is practically absent about glassy and properties of solid electrolytes in the oxide system Li_2O-Li_2WO_4-B_2O_3. In the work [1] devoted to investigated of the indicated system, properties of the given system are studied with high contents of oxide of lithium in amounts more 35 mol.%, practically all cations of tungsten are found in the hexavalent state. In work it is marked also, that the increase of concentration of the ions W^{+6} results in polymerization of tungsten groups, that stipulates high ionic conductivity of such solid electrolytes. For the increase of conductivity on the ions of lithium in their composition salt additions are entered (LiF, Li_2SO_4 and others) [2].

Development of composition of the solid electrolyte Li_2O-LiF-Li_2WO_4-B_2O_3 from high ionic conductivity of intended for the use in the lithium power sources is the purpose of investigations.

Experimental

Investigation of impedance of solid electrolytes for determination of ionic conductivity was conducted by a multifunction device for the electrochemical investigations VoltaLab 40 (PGZ 301) in a thermostat in the interval of temperatures (from 26°C to 110°C). Amplitude of variable tension made 10 mV, in area of frequencies from 100 kHz to 100 mHz. Treatment of results of the impedance measuring was conducted on the equivalent chart [3] grounded for solid electrolytes.

Experimental data, obtained at the SE research processed by the method of plural correlation. The equalization 1 describes dependence of conductivity of solid electrolyte on his composition. The equalization 2 describes dependence of activation energy on composition of solid electrolyte.

Electronic conductivity of solid electrolytes was determined by VoltaLab 40 (PGZ 301) with the use of method of step change of potential in cell (electrode / solid electrolyte / electrode) with blocking electrodes.

X-ray analysis (XRD) solid electrolytes was determined on DRON-3.0 in the Cu_{Ka} radiation.

Results and discussion

How it is shown [4], that for the increase of conductivity on the ions of lithium in the content of the solid electrolyte Li_2O-LiF-P_2O_5 fluorine of lithium is entered.

it is possible that partial replacement in composition solid electrolyte of the Li_2O-Li_2WO_4-B_2O_3 lithium oxide on his fluorine will be accompanied by formation in the structural net of the SE electro-neutral oxide-fluoride, for example, $[WO_4F_2]^{4-}$. Thus localization of anions of fluorine near cations of tungsten can cause change coordination number of the last from the four to six (fig.1).

a) b)

Fig.1: *Structural groups $[WO_4]^{2-}$ (fig.1a) and $[WO_4]F_2^{4-}$ (fig.1b).*

Such polyhedron, not containing multiple communications, can be bound in a three-dimensional spatial structural net. The increase of degree of coherent of spatial framework of solid electrolyte, sure, must be accompanied increases of degree of amorphous (fig.2) and increase of free volume. The last in turn one ought to result in the increase of ionic conductivity of solid electrolytes.

The results of measuring of ionic conductivity of the investigated solid electrolytes in the system by the Li_2O-LiF-Li_2WO_4-B_2O_3 method of impedance spectroscopy fully confirmed the outspoken suppositions (table 1).

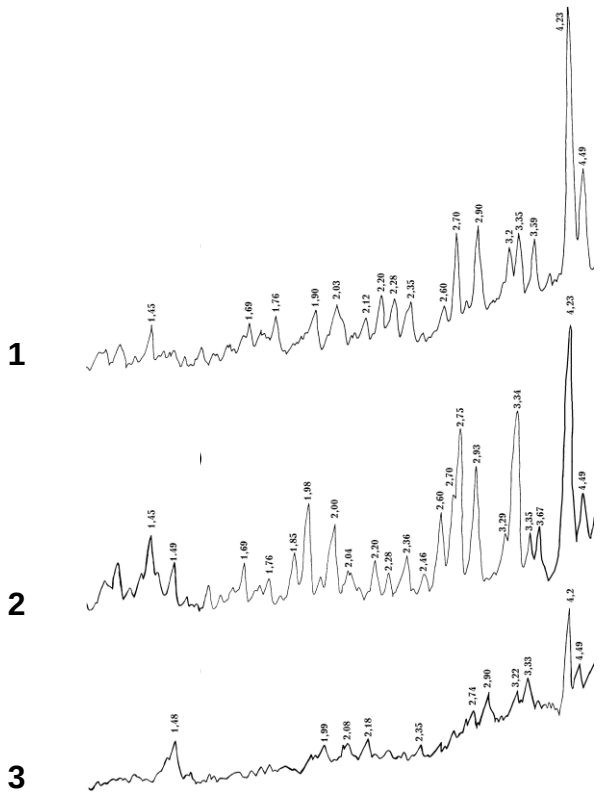

Fig.2: *X-ray photograph solid electrolyte on basis of Li_2O-Li_2WO_4-B_2O_3 system: 1 – content LiF – 0 mol.%; 2 – content LiF - 10 mol.%; 3 – content LiF - 20 mol.%.*

Tab. 1: *– Ionic conductivity of solid electrolyte in the system Li_2O-LiF-Li_2WO_4-B_2O_3*

№ composition - Li_2O	***Content SE, mol. %***				Ionic conductivity SE κ, $Sm \cdot cm^{-1}$ at 25°C
	Li_2O	***LiF***	Li_2WO_4	B_2O_3	$κ_{экс.}$
1 - 52	40	10	20	30	$0,97 \cdot 10^{-6}$
2 - 53,8	40	20	20	20	$0,114 \cdot 10^{-6}$
3 - 54,2	45	10	15	30	$0,10 \cdot 10^{-6}$
4 - 56,5	50	10	10	30	$0,48 \cdot 10^{-6}$
5 - 58,3	50	10	15	25	$1,26 \cdot 10^{-6}$
6 - 58,3*	50	0	20	30	$2,45 \cdot 10^{-7}$
7 - 60	50	10	20	20	$0,79 \cdot 10^{-6}$
8 - 60,9	55	10	10	25	$1,07 \cdot 10^{-6}$
9 - 64	55	10	20	15	$1,34 \cdot 10^{-6}$
10 - 65,2	60	10	10	20	$1,74 \cdot 10^{-6}$

Note: * - ionic conductivity from data [1].

At the processing experimental data method of plural correlation [5] obtained linear equalizations of regression of two kinds $Y = b_0 + \sum (b_i * x_i)$ and $Y = \sum (a_i * x_i)$, where $a_i = b_0 + b_i$ (R = 0,918; Δlgκ = ±0,1; [κ, $Sm \cdot cm^{-1}$]), linking intercommunication between ionic conductivity of the investigated solid electrolytes in the system Li_2O-LiF-Li_2WO_4-B_2O_3 and their chemical composition (mol.%) (equalization (1) and (2)):

$$\lg \kappa = -6{,}295 + 0{,}00854 \cdot C_{Li_2O} + 0{,}041 \cdot C_{LiF} - 0{,}00513 \cdot C_{Li_2WO_4} - 0{,}021 \cdot C_{B_2O_3}, [\kappa, Sm \cdot cm^{-1}] \quad (1)$$

$$\lg \kappa = -0{,}054 \cdot C_{Li_2O} - 0{,}022 \cdot C_{LiF} - 0.068 \cdot C_{Li_2WO_4} - 0{,}084 \cdot C_{B_2O_3}, [\kappa, Sm \cdot cm^{-1}] \quad (2)$$

It is necessary to notice that introduction of lithium fluoride in the composition of solid electrolyte in the system Li_2O-Li_2WO_4-B_2O_3 as results the increase of ionic conductivity. So, for example, at identical content of lithium oxide (58,3 mol.%) in the system Li_2O-Li_2WO_4-B_2O_3 introduction to its composition of 10 mol,% of lithium fluoride as results the increase of ionic conductivity. Thus conductivity total $1{,}26 \cdot 10^{-6}$ Sm·cm^{-1} (system 5, table 1), on comparison with a similar system without content of lithium fluoride [4] and total $2{,}45 \cdot 10^{-7}$ Sm·cm^{-1} (system 6, table 1).

Legitimacy of supposition at the increases of ionic conductivity of solid electrolyte in the system Li_2O-Li_2WO_4-B_2O_3 at the expense of introduction of lithium fluoride is confirmed by investigated results.

Thus, totality of the obtained results testify to high quality of the developed solid electrolytes in the system Li_2O-LiF-Li_2WO_4-B_2O_3 and is the optimum variant of decision of task of increase of ionic conductivity of solid electrolytes and saving of their technological. Thus in the composition solid electrolytes be found a minimum of traditional glass-forming element (B_2O_3 – 15-25 mol.%), providing good cooking and workability characteristics, but to substantially decreasing conductivity of solid electrolytes on the ions of lithium.

Conclusions

The developed solid electrolytes Li_2O-LiF-Li_2WO_4-B_2O_3 possess high ionic conductivity on the ions of lithium $1{,}26 \cdot 10^{-6}$ Sm·cm^{-1} and the low electronic conductivity $3{,}0 \cdot 10^{-13}$ Sm·cm^{-1}.

It is shown, that the presence of fluoride ions in composition the oxide-salt solid electrolytes Li_2O-LiF-Li_2WO_4-B_2O_3 allows to increase the degree of their amorphous and ionic conductivity.

Linear equalizations are found, is numeral reflecting influencing of chemical composition of solid electrolytes on the basis of Li_2O-LiF-Li_2WO_4-B_2O_3 on ionic conductivity.

Established chemical stability of the developed solid electrolytes in relation to metallic lithium in the interval of temperatures (18 - 250°C) and electrochemical stability of solid electrolyte in an interval 0 - 4,5 V, that will provide high efficiency of work of lithium power sources.

References

[1] Kvasha A. M. Ph.D. thesis - candidate of science: 05.17.03. – Dnepropetrovs'k, 2004. – p. 147 - (in Russian).
[2] Julien C. и Nazri G.A. - Kluwer Academic publishers, 1994. 625 c.
[3] Tron' A. V., Nosenko A. V., Shembel' E. M. // Materials of the X International conference: Theses of lectures of fundamental problems of transformation of energy in the lithium electrochemical systems. – Saratov. – 2008. - P. 199-201. -(in Russian).
[4] Tron' A. V., Nosenko A. V., Shembel' E. M. // Russian Journal of Electrochemistry. – 2009. – Vol. 45. – No. 5. – p. 527–532 - (in Russian).
[5] Ahnazarova S. L., Cafarov V. V. – M.: Higher school, 1978. – p.319 - (in Russian).

SULFOLANE AS A SOLVENT FOR APROTIC ELECTROLYTES

J. Vondrák[2], *M. Sedlaříková*[1], *M. Zatloukal*[1], *P. Dvořák*[1]

[1] *Department of Electrical and Electronic Technology, University of Technology Brno, 602 00 Brno, Czech Republic*
[2] *Institute of Inorganic Chemistry of the ASCR, v. v. i., 250 68 Řež near Prague, Czech Republic*

Corresponding author: J. Vondrák (vondrak123@seznam.cz)
Phone: +420607285434

Introduction

The importance of aprotic solvents for preparation of especial electrolytes has increased in ast two decades. Among them, the sulfur containing solvents have not attracted too much attention yet. One of them is sulfolane (1,4-butylene sulfone, further abbreviated as SL , formula see in Fig. 1). Its fundamental properties were reviewed several times,, see Tab. 1. As its formula is similar to that of cyclic carbonates, some important properties of propylene carbonate (PC), ethylene carbonate (EC) and sulfolane (SL) are compared in Table 1.

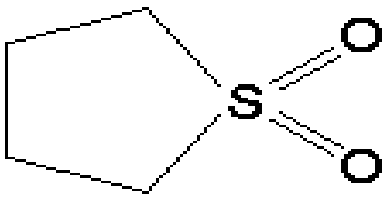

Fig. 1: *Formula of sulfolane*

Any solvent suitable for aprotic electrolytes must possess high dielectric permittivity as well as not too high viscosity in order to obey Walden and Stokes rules. For application in technology, also the effect of low temperatures and the inflammability are of importance.

The subject of present paper is the consideration and evaluation of several parameters of sulfolane from the viewpoint of applicability in the electrochemistry of anhydrous aprotic systems. Mainly, the freezing, electrical conductivity of inorganic salts, thermal decomposition and flash point were evaluated by us.

The use of SL and similar compounds in electrochemistry is rather seldom for many reasons (their high melting point and viscosity and lower conductivity) see [1], [2], [3].

Tab. 1: *Selected properties of sulfolane, PC and EC*

solvent	PC	EC	sulfolane
Molecular mass	102.09	88.06	120.17
Boiling point / °C	242	238	287.3
Meeting point / °C	-54.53	36.53	28.15
Permitivity ε	64.95	90.36	43.3
Viscosity / cP	2.21	1.9	1.262
Flash point	132°C	150°C	165°C

Experimental

Sulfolane and propylene carbonate used for experiments were purchased at Aldrich Co. And distilled in vacuum. Lithium salts were dried at 100oC in vacuum.

Cryoscopy, DTA-TG and flash point estimations were performed with the samples. As an attempt, the gel polymer electrolytes from MMA in which PC solution was replaced by a solution of Li salt in SL were prepared.

Results and Discussion

a) Freezing point

Freezing point of a 0,5 M LiClO4 in SL was lowered from, more than 26oC to +10+C, thus indicating rather high cryoscopic constant of SL. Moreover, the same concentration of LiClO4 in a mixture of 20%PC and 80%SL is even more resistant to freezing; it remains liquid below -20°C. This opens the possibility to improve the applicability of SF electrolytes.

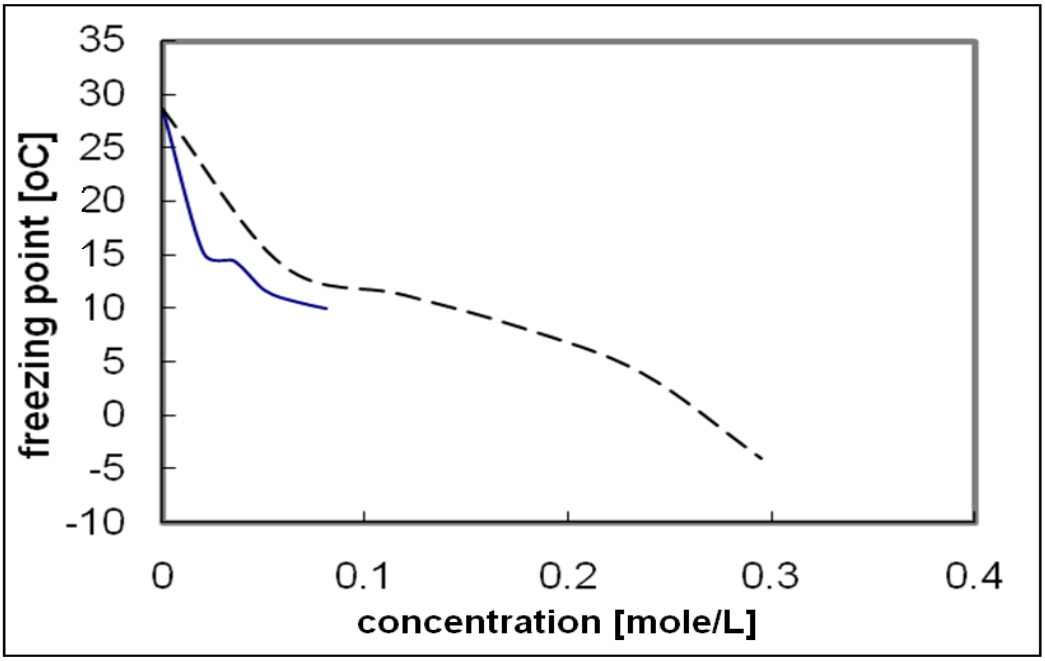

Fig. 2: *Freezing point*

b) Flash point

The increase of flash point in the mixtures of PC and SL indicates the positive influence of SL on improved safety of lithium cells.

DTA – GT measurements at which the mass spectrometric detection of SL decomposition indicates that the decomposition begins at temperatures between 250 and 350°C.

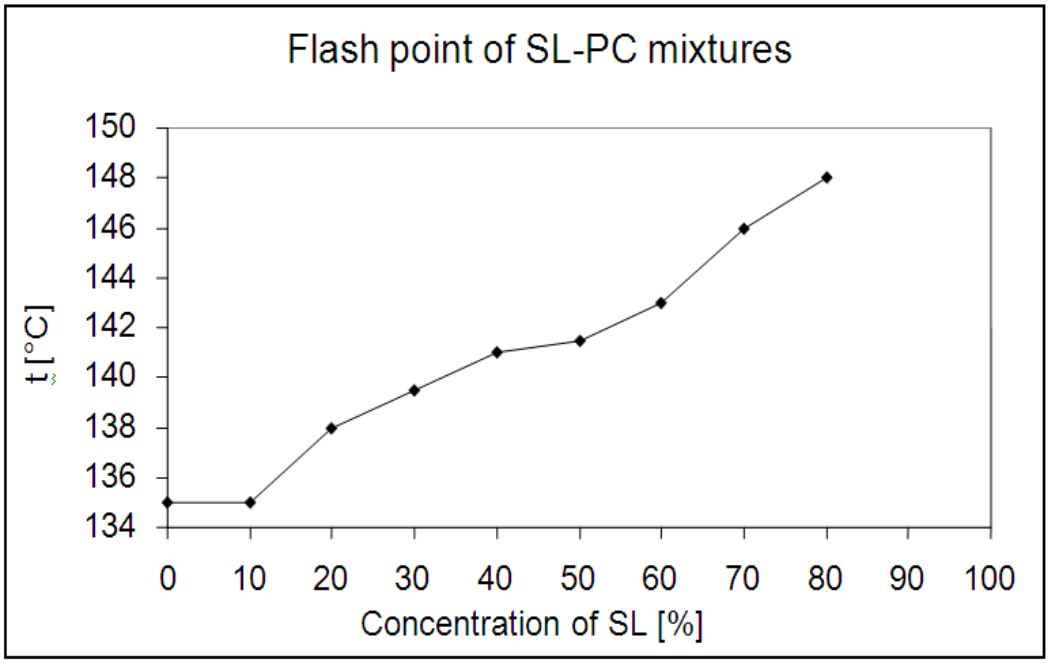

Fig. 3: *Flash point of SL-PC mixtures*

c) Electrochemical observations performed

1. The conductivity at r.t. – it is cca ¼ od that of PC solutions , should be improved by addition of other less viscous substances (similar to replacing PC by EC-DMC mixtures)
2. Potential window (left) and purified (right) SL – $LiClO_4$

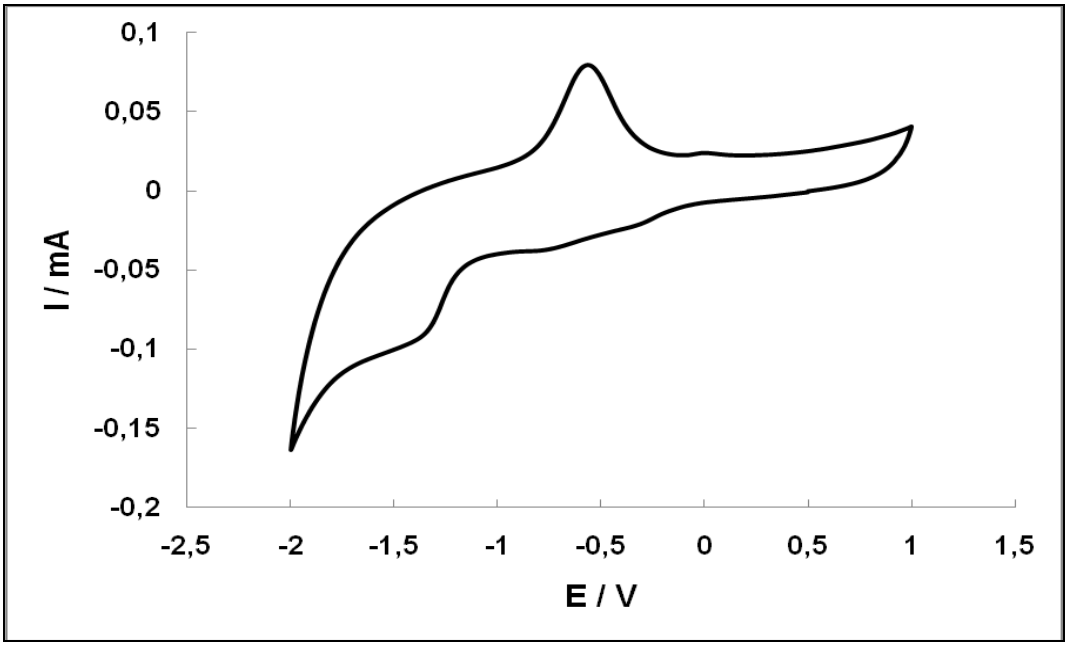

Fig. 4: *Voltammogram of raw SL*

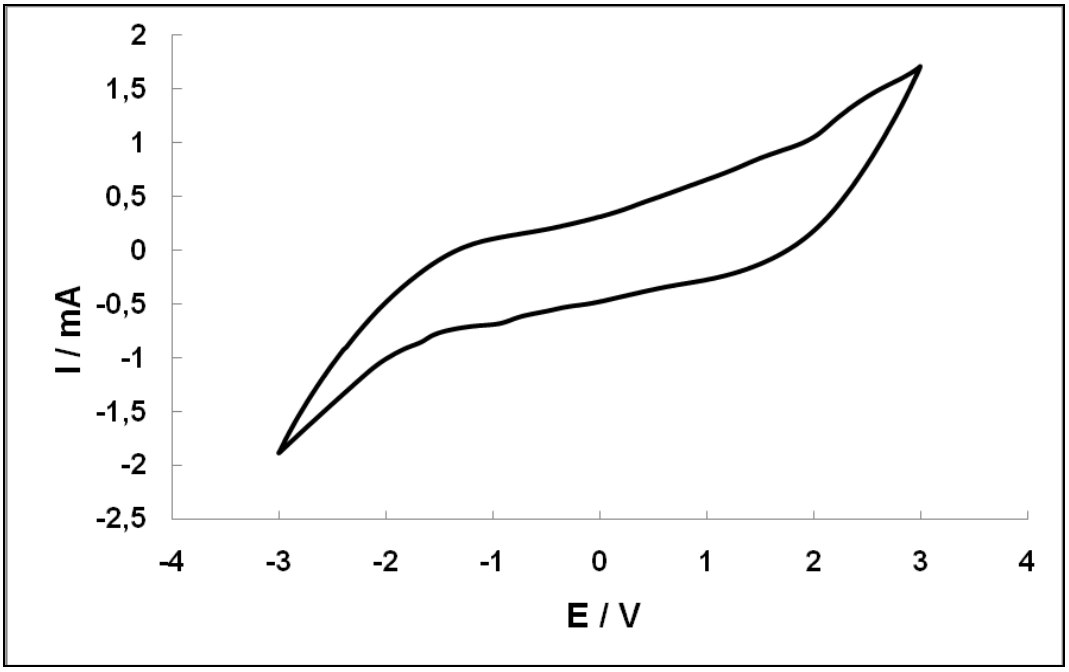

Fig. 5: *voltammogram of SL distilled in vacuum*

These voltammograms show the necessity of using distilled SL exclusively. Further. The potential window seems to be fairly broad for any application.

Sulfolane can be used as an aprotic solvent. This was verified by the solution of ferrocene in lithium – SL electrolyte. Voltammogram of the system is shown in Fig. 5; the redox system is apparently rather reversible.

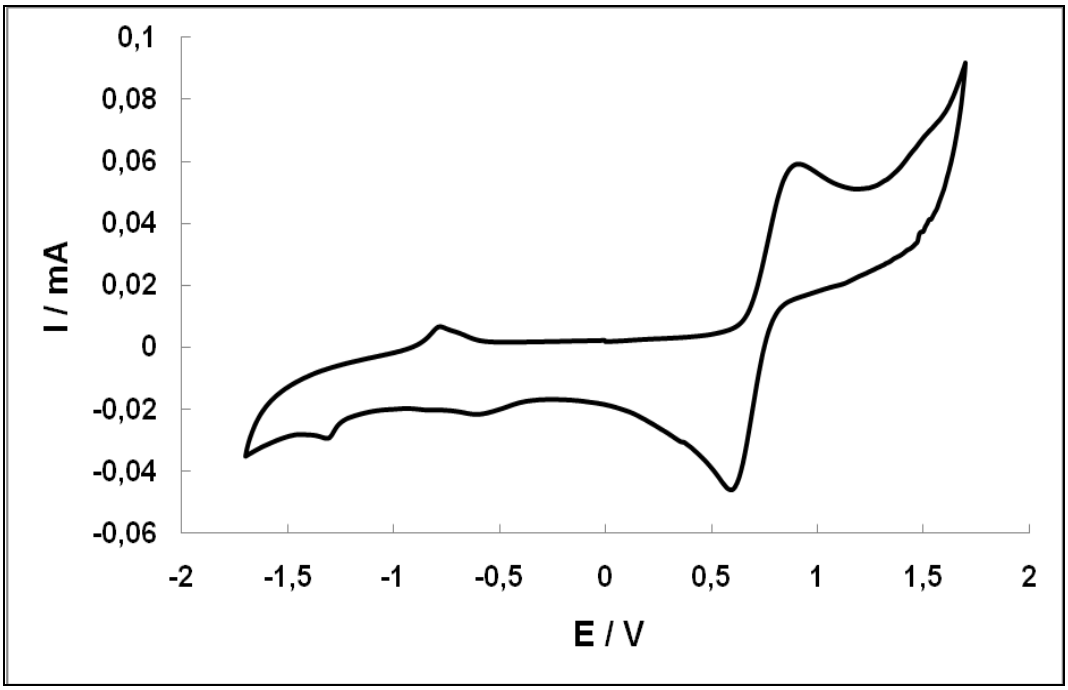

Fig. 6: *Voltammetry of 0.01 M ferrocene in $LiClO_4$, scan rate 1 mV/s*

Conclusions

Sulfolane is a solvent which can be used for various purposes in lithium batteries and similar devices. Two disadvantages, i.e. , high melting point and low conductance of lithium salts, could be weakened by the addition of other solvents. On the other hand, high flash point would improve the safety of the batteries against incineration.

Acknowledgements

MinIstry of Education, project MSM 0021630516 , to The Electrochemical Society, Czech Science Foundation No. P103/10/2091 and ASCR Research Plan No. AV/ 0Z403 0502. Moreover, this work was a part of Student Chapter of thé Electrochemical Society.

References

[1] Electric double layer capacitor, US pat. 5,754,393, May 19, 1998
[2] V. Steele, R. D. Chirico, S. E. Knipmeyer, and A. Nguyen J.Chem. Eng. Data(1997) 42>1021-1036
[3] Kolosnitsyn V.I., E.V. Karaseva, Al Ivanov, Russian Journal of Electrochemistry (2008)44:564-569

RECENT DEVELOPMENTS IN THE RESEARCH OF GEL POLYMER ELECTROLYTES

J. Vondrák[1], M. Sedlaříková[1], J. Velická[2] , M. Macalík[1]

[1] Faculty of Electrical Engineering and Communication, Department of Electrotechnology, Údolní 53, 602 00 Brno, Czech Republic
[2]Department of Inorganic Chemistry, Academy of Science, Husinec, Řež near Praque, Czech Republic

Corresponding author: Jiří Vondrák (vondrak123@seznam.cz)
Phone: +420 607 285 434

The application of gel polymer electrolytes which contain lithium salt is essential for lithium polymer batteries. The durability, conductivity, resistance to extreme temperatures fire and mechanical properties are the most important parameters to be emphasized. Our recent results are concerned in the methacrylate based composites prepared by polymerization of monomer - organic Li solution mixtures. The composite (gel) electrolytes prepared from MMA and Li salts dissolved in PC exhibit reasonable value of conductivity (10^{-3} S/cm) and freeze resistance down to -25°C at least.

Lithium salts should be considered as strong electrolytes, the molar (or equivalent) conductance conductance$\Lambda=\kappa/c$ should decrease slowly with increasing concentration (ionic strength). The theory initiated by Kolrausch implies the model of ions as charged spheres containing ion surrounded by a solvatation envelope; its movement in electric field is governed by Stokes law.

The behavior of our gels is somewhat different. As Fig. 1 shows, the molar conductance passes through *a maximum* at intermediate concentration. This indicates some changes in the gel structure, which facilitate the movement of ions. (From top to down: molar conductances from +25 to -15°C with the step 5°C)

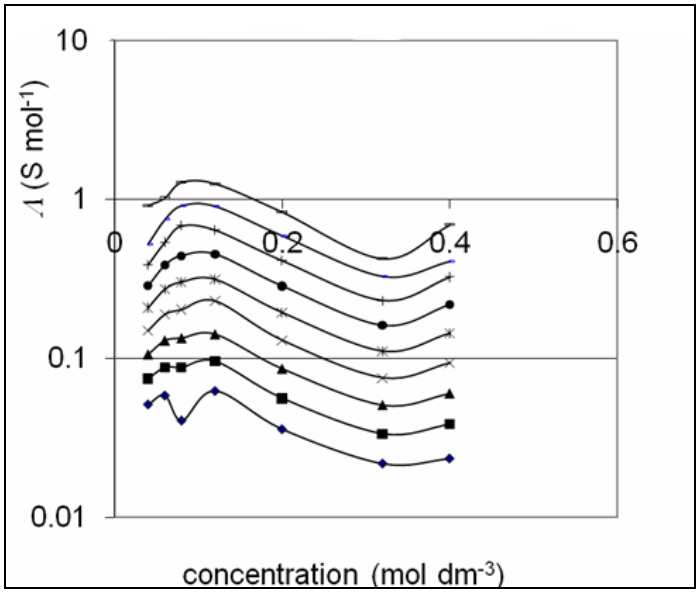

Fig.1: *The molar (equivalent) conductivity Λ (in S.mol-1) of gel containing LiClO4 in different concentrations. From up to down: temperatures from +25 to –15oC*

We have shown that the rheologic properties expressed as Young module Y show an inverse character (see Fig. 2).

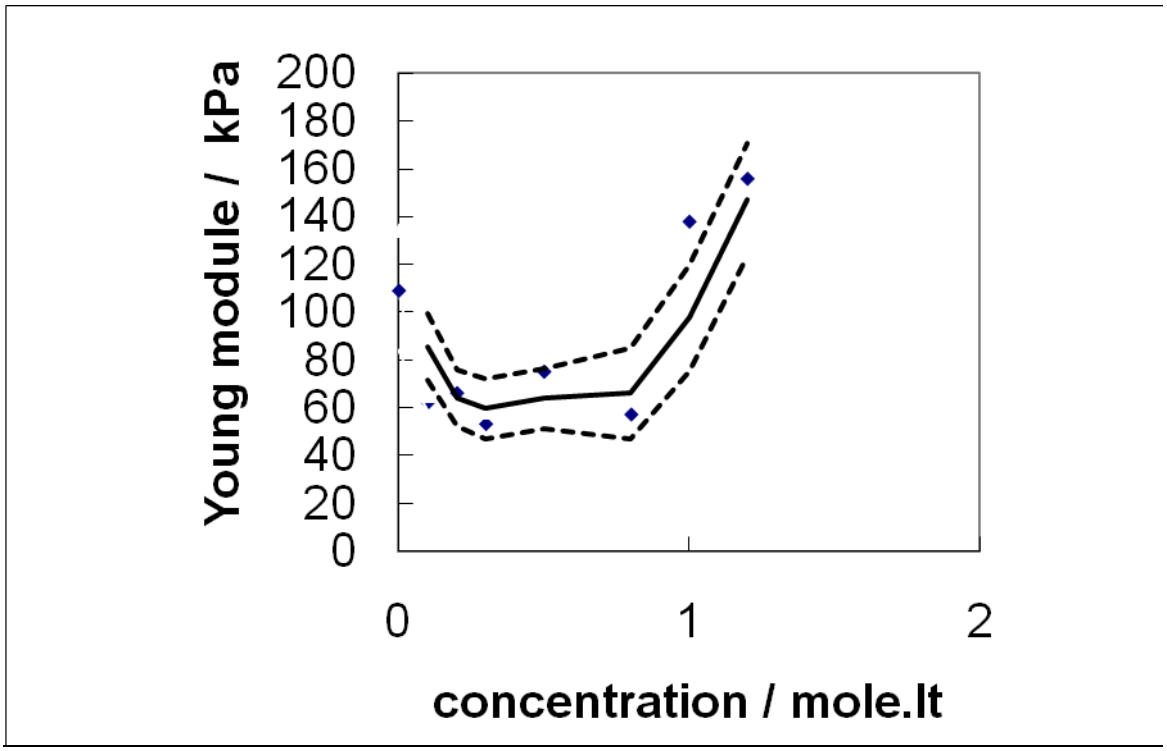

***Fig.2**: The influence of concentration on Young module of elasticity. Broken lines: statistic reliability of results.*

We suppose therefore that ions can move more easily in a medium the rigidity of which is lowered.

We have demonstrated that the thermal evolution of complex module and its real and imaginary components Y´and Y´´ is similar to the thermal evolution of ionic conductivity,

Therefore we suppose that the ions “swim” in a random network of polymeric chains in the voids filled by liquid electrolyte amd that their movement depends on the organization of the macromolecules. Our model is sketched diagrammatically in Fig.3.

The interactions between the ions and polar groups of the polymer are important too. This is most likely the reason why the conductivity of the composite *increased* when sodium salt was introduced into the composite instead of those of lithium.

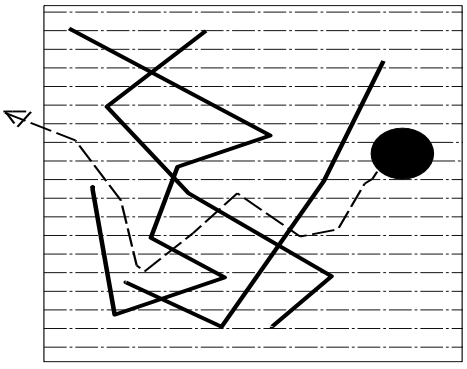

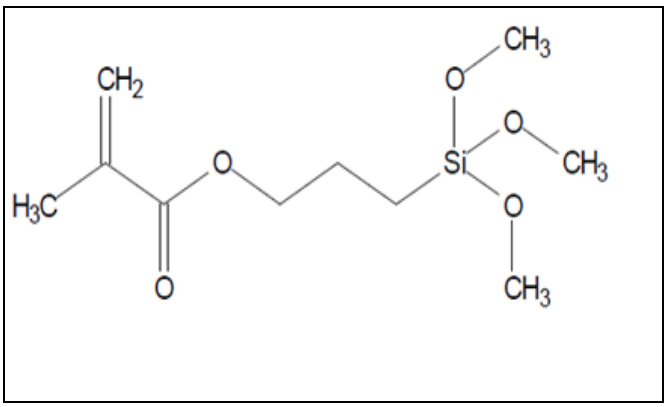

***Fig. 3:** (left) Ideal model of ionic movement between polymeric chains*
***Fig. 4:** (right)Formula of trimethoxysilyl propyl methacrylate, TMSPMA*

Our model is supported by other data. For example, we can observe the diffusion coefficients in the system of ferrocene – ferricinium by cyclic voltammetry.

Recently, we started to study other polymers with the aim to decrease the fire hazard of lithium batteries. Therefore we have introduced the methacrylate which contains silicium in side branches of its molecules (trimethoxysilyl propyl methacrylate, TMSPMA, formula see Fig. 4 [1]). It can replace the commonly used MMA for gel preparation. Actually, the non-volatile silico-organic fragments mean that the composite if hezted does not burn off totally even at 500°C and inflammable residuum is left (see results of thermogravimetry in Fig. 5, where sample 1 is MMA gel and sample 4 means gel prepared from TMSMA).

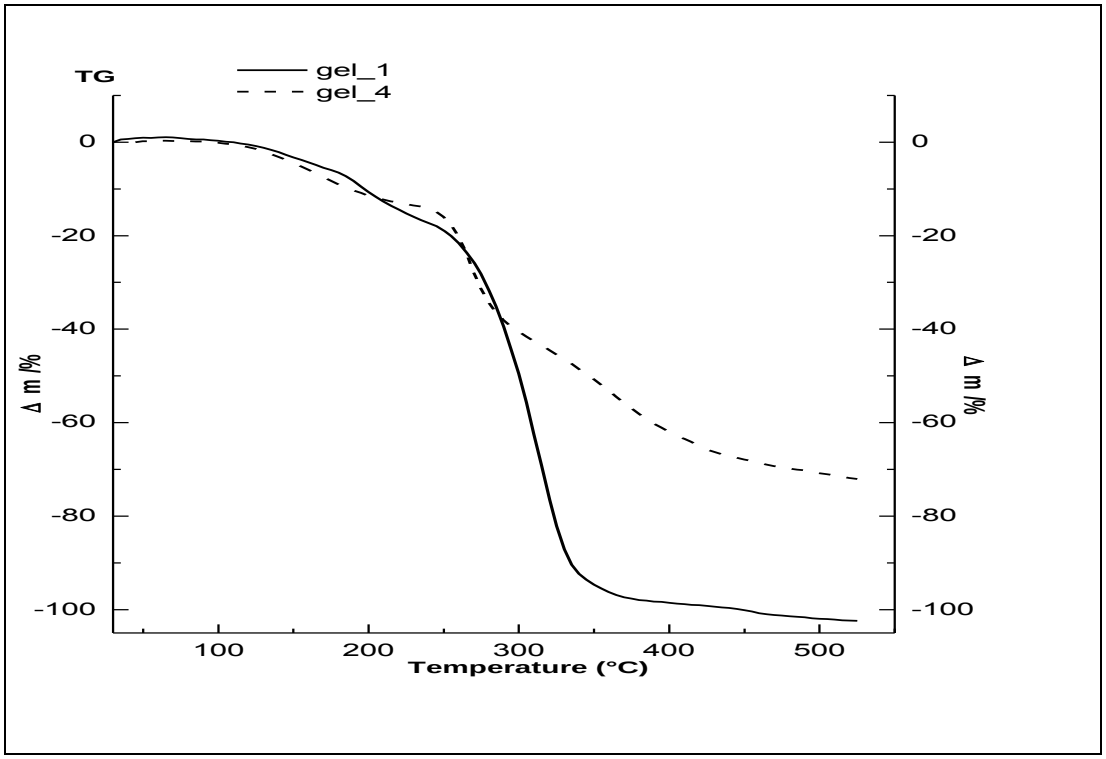

Fig,5: *Thermogravimetry of gel polymer electrolytes. Solid line – gel – 1 prepared from monomer MMA, broken line – gel prepared from TMSPMA monomer TMSPMA*

Samples: gel – 1: MMA based, gel-4 : gel based on TMSPMA Fig. 5. The conductance of TMSPMI containing gels is surprisingly higher almost by an order of magnitude.

Another interesting group of phenomena is the low – frequency component of electrode impedance. It has the nature of a spatial effect and may be connected with the ease of difficulty of macromolecules adjacent to the surface to move according to the ac voltage applied on the system.

Conclusions

The electric properties of composite gel electrolytes are undoubtedly influenced by the mechanical properties, which is strongly dependent on the arrangement of macromolecules in the composite. Molecular effects plays role in more detailed view, for example, in answering the difference between sodium and lithium salts in the composite gel.

Acknowledgements

This work at Brno Technical University was supported by Czech Science Foundation, Grant No. P102/10/2091 and FEKT-S-10-14., CVVOZE CZ.01.05/2.1.00/01.0014

Moreover, the work at the Institute of Inorganic chemistry was supported by the Academy of Sciences, Research Plan AV/ 0Z403 0502

Reference

[1] Vraštil J, Matějka L, Špaček V, Večeřa M, Prokůpek L (2009) 46: 112323-11240 AND REFERENCES THEREIN

11th ABAF

BRNO 2010

Advanced Batteries, Accumulators and Fuel Cells

New Materials

NANOSTRUCTURAL COMPOSITES FOR POWER CELLS BASED ON MOLYBDENUM-MODIFIED CARBON NANOTUBES

M. O. Danilov[1], N. D. Ivanova[1], E. I. Boldirev[1], O. A. Stadnik[1], A. V. Filatov[2]

[1] Institute of General and Inorganic Chemistry of the Ukrainian National Academy of Sciences, Kyiv, Ukraine
[2] Institute of Metal Physics of the Ukrainian National Academy of Sciences, Kyiv, Ukraine

Corresponding author: Danilov M.O. (danilovmickle@rambler.ru)

Abstract

It is shown that the molybdenum compounds are good catalysts for oxygen electrodes of the power cells based on carbon nanotubes working in the alkaline electrolyte. With the help of electrochemical method were obtained the molybdenum compounds applied on the nanotubes. It was established that it was a compound with molybdenum oxidation degree ~ +4. The catalytic characteristics of molybdenum oxide compound deposited on carbon nanotube are equal to those of platinum catalysts.

Keywords

carbon nanotubes, catalyst, fuel cells, oxygen electrodes, molybdenum oxide.

Introduction

Chemical power cells in which the electrocatalytic processes are taking place refer to alternative or small-scale power generation. At the present time according to the total energy capacity the energy which is produced by all current sources existing in the world is equal to the energy generated by nuclear power stations, thermal electric power stations and hydroelectric power stations taken together. As a result, the investigations connected with generation of current flow are of interest at the present time. The application of air or oxygen electrode in facilities generating the electric power is quite prospective because it does not cause any ecological problems and allows saving natural resources such as oil and gas. Air and oxygen electrode is an electrode-electrolyte-gas three-phase system in which the processes of current flow generation are concentrated at the phase boundary. The current magnitude generated at such gas diffusion electrode depends on the percentage of the triplex contact of these three phases. In its turn, the electrode itself is composed of catalyst and carrier. The interaction between them defines the quantity of generated current which depends on the catalyst being used. At present, the most effective catalyst for oxygen reduction is platinum, but it is very expensive. There is the great amount of works oriented to the investigation of other effective but less costly catalysts. Another main problem is catalytically active and stable carrier. In works [1-4] the benefits of carbon nanotubes used as the carrier are shown. The application of platinum on the carbon nanotubes (NT) enabled to improve the characteristics of oxygen electrodes as compared with the same electrodes with platinum applied on activated carbon [3].

Carbon nanotubes are characterized by high conductivity and specific suppression. They also can form the mesoporous three-dimension structures, what makes them prospective as the carriers. An additional point is that tubular carbonic structure enables the extension of triple contact zone electrode-electrolyte-oxygen where takes place the process of current flow generation. This leads to the growing of operating current density as compared to activated carbon. This amount is also influenced by low bulk density of carbon nanotubes as compared to activated carbon. It follows from the data [5] that molybdenum deposited from the gas phase has the electrocatalytic characteristics in reactions of oxygen reduction. Molybdenum oxides have high melting point and high corrosion stability in alkaline and acidic media, in which the oxygen electrodes of power cells are working. Therefore, the investigation of catalytic activity of molybdenum compounds supported on carbon nanotubes with the help of galvanic method was of special interest. The galvanic method of molybdenum electrodeposited on carbon nanotubes allows regulating the cluster size and the mass of coated compound with the help of current density variation.

It was the purpose of our work to investigate the electrocatalytic characteristics of carbon nanotubes with the molybdenum oxides supported on them by the electrodeposition as the electrode material of oxygen electrode for power cell.

Experimental

The multiwalled carbon nanotubes (MWCNT) were taken in our investigation as the carriers and electrode material [6]. The product was the black powder with the tapped density of 25-35 g/dm^3. The outer diameter of nanotubes was about 10-30 nm, the specific surface area was 230 m^2/g.

Two-layer oxygen electrodes were prepared by press molding. Hydrophobic layer contained 0,07 g/cm^2 acetylene black with 25 % of polytetrafluorethylene. The effective layer contained 0,02 g/cm^2 MWCNT, modified by different molybdenum compounds with 5% of polytetrafluorethylene. The research was conducted on the power cell mock-up with zinc as an anode. The mock-up for the gas diffusion electrodes testing is described in the work [7]. The solution of 5M KON and 1M LiOH was taken as an electrolyte. All potentials were measured compared to the standard silver chloride electrode connected via salt bridge The characteristics were measured in the galvanostatic mode. The source of oxygen was the U-shaped electrolyzer with the alkaline electrolyte. The oxygen was fed to the gas electrodes under surplus pressure of 0.01 MPa. Before the research the oxygen electrode was being oxygen cleaned during one hour. The methods of applying the molybdenum oxide are described in the work [8]. The electron microphotographs are obtained with the help of electronic microscope JEM-100 CXII. The X-ray phase analysis was carried out with the help of X-ray diffractometer “DRON – 4” (Russia).

Results and Discussion

With the help of electrochemical deposition method [8] we have obtained the nanostructural compositions on the base of carbon nanotubes with applied on them oxide molybdenum compounds in different proportions. Different compositions of electrolytes with the same containing of molybdenum (10 g/dm^3) but with the different containing of hydrofluoric acid in electrolyte: 1; 2; and 4 g/dm^3, were investigated and developed. With

the same current density of 0,25 A/dm^2 and time of electrolysis of 0,5 hour and the temperature of 22°C, the nanocomposites on the base of oxide molybdenum compound and multiwalled carbon nanotubes with different containing of molybdenum and its oxide compounds: 5, 4 and 3,5 mass %, were obtained. Fig.1-2 shows the electron microphotographs of obtained composites. As it seen from the photographs, the size of obtained particles is growing simultaneously with the growing of hydrofluoric acid concentration. We presuppose that it is connected with the fact that while the acid concentration is growing, the centers of molybdenum oxide concentration on the surface of nanotubes are decreasing, and that leads to the increase in average size of applied particles. For the identification of applied particles the X-ray phase analysis of obtained composites was carried out. Fig. 3 displays the X-ray pattern of composites obtained from the solutions containing the hydrofluoric acid 1 and 4 g/dm^3. They are curves 1 and 2 respectively. As it seen from the results of X-ray phase analysis, the obtained specters are similar, which gives evidence of the obtaining of identical molybdenum compounds after the similar modes of electrolyze but with the different concentrations of hydrofluoric acid. The obtained apexes as a result of roentgen-amorphism of carbon nanotubes were succeeded to identify as the molybdenum compound MoO_2 at 2θ=26.04 degrees. However, the lines from synthesired oxide are marginally displaced from theoretical diffractogram. This points to the fact that the lattice constant doesn´t correspond to oxide balanced state, for example, due to nonstoichiometric structure.

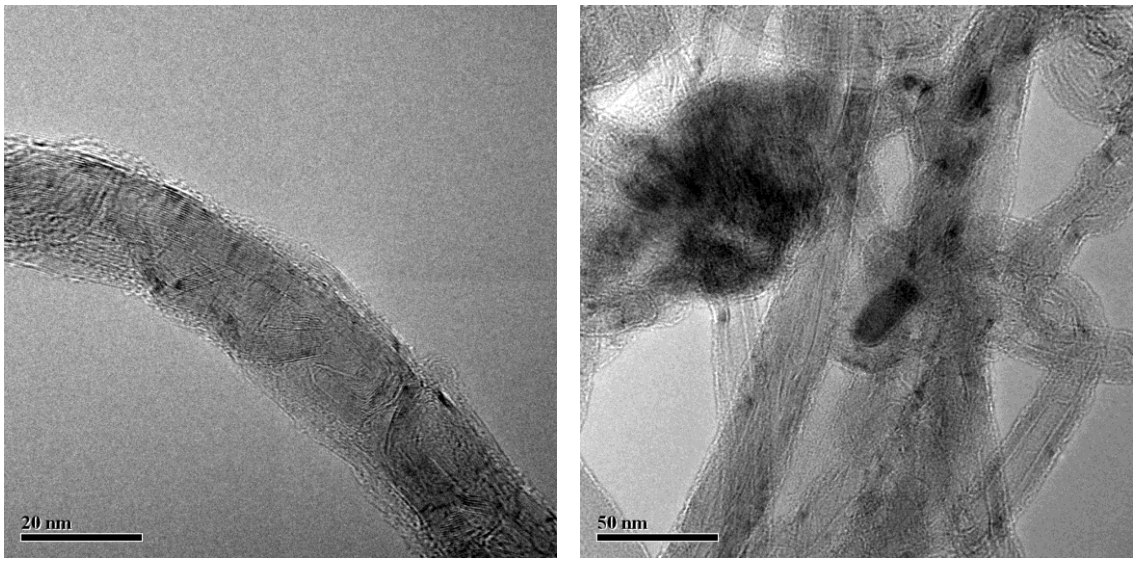

Fig. 1: *Electron microphotography of molybdenum oxide nanostructural composites on the nanotubes. Elemental molybdenum containing is 5 mass %.*

Fig. 2: *Electron microphotography of molybdenum oxide nanostructural composites on the nanotubes. Elemental molybdenum containing is 3.5 mass %.*

The oxygen electrodes were produces from the obtained composites. Fig. 4 displays the correspondences of potential from the current density for the oxygen electrode on the base of nanostructural composites from the nanotubes with the molybdenum oxide applied on them. It follows from the figure that the best characteristics has the electrode which contains 5 mass % of molybdenum. Next to them, according to activity descending, are arranged the electrodes on base of nanotubes composites with the molybdenum oxide containing molybdenum in amount of 4 and 3 mass %. As a comparison, in figure is described a curve for electrodes on base of initial nanotubes. Such dependence of

electrical characteristics of oxygen electrodes is determined by dispersion increase of supported molybdenum oxide compounds. It is also confirmed by photographs from electron microscope: Fig.1 and Fig.2 for 5 mass. % of molybdenum and for 3.5 mass. % of molybdenum respectively. It follows from the photographs that the average size of molybdenum oxide particle increases with the concentration growth of hydrofluoric acid in electrolyte. Calculated electrochemical characteristics of oxygen electrode of the power cell on base of molybdenum oxide compound applied on multiwalled carbon nanotubes are 300 mW/cm^2 with the polarization of 250 mV at room temperature. This data is comparable to samples containing platinum.

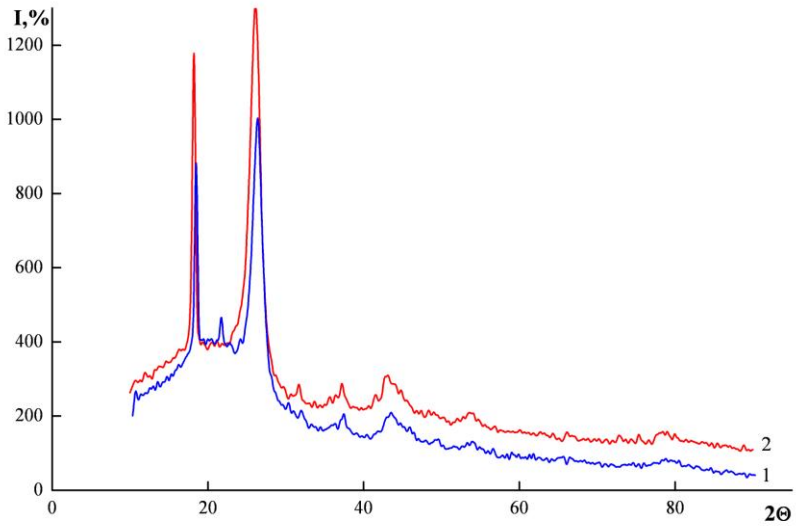

Fig. 3: *X-ray phase analysis of composites sample based on molybdenum oxide and carbon nanotubes containing elemental molybdenum with mass % of 1 – 5.0; 2 – 3.5.*

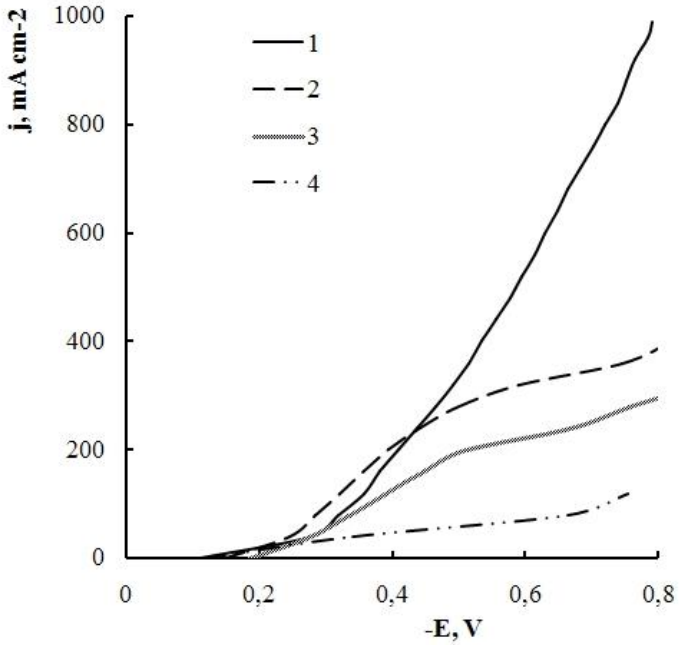

Fig. 4: *The dependence of potential from the current density for the oxygen electrode on base of nanostructural composites of nanotubes with the applied molybdenum oxide in the amount of 0,02 g/cm^2 with the containing of elemental molybdenum with the mass % of 1 – 5.0; 2 – 4.0; 3 – 3.5; 4 – pure CNT.*

Conclusions

The electrochemical method of production of the nanostructural composites based of carbon nanotubes and molybdenum oxide compounds is suggested.

It is shown that the obtained electrode materials are the prospective catalysts for oxygen electrodes of the power cells and that they can substitute the catalysts containing platinum.

References

[1] 1. Xie X., Gao L.Carbon 45 (2007) 2365.
[2] 2. Yang S., Zhang X., Mi H., Ye X. J.Power Sources 175/1 (2008) 26.
[3] 3. Wang X., Waje M., Yan Y. Electrochem. Solid-State Lett. 8/1(2005). A42.
[4] 4. Danilov M.O.. Melezhyk A.V J. Power Sources 163/1 (2006) 376.
[5] 5. Falkenberg F., Ahlberg E. 55 ISE Thessaloniki, Greece, (2004) 736.
[6] 6. Melezhik A.V., Sementsov Yu.I., Yanchenko V.V. J. Applied Chem.(Russian),78**/**6 (2005) 917.
[7] 7. Danilov M.O., Melezhik A.V., Danilenko N. I. J. Applied Chem. (Russian), 78**/**11 (2005) 1849.
[8] 8. Ivanova N.D., Ivanov S.V., Russian Chemi. Reviews, 62/10 (1993) 907.

NANOSTRUCTURED BINARY TIN ALLOY FABRICATION

G. Ferrara, F. Vergottini, R. Inguanta, S. Piazza, C. Sunseri

Dipartimento di Ingegneria Chimica dei Processi e dei Materiali
Università di Palermo, Viale delle Scienze, 90128 Italy

Corresponding author: Germano Ferrara (g.ferrara@dicpm.unipa.it)
Phone Number +39 091 23863732, Fax Number +39 091 7025020

Introduction

Owing to the growing importance of lithium ion batteries in the field of power supply for portable devices, new materials are being extensively investigated in order to improve battery performances in response to the enhancing power demand of the new devices. Challenging efforts are currently devoted to synthesis and characterization of innovative active materials to be used as anodes. Materials like tin, silicon, aluminium and others have been studied with increased attention because of their high theoretical specific capacity, compared to that of currently employed carbonaceous materials. Unfortunately, they suffer dimensional decay due to swelling and relaxing process coupled to intercalation/deintercalation of lithium ions during battery cycling. Above cited materials react with lithium forming binary alloys, e.g. $Li_{4.4}Sn$ when tin is fully lithiated. Owing to density differences among unlithiated and lithiated phases, mechanical stresses are localised in the region between the two phases, determining the breakdown, up to pulverization, of metals and alloys employed as anodes. Mechanical damage of the host metal causes loss of electric contact between current collector and electroactive material, with consequent failure of the battery. To prevent this event, it has been proposed to use nanostructured materials. In fact, it has been shown that a nanosized anode can accommodate lithium ions better than bulk materials [1], because host materials can be entirely lithiated with disappearance of highly stressed interface [2]. In the case of tin, use of tin-based alloy instead of pure metal, could help in preventing material crumbling: a commercially available battery, Sony Nexelion™ [3], confirms that this approach is useful to have a stable metallic anode with high specific capacity. Starting from these findings, our group has devoted attention to the fabrication of binary tin alloys and a facile and cheap method has been developed. Here, we will show that it is possible to fabricate nanostructured tin alloys by electrochemical deposition inside the cylindrical channels of a porous template. In particular, we will show the results concerning the synthesis and characterization of Sn-Co and Sn-Cu alloys. These materials have been chosen because the former, introduced by Sony, is, according to Dahn and co-workers [4], the tin alloy with the best performance, while the latter is cheaper and more health-friendly than the cobalt alloy. Independently of the possible application, the attention has been devoted to study in detail the electrodeposition process of alloys in a confined ambient, like template channel, that was already investigated in previous works [5, 6]. Here, a polycarbonate membrane was used, in place of anodic alumina membrane, which shows cylindrical and parallel channels with high surface population (about 10^{13} m^{-2}), whereas the former template shows interconnected pores with surface population less than one order of magnitude. A different morphology of pores implies a different nanostructured reaction ambient, so that the investigation of the electrodeposition procedures was considered of some relevance in

order to verify the extendibility of the experimental conditions previously founded to polycarbonate membrane.

Experimental

A track etched polycarbonate membrane commercially available (Whatman, Cyclopore™), characterized by interconnected pores of about 200 nm in diameter, was used as template. In order to fabricate tin alloy NWs directly and firmly onto the current collector, a special holder was designed allowing electrodeposition, in two successive steps, of both copper current collector layer (on one side of the template) and tin alloy NWs inside the channels of the template. Electrodepositions were performed using an EG&G Potentiostat/Galvanostat (mod. 273A). Copper film electrodeposition was performed for 1 h at constant current density and room temperature. Electrolytic solutions employed for NW growth are reported in table 1 along with the operative conditions. Electrodepositions were conducted at constant potential, referred to Saturated Calomel Electrode (SCE), in a three electrode cell with platinum wire as counter electrode.

Tab. 1: *Composition of electrolytic baths and operative conditions for deposition of tin alloys*

	Sn-Co	**Sn-Cu**
$SnSO_4$	$20 \cdot 10^{-3}$ M	$20 \cdot 10^{-3}$ M
$CoSO_4$	$5 \cdot 10^{-3}$ M	—
$CuSO_4$	—	$10 \cdot 10^{-3}$ M
Na_2SO_4	0.2 M	0.2 M
Sodium gluconate	0.2 M	—
H_3BO_3	—	0.2 M
Thiourea	—	0.2 M
pH	4.6	1.0
T [°C]	60	25
t [min]	60	30
E [V vs. SCE]	-1.0	-0.55

Deposits were characterized by X-ray diffraction (XRD) analysis (APD2000™ Italstructures diffractometer working with Cu Kα radiation (λ = 1.54 Å)). Morphological analysis of deposits was carried out by a Field Emission Gun - Environmental Scanning Electron Microscope (FEG-ESEM, FEI Quanta™ 200 F).

Results and Discussion

Electrodeposition of nanostructured binary tin-based alloys was potentiostatically conducted to better control the current deposition of each ion constituting the alloys. Usually, higher applied potential favours reduction of ions with large charge transfer overpotential, consequently it is easier to control the composition of the alloy by adjusting the electrode polarization, like in potentiostatic deposition. Fig. 1a shows a typical XRD pattern of the electrodeposited SnCo NWs: in addition to copper peaks, the presence of two weak peaks located at 30.64 and 32.92 degrees can be observed. The identification of these two weak peaks is rather difficult because at least three peaks are required. The peak at 2θ = 30.64 can be attributed to tin because it is coincident with the diffraction of the plane (200) of tin (JPS card # 04-0673), whilst the identification of the second peak is

more uncertain, but it might be attributed to an unknown tin-cobalt phase, according to [7]. Besides, Gómez et al. [8] have electrodeposited a crystalline tin cobalt alloy and have proposed a new SnCo tetragonal phase with a main peak at 2θ = 32.77, very close to the second unknown peak of fig. 1a. However, taking into account that, except for copper peaks, the other ones were broad and weak, it can be concluded that low crystalline SnCo NWs were electrodeposited. In the case of SnCu alloy, fig. 1b shows the presence of two phases Sn and Cu_6Sn_5 (JPS # 45-1488) which confirm that in the found experimental conditions, a co-deposition of copper and tin can be achieved despite the difference in their standard reduction potentials. In this case, the alloy was crystalline.

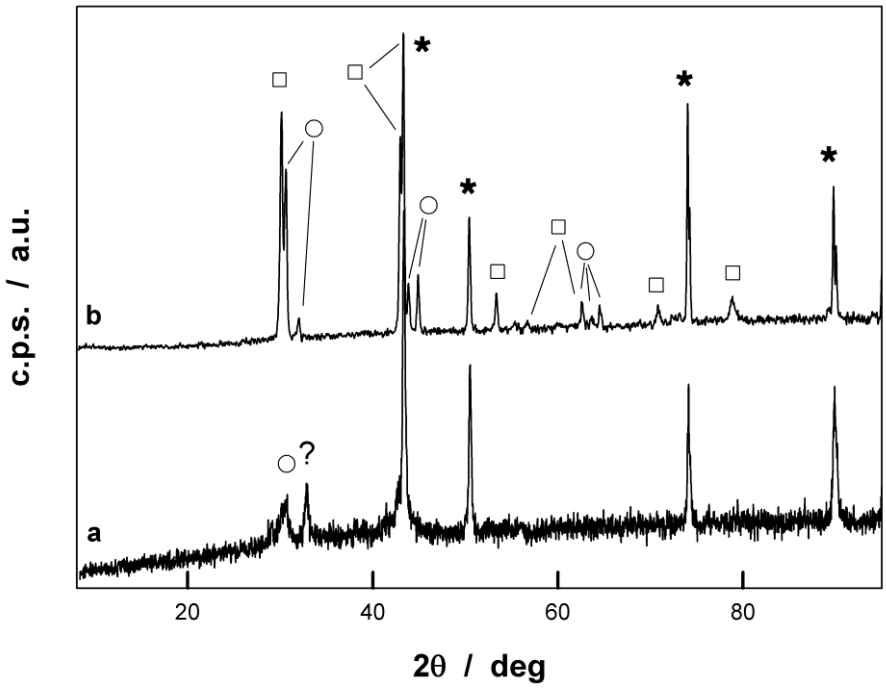

Fig. 1: *XRD of SnCo NWs (a) and SnCu NWs (b) after template removal in $CHCl_3$ (✱ Cu # 04-0836; ○ Sn # 04-0673; □ Cu_6Sn_5 # 45-1488; ? unknown phase).*

Morphologies of the two deposits are quite similar because same kind of template was used. Fig.2 shows that NWs are interconnected, but there is sufficient free space around every NW that may guarantee good performances as anode of Li-ion battery. In this application, electrode is subjected to large volume changes due to intercalation/deintercalation of Li, that, in the case of pure tin, can reach a value of 300%. Consequently, free space is fundamental to accommodate large change volumes avoiding damage of the NWs. Another advantage related to the distance among NWs, is the complete wetting of the surface by the electrolytic solution leading to a high utilization degree of the electrode. Low free space between NWs, like in the case of NWs grown inside anodic alumina membrane, can more or less hindering the penetration of the solution leading to a low utilization degree of active material in addition to possible damage due to volume expansion.

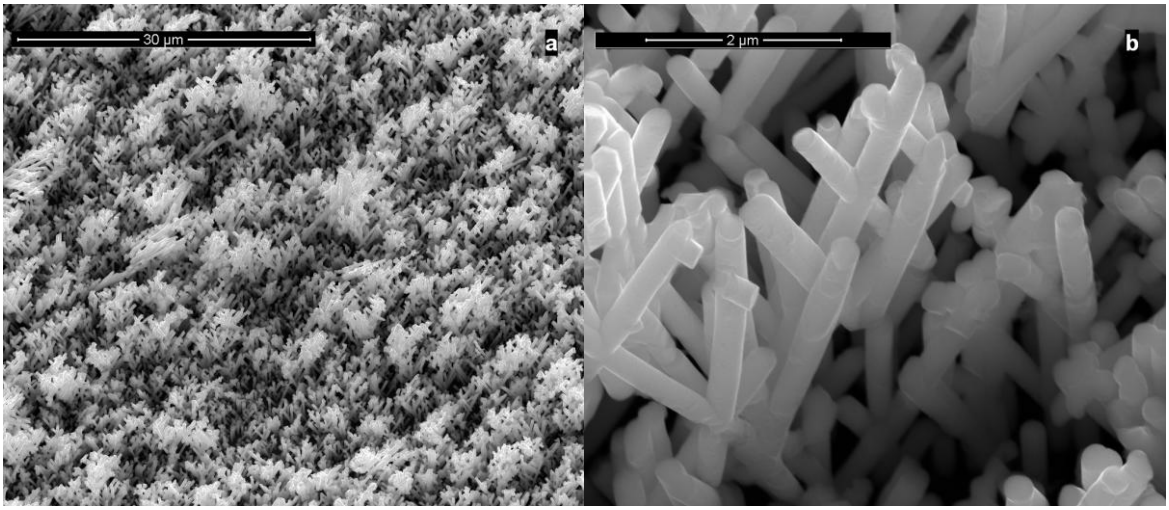

Fig. 2: *Typical morphology of SnCu alloy grown inside the channels of track etched polycarbonate membranes. In (b), a high magnification view shows how nanowires are interconnected. Similar morphology was shown by the SnCo alloy.*

Conclusions

In the present work, we proposed a simple, cheap and easily scalable procedure, in place of expensive physical methods, for synthesizing nanostructured tin alloys which may be used for fabrication of high capacity anodes for lithium-ion batteries. Crystalline structure and morphology of NWs, deposited inside the channels of polycarbonate membrane, can be controlled by adjusting bath composition and electrode polarization. Interconnected nanostructures of binary tin-based alloys were electrodeposited with different crystalline structure. SnCo alloy showed low crystallinity degree, while SnCu was synthesized with a crystalline structure.

In view of possible application of these alloys as anodes of Li-ion battery, the free space among NWs should allow to accommodate the large volume changes due to Li intercalation/deintercalation and to enhance the utilization of the active material.

Acknowledgements

This work was financially supported by Università di Palermo.

References

[1] C. K. Chan, H. Peng, G. Liu, K. McIlwrath, X. F. Zhang, R. A. Huggins, Y. Cui: Curr. Nanosci. 3 (2008) 31.
[2] R. Deshpande, Y-T. Cheng, M. W. Verbrugge: J. Power Sources 195 (2010) 5081.
[3] Information on http://www.sony.net/SonyInfo/News/Press/200502/05-006E/
[4] A. D. W. Todd, R. E. Mar, J. R. Dahn: J. Electrochem. Soc. 153 (2006) A1998.
[5] G. Ferrara, R. Inguanta, S. Piazza, C. Sunseri: Electrochem. Solid-State Lett. 12 (2009) K17.
[6] G. Ferrara, R. Inguanta, S. Piazza, C. Sunseri: J. Nanosci. Nanotechnol. In press
[7] J. R. Dahn, R. E. Mar, A. Abouzeid: J. Electrochem. Soc. 153 (2006) A361
[8] E. Gómez, E. Guaus, J. Torrent, X. Alcobe, E. Vallés: J. Appl. Electrochem. 31 (2001) 349.

LOW-TEMPERATURE ANOMALY IN IONIC CONDUCTIVITY OF SCANDIA-STABILIZED ZIRCONIA

V.I. Barbashov, G.G. Levchenko, E.V. Nesova, N.E. Pismenova

Donetsk Phys. Tech. Institute, National Academy of Science of Ukraine, R. Luxemburg St. 72, 83114 Donetsk, Ukraine

Corresponding author: Barbashov V.I. (v.barbashov@mail.ru)

Introduction

Numerous observations show preference for using scandia oxide as stabilizer for zirconia's cubic phase to synthesize ceramic with extremely high ionic conductivity. However, one of the most important shortcomings of the ZrO_2-Sc_2O_3 system is the degradation of its high conductive properties at region of characteristic temperatures for fuel cell operation (750 – 1000^{0}C) because of the decrease for the concentration of scandia ions due to the migration to the surface and to the grain boundaries [1]. Thus, for decrease the diffusion coefficient of scandia ions, ZrO_2-Sc_2O_3 system is doped by ions with larger radius than zirconium radius [2-7]. Phase diagram for the ZrO_2-Sc_2O_3 system shows stability of a rhombohedral phase at room temperature in the concentration range 9,3-14,0 mol% Sc_2O_3 [8]. The transformation of the low conducting rhombohedral phase to high conductivity cubic phase accompanies heating in the 500-600^{0}C temperature range (in dependence from the Sc_2O_3 concentration). Clear hysteresis properties of discovered phase transformation are due to polymorphic transformations. The only difference is the exact definition of the phase transformation in order with Arrhenius dependences ($\lg(\sigma T) - 1/T$)[9,10].

As a rule, in ionic conductivity observations for ScSZ, the authors of indicated papers work in temperature range from 650 K. In present research, we put the accent on zirconia's ionic conductivity behavior in low-temperature range.

Experimental

Experimental procedures were performed on ceramic composition (for 89 mol.% ZrO_2 + 10 mol. % Sc_2O_3 + 1 mol. % CeO_2 (1)) sintered at 1550^{0}C for 2 h from powder prepared by method of reverse coprecipitation which increases the chemical homogeneity of system in comparison with ceramic method for preparing of the necessary compositions. For comparison, DKKK (Japan) (2) and Praxair (USA) (3) powders with 89 mol% ZrO_2 + 10 mol % Sc_2O_3 + 1 mol% CeO_2 was sintered. The density and the average grain size of sintered ceramic compositions (1-3) were 2; 16; 8 mkm и 4,88; 5,59; 5,52 g/cm^3, respectively.

Microstructure observation was performed by a field-emission scanning-electron-microscope. Fig. 1 shows typical structures for the fracture surface of (1), (2) and (3) specimens.

The observed conductivity behavior also supported the XRD observations using Cu – Kα radiation.

Heating and cooling of compositions used 2 K/min rate.

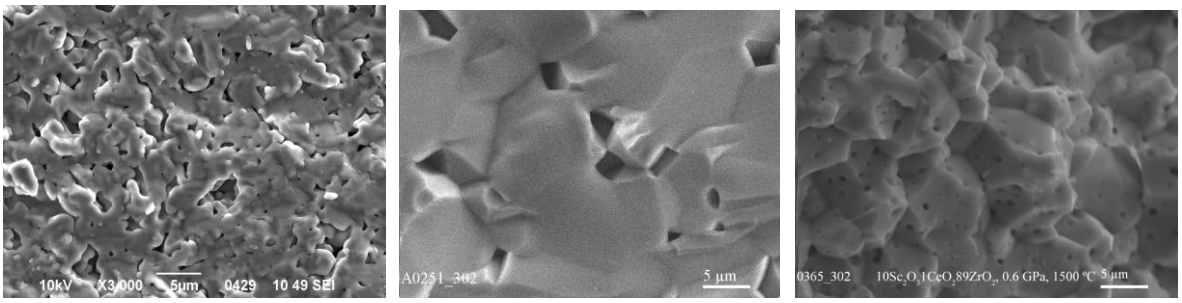

(a) (b) (c)

Fig.1: *Structure for the fracture surface of specimens: (a) 89 mol.% ZrO2 + 10 mol. % Sc2O3 + 1 mol. % CeO2; (b) from DKKK powder; (c) from Praxair powder.*

Results and Discussion

Fig.1, 2 shows Arrhenius dependences of conductivity with the reverse temperature in the regimes of slow heating and slow cooling with indicated rate for all studied specimens.

For specimen (1), dependence lg(σT) - 1/T shows the jumping behavior in conductivity for both the high-temperature region (750-900 K) and the low-temperature region (500 – 645 K) (fig.1). For the high-temperature region, the jumping behavior in conductivity has hysteresis character, and it is connected with zirconia's polymorphic transformation from the rhombohedral phase to the cubic phase as shown earlier. As far as the authors know, the low-temperature jumping in ionic conductivity wasn't observed for this ceramic composition. Characteristic features of this temperature anomaly in ionic conductivity are absence of the hysteresis loop and significantly bigger value of the activation energy in the 625-740 K temperature range for cooling curves.

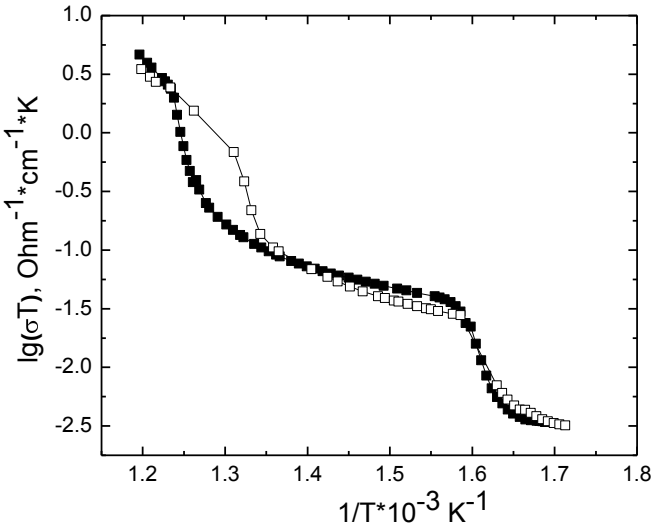

Fig. 2: *Arrhenius dependences for conductivity of (1) specimen where light signs are cooling, and dark signs are heating.*

All sintered specimens from powders with announced concentration don't show the jumping behavior in conductivity for lg(σT) - 1/T dependences (fig. 2).

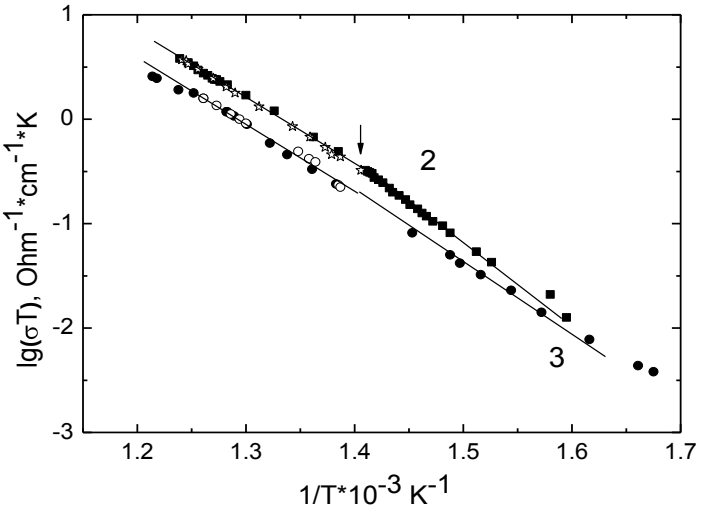

Fig. 3: *Arrhenius dependences for conductivity of specimens sintered from DKKK (2), Praxair (3) powders where light signs are cooling, and dark signs are heating.*

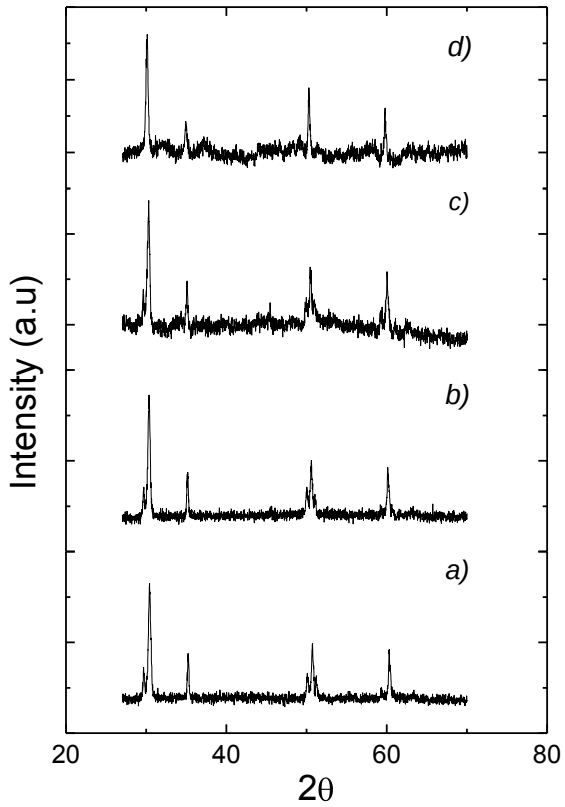

Fig. 4: *XRD patterns of (1) specimen were compared between 20° and 70° (2θ) for T: (a) 20℃, (b) 290℃, (c) 410℃, (d) 630℃.*

The absence for these anomalies is due to the deflection of real values for the Sc_2O_3 и CeO_2 concentration from the enter values or/and to significantly larger grain size and, thus, a less value of Laplace pressure as discovered earlier [2, 3]. The real concentration of Sc_2O_3 for ceramic was equaled to 9.3 ± 0.7 mol. %. X-ray spectral analysis displayed that ceramics was in the tetragonal phase. It is possible that polymorphic transformation from the tetragonal phase to the cubic phase will not show the jumping in ionic conductivity. In terms of our baric model for zirconia's conductivity [11], absence of the rhombohedral

phase for these specimens may be corresponded to the low value for the ceramic grains' total pressure (Laplace pressure and pressure due to stabilizer's effect) which is necessary for this transformation.

Due to connectedness of discovered low-temperature anomaly with polymorphic phase transformation, in this research phase composition for specimen (1) was observed for different temperatures (T = 20°C; 290°C; 410°C; 630°C) by X-ray method.

In the 300 – 750 K temperature range, phase composition of specimen (1) doesn't practically show changes due to the single-valued fact in the presence of the rhombohedral phase as follows from XRD patterns (fig. 3). The present result doesn't give the reason to connect the low-temperature jumping in ionic conductivity with polymorphic transformation. As is generally known, the rhombohedral phase has much lower symmetry in comparison with the cubic phase. Its formation is the inheritance for the anisotropic properties of dopant clusters. Last point gives the reason to suppose the presence of anisotropy in ionic conductivity for the rhombohedral phase of each grain. In terms of this supposition, discovered low-temperature anomaly in ionic conductivity has the orientation character due to the synchronous ordering of grains for T ≥ 500 K. Possibility of the analogous effect was shown by J.A. Kilner at [12]

Conclusions

Low-temperature anomaly in ionic conductivity of scandia-stabilized zirconia was detected experimentally. Disconnectedness of indicated anomaly with polymorphic transformation and its relatedness with the ordering of grains with presence of the rhombohedral phase were shown.

References

[1] S. P. S. Badwal, F. T. Ciacchi, D. Milosevic, Solid State Ionics **91** (2000) 136.
[2] R. Chiba, F. Yoshimura, J. Yamaki, T. Ishii, T. Yonezawa, K. Endou, Solid State Ionics **104** (1997) 259.
[3] O. Yamamoto, Y. Arati, Y. Takeda, N. Imanishi, Y. Mizutani, M. Kawai, Y. Nakamura, Solid State Ionics **79** (1995) 137.
[4] M. Yashima, M. Kakihana, M. Yoshimura, Solid State Ionics **86-88** (1996) 1131.
[5] M. Hirano, T. Oda, K. Ukai, Y. Mizutani, J. Amer. Ceram. Soc. **85** (2002) 1336.
[6] I. Kosacki, NATO Science Series, II: Mathematics, Physics and Chemistry **202** (Fuel Cell Technologies) (2005) 395.
[7] A.J. Feighery, J.T.S. Irvine, Solid State Ionics **121** (1999) 209-216.
[8] R. Ruh, H.I. Garrett, R.F. Domagala, V.A. Patel, J. Amer. Ceram. Soc. **60** (1977) 399.
[9] Jong Hoon Joo, Gyeong Man Choi, Solid State Ionics **180** (2009) 252.
[10] V. I. Barbashov, V. M. Timchenko, E. V. Nesova, ECS Transactions **25** (2009) 1659.
[11] V. I. Barbashov, Yu. A. Komysa, E. V. Nesova, High Pressed Physics & Technologies **18** (2008) 148.
[12] J.A. Kilner and B.C.H. Steele. In: O.T. Sorensen, Editor, Non-stoichiometric Oxides, Academic Press, New York (1981), page 233.

COUNTER ELECTRODES FOR ELECTROCHROMIC DEVICES

J. Vondrák[1], M. Sedlaříková[1], M. Macalík[1],M. Zatloukal[1], J. Mohelníková[2]

[1] Faculty of Electrical Engineering, Brno University of Technology, Údolní 53, 602 00 Brno, Czech Republic
[2] Faculty of Civil Engineering, Brno University of Technology, Veveří 95, 602 00 Brno, Czech Republic

Corresponding author: Jiří Vondrák (vondrakj@iic.cas.cz)
Phone: 54114 6117

Introduction

Laboratory testing of thin films of V_2O_5 for electrodes of electrochromic devices could find applications for electrochromic glazings or mirrors with controlled solar transmittance which are used in automotive industry and in architecture as well as in many applications of solar thermal and lighting appliances.

Experimental

The counter electrode was carried out from the vanadium pentoxide V_2O_5 deposited on FTO substrates by the dip-coating coating method. The deposition laboratory apparatus was constructed for the experiment, Fig. 1. There are three time intervals for the dip-coating and 20 cm of the lifting height.

Fig. 1: *Dip-coating laboratory apparatus.*

The powder of 0,5 g of V_2O_5 (Sigma-Aldrich, 99,9%) was diluted inside of 30 ml H_2O_2 (Penta, p.a.) of 15% concentration. The vanadium pentoxide V_2O_5 is strongly reactive with hydrogen peroxide and gives light orange solution of peroxo-vanadium acid which is non-stabile not even after several days. The solution has very high surface tension and it is hardly wettable on the surface. The proper compound of $V_2O_5 \cdot nH_2O$ is obtained by tempering of the solution in the water bath at the temperature 80 °C for continual mixing by

the magnetic stirrer. The compound viscosity is increased rapidly because of gelation effect. The compound colour is change to dark brown. This phase is critical for the final properties of the thing films. There might appeared some sediments or surface membrane.

The sample preparation for the laboratory testing was completed four times in the following way:

- the first sample was diluted by 20 ml of distilled water,
- the second one by 40 ml of distilled water,
- the third one by 60 ml of distilled water,
- the fourth sample was not diluted.

The samples were burnt at temperatures 60 °C and 120 °C and 200 °C. One set of samples were without burning. The samples were taken out of the solution in speed 5 cm/s, the area of the deposition was 6 cm^2.

Optical and electric properties of V_2O_5 layers were monitored in 0,5M solution of u $LiClO_4$ diluted in polycarbonate which was used to obtain Li^+ ions. Potentials of the working electrode of the potentiostat μAutolab were in the range from –0,5 V to 1,25 related to Cd/Cd^{2+} referent electrode. As the counter-electrode the platinum plate was used. Spectroscopic and electrochemical measurements were taken in the measurement cell with the defined positions of the individual electrodes.

Results and Discussion

The spectral measurements were provided for the spectral range 325–900 nm by the apparatus UNICAM Helios δ. Results of the ,measurements proven that the layer prepared from the non-diluted solution is very low transparent and maximal value of transmittance T_S is only 38 % between 550 and 620 nm. In contrary the diluted solution gave higher optical transmittance. It was probably cause by the influence of the smaller thickness of the layer. The Roentgen analysis by the apparatus SIEMENS D5000 confirmed the existence of the hydrated form of V_2O_5 rhombic structure. Except $V_2O_5 \cdot 1{,}6H_2O$ any other vanadium compounds were not obtained. The bound water is important for the correct function of the electrochromic layers.

Layers of V_2O_5 for the electrochromic applications have not modulation of optical properties because of the layer polarization.

Conclusions

The counter electrodes of V_2O_5 for electrochromic devices were prepared by the dip-coating method from peroxo-vanadim solution. The layers were deposited by the differently diluted solution (dilution by the distilled water) and after the deposition they were burnt under different burning temperatures. The measurements gave results, that the non-diluted solution is not convenient for thing films with high light transmittance requirements. They have higher thickness which causes lower transmittance. Influence of the diluted solution is obvious in case of the layer oxidation (positive potential). No important influence of the annealing process for the final optical and electro-chemical properties of the samples was found.

Acknowledgements

This work at Brno University of Technology was supported by Ministry of Education of Czech Republic project MSM 0021630516 and research project GAAV KJB 208130902. Moreover, we thank to The Electrochemical Society.

References

[1] Reiter, J., Vondrák, J., Mička, Z. Solid-state Cd/Cd2+ reference electrode based on PMMA gel electrolytes. *Solid State Ionics.* **177** (2007), 3501-3506.

ELECTROCHROMIC LAYERS

J. Vondrák[1], M. Macalík[1], J. Kazelle[1], J. Mohelníková[2]

[1] Faculty of Electrical Engineering, Brno University of Technology, Údolní 53, 602 00 Brno, Czech Republic
[2] Faculty of Civil Engineering, Brno University of Technology, Veveří 95, 602 00 Brno, Czech Republic

Corresponding author: Jiří Vondrák (vondrakj@iic.cas.cz)
Phone: +420 54114 6117

Introduction

Dip-coating method was selected for deposition of thin films with electrochromic properties. In accordance with publication [1] it is possible to obtain tungsten acid from water solution of $Na_2WO_4 \cdot 2H_2O$ due to ion-changing column. Its mixing with hydrogen peroxide gives peroxi-poly-tungsten acid. Another procedure is published on [2] where peroxi-tungsten acid is obtaind directly by solution of tungsten powder in hydrogen peroxide. It is convenient for the pyrolythic method deposition which was described in [3]. The described method is based on the solution powdered tungsten oxide inside of hot water soluent of ammonia. The result of the chemical reaction is ammonia tungstate compound $(NH_4)_2WO_4$. No of the above mentioned procedures gave high quality of thin tungsten oxide films with convenient electrochromic properties. Solutions were badly hydrophilic on TCO substrate. It means they did not create continual thin films or they were not transparent white coloured and without the electrochromic effect.

The article presents the main results of laboratory deposition and testing of electrochromically active and passive thin films. The different deposition temperatures gives the set of laboratory samples of glass substrates with electrochromic films and their laboratory testing has brought information about the optimal solution for the most convenient electrochromic properties.

Experimental

The chemical solution for the tungsten oxide deposition was prepared from tungsten powder (6,5 g of Sigma-Aldrich, 99,9%) diluted in 40 ml hydrogen peroxide (30% concentration, Penta, p.a.). Process of the dilution was completed under lower temperature (5–10 °C) and steady mixing [4]. The low temperature mixing limits sediments creation. After 24 hours the solution was taken out of the fridge and filtrated. This solution of peroxi-tungsten acid with addition of 40ml of ice acetic acid [5], which is convenient for its low content of carbon, chemical stability and applicability for the pyrolitic deposition. The solution was tempered for 3 hours which is enough for the decomposition of non-reactivated hydrogen peroxide and for the peroxi-tungsten acid acetylation. The final solution of light yellow-green colour was diluted in the ratio 1:1 with pure ethanol because of wettability enhacement.

Electro-deposition of layer WO_3 from the solution was carried out for the determined laboratory conditions [6] using the apparatus μAutolab (Ecochemie, Netherland). The electrode Ag/AgCl was used as the reference electrode and the platinum plate for the contra-electrode. The deposition potential of the wprking electrode of FTO layer (Flabeg, Germany, R_{sh} = 35 Ω/ϒ, area 2x3 cm^2) was U_{dep} = -0,45 V against the reference electrode (at the room temperature). The exposition time was changed in several time-interval alternatives 5, 8, 10, 12 and 15 minutes.

After the deposition the sample was taken out of the solution washed in the diluted ethanole and dried Deposited layer is blue coloured which is bleached in several hours. The deposition time has influence on the thickness of the deposited layer. The layer thickness is grown with the exposition time. The layer thickness was measured by the profile-meter Talysurf CLI 1000.

The quartz microbalance (QCM) was used for the determination of an active weight increasement during the layer deposition. The WO_3 layer was deposited 10 minutes on the quartz with platinum plated (firm Maxtec). After the deposition the weight 264,5 μg was determined for the layer thickness 380nm and diameter of the quartz active area 1,37 cm^2 , density WO_3 layer was 5,08 g/cm^3.

The dip-coating or spin-coating deposition methods require firing process. The firring is carried out because of the layer stabilisation and proper optical characteristics. The one hour firing at temperatures 60 and 120 and also 200 °C were tested.

Results and Discussion

Measurement of optical and electric properties of the deposited layers were completed by apparatus μAutolab by the referent electrode Cd/Cd^{2+} and the contra-electrode of the platinum plate [7]. Limit values of the working electrode with the sample were -0,5 V after the intercalation and 1,5 V after the de-intercalation Li^+ ions.

Optical properties were measured by the spectrophotometer UNICAM Helios δv. Spectral transmittance as determined in the spectral range 325–900 nm. In the coloured state the electrode with WO_3 layer was polarised by voltage -0,5 V, for the bleaching state by voltage 1,5 V, switching time 3 minutes.

The scanning microscope TESCAN VEGA 3135 was used for the evaluation of the deposited layers surface quality. It was proven that the layers which were not annealed are porous compared to the annealed layers at the temperature 120 °C. But the annealed layer porosity is increased for annealing at the temperature 60 °C.

The used of method of the cyclic voltammetry offered results of the characteristic volt-metric diagrams for WO_3 layers. Scanning starts at the potential of the working electrode 0,5 V and decreased by 20 mV/s to the value -0,5 V. Positive Li^+ ions intercalate into the WO_3 layer and cause colouration. After the the reaching of voltage -0,5 V the electrode potential is reversed to 1,5 V. The negative current of ions reaches zero and then is increased to positive values. The ions begin to intercalate and thin layer is bleached.

Conclusions

The laboratory investigation of the optimal time of the electrochromic layers deposition was presented in the article. The electrochromic thin films of tungsten oxide were tested. The layers were deposited by the dip-coating deposition method and the following firing at the determined thermal conditions adequate the firing temperature requirements. Optical measurements and determination of volt-metric diagrams were completed on basis of the tested data.

It was proven that in the laboratory conditions it is possible to deposit thin films of tungsten oxide with convenient electrochromic properties which can be applied for many practical applications.

Acknowledgements

This work at Brno University of Technology was supported by Ministry of Education of Czech Republic, project MSM 0021630516 and project GAAV KJB 208130902. Further, a support was obtained from The Electrochemical Society.

References

[1] Wang, H., Zhang, M., Yang, S., Zhao, L., Ding, L. Preparation and properties of electrochromic tungsten oxide film. *Solar Energy Materials and Sollar Cells*. **43** (1996), 345-352.

[2] Deepa, M., Saxena, Tk.K., Singh, D.P., Sood, K.N., Agnihotry, S.A. Spin coated versus dip coated electrochromic tungsten oxide films: Structure, morphology, optical and electrochemical properties. *Electrochimica Acta*. **51** (2006), 1974-1989.

[3] Patil, P.S., Nikam, S.B., Kadam, L.D. Influence of substrate temperature on properties of sprayed WO_3 thin films. *Materials Chemistry and Physics.* **69** (2001), 77-83.

[4] Patra, A., Auddy, K., Ganguli, D., Livage, J., Biswas, P.K. Sol-Gel electrochromic WO_3 coatings on glass. *Material Letters*. **58** (2004), 1059-1063.

[5] Deepa, M., Saxena, Tk.K., Singh, D.P., Sood, K.N., Agnihotry, S.A. Spin coated versus dip coated electrochromic tungsten oxide films: Structure, morphology, optical and electrochemical properties. *Electrochimica Acta*. 2006, roč. 51, s. 1974-1989. ISSN 0013-4686.

[6] Leftheriotis, G., Yianoulis, P. Development of electrodeposited WO_3 films with modified surface morphology and improved electrochromic properties. *Solid State Ionics*. **179** (2008), 2192-2197.

[7] Reiter, J., Vondrák, J., Mička, Z. Solid-state Cd/Cd2+ reference electrode based on PMMA gel electrolytes. *Solid State Ionics.* **177** (2007), 3501-3506.

SODIUM INSERTION INTO THIN LAYER V_2O_5 ELECTRODES

J. Vondrák, P. Špičák, J. Kazelle

Faculty of Electrical Engineering and Communication, Department of Electrotechnology, Údolní 53, 602 00 Brno, Czech Republic

Corresponding author: J. Vondrák (vondrak123@seznam.cz)
Phone: +420607285434

Thin layers of V_2O_5 were vacuum deposited onto glass substrates covered by SnO_2. The electrochemical insertion of sodium ions was investigated and the diffusion behavior of the electrodes was investigated.

The experiments were performed in a solution of dry $NaClO_4$ in propylene carbonate in standard voltammetric arrangement. Supplementary investigation was done using MAXEC quartz crystal microbalance QCM, which was calibrated by electrodeposition and dissolution of copper.

Some voltammetric curves (at scan rate 3 mV/s) are plotted in Fig.1. Their closer analysis showed that the process od insertion should be diffusion controlled.

In order to investigate this, a potentiostatic analog of GITT techniques was applied. The electrodes were exposed to a stepvise potential in the potential range where the insertion occurred (see Fig. 2). According to the theory of diffusion in thin layers, the current response in first few seconds after the step should be governed by the Cotrell equation modified for the diffusion in a layer of limited thickness [1]. An example of the voltage profile and corresponding response is given in there.

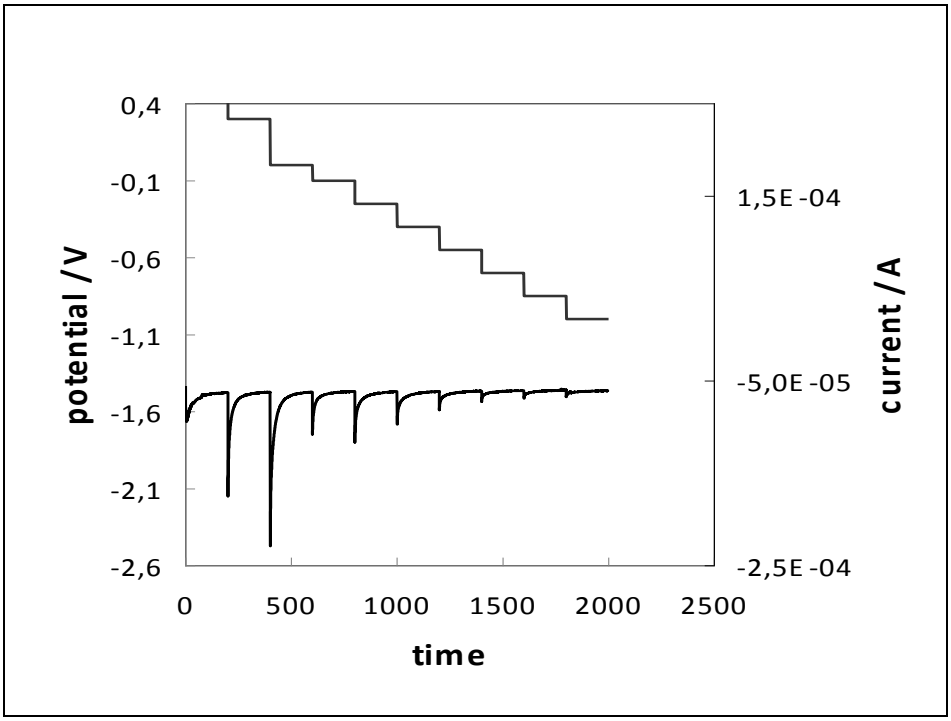

Fig. 1: *The waveform of potential chane during an experiment witn conductive glass covered by V3O5. Upper curve: potential, lower curve: current response.*

Therefore, the increment of concentration could be obtained approximately by numeric integration of the peaks, and the diffusion coefficient from 2. Similar experiments were done also with $LiClO_4$ electrolyte for comparison.

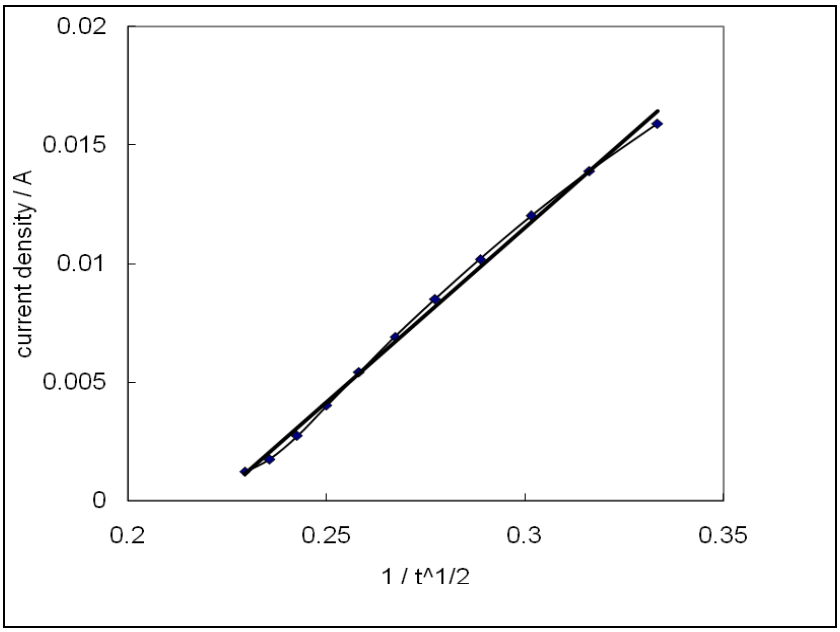

Fig.2: *The current at the potential just after the potential step (first 11 points); time plotted as t-1/2.*

Tab. 1: *The estimation of diffusion coefficient for potential range between two neighboring potential steps. Upper part: from positive to negative values of potential lower part. opposite direction.*

potential	D, Na	D,Li
0.3	6.4E-10	9.0E-15
0	1.2E-08	7.1E-15
-0.1	6.8E-09	9.3E-16
-0.25	6.8E-10	1.2E-15
-0.4	7.1E-10	1.1E-16
-0.55	2.4E-10	2.7E-17
-0.7	5.0E-11	2.4E-17
-0.85	6.7E-12	3.6E-17
-1	1.1E-11	3.4E-17
-0.85	4.6E-17	2.1E-16
-0.7	4.9E-11	3.8E-16
-0.55	1.2E-15	8.7E-17
-0.4	1.7E-15	1.0E-16
-0.25	3.7E-15	6.0E-17
-0.1	6.7E-14	2.4E-17
0.1	4.4E-14	2.8E-17
0.3	1.7E-13	5.3E-16
0.5	3.9E-13	9.0E-16

QCM observations

On contrary to similar measurements with WO_3 electrodes, the QCM measurements revealed that the effective mass of the inserted ions is close to 23 and therefore, no coinsertion of solvent occurs.

Moreover, the lifetime in 10 following cycles has shown to be sufficient (see Fig. 3).

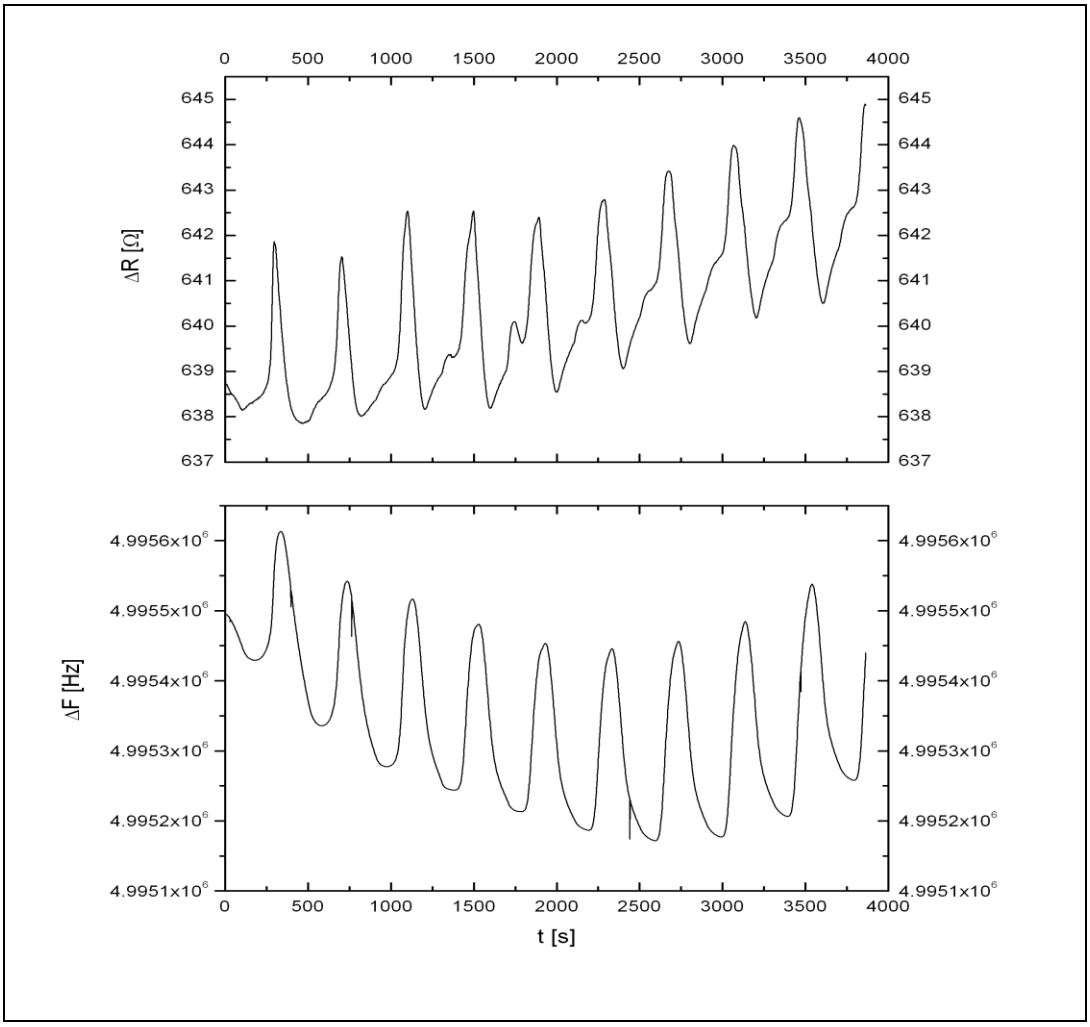

Fig.3: *Real and imaginary component of the QCM response during 10 cycles*

The change of real component of the QCM response is given there too. It may be connected to the change of oxide elasticity and/or friction at the boundary with surrounding electrolyte.

Acknowledgements

This work was supported by Ministry of Education of Czech Republic, Project MSM 0021630516, and by The Electrochemical Society .

Reference

[1] Vondrak J, Reiter J, Velicka J, Klapste B, Sedlarikova M, Novak V (2003) 7: 361-367

PROBLEMS OF "IN SITU" SPECIMEN OBSERVATION IN ESEM

J. Jirák[1], J. Runštuk[2], J. Špinka[1]

[1] Department of Electrotechnology, FEEC, BUT Brno, Technická 10, Brno, Czech Republic
[2] Institute of Scientific Instruments ASCR, Královopolská 147, 61264 Brno, Czech Republic

Corresponding: Jiří Špinka (spinka@feec.vutbr.cz)
Phone: +420 54114 6145, Fax Number: +420 54114 6147

The paper deals with the possibility of observing the surface of specimens (such as battery mass, hydrated samples, etc.) using scanning electron microscopy, especially by means of ESEM. We are engaged at our department for a long time - with cooperation with the Institute of Scientific Instruments, Academy of Science, the Czech republic – in the issues of ESEM [1].We participate in the development of ESEM first produced in the Czech republic by TESCAN company. We focused our work in the long term on the problem of signal generation and its suitable detection. As it is known, ESEM enables us to observe the samples at higher pressures than the pressure needed at the area of cathode and a column microscope (e.g. at the pressure over 609 Pa for water), so it is possible to observe due to electron optics also samples, which contain certain amount of liquid in it. Another advantage is (because there is water vapor, aerosols and others present in the sample and get to anodized) that at the samples of insulating character, the charging of sample is avoided. This surface charging is cause by incident electrons. The resulted charge is then eliminated by ions. We can also observe the samples in their native condition, for certain time, thanks to higher pressures. The ideal case happens when it is possible to prepare such conditions during observing that it is possible to observe dynamic acts and changes going on in the sample of in situ. If it goes well to create appropriate conditions for example when observing the changes of accumulator mass at the model accumulator while charging and discharging, we obtain important information about the structure changes of accumulator mass. Initially we focused our work towards the usage of a typical ESEM microscope for the observing of structure of battery mass, without any preparation and changes needed to be done. We were aware of the fact that the electrolytes soaked in the substances create very aggressive environment (either speaking about the solution H_2SO_4 or KOH) and this aggression is the biggest problem in the long term observing of samples. We were trying to get the situation when aggressive aerosols and evaporation loosened from the surface of electrode mass have done the smallest possible damage to the microscope. For this reason we used differential pumping to protect the surface of the sample, which splits the sample (area with higher pressure) from the column, thin layer of gold plating. To detect the signal we use a scintillator from YAG single crystal doped with Cerum, which is very chemically resistant. Thanks this we protected those parts of the microscope which will get in imminent contact with aggressive aerosols, but neither the whole vacuum pumping system nor the column were protected. We used an old type of microscope with directly heated tungsten cathode and pumping via diffusion pump. After certain time it was needed to disassemble the whole microscope, withdraw the impacts of aggressive impingement (clean the column, clear the apertures, to change oil in both the diffusion pump and rotary pumps. The problems greatly complicate the possibility of using ESEM for observing battery mass.

Another option is to prevent the aggressive substances from escaping into functional parts of microscope. For that reason we enclosed the sample with the suitable resistant vessel, which is pumped individually [2]. For pumping, Roots pump with front-end filter is the most suitable to use. The pressure in the vessel must be few pascals lower than the pressure in the sample chamber, so the aggressive environment does not infiltrate into the microscope. In the upper part of this vessel there is a small loophole which enables incident of primary electrons. Simultaneously a suitable detect system is created, for detection by ionic detector and also by scintillation detector. The whole matter is complicated by creation of a suitable micromanipulation system for shifting of samples.

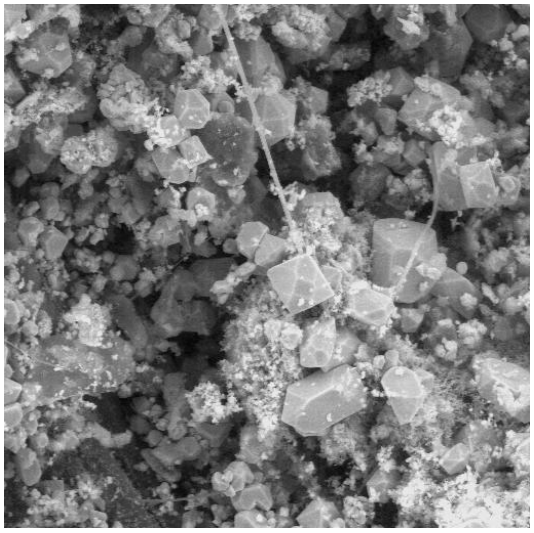

Fig. 1:

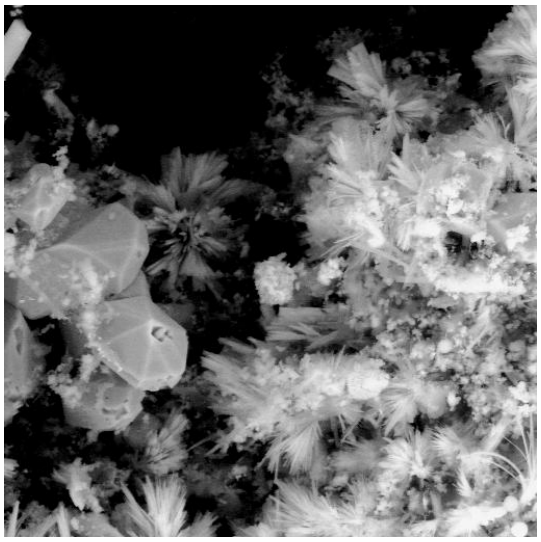

Fig. 2:

Acknowledgment

This work was supported by Ministry of Education Czech Republic, VZ MSM 002130516.

References:

[1] Autrata, P., Schauer, P., Špinka, J., Romanovský, V.: Scintillation and Ionisation Detectors for Environmental SEM. *European Microscopy and Analysis.* 1999(19). p. 59 - 62. ISSN 0958-1952.

[2] Neděla V. , Runštuk J.: Study of highly-aggressive samples using the variable pressure SEM. EMC 2008 - 14th European Microscopy Congress - Volume 1: Instrumentation and Methods. Berlin : Springer, 2008 - (Luysberg, M.; Tillmann, K.; Weirich, T.) S. 589-590. ISBN 978-3-540-85154-7.

SPECIMENS OBSERVATION IN ESEM

J. Špinka

Department of Electrotechnology, FEEC, BUT Brno, Technická 10, Brno

Corresponding: Jiří Špinka (spinka@feec.vutbr.cz)
Phone: +420 54114 6145, Fax Number: +420 54114 6147

Questions of specimen observation in ESEM have been solved at our department in cooperation with the Institute of Scientific Instruments, Academy of Science since 1989, one of the first publications in this area was [1]. We have been solved for a long time matters of gas pumping in ESEM, detection of signals and detectors and also with the issue of humidity measurement and adjustment at environmental conditions [2].

In the microscope there is a possibility of damage to wet samples caused by electron beam, which I is undesirable, it is the case of e.g. polymer and biologic materials, which are sensitive to drying in vacuum and damage by downfall of highly energetic electrons.

Damage is a major problem, given to the sample sensitive to electron beam and also because water is the source of highly mobile free radicals which can accelerate a sample degradation quicker. From the study of interaction electron – water it is known that electron undergoes nonflexible collisions during which 6 reactive elements emerges. These are to e^-, H., H_2O_2, H^+_{aq}, OH., OH^-_{aq}. From which the radical of hydroxyl occur with the highest concentration. Significant effect on the concentration of reactive elements and particles is especially energy beam. Because increase of radiation damage is non-linear dependent on beam energy, we achieve the lower radiation damage if we use the lower energy of beam.

EREM enables us to observe wet samples when we substitute dry air in the sample chamber with the air which is saturated by water vapor. During pumping, we can observe evaporation or condensation of water on the sample, which my indicate that the sample, which we want to observe, does not have to stay in its natural state. Because of that we need to optimize humidity in the sample chamber and to find pumping cycle, which is optimal from this point of view. We have an optimal pumping cycle, thanks which we achieve the highest humidity in the sample chamber EREM [2]. Few parameters can influence these cycles. The main ones are these: sample temperature, water temperature in developer of water steams, number of pumping cycles x floatation, initial humidity in the sample chamber and also a range of pressures between which we carry out the floatation cycles.

Following findings were brought from performed measuring: We achieve optimum initial humidity in the sample chamber by injection of water droplets of minimum 0,3ml, with back up we rather pick 0,5ml. We perform the pumping floatation cycle between the pressures 700 – 1100 Pa and we can finish it after the fourth cycle. Under these conditions we achieve an optimum amount of water steam in the microscope sample chamber at the end of the pumping cycle.

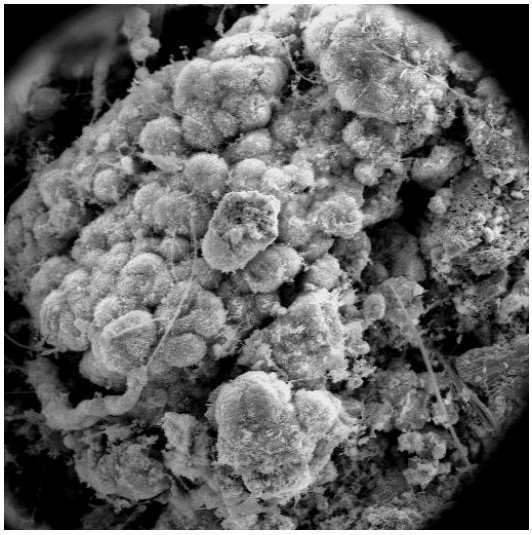

Fig.1:

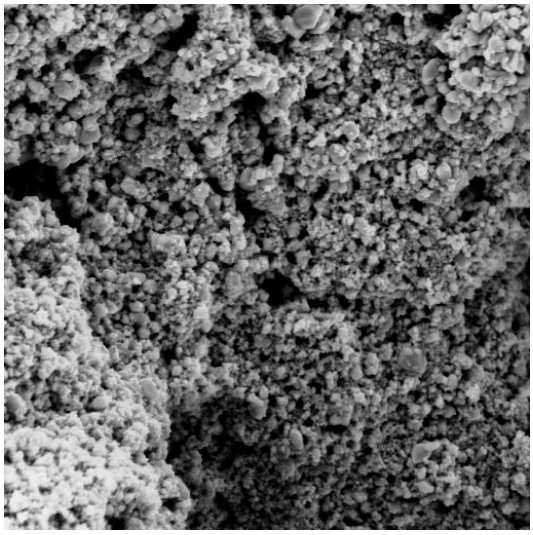

Fig.2:

Acknowledgment

This work was supported by Ministry of Education Czech Republic, VZ MSM 002130516.

References:

[1] Autrata, R., Jirák, J., Špinka, J.:Backscattered electron detector for environmental scanning electron microscopes. Beiträge zur elektronenmikroskopischen Direktabbildungen der Oberfläche. Roč. 26, - (1993), s. 13-18. ISSN 0340-3815

[2] Royall, C. P., *et al.*: Radiation Damage of Water in environmental scanning electron microscope, Reference and Application Data, The Royal Microscopical Society, Journal of Microscopy 204, str. 185 – 194, 2001.

[3] Autrata, R., Jirák, J., Neděla V., Špinka, J.:Humidity Measurement and Adjustment at Environmental Conditions. Proceedings of the 9th International Seminar Recent Trends in Charged Particle Optics and Surface Physics Instrumentation. Brno : Institute of Scientific Instruments AS CR, 2004 - (Müllerová, I.) s. 7 - 8. ISBN 80-239-3246-2.

11th ABAF

BRNO 2010

Advanced Batteries, Accumulators and Fuel Cells

Supercapacitors

ELECTROLYTIC NICKEL SULFIDE FILMS IN ELECTROCHEMICAL CAPACITOR

R. Apostolova[1], O. Kolomoyets[1], U.Tkachenko[1], E. Shembel[1, 2]

[1]Ukrainian State Chemical Technology University, Dnepropetrovsk,
[2] Enerize Corporation, Coral Springs, Fl, USA

Corresponding author: E.Shembel (shembel@onil.dp.ua)
Phone, Fax:+380562 470391

Introduction

Recently semiconducting metal sulfides were investigated as superior electrode materials in electrochemical capacitors (ECs) [1]. Electrolytic (e) sulfides of transition metals (Me=Co, Ni, Fe) that revealed good electrochemical characteristics in the lithium thin-layer accumulator models [2] have been studied by us in electrochemical capacitor.

In the present work capacitor studies of electrolytic nickel sulfide in alkaline solutions are reported.

Experimental

Nickel sulfide was synthesized on stainless steel sheet (SS) -10x10 mm from aqueous electrolyte containing nickel sulfate and sodium thiosulfate [2]. The experiments were conducted using electrochemical cell (200 cm^3) with 1.7-2.0 mg/cm^2 nickel sulfide on SS as a working electrode, (5.0 cm^2) acetylene carbon black on nickel sheet as counter electrode and Ag/AgCl (saturated) was a reference electrode. Capacitive studies were carried out by cycling voltammetry (CV) at the different scan rates using analytical radiometer VoltaLab PJZ 301. The structure of nickel sulfide was examined by X-ray diffraction analysis (DRON-2). 6.00; 2.00; 0.20; 0.05 M KOH solutions were used as an electrolyte in capacitor model.

Results and Discussion

Fine crystal nickel sulfide was identified within the deposit obtained on SS support (Fig. 1). Nickel sulfide is presents in one phase, its structure corresponding to NiS structure.

Cycling voltammograms of NiS electrode recorded in several electrolytes are shown in Fig.2. In 6.0 M KOH there is an oxidation peak at 0.29 V, current increasing corresponds to oxygen evolution at about 0.42 V. The cathodic current peak is at about 0.195V. These features of voltammogram suggest a diffusion-controlled quasi- reversible redox reaction with capacitive behavior within the limited potential range. The analysis of e-NiS cycling voltammograms within the different sweep rate (Fig.3a) shows the characteristic plotting I_{peak} vs $v^{1/2}$ for diffusion controlled electron transfer reaction (Fig.3 b).

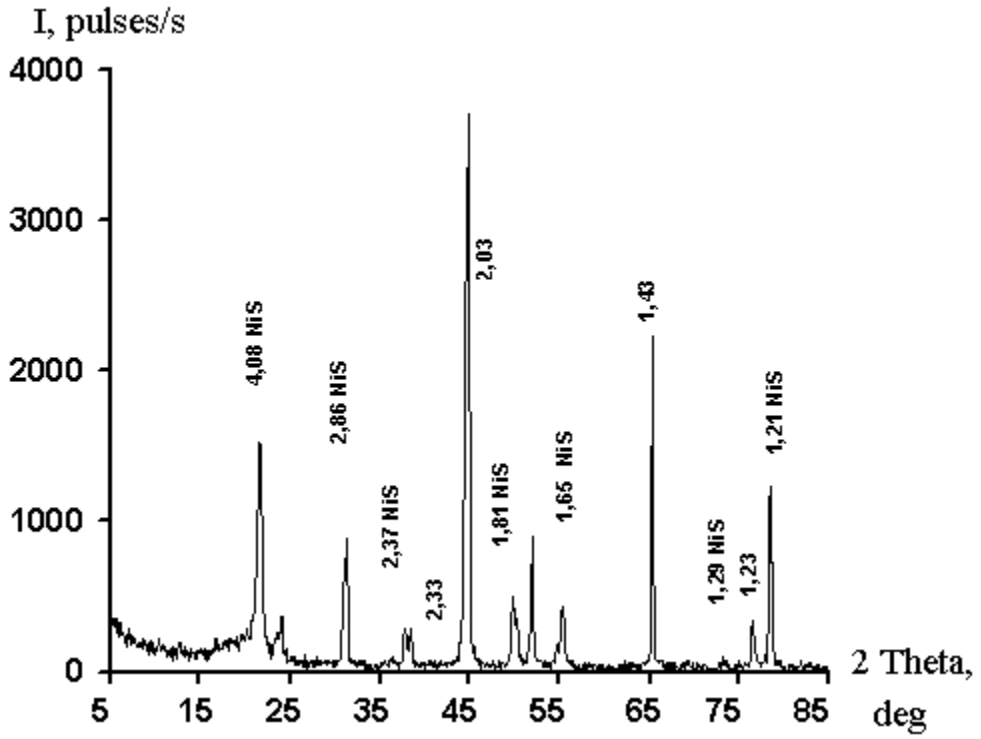

Fig. 1: *X-ray diffractogram of electrolytic NiS deposit on SS. Co-K_α radiation.*

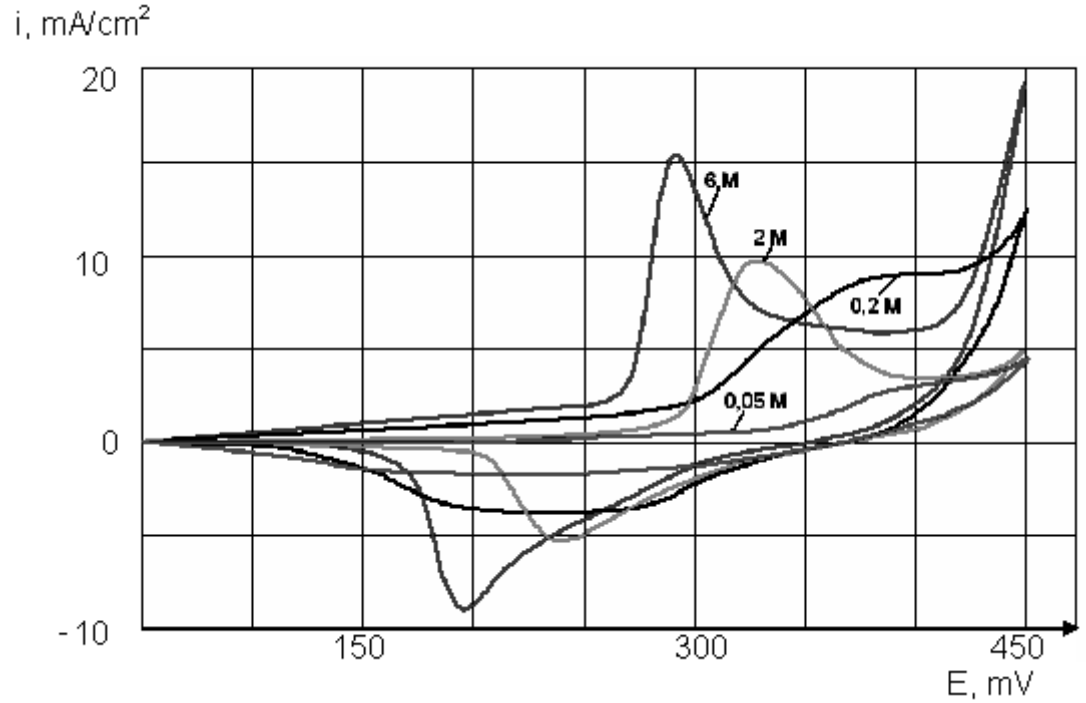

Fig.2: *Cycling voltammograms of e-NiS electrode at 10 mV/s sweep rate in 6.0 M KOH, 2.0 M KOH, 0.2 M KOH, 0.05 M KOH.*

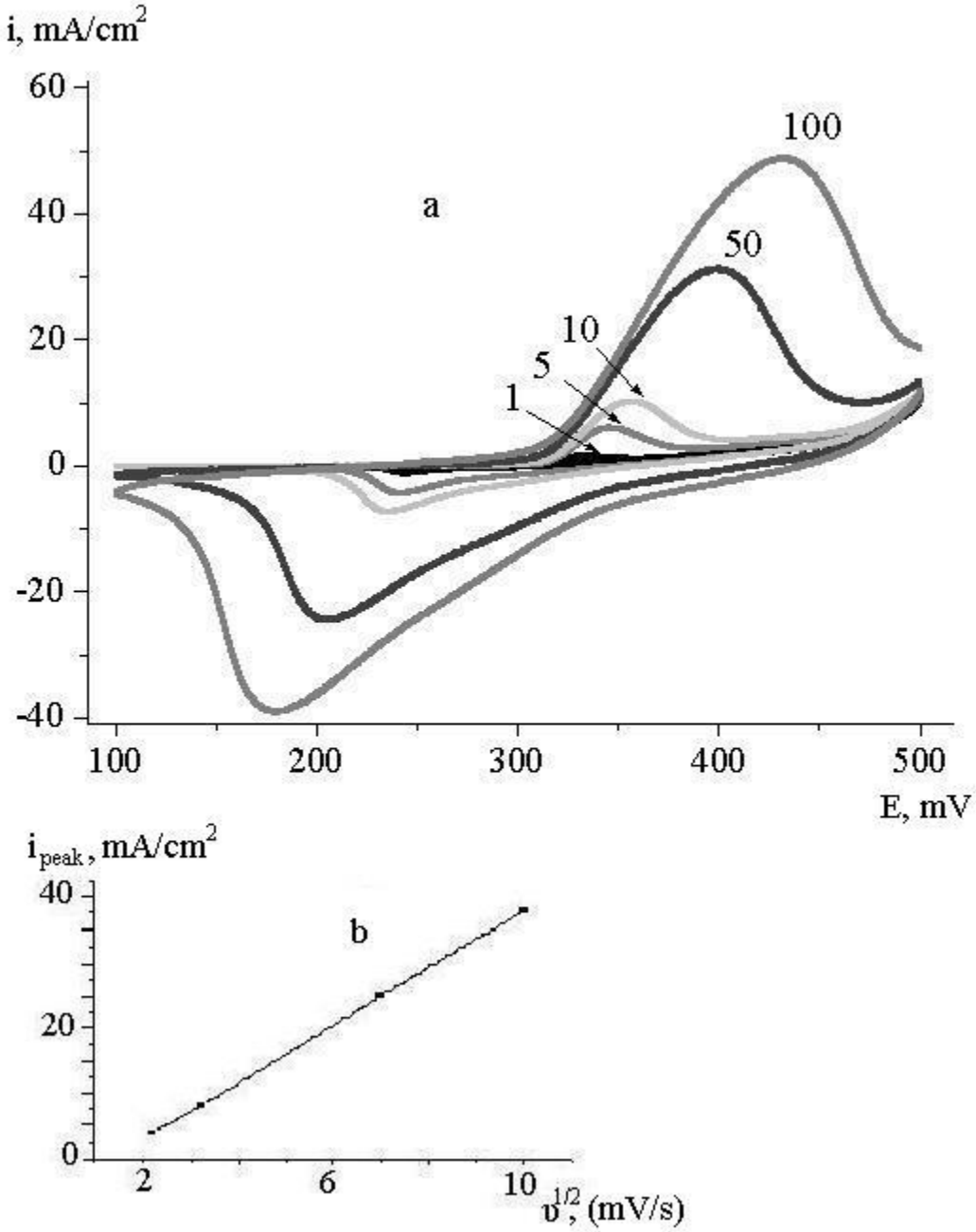

Fig. 3: *Cycling e-NiS voltammograms within the different sweep rate (υ), mV/s: 1; 5; 10; 50; 100 (a) and the plotting* I_{peak} *vs* $\upsilon^{1/2}$ *(b).*

The e-NiS CV shape is the same as that of the reported e-NiO oxide in the KOH electrolyte. The formation of NiOOH phase during e-NiS cycling is proposed as follows (1):

$$NiS + 3OH^- - 3\bar{e} \rightarrow NiOOH + S + H_2O \qquad (1)$$

The XRD e-NiS electrode pattern shows the presence of NiOOH phase inhere (d=3.2; 2.38; 1,58; 1.44; 1.40 Å) when the fresh electrode is submitted to anodic scan (27-956).

The high-efficiency e-NiS cycling was realized in 2 M KOH electrolyte at 10 mV/s sweep rate during 200 cycles (Fig.4). A specific capacitance (C) of 143 F/g obtained after 200 cycles. $\Delta = C_{disch.}/C_{charge} = 0.96$.

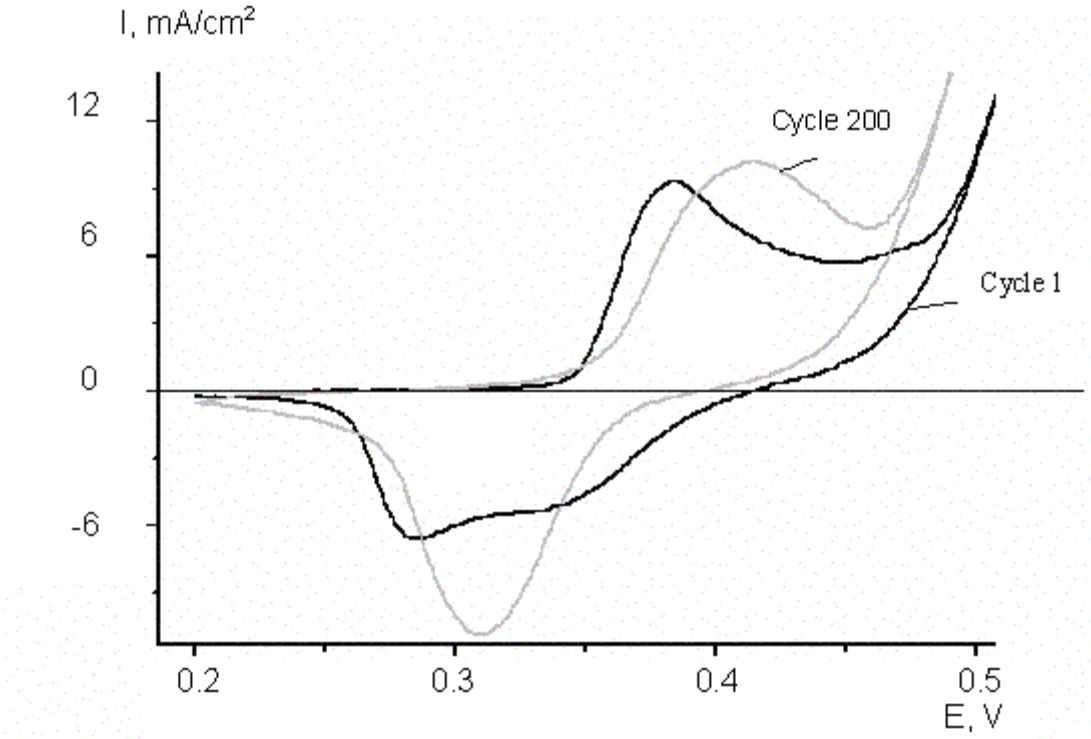

Fig. 4: *Cycling voltammograms of NiS electrode at 10 mV/s sweep rate in 2.0 M KON, obtained in the 1st and the 200 th cycles.*

Conclusions

Capacitor properties of electrolytic NiS on SS substrate are studied in KOH electrolytes of various concentrations and sweep rate. 143 F/g obtained after 200 cycles in 2 M KOH at 10 mV/s sweep rate as the potential window is 0.3 V.

References

[1] Changzhou Yuan, Bo Gao, Linhao Su, Li Chen, and Xiaogang Zhang // J. Electrochem. Soc. 156 (2009) A 199-A 203 (and references therein).

[2] V.M.Nagirny, R.D. Apostolova, E.M. Shembel. Synthesis and electrochemical characteristics of electrolytic metal-oxide and metal-sulfide materials for lithium accumulator systems, USCTU, Dnepropetrovsk, 2008. p. 260.

SYNTHESIS, CHARACTERIZATION AND ELECTROCHEMICAL PROPETIES OF NANOSTRUCTURED ELECTRODE MATERIALS FOR SUPERCAPACITORS

M. Mladenov[a], N. Petrov[b], T. Budinova[b], B. Tsyntsarski[b], T. Petrov[d], D. Kovacheva[c], R. Raicheff[a]

[a]Institute of Electrochemisty and Energy Systems, Bulgarian Academy of Sciences, Ak. G.Bonchev str., BL.10, 1113 Sofia, Bulgaria
[b]Institute of Organic Chemistry, Bulgarian Academy of Sciences, Ak. G. Bonchev str., BL.9, 1113 Sofia, Bulgaria,
[c] Institute of General and Inorganic Chemistry, Bulgarian Academy of Sciences, Ak. G.Bonchev str., BL.11, 1113 Sofia, Bulgaria
[d] University of Chemical Technology and Metallurgy, 8 St. Kliment Ohridski blvd., 1756 Sofia, Bulgaria

Corresponding author: M. Mladenov (mladen47@bas.bg)
Phone: +359-885450062, Fax: +3592-8722544

Introduction

In the last years the electrochemical double-layer capacitors (supercapacitors) have attracted worldwide interest, due to their potential applications as energy storage devices. Porous carbons are among the most attractive materials for preparation of electrodes for electrochemical capacitors. The main advantage of these materials is the possibility to produce highly porous structures with high specific surface area and to adjust the porosity texture of the electrodes. On the other hand, the carbon materials give possibilities to develop various composite electrode structures by adding electrochemically active materials to the carbon matrix [1, 2]. The electrochemical cells in the carbon-based supercapacitors are usually symmetrical with identical carbon electrodes. In order to improve the energy density while keeping long cycle life, asymmetrical cells consisting of different types of electrodes were introduced. Thus, hybrid capacitor configurations consisting of active carbon as a positive electrode and a negative electrode based on metal oxides (nickel, lead or manganese oxides) [3-5], conducting polymers [6], or Li intercalation oxides [7-8] were suggested, and promising results were obtained. An interesting approach in this respect is also so called Li-ion capacitor, using lithiated graphite and activated carbon for the negative and positive electrodes, respectively [9]. In our previous studies [10, 11] it was shown that nanoporous carbon materials can be synthesized from waste biomass (apricot stones and spent coffee grounds), and their pore texture could be readily regulated by appropriate thermal and hydrothermal treatment. The electrochemical tests showed promising characteristics (capacity values up to 60 $F.cm^{-2}$, cycling efficiency 85-90%) of symmetrical sandwich-type capacitor cells, with the carbon electrodes obtained and with organic electrolyte Et_4NBF_4 – PC. The main objective of the present work is to study the electrochemical properties of newly synthesized carbon electrode materials on the base of waste biomass for supercapacitors. Another aim of this work is to compare the capacitance behaviour of the symmetrical carbon-based

supercapacitors with those of an asymmetrical suprecapacitor, composed by carbon and carbon- $Li_4Ti_5O_{12}$ oxide composite electrodes.

Experimental

Synthesis and physico-chemical characterization of the electrode materials

The mixtures of coal tar pitch and furfural in different proportions were treated with concentrated H_2SO_4 at 120 ºC until solidification. The obtained solid product was heated at 600 ºC with a heating rate of 10 ºC min^{-1}, under nitrogen atmosphere, and after carbonization it was further submitted to steam activation at 800°C for 1 h [12]. The samples obtained were labelled with C (carbon) and F (furfural), followed by the content in furfural (CF-50 and CF-55). In order to explore the effect of the high temperatures on the electrochemical performance, CF-50 was treated at 1100 ºC and sample CF-55 - at 1400 ºC, both in nitrogen athmosphere. These samples were labelled as CF-50H and CF-55H, respectively. Powder X-ray diffraction spectra were collected using Bruker D8 Advance diffractometer with Cu Kα radiation. Nanotexture of the synthesized carbon materials was characterized by N_2 adsorption at −196 °C, carried out in an automatic volumetric apparatus Micromeritics ASAP 2020.

Electrochemical tests

The electrodes were prepared from a mixture of 90 wt.% activated carbon (with addition of graphite 10% or $Li_4Ti_5O_{12}$ – 20%) powder and 10 wt.%. polytetrafluoroethylene (PTFE binder - Aldrich, 60% suspension in water), and then pressed on aluminum discs (surface area 1.75 cm^2). The electrodes were soaked in the electrolyte before the cell assembly. Sandwich-type symmetric cells constituted of two identical carbon electrodes of comparable mass. The electrodes were electrically isolated by a ceramic-mat separator, soaked with an organic electrolyte, and the cell was assembled in dry-box under argon. Tree type of organic electrolytes–Et_4NBF_4, $LiBF_4$ and $LiPF_6$ (Aldrich p.a.) were used. The composite electrodes were prepared from electrochemically active nanostructure $Li_4Ti_5O_{12}$ oxide, carbon CF-50 and two conductive materials (natural graphite NG-7 and acetylene black), in ratio 1:1:1. The capacitor cells were subjected to galvanostatic charge-discharge cycling at different current rates using an Arbin Instrument System BU-2000 [11].

Results and discussions

Physicochemical characterization

The data for powder X-Ray diffraction of the samples and for PSD are presented in Table 1 and Table 2, respectively. The results indicate formation of graphite domains with higher crystallite sizes after additional heating of CF-50 (Fig. 1, Inset).

Tab. 1: *Main parameters obtained from XRD patterns of the samples*

Sample	CF-50	CF-50H	CF-50H (graphite)	CF-55	CF-55H
(002)-position [A]	3.719	3.732	3.379	3.711	3.684
Size[nm] perpendicular to graphene layers	0.56	0.75	3.23	0.51	0.59
(100)-position [A]	2.081	2.079	2.132	2.083	2.071
Size[nm] within the graphene layers	0.86	1.42	14	1.23	1.14

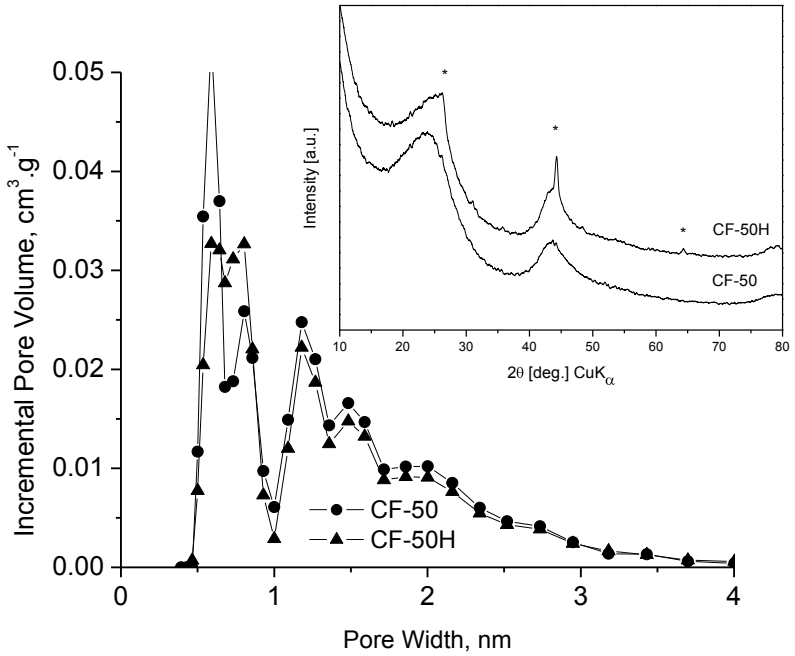

Fig. 1: *Pore size distribution of the activated carbons: CF-50 and CF-50H, (Inset: X-ray diffraction patterns of CF-50 and CF-50H.)*

The main textural parameters obtained from pore structure analysis of the samples, performed using nitrogen gas adsorption isotherms at -196 ºC, are compiled in Table 2. The results show that the furfural content has a strong effect on the porosity of the carbons. The isotherm (not shown) for the sample with the lowest proportion of furfural (CF-50) are characteristic for microporous materials. As the content of furfural rises, the results indicates development of mesoporosity and widening of the microporosity in the sample CF-55.

Tab. 2: *Main textural parameters of the samples from N_2 adsorption isotherms at 77 K.*

Samples	S_{BET} [m^2g^{-1}]	V_{TOTAL} [cm^3g^{-1}]	V_{MICRO} [cm^3g^{-1}]	V_{MESO} [cm^3g^{-1}]	Wo N_2 [cm^3g^{-1}]
CF-50	1173	0.551	0.374	0.033	0.533
CF-50H	1071	0.486	0.338	0.033	0.473
CF-55	1613	0.761	0.492	0.177	0.604
CF-55H	1397	0.620	0.440	0.074	0.509

This was confirmed by the analysis of the pore size distribution by the DFT method (Table 2). Rising the furfural content in the initial mixture from 50% to 55% (CF-50 and CF-55) leads to increase of the micropore and the mesopore volume (Table 2). It has been reported that the presence of oxygenated groups enhances the inner resistance and the leakage current of carbon electrodes [13]. Consequently, carbon samples were submitted to high thermal treatment in order to remove the surface functionalities (CF-50H and CF-55H). It is also known that heating at high temperature may favour internal rearrangements in the carbon structure, which can end up with an increase in the electrical conductivity, if graphitic-like domains are created during the rearrangements. The results show a decrease in the surface area and pore volumes of the thermally treated carbons, which is

more strongly expressed in the case of CF-55H (treated at a higher temperature), and more precisely for the mesopore volume.

Electrochemical performance

A beaker with two electrode symmetric cells has been used to evaluate the electrical characteristics of the electrode material CF-50 in different electrolytes: Et_4NBF_4-PC, $LiBF_4$-PC and $LiBF_6$-DMC/EC. Fig. 2 compares discharge capacity of the samples at different current rates. At low current rate, 20 $mA.g^{-1}$, all three type capacitors have very close capacity values. At high current rate, 100 $mA.g^{-1}$, however the capacitors with Li^+ in the electrolyte demonstrate quite different behavior from those of cell with Et_4N^+ in the electrolyte. As seen from Fig.2 the capacitance value of the latter is much higher than those of the other two cells. Fig.2 (inset) shows the charge-discharge profiles of the above described capacitors after 50 cycles. The capacitance of the cell when using Et_4NBF_4 demonstrates very stable cycleability. The initial discharge capacity values for all electrolytes are very close.

Fig. 3 shows that all prepared carbons show satisfactory capability of charge accumulation in the electric double layer up to 160 $mA.g^{-1}$. The capacitance values of carbon CF-50 however, is much higher than this of CF-55. CF-50 and CF-55 show quite different porous texture characteristics - pore volume, surface-area and micropore size distribution. There are contradictory reports in the literature on the effect of the increasing surface area and the porosity on the intrinsic electronic conductivity of compact carbon powders. It seems rather soundly to expect that the volumetric conductivity decrease as the microporosity and surface area increase. However the results of some authors [13] oppose to this common consideration.

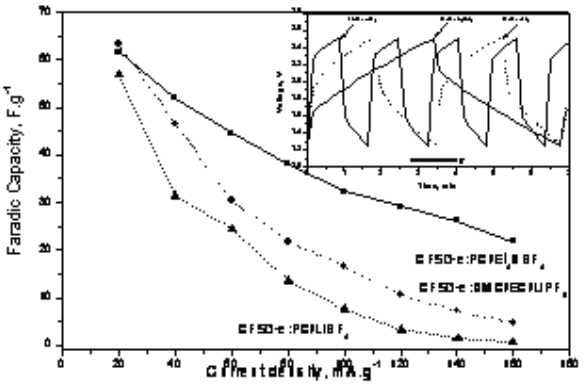

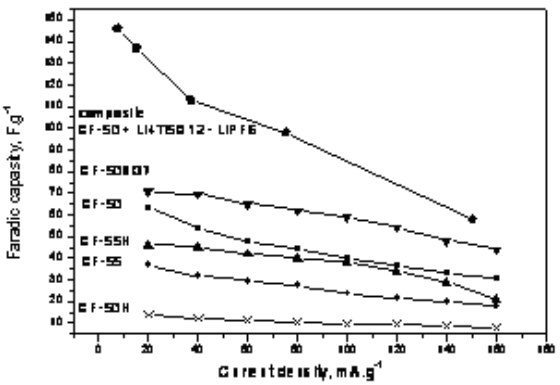

Fig. 2: *(left) Dependence of capacity on discharge current for symmetric cells with different electrolytes (Inset: Cycling performance of symmetric cells with CF-50.)*

Fig. 3: *(right) Dependence of capacity on discharge current for symmetric cells using Et_4NBF_4 and for asymmetric cells*

Fig.1 (Inset) and Table 1 show that thermal treatment leads to rearrangements in the carbon structure, and graphitic-like domains are formed, proved by XRD analysis of CF-50H (10% degree of crystallinity) and CF-55H. This process can end up with increased conductivity and capacity of the samples. Fig. 3 shows that the capacity of CF-55 increase after thermal treatment, but the capacity of CF-50 at these conditions drastically decrease. The possible rearrangements in CF-55 during thermal treatment cause changes of the textural and structural properties of the carbon skeleton (annealing effects).

Significant increase of capacity was observed for the composite carbon-$Li_4Ti_5O_{12}$ (Fig. 3).

Conclusions

1. Organic electrolyte strongly influences the capacitance performance of symmetric carbon/carbon non-aqueous supercapacitors.

2. The conductivity, pore size distribution and surface properties of the carbon have major impact on the charge storage behavior of carbon electrodes in symmetric supercapacitors.

3. Supercapacitors using Li^+-based electrolyte show different behavior from quarternary alkyl ammonium-based electrolyte, which mainly is due to both processes – adsorption and intercalation of the PC (DMC/EC) – solvated Li^+ on the negative electrode.

Acknowledgment

This work is supported by Bulgarian NSF under Proj TK-X-1705/2007

References

[1] R.Kotz, M.Carlen, Electrochim. Acta 45 (2000) 2483.
[2] R.S. Brood, K. R Bulock, R.A. Leising, R.L. Middouh, J.R. Miller, E. Takeuchi, J. Electrochem.Soc. 151(2002) LOK1.
[3] S. Razumov, A. Klementov, S. Letvinenko, A. Beliakov, US Patent 6,222,723 (2001).
[4] W.G. Pell, B.E. Conway, J. Power Sources 136 (2004) 334-345.
[5] V. Khomenko, E. Raymundo-Pinero, F. Beguin, J. Power Sources 153 (2006) 183-190.
[6] C.A. Fabio, A. Giorgi, M. Mastragostino, F. Soavi, J. Electrochem. Soc. 148 (2001) A845-850.
[7] G.G. Amatucci, F. Badway, A. Du Pasquier, T. Zheng, J. Electrochem Soc. 148 (2001) A930-939.
[8] A. Du Pasquier, I. Blitz, J. Gural, S. Menocal, G.G. Amatucci, J. Power Sources 143 (2003) 62-71.
[9] V. Khomenko, E. Raymundo-Pinero, F. Beguin, J. Power Sources 177 (2008) 643-651.
[10] M. Mladenov, P. Zlatilova, R. Raicheff, S. Vassilev, N. Petrov, K. Belov, V. Trenev, Bulgarian Chem. Commun. 40 (2008) 360-366.
[11] M. Mladenov, R. Raicheff, N. Petrov, D. Kovacheva, R. Nickolov, V. Trenev, D. Bachvarov, K. Belov, Proc. 4M/ICOMM 2009 Conference, Karlsrhue, Germany, (2009) 223-226.
[12] B. Petrova, B. Tsyntsarski, T. Budinova, N. Petrov, C.O. Ania, J.B. Parra, M. Mladenov, P. Tzvetkov, Synthesis of nanoporous carbons from mixtures of coal tar pitch and furfural and their application as electrode materials, Fuel Process. Technol. (2010), doi:10.1016/j.fuproc.2010.07.008
[13] H. Wang, M.Yoshio, Electrochemical Communication, 10, (2008),382-396.

11th ABAF

BRNO 2010

Advanced Batteries, Accumulators and Fuel Cells

Fuel Cells

NEW TYPE OF CARBON MATERIALS FOR CATALYTIC LAYER OF MEA STRUCTURES FOR PEM FUEL CELLS

L. Chladil [2], V. Novák [2], P. Barath [1, 3]

[1] Institute of Inorganic Chemistry of the ASCR, v. v. i., 250 68 Řež near Prague, Czech Republic
[2] Institute of Electrotechnology, Technical University of Brno, 602 00 Brno, Czech Republic
[3] Metrohm Česká republika Ltd., Na Harfě 935, Prague, Czech Republic

Abstract

Our article contains one part of our research activity which is focus on various carbon materials as conductive matrix for fuel cells electrodes. We would like to find a good material with hight electrical conductivity, geometrical area and porous structure. We have studied carbon black Chezacarb A, Chezacarb B and Vulcan XC-72. We have used as a catalyst platinum in a different contents. The catalytic activity was studied by cyclic voltammetry and linear sweep voltametry on RDE. The electrode materials were tested in experimental fuel cell. We have measured all experiments on PGSTAT12, produced by Metrohm AUTOLAB BV. All experimental setup was fully automatically controlled with NOVA 1.6. software developed by METROHM AUTOLAB BV.

Introduction

Proton exchange membrane fuel cells (PEMFCs) are devices, which convert chemical energy, stored in hydrogen, direct into electrical energy. Fuel cells achieve higher efficiency (compared to conventional sources) and have the ability to work without greenhouse gas emission. These advantages make fuel cells an attractive source of future applications. The biggest disadvantage is in the high price of used catalytic materials and ionexchange polymer membrane. Catalytic materials consist of a catalyst and support material, typically carbon material. In commercial application is used for example carbon Vulcan XC-72. Our previous research in the area of building materials showed, that carbon Chezacarb A and Chezacarb B by Unipetrol RPA Ltd. can be used as a cheapest alternative to commercial used carbon Vulcan XC-72. These materials have comparable conductivity and structural properties.

Experimental

Preparation and measured of catalytic ink

We prepared the mixtures of carbon and 96% acid H_2PtCl_6 in ratios 1:20, 1:10, 3:20, 1:5 for each carbon materials (Vulcan XC-72, Chezacarb A, Chezacarb B). This correspond to Pt loading 2,3 wt%; 4,7 wt%; 7 wt%; 9,4 wt%. Resulting mixtures were insert for 0,5 hour into the furnace heated at 400°C. After that, each 100 mg catalytic material was diluted on the suspension (catalytic ink) by adding 2,6 ml water and 1,3 ml isopropylalcohol.

5 µl of suspension was dropped on tip of rotating ring disc electrode. Active area of electrode is 19,6 mm^2. Materials were measured in 1M H_2SO_4 with standard calomel electrode as reference. Solution was saturated by bubbling H_2.

Preparation and measured of MEA structures

MEA structures were prepared on base Nafion® membrane and as diffusion layer was used carbon cloth, which was cover with PTFE in amount 0,33 mg PTFE per cm^2. Catalyst ink was coated on carbon cloth using spraying technique. Nafion® membrane and carbon cloth coated by catalyst ink were pressed at 80°C and pressure 4 kN.

Active region of MEA structures is 4,4 cm^2. Before start measurement, MEA structure was inserted into distilled water for 2 hours. All load characteristic was measured at 50°C.

Result and discussion

Fig.1 showed cyclic voltamogram of catalytic materials with different type of carbon. On the catalytic activity can be deduced form the slope in the beginning of the voltammetric curves. The highest catalytic activity have sample with carbon Vulcan XC-72. The lowest activity showed carbon Chezacarb B.

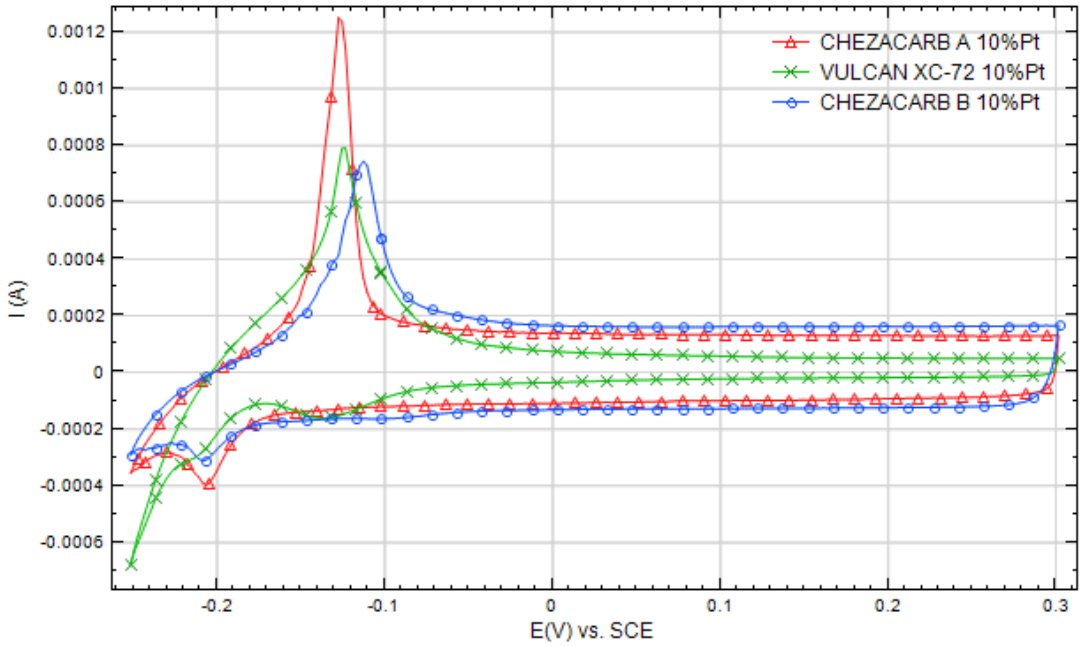

Fig. 1: *Cyclic voltamograms of catalytic materials with different type of carbon for 4,7 % Pt loading*

Fig.2 presents the load characteristic of MEA structures s 4,7 % Pt loading. MEA structures with Carbon Vulcan XC-72 have the best power characteristic, but carbon Chezacarb A have comparable characteristic with smaller amount of catalytic material in cm^2. MEA structure with Carbon Chezacarb B, have the lowest power characteristic. This MEA have the biggest over potential loss, which are caused by low electrode kinetics. Carbon Chezacarb A and commercial used carbon Vulcan XC-72 have almost the same over potential loss.

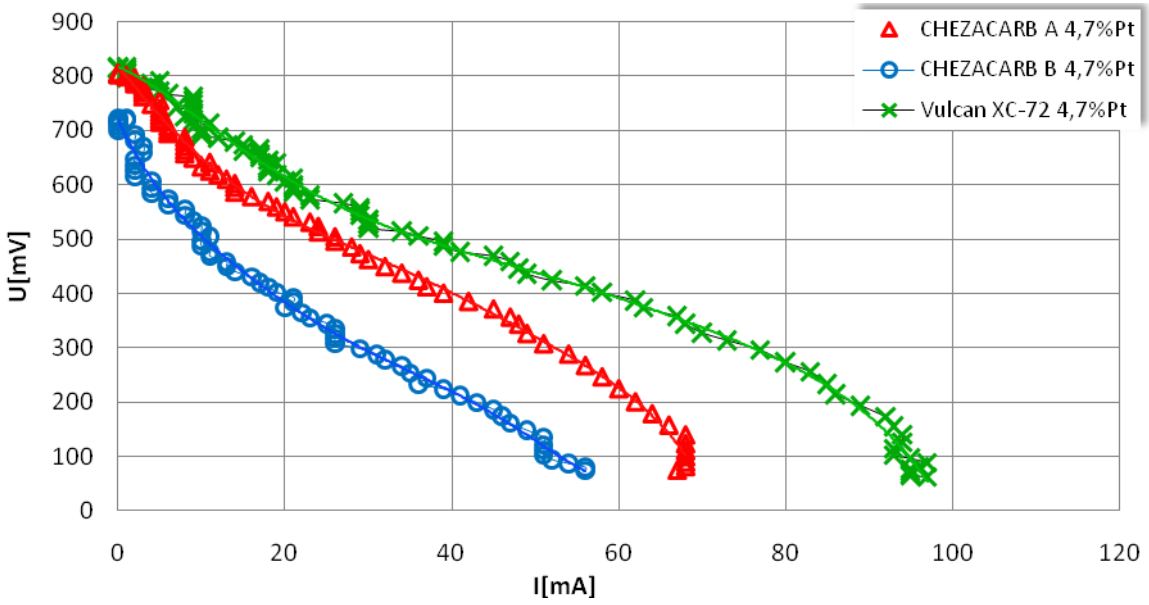

Fig. 2: *Load characteristics of MEA structures with different type of carbon for 4,7 % Pt loading*

In Tab.1, we can see measured parameters such as maximal current, maximal voltage, maximal power ect. Because each MEA structure have different amount of catalytic material, the most important values are power per gram catalytic material. P_{Pt} is power per gram of platinum. From this value we can see efficiency of platinum catalyst

Tab.1: *Table with measured parameters of all of type MEA structures*

CHEZACARB A								
Contain Pt [%]	m [mg]	Imax [mA/cm^2]	Umax [mV]	Pmax [mW/cm^2]	Ipmax [mA/cm^2]	Upmax [mV]	P [mW/g]	P_{Pt} [W/g$_{Pt}$]
2,3	37,9	7,3	853	2,5	5,4	479	316,6	12,66
4,7	36,9	15	788	3,5	10,6	322	452,6	9,05
7	34,5	13,8	858	4,2	10,4	397	582,6	7,77
9,4	37,2	41,5	769	8	24	332	1034,9	10,35
CHEZACARB B								
2,3	41,8	4,4	786	1,1	2,5	439	26,4	1,06
4,7	48,8	11,7	722	1,9	7,5	263	38,4	0,77
7	54,3	11,9	824	2,4	6,9	342	43,7	0,58
9,4	53,8	28,3	856	7	20	353	130,9	1,31
VULCAN XC-72								
2,3	55,9	10	774	3	6,7	444	255,8	10,23
4,7	55,2	20,2	818	5	14	360	434,8	8,7
7	57,8	31	813	7,4	17,1	435	610,7	8,14
9,4	64,7	81	900	19,6	57,1	350	1457,5	14,58

Conclusion:

MEA structures with different type of carbon materials and with different Pt loading were prepared. Catalyst with carbon Chezacarb B, have the lowest catalytic activity studying by cyclic voltammetry. This statement was confirmed by loading characteristic of prepared MEA structures. For this reasons, Chezacarb B isn't suitable as support material for fuel

cell. Chezacarb A achieved better result, especially for lowest Pt loading – 2,4% and 4,7%. This type of carbon seems to be an appropriate alternative to supported material for fuel cells.

Acknowledgement

This work was supported by Ministry of Education, Youth and Sports, Czech Republic project MSMT 0021630516, MSMT (LC 523), AV ČR (AV0Z40320502) and AV CR (KJB200320801)

References

[1] Material for fuel cells. Edited by Michael Gasik. Vyd. 1. Cambridge : Woodhead publishing limited, 2008. 498 s. ISBN 978-1-84569-330-5.

[2] NORES-PONDAL, Federico, et al. Catalytic activity vs. size correlation in platinum catalysts of PEM fuel cells prepared on carbon black by different methods. International Journal of hydrogen energy 34. 2009, 19, s. 8193-8203.

[3] SONG, Datong; WANG, Qianpu; LIU, Zhongsheng; EIKERLING, Michael; XIE, Zhong; NAVESSIN, Titichai; HOLDCROFT, Steven. A method for optimizing distributions of Nafion and Pt in cathode catalyst layers of PEM fuel cells. In Electrochimica Acta 50, 15 October 2004, Elsevier B.V., s. 3347–3358.

[4] SONG, Datong; WANG, Qianpu; LIU, Zhongsheng; NAVESSIN, Titichai; EIKERLING, Michael; HOLDCROFT, Steven. Numerical optimization study of the catalyst layer of PEM fuel cell cathode. In Journal of Power Sources , 2003, Elsevier B.V., s. 104–111.

NEXA FUEL CELL CHARACTERISTIC

P. Procházka, V. Minárik

VUT Brno, FEKT UVEE, Technická 8, 616 00 Brno, Czech Republic

Corresponding author: Petr Procházka (prochazkap@feec.vutbr.cz)
Phone Number: +420 54114 2536

Introduction

This article deals with detailed description of results from measurement on the NEXA fuel cell to get more detailed pictured about it. Statistic and dynamic characteristics where measured for the experimental determination of the behavior and characteristics of this fuel cell. The inner resistance was measured too.

Fuel cell

There comes to direct conversion of inner energy of the fuel to the electric energy based on electrochemical actions in the fuel cell. Based on this fact, these cells are similar to batteries. The basic difference is in the fact that chemical mediums are delivered to the cell from outside during the function. Both electrodes are like catalysts of chemical metamorphoses and they do not get used and hold they chemical structure during function. Fuel cells can work without any time limitation from the theoretical view. However, from the practical view is by the influence of soiling of the polymer diaphragm the working live limited.

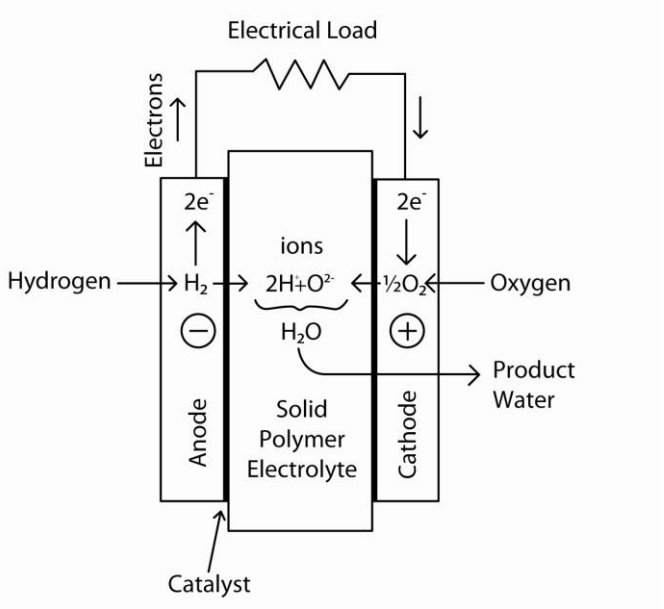

Fig. 1: *Principle function of the fuel cell (inspirited by [1]).*

The principle function of the fuel cell is easy. There is supplied fuel on the negative electrode. Like the fuel, we can use hydrogen H_2, coaly oxide CO, hydrazine N_2H_4,

methanol CH_3OH or some of the metals like sodium Na, magnesium Mg, zinc Zn and cadmium Cd. The fuel is on the negative electrode oxidizing and his atoms are releasing (by using of catalysts) one or some electrons from the valence orbit. The released electrons (representing electrical current) are moving to the positive electrode thru the output circuit. Positive electrode is supplied with oxidant. In general oxygen O_2, but it can be also chlorine Cl_2, oxide mercuric HgO, oxide manganese MnO_2. Reduction is in progress here (atoms of oxidant are accepting free electrons) by the reaction with the positive ions in the same time, which are getting to cathode thru electrolyte. The chemical reaction stops when the flow of the output current aborts. This chemical reaction is called "cold burning". The gas fuel, most of the time hydrogen is supplied from one side of the cell and the oxidant (oxygen, but from the practical view most of the time air) from the other. There is electrolyte from special plastic film in acidic or alkaline solution between both electrodes. The goal of it is also to avoid the contact of bout gases. Electrolyte is an electric insulator, which has to guarantee that the electrons will exchange only thru the outside current circuit. Between the electrodes arises voltage of 1,2V. We connect the cells in series to "bundles" to get the required voltage. There are bipolar plates between cells, which are conducting current and caulk them from each other.

Measurements were executed on fuel cell Nexa (Figure 2.). The cell affords the nonadjustable nominal power of 1,2kW. The basic parameters of the cell are in Table 1.

Fig. 2: *Hydrogen fuel cells Nexa build in a hydrogen car SEM H2.*

Tab. 1: *Parameters of hydrogen fuel cell Nexa.*

	Rated Power		1200W
	Voltage	Operating voltage range	22V to 50V
		Voltage at Rated Power	26V
	Start-up Time	Minimum time to achieve Rated Power from a Cold Start condition	2 minutes
Emissions	Noise	Maximum noise emission at 1m	72dBA
	Water	Maximum quantity of liquid water produced at Rated Power	870 mL/hr
Lifetime	Operating Life	Minimum number of operating hours before EOL	1500 hours
	Cyclic Life	Minimum number of start-up & shut-down cycles before EOL	500
	Shelf Life	Minimum storage (non-operation) before EOL	2 years

Load characteristics

Load and static characteristics represent the steady state of fuel cell by different loads. Measurement was executed by constant temperature and the final diagram is on the Figure 3.

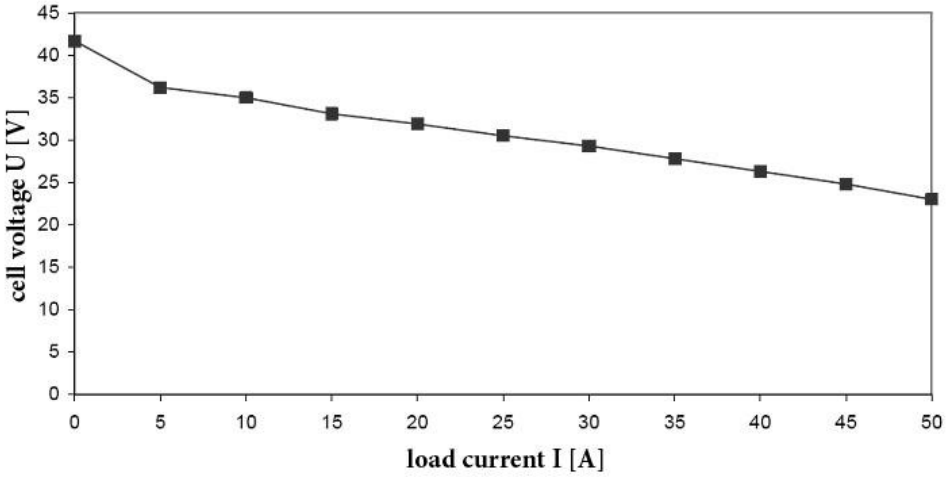

Fig. 3: *Fuel cell load characteristics.*

It is obvious from the diagram, that the fall of voltage is constant from the value of 5A and there for it is possible to interpolate the values without to make a big mistake. By using a simple formula (1) and the curve addiction, we can set the inner dynamic resistance R_d =0.29Ω of the fuel cell.

$$R_d = \frac{\Delta U}{\Delta I} \qquad (1)$$

Dynamic characteristics

Diagrams on figures 4 and 5 represent values measured by step loading and step loading off the fuel cell.

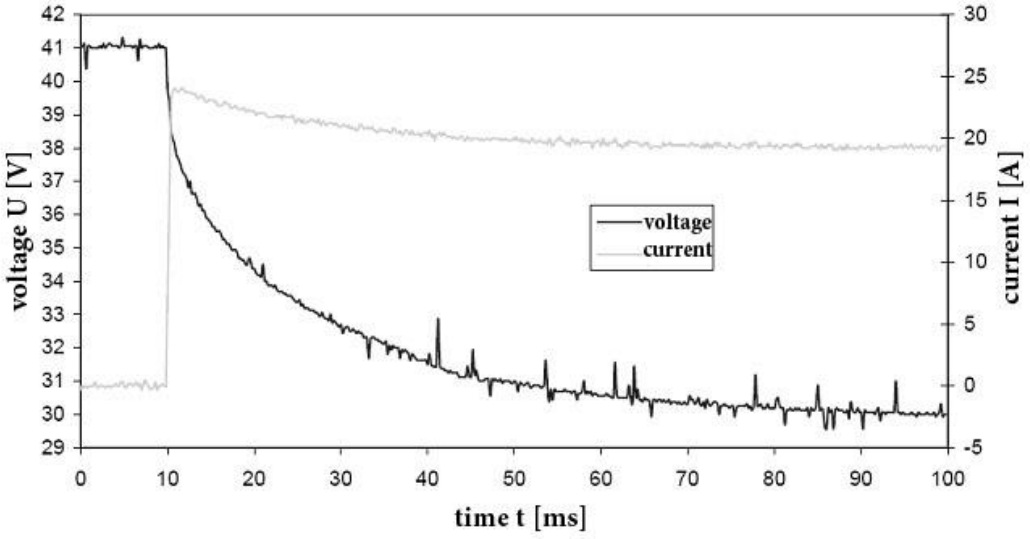

Fig. 4: *Adjunction of 20A load.*

The increase of the current is radically, all most by step, but the voltage is falling slowly as shows Figure 4. It is by virtue of inner capacity of fuel cell. The load was resistive. Higher current by adjunction of load is caused by higher cell voltage.

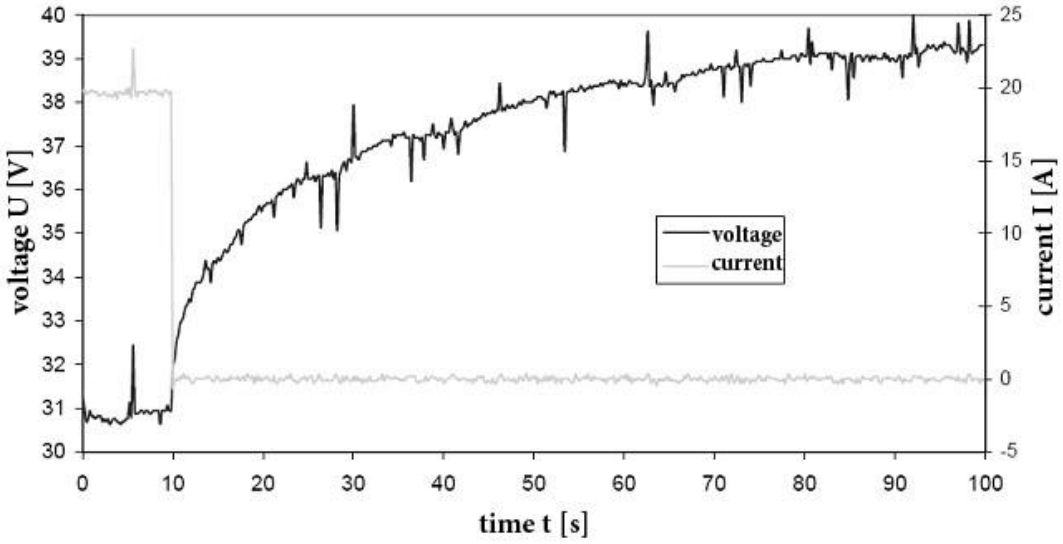

Fig. 5: *Disconnection of 20A load.*

The reason for the slower increasing of the cell voltage is charging of inner capacity, as shows Figure 5. Moreover, the charging process is slower than discharging process, which is given by the inner consumption of the fuel cell.

Measurement of internal fuel cell impedance

The followed diagrams show measured values by four different loads, than on the cell turned off and on designed substitution diagram of fuel cell.

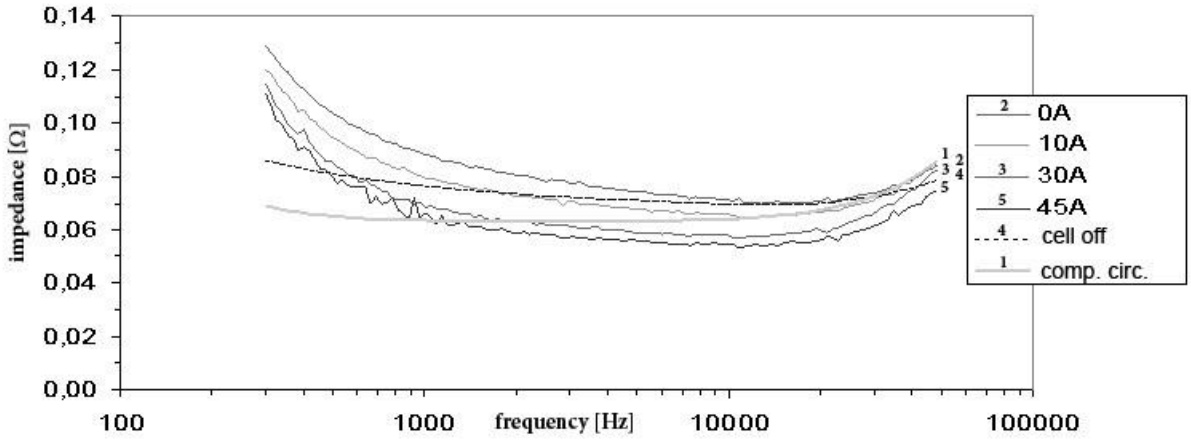

Fig. 6: *Dependency of fuel cell impedance modulus on measured signal frequency.*

The impedance modulus shows Figure 6. It is obvious that the modulus is falling until the frequency of 13 kHz. The steepness of falling is harder until the frequency of 1 kHz. After the frequency of 13 kHz is the modulus rising. The impedance modulus is falling down with the rising load.

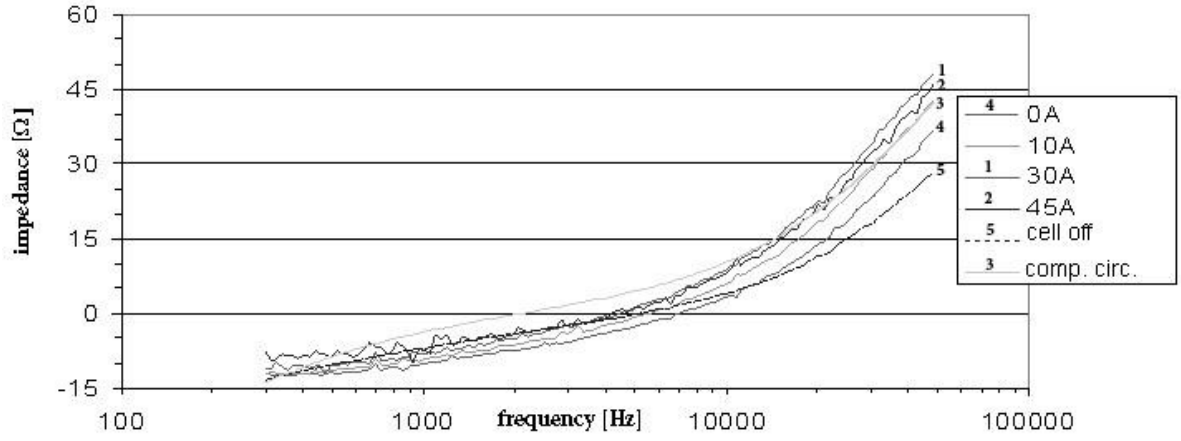

Fig. 7: *Dependency of impedance phase of the fuel cell on the measured signal frequency.*

The phase of impedance shows Figure 7. We can tell that the cell is acting like capacity under the frequency of 5500 Hz and upward of this frequency is acting like inductance. Phase is with the load rising up. That means that frequency with zero phases is falling with load.

The substitution diagram of fuel cell has been set based on measured values by different loads. The circuit is just approximate, because we are not possible to formulate the active resistance changing with frequency and characteristics are changing with load. There for have the substitution diagram aberrancies by low frequencies from the measured values. The schematic of the substitution diagram shows Figure 8.

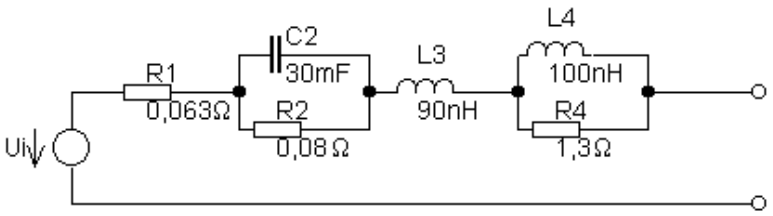

Fig. 8: *Fuel cell substitution diagram.*

Conclusion

The article present results of measurement of static and dynamic characteristics of the fuel cell. The measured values of inner resistance are presented too.

This research has been supported by the European Commission under the ENIAC CA-E3Car-2008-120001 E3CAR - Nanoelectronics for an Energy Efficient Electrical Car project. Further this was supported by the project MSM0021630516 “Zdroje, akumulace a optimalizace využití energie v podmínkách trvale udržitelného rozvoje”.

References

[1] Nexa Power Module User’s Manual, 16.6.2003, MAN5100078

STUDY OF MANGANEESE OXIDES PROPERTIES BY THE EQCM METHOD

D. Pléha[1], V. Novák [1]

[1] Department of Electrical and Electronic Technology, Brno University of Technology, 602 00 Brno

Corresponding author: Vítězslav Novák (novakv@feec.vutbr.cz)
Phone: +420 541 146 121, Fax: +420 541 146 147

Introduction

Manganese dioxide has a great use in batteries as a positive electrode. Types of electrolytic manganese dioxide used in this sphere are EMD and γ-MnO_2. Electrolytically deposited layer is catalytically active and there is the following reaction:

$$MnOOH + OH^- \leftrightarrow MnO_2 + H_2O + e^- \quad (1)$$

However, the reaction is rather unstable and the cycling effect causes its dissolution. All forms prepared at low temperatures contain relatively large amounts of water. For the use in lithium batteries, it is necessary to remove this water to prevent transition to inactive β-phases, e.g. by heating to a temperature of 300 °C. Most production is currently based on electrochemical oxidation of manganese salts.

Removal of structural water in the electrodeposition and cyclic voltammetry is important for further development. Using the electrochemical quartz crystal microbalance (EQCM) can clarify the changes in weight during the electrodeposition and cyclic voltammetry. We are also able to examine the effect of dopants on the stability of the disposed oxide and other relevant parameters.

Experimental

The measuring centre was composed of a VSP potentiostat, a computer with programming environment, a microbalance QCM 200 and a 5 MHz oscillator QCM25. Electrodeposition was carried out on platinum crystals with the contact area size of 1.37 cm^2. The resonant frequency of the crystal is 5 MHz and its sensitivity is 56.6 Hz μg^{-1} cm^2. Electrodeposition was performed in 0.1 M MnSO4 solution in distilled water. Cyclic voltammetry was performed in 1 M KOH. Hg / HgO electrode was used as the reference electrode. The method used was based on the measurement of electrolytically disposed manganese dioxide to which divalent metal salts were added during the electrodeposition. The aim of the work was to measure the solution and observe how the dopants used affect the properties of the resulting oxide in terms of size of the transferred charge and cycling stability.

Tab. 1: *Dopants charges for the preparation of the test solution for electrodeposition*

Sample designation	Dopant used	Backfills	
		1 M $MnSO_4$	0,01 M dopant
MnO_x	-	1,69 g	-
MnO_x + Co	$Co(NO_3)_2.6H_2O$	1,69 g	0,291 g
MnO_x + Mn	$Mn(NO_3)_2$	1,69 g	0,251 g
MnO_x + Cu	$Cu(NO_3)_2.3H_2O$	1,69 g	0,241 g
MnO_x + Ag	$AgNO_3$	1,69 g	0,169 g
MnO_x + Mg	$Mg(NO_3)_2.6H_2O$	1,69 g	0,256 g
MnO_x + Zn	$Zn(NO_3)_2$	1,69 g	0,261 g

Results and Discussion

Redox reactions of the material deposited on the electrode are limited by quantities of substance that can participate in the reaction. Quantities of reactive substances correspond to the peak area, which doesn´t depend on the scan rate change.

Quantity of the portable charge in the reductive branch does not correspond to the quantity of charge q in the oxidative branch; hence the process can be described as hardly reversible. The biggest peak area on the reductive branch had the MnOx + Ag sample.

In cyclic voltammetry the peak area due to repeated measurements for all samples decreased. The reason why there is a decrease in charges may be that the negative potentials lead to the dissolution of the active mass.

All materials disposed are catalytically active. This is reflected in the wave of oxygen reduction between -0.15 – 0 V against the reference electrode Hg / HgO. The highest value of the E_{ON} onset potential had a sample with the addition of dopant $Zn(NO_3)_2$.

In Figure # 1 the cyclic voltammetry for a sample MnO_x, MnO_x + Zn and MnO_x + Mg is depicted. The chart clearly shows that the MnO_x + Zn sample has a large influence on the final course of cyclic voltammetry.

Tab. 2: *Summary of wave and peak analysis parameters, at the scan rate of 10 mV/s on platinum crystal.*

Sample	$E_{1/2}$ [V vs. Hg/HgO]	I_{lim} [mA]	$\alpha \cdot n$ [-]	q mC	E_{ON} [V vs. Hg/HgO]
MnO_x	-0,043	-0,034	1,766	-2,882	-0,016
MnO_x + Co	-0,044	-0,056	0,036	-0,113	-0,010
MnO_x + Mn	-0,060	-0,384	2,221	-2,693	-0,017
MnO_x + Cu	-0,058	-0,244	1,69	-1,673	-0,021
MnO_x + Ag	-0,062	-0,454	2,722	-4,092	-0,022
MnO_x + Mg	-0,040	-0,028	0,288	-0,016	-0,015
MnO_x + Zn	-0,033	-0,262	1,754	-1,548	-0,005

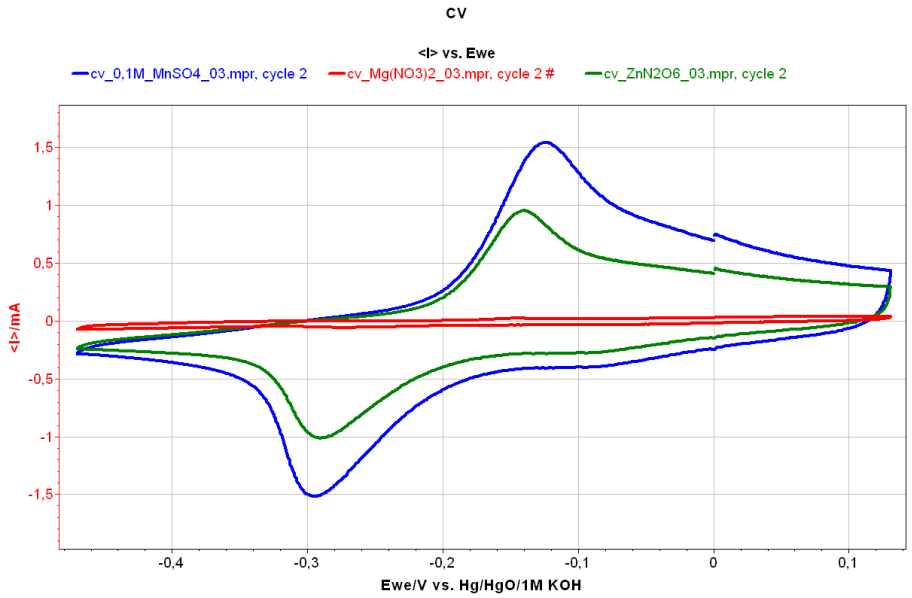

Fig. 1: *Cyclic voltammetry of the sample MnO_x + Zn and MnO_x + Mg, scan rate 10 mV/s, a solution of 1 M KOH, platinum crystal with an electrolytically coated layer of MnO_2, auxiliary electrode Pt, reference electrode Hg/HgO, 2nd cycle.*

Using the QCM made it possible to determine how the used dopants influence the deposited layer during cyclic voltammetry.

The smallest change in weight was achieved with the MnO_x + Mg sample, when there was a decrease in weight between the initial and final scan of 0.21 μg. With the MnO_x + Mn sample, the decrease in weight after six cycles was equal to 2.67 μg, which is 94.87 % of the total deposited layer. The greatest weight decrease was noticed in MnO_x + Cu sample. With the MnO_x + Zn sample, which had very good properties at the wave and peak analysis evaluation, a decrease of 10.17 μg between the initial and final scan was observed. Compared with the weight loss in MnO_x sample, the MnO_x + Zn sample in the first three cycles was more stable and there was not such a large weight loss. In the time of 450 s between the third and the fourth cycle there was a rapid weight decrease of about 5 μg. In subsequent cycles there was a minimal change in weight. The rapid decrease in weight could be caused by the layer unstuck from the crystal due to its structure disruption. Figure 2 shows a chart of weight change in MnO_x + Zn sample and MnO_x sample in cyclic voltammetry. From the chart in Figure 2 is apparent that the repetitive scan causes weight decrease, therefore the ongoing electrochemical reaction is not fully reversible. With the increasing number of cycles the weight loss occurs, but the difference between the top and bottom gets smaller with each successive cycle. From the charts is easily recognizable whether the deposited layer is stable or unstable. In MnO_x, MnO_x + Ag, MnO_x + Cu, and MnO_x + Zn samples a certain period of cycles with weight loss was observed, therefore with a certain stable layer. In the other samples there was visible layer instability and rapid changes in weight. Samples with the unstable layer, MnO_x + Co and MnO_x + Mg, were clearly recognizable even on the voltammogram and massogram, where they significantly differ from the stable samples outputs.

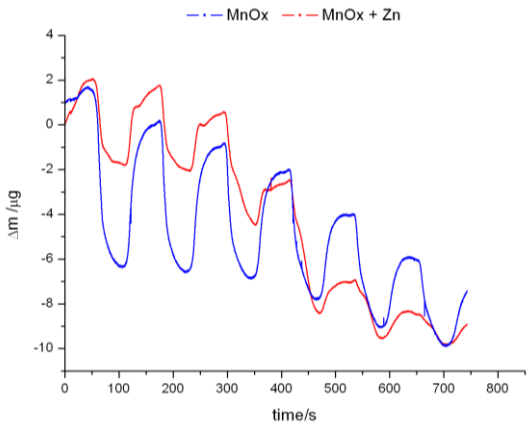

***Fig. 2**: Time course of weight loss during cyclic voltammetry, Pt crystal with a layer of MnO_2 in 1M KOH solution, auxiliary electrode Pt, reference electrode Hg/HgO, scan rate 10 mV.*

Conclusions

Measurement and subsequent evaluation found a gradual weight loss caused by dissolution of the deposited layer, suggesting that ongoing electrochemical reaction is not too reversible. It was found that the sample doped with manganese and magnesium had the smallest weight loss during cyclic voltammetry. Sample doped with zinc, which had a higher catalytic activity, had during the first three cycles a good stability with minimal weight loss. During the remaining cycles, however, a weight decrease of the applied layer occurred in this sample, which could be caused by disruption of the crystal layer. In the sample doped with cobalt and copper the largest weight loss during a 6-cycle voltammetry was found.

From the results it was evident that with the increasing number of cycles, weight loss occurred, but the difference between the maximal and minimal weight declined with each successive cycle.

Acknowledgements

Ministry of Education of Czech Republic, Project MSM002130516

References

[1] PLÉHA, D. Měření vlastností oxidů manganu (MnOx) metodou EQCM. Brno: Vysoké učení technické v Brně, Fakulta elektrotechniky a komunikačních technologií, 2010.

[2] OWEN, Michael P.; LAWRENCE, Geoffrey A.; DONNE, Scott W., *An electrochemical quartz crystal microbalance study into the deposition of manganese dioxide.* Callaghan: University of Newcastle, 2007.

[3] CHABRE, Y.; PARMETIER, J..; *Structural and electrochemical properties of the proton / γ-Mn02 system.* Laboratoire de Spectrometrie Physique, Universite Joseph Fourier and CNRS BP 87, France and Institut Laue-Langevin, BP 156,38042 Grenoble, France.

[4] Novák, V..; *Katalyzátory na bázi MnOx pro palivové články*. 2008, 76 s., Ústav elektrotechnologie FEKT VUT v Brně.

11th ABAF

BRNO 2010

Advanced Batteries, Accumulators and Fuel Cells

Electrolysis

ONE-DIMENSIONAL NANOSTRUCTURES AS ELECTRODE MATERIALS FOR WATER ELECTROLYSIS

R. Inguanta, G. Ferrara, S. Piazza, C. Sunseri

Dipartimento di Ingegneria Chimica dei Processi e dei Materiali
Università di Palermo, Viale delle Scienze, 90128 Italy

Corresponding author: Germano Ferrara (g.ferrara@dicpm.unipa.it)
Phone: +3909123863732, Fax: +390917025020

Introduction

Today, about 95% of the hydrogen comes from reforming of natural gas, the remainder being high-purity hydrogen produced by water electrolysis. In order to gain benefits of a hydrogen economy, this must be produced cleanly, efficiently and affordably from renewable resources, preferentially available close to the end-users. The goal is a sustainable cycle of hydrogen production and use: in the first stage of the cycle, hydrogen is produced from renewable resources and then used to power a fuel cell [1]. This cycle produces no pollution and no greenhouse gases. In this context, development of low size electrolysers producing high-purity hydrogen with high efficiency and low cost is of great importance. Electrode materials play a fundamental role in influencing electrolyser performances; consequently, in the last years considerable efforts have been made to obtain highly efficient and inexpensive catalysts. To reach both goals, we have developed nanostructured electrodes constituted by PdCo alloys (cathode) and RuO_2 (anode) that could be potentially used in Proton Exchange Membrane Electrolyzers (PEMEL). In fact, PdCo alloy is a valid alternative to Pt for hydrogen evolution [2], whilst ruthenium oxide is one of the most active catalysts for oxygen evolution [3].

In this work, both these materials were electrodeposited using two different types of support: carbon paper, in order to fabricate a porous nanostructured film, and anodic alumina membrane, in order to obtain regular arrays of nanostructures. The goal was to obtain porous electrodes having very large active surface area with little amount of material, and hence with a low cost. We will show that the electrochemical method is an ideal technique to obtain nanostructured materials with good catalytic properties for both hydrogen and oxygen evolution reactions. Besides, for electrodeposition of both RuO_2 and PdCo alloy, an electrochemical cell has been specifically designed in order to employ only 0.5 mL of electrolytic solution. The deposition from a very small volume of solution was specifically addressed owing to the high cost of precious metal compounds, which could be of some relevance from an applicative point of view. We will show, also, how PdCo alloy composition can be controlled by adjusting electrodeposition parameters, like bath composition, current density and time. In the case of RuO_2 electrodeposition, interesting results have been obtained when alumina membranes were used as support. In fact, we have obtained ruthenium oxide nanotubes in a single-step by a simple, low cost procedure that is easily scalable [4]. The main results concerning fabrication process and the morphological and chemical characterizations will be presented.

Experimental

A two-electrode cell, specifically designed, was used in order to reduce electrolyte volume. For this aim, we have used a tube glass with a screw-thread (SVL® 15) that was modified in order to get a pipe-like support [4]. Two different types of support (carbon paper (CP) and anodic alumina membrane (AAM)) were used as working electrode with an area exposed to the solution of 0.5 cm^2. The cathodic electrodeposition of RuO_2 and PdCo alloy was carried out in aqueous solution at room temperature with the experimental conditions reported in Table 1.

Tab. 1: *Electrodeposition conditions of RuO_2 and PdCo alloy.*

	Substrate	*Electrolyte*	*c.d. mA/cm²*	*Time*
	CP	$RuCl_3$	5	3h
RuO_2	AAM	Na_2NO_3		
	CP	$Pd(NH_3)_4(NO_3)_2$	1.56÷156	60÷1800s
PdCo		$CoSO_4$		

The crystallographic structure of samples was investigated by X-ray diffractometry (APD2000 ItalStructures,) while elemental composition was determined by energy dispersive spectrometry (EDS). Morphology was investigated using a scanning electron microscope (FEG-ESEM, QUANTA 200 FEI). Micro-Raman spectra were obtained at room temperature using a Renishaw spectrometer (inVia micro-Raman system). Electrochemical characterization, cyclic-voltammetry and chrono-potentiometry, were carried out in 2M H_2SO_4 aqueous solution, by PARSTAT 2273 P.A.R.

Results and Discussion

RuO_2 film and nanotubes (NTs) were fabricated in a single-step by electrogeneration of base [4]. In order to identify the deposit, XRD, EDS and Raman analyses were performed on as-prepared samples. In both Raman spectra of NTs and film, Eg, A_{1g} and B_{2g} vibration modes of RuO_6 structural units of the tetragonal form of RuO_2 were present. In the spectra, a weak and broad peak at 390 cm^{-1} are also present, that may be assigned to some hydrated form of ruthenium oxide. Results of Raman spectroscopy are summarized in Table 2, where position of Raman peaks are listed. In comparison to RuO_2 single crystal, all Raman modes show a red-shift attributable to the nanostructured nature of the as-deposited oxide. On the basis of these results, it can be inferred that deposit is a subnano-crystallyne, rather than isotropic amorphous RuO_2 likely partially hydrated. This conclusion is supported by the presence of characteristic peaks in the Raman spectra and the absence of RuO_2 peaks in the XRD patterns.

Tab. 2: *Raman modes position of as-deposited ruthenium oxide.*

	Raman Position / cm^{-1}			
	Eg	*A_{1g}*	*B_{2g}*	*Red-shift*
Film	515	624	695	13
Nanotubes	508	626	693	20
Single Crystal	528	646	716	/

Figure 1 shows FEG-SEM pictures of RuO_2 film (Fig. 1a) and NTs after total template dissolution (Fig. 1b). Fig. 1a shows that all fibers of CP were covered with RuO_2 deposit that, in many areas, led to the formation of a continuous and compact film. RuO_2 NTs are clearly visible in Fig. 1b: their population density is of the order of 10^{13} NTs m^{-2}. The mean external diameter is 210 nm and the tubular structure extends throughout the length of NTs, although mean wall thickness changes from 65 nm at the bottom to 40 nm at the top.

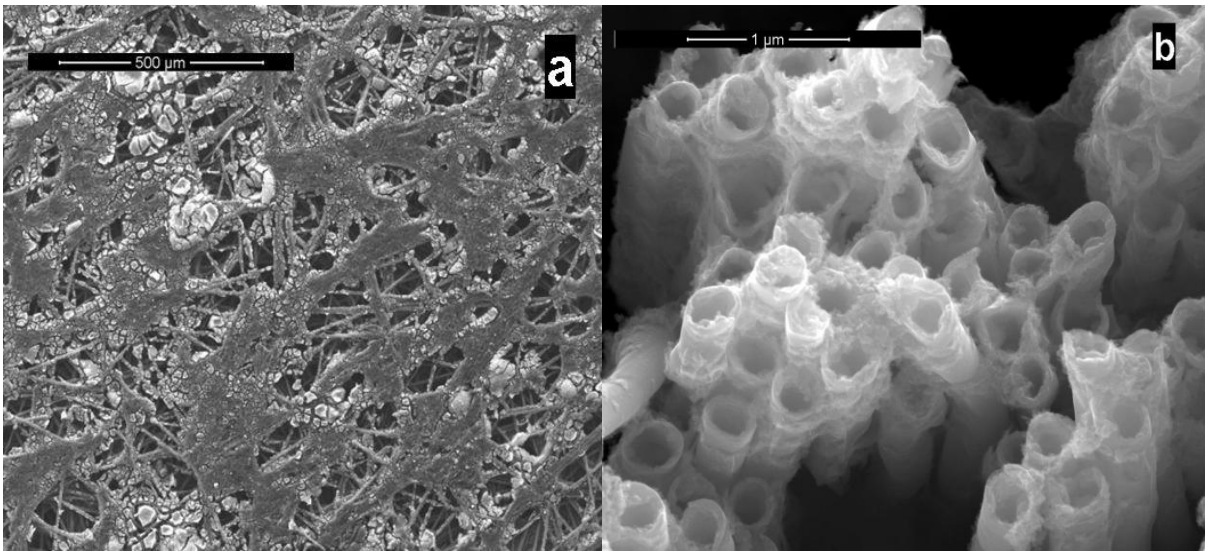

Fig. 1: *Morphology of RuO_2 film on CP (a) and NTs after total dissolution of AAM (b).*

As regards PdCo alloy, composition and morphology of deposit can be varied by adjusting electrodeposition conditions (time, electrolyte composition, current density). In particular, Figure 2 shows that morphology changed from nanoparticles (Fig. 2a), uniformly distributed on CP fibers, to a dense film (Fig. 2b) that fully covered fibers. We have found that 900 sec is the optimal deposition time because for longer time than 900 sec, we found that PdCo deposit was tending to detach from the fibers.

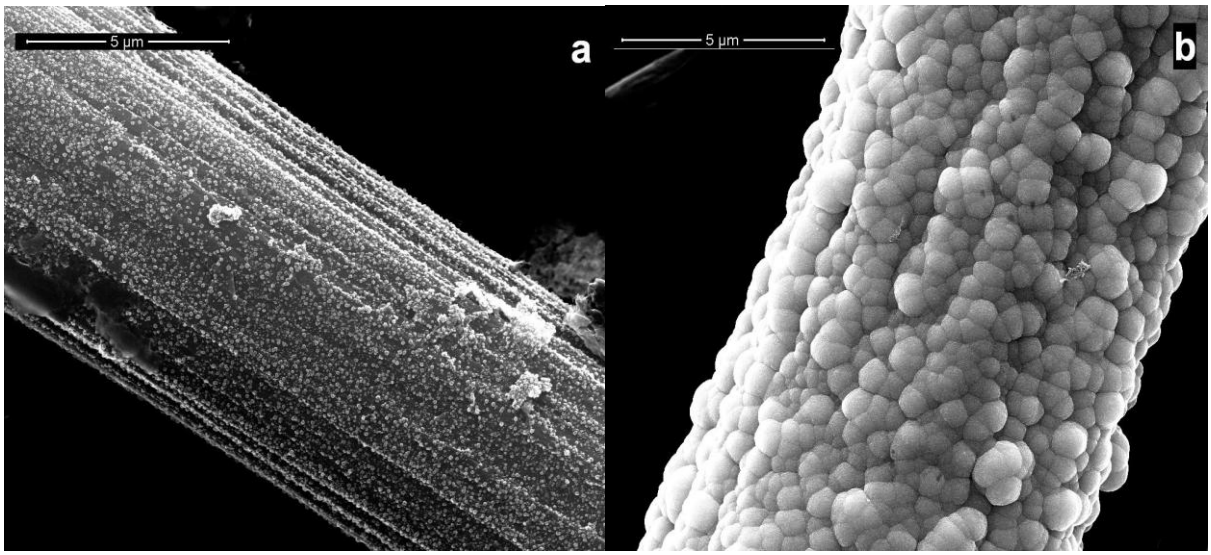

Fig. 2: *Morphology of PdCo alloy obtained at different electrodeposition conditions: (a) 60sec, 15.6 mA/cm^2; (b) 900sec, 15.6 mA/cm^2.*

Electrochemical behaviour of these deposits changed with alloy composition and morphology. As shown in Figure 3, PdCo alloys obtained at higher current density exhibit higher hydrogen evolution rate.

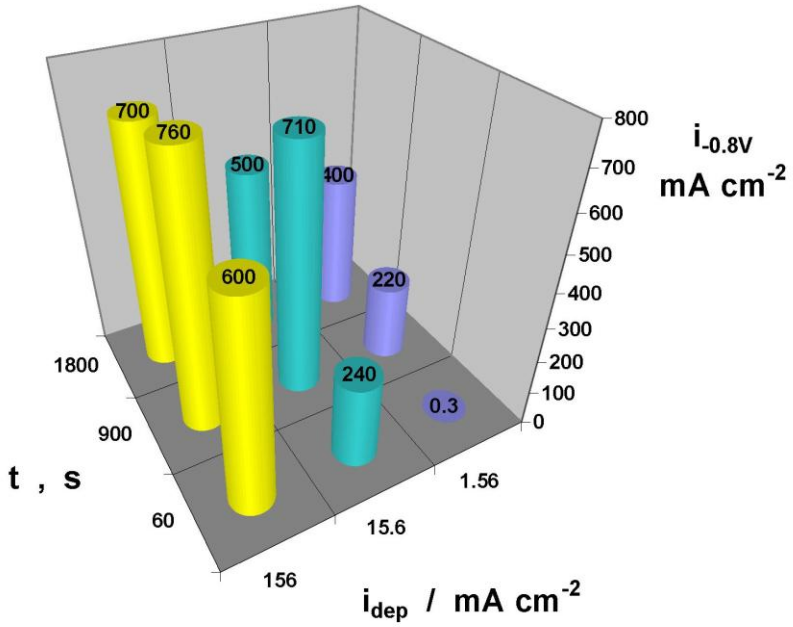

Fig. 3: *Current density at -0.8 V(NHE) for hydrogen evolution reaction on PdCo electrodes obtained at different electrodeposition conditions.*

Conclusions

Using a specifically designed electrochemical cell, we have fabricated RuO_2 and PdCo alloys in a single-step by galvanostatic deposition on two different substrates. This cell allows to reduce consumption of electrolyte containing precious metals and hence fabrication cost.

RuO_2 film and NTs were obtained with a nano-crystalline structure as confirmed by both XRD and Raman analyses. SEM investigations of NTs showed an uniform average external diameter with a wall thickness that changed throughout length.

PdCo alloys were obtained with different composition and morphology in dependence on electrochemical parameters. These electrodes, tested for hydrogen evolution reaction, showed different performance. Deposit obtained at higher current density exhibit higher hydrogen evolution rate.

Acknowledgements

This work was financially supported by Università di Palermo.

References

[1] National Renewable Energy Laboratory "New Horizons for Hydrogen" Research Review article 2003. Available at http://www.nrel.gov/learning/eds_hydrogen.html
[2] O. Savadogo, K. Lee, K. Oishi, S. Mitsushima, N. Kamiya, K-I. Ota, Electrochem. Comm. **6** (2004) 105.
[3] S. Song, H. Zhang, X. Ma, Z. Shao, R. Baker, B. Yi, Int. J. Hydrogen Energy **33** (2008) 4955.
[4] R. Inguanta, G. Ferrara, P. Livreri, S. Piazza, C. Sunseri, Submitted to Current Nanoscience.

RESEARCH OF MATERIAL FOR ELECTROLYZER

T. Knotek, J. Vondrák

Faculty of Electrical Engineering and Communication, Department of Electrotechnology, Údolní 53, 602 00 Brno, Czech Republic

Corresponding author: Tomáš Knotek (xknote06@stud.feec.vutbr.cz)

Abstract

The electrochemical properties were studied on Fe, Ni, non-corroding steel, nickel coated Fe, nickel-zinc alloy coated Ni (Ni-NiZn, leached Zn) and nickel (under layer)/nickel–zinc alloy coated (top layer) Fe electrodes (Fe-Ni-NiZn, leached Zn). Zn component was extracted from the layers by HCl solutions for their activation. Electrocatalytic properties of the layers were estimated by the current-voltage curves in 1M KOH solution at room temperature.

Key words

Electrode, electrolysis, alloy, NiZn, coating

Itroduction

Fossil fuels constitute the major part of energy sources consumed in the world today. These fuels cause environment pollution. On that account we must find new alternative source of energy. Hydrogen gas could be an alternative source of energy. One of the techniques of producing hydrogen is the electrolysis of water. However, this technique is quite expensive due to its high energy consumption. One improvement could be alkaline solutions in water electrolysis. And second improvement could be better electrode: large active surface area, electrochemical stability, good electrical conductivity and low overpotential, low cost and ease of use. Several active electrodes have been developed for hydrogen evolution, and the performance of nickel based is the best at all. If we use nickel alloy, it will be cheaper this way.

This work was created for better understanding of galvanic deposition of metals and electro catalytic properties of these depositions. This knowledge will be used to design the best electrodes for electrolytic cell for hydrogen production.

Experimental

Many methods are possible for coating layers. Chemical and galvanic deposition was used in this case. Chemical deposition was used to copper a nickel layers. Galvanic deposition vas used for NiZn alloy. NiZn alloys are very good for corrosion protective coatings. Electrical conductivity will be increased if we leach zinc component from NiZn alloy.

Ni-Zn alloys were electrodeposited, onto Fe and Ni electrodes, using a commercial alkaline electrolyte (SLOTOLOY ZN 80 - produced by Dr.-Ing. Max Schlötter GmbH & Co.KG, SRN) of composition strictly identical to the industrial electrolyte, at 32 °C temperature.

Chemical coating of nickel was created in plating bath SLOTONIP 70 A for 30 minutes at temperature 92°C. We can see operating conditions for each sample in table 1.

Tab. 1: *Operating conditions*

	chemical coating		galvanic coating NiZn		
Samples	**time [min.]**	**temperature [°C]**	**time [min.]**	**current density [A/dm2]**	**temperature [°C]**
Fe + Ni	30	92	-	-	-
Ni + NiZn	-	-	10	2	32
Fe + Ni + NiZn	30	92	10	2	32

The working electrode area varied according to the method of surface characterization. The plating cell was provided with an air bubbling. The samples were immersed after deposition in hydrochloric acid (5% HCl, for 10s) for their activation consisting in dissolution of zinc from them.

Experiments were carried out in a three-electrode cell with a capacity of 2 dm3 supplied by a PGSTAT12 Autolab potentiostat (ECO Chemie). The samples were connected as a work electrode, a Saturated Calomel Electrode was connected as a reference electrode and a platinum electrode was connected as a counter electrode. Samples were tested in the described way by means of cyclic voltammetry by GPES program.

Results and discussion

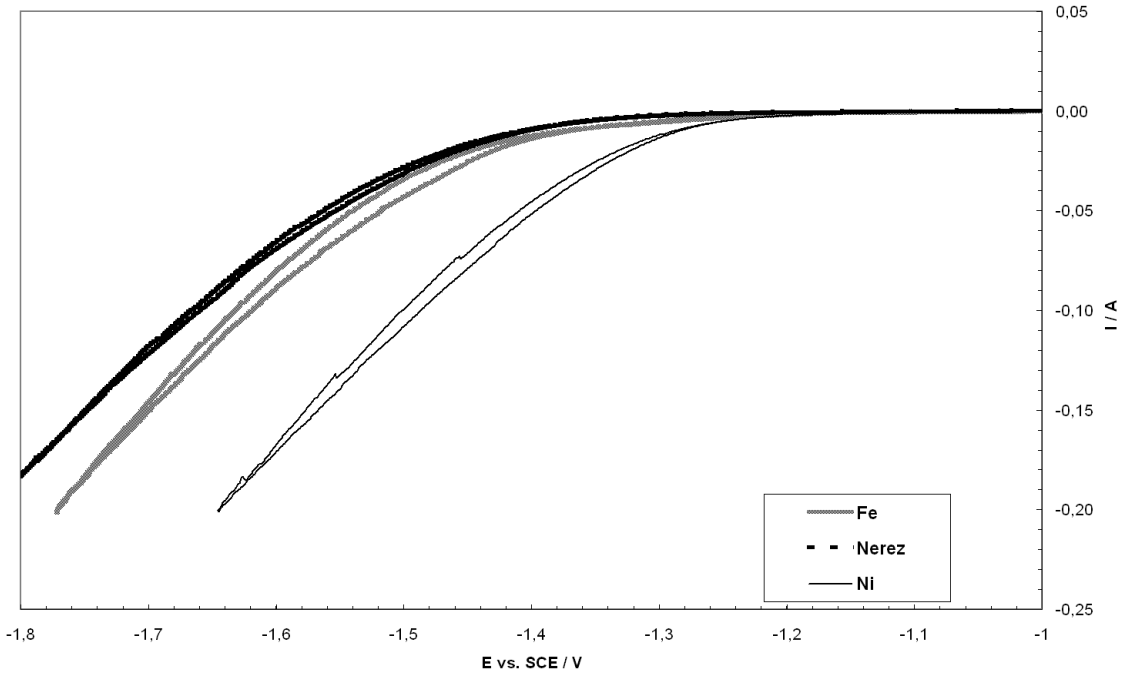

Fig. 1: *Voltage-current curves*

We can see a comparision of the three materials in graph 1. As we can see optimal material for hydrogen production at lowest consumption of energy is nickel. By this It was confirmed, that Ni is very suitable for an electrode system. We chose to create layers of nickel because pure nickel is very expensive. By modification of nickel-coated surface is possible to obtain major active surface. Nickel and alloys NiZn ware created. Alloy NiZn has a high corrosive protectiveness. We need it, because we use hydroxide as electrolyte in electrolyzer. Zinc component was leached from alloy by strong KOH.

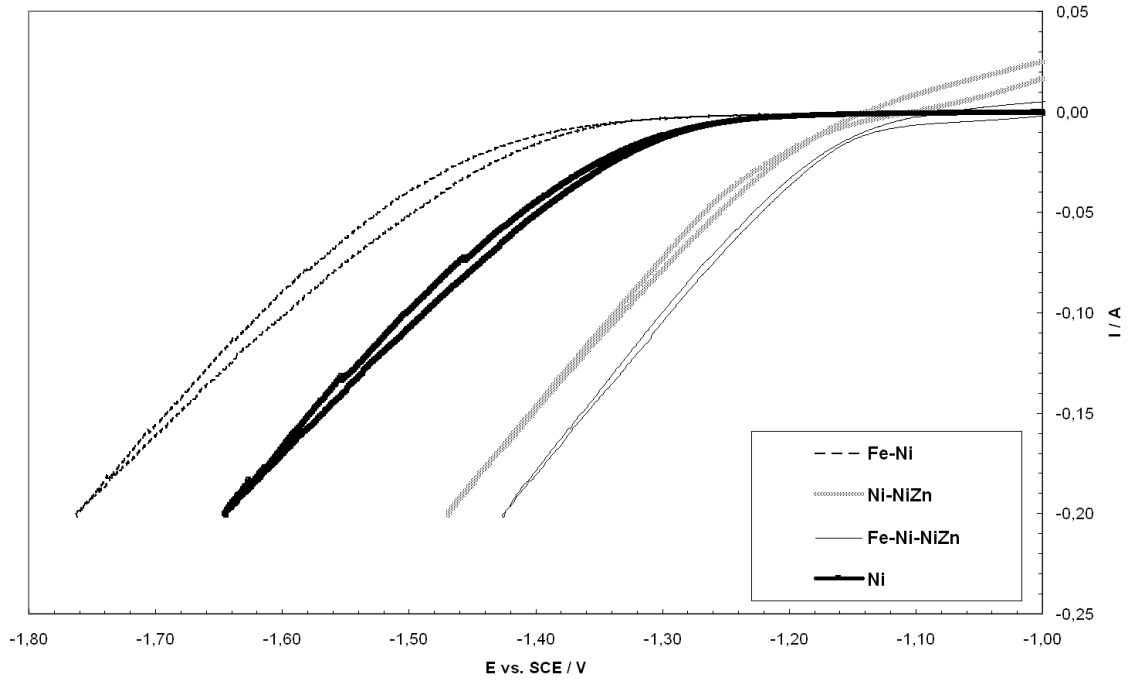

Fig. 2: *Voltage-current curves*

We can see curves of materials with layers in graph 2. Only the sample Fe-Ni was worse than pure Ni. It was caused by more phosphorus component in the deposit layer. It will be interesting to try galvanic depositing of nickel. The sample Fe-Ni-NiZn is the most acceptable. Difference potentials between pure nickel and Fe-Ni-NiZn are about 0,22 V.

Conclusion

Nickel is the best material for electrode on electrolysis waters, as we can see in graph 1. But nickel is very expensive so we must create nickel layers on cheaper base material. We can see in graph 2 that sample with 2 layers is better than the others. NiZn alloy has a good electrochemical stability and a better electrical conductivity then the others. This galvanic deposition will be used to create the best electrodes for electrolysis cell for hydrogen production. It is clear, that we can create suitable surface for electrodes. Hence, the reduction of energy by their use is possible.

Purpose of this work was to create galvanic deposits of metals with electro catalytic properties. This galvanic deposition will be used to create the best electrodes for electrolysis cell for hydrogen production. It is clear, that we can create suitable surface for electrodes. Hence, the reduction of energy requirement by their use is possible. Further, the starting preposition of activation by addition of zinc was proved successfully.

Acknowledgments

This work was supported by Grant Agency of the Czech Republic (grant NO. MSM0021630516)

References

[1] G. Vatankhah, J. Lessard, G. Jerkiewitz: Electrochimica Acta 48 (2003) 1613-1622
[2] Barek J., Opekar F., Štulík K. Elektroanalytická chemie KAROLINUM
[3] Regner A. Elektrochemické pochody v anorganickém průmyslu SNTL
[4] Ramazan Solmaz, Gülfeza Kardas: Hydrogen evolution and corrosion performance of NiZn coating, received in revised form 9 December 2005; Dostupné online z www.sciencedirest.com.
[5] Vladimír Krejčík: Povrchová úprava kovů I (Pro 2. ročník SOU), SNTL Praha 1987, 168 stran, 04-203-87
[6] Vladimír Krejčík: Povrchová úprava kovů I (Pro 2. ročník SOU), SNTL Praha 1988, 312 stran, 04-229-88

USE OF NONWOVEN TEXTILES AS MEMBRANES FOR ELECTROLYSER

M. Kunovjánek[1], J. Vondrák[1,2], M. Sedlaříková[1]

[1] Department of Electrical and Electronic Technology, University of Technology Brno, 602 00 Brno, Czech Republic
[2] Institute of Inorganic Chemistry of the ASCR, v. v. i., 250 68 Řež near Prague, Czech Republic

Corresponding author: Miroslav Kunovjánek (kunovjanek@phd.feec.vutbr.cz)
Phone: +420 605 933 898

Introduction

In this article we will deal with the production of hydrogen by decomposition of water into hydrogen and oxygen. Hydrogen can also be produced by other ways, for example processing of natural gas, but it is not as environmentally beneficial as electrolysis. In addition, by using electrolysis we are producing very clean hydrogen. Water is decomposed in a machine called Electrolyser. For our measurements a simple laboratory electrolyser, separated by an appropriate membrane, with two electrodes, has been designed,. Distance between electrodes is 2 cm and area of each is 25 square centimetres. Electrolyser was filled for the measurement of 1 MOL KOH electrolyte up to 80% of its height.

Experimental

For the electrolyser membrane we have a few basic requirements. The primary requirement is the absolute impermeability of produced gases to prevent formation of explosive mixture. What is also required is a sufficient strength and stability of parameters in a strongly alkaline environment. The membranes for electrolysis must also have ionic conductivity, which is necessary for decomposition of water into hydrogen and oxygen. Commercially produced membranes meet these requirements, but due to their high cost they are less available and their use would greatly raise the price of terminal equipment. The fabric used for membranes was non-woven fabric selected from the company BTP from Brno, specifically fabrics PDC 95, PEG 50, VPK PES / SOL, then the membrane produced by DEC company and last Sontara® membrane by DuPont company. Measurement of each membrane was realized in electrolyser under given conditions at constant current 400 mA for 24 hours.

During the measurements the level of electrolyte in the electrolyser was continuously monitored to avoid its loss and consequently to influence the measurements. Electrolyte was also continuously being changed, owing to its gradual degradation during the measurement. One of the negative properties of non-woven fabrics is their permeability to gases. This negative feature in our case is partly eliminated by sealing of a part of the membrane, which is not immersed in electrolyte, into gas impermeable plastic foil. In the final case we don´t separate two gases, but only the individual bubbles of gas dispersed in the liquid. Very important point in this case is the density of membranes fiber. The

following pictures are photos of each membrane under a microscope at a magnification of 90x.

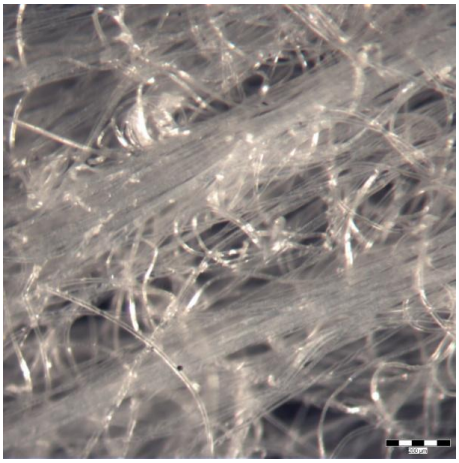

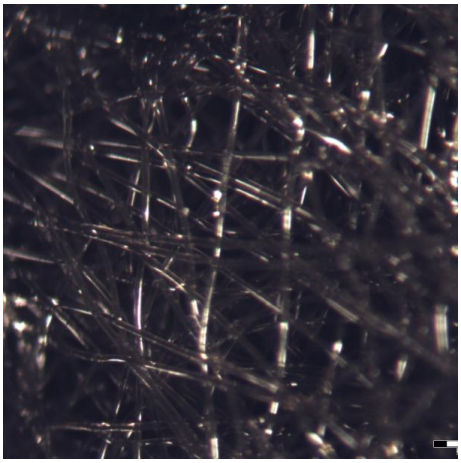

Fig. 1: *(left) DEK white*
Fig. 2: *(right) PEG 50*

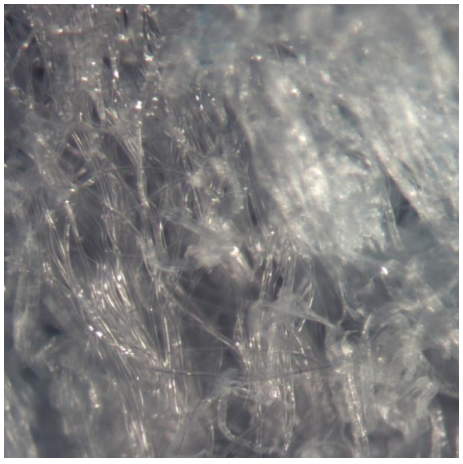

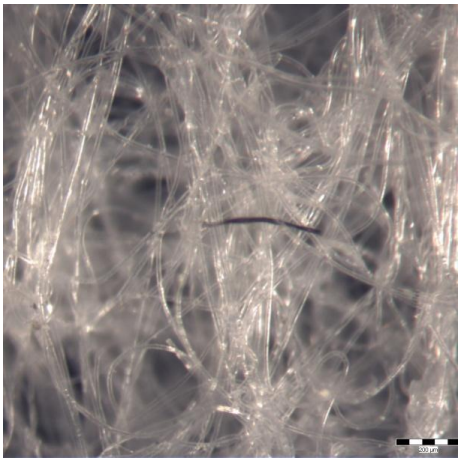

Fig. 3: *(left) Sontara® Dupont*
Fig. 4: *(right) PDC 95*

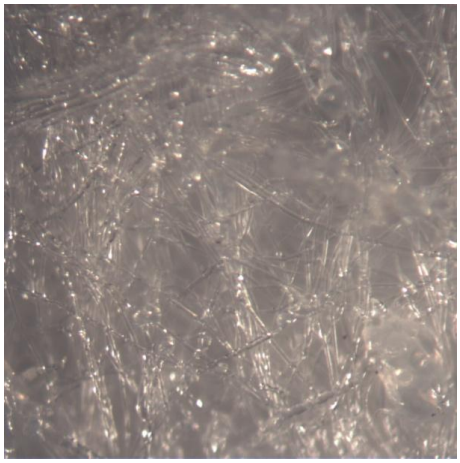

Fig. 5: *VPK PES/SOL*

You can see in the pictures that the greatest fiber density is that of the membrane VPK PES/SOL by BTP Company. The lowest density has the membrane PEG 50 by the same

company. Fiber density of other membranes is approximately the same. Generally speaking, if the fiber density is higher, the gas impermeability of membrane is better.

Results and Discussion

Membrane resistivity is factor which shows how membrane increases voltage of electrolyser if the current is constant and also how it reduces the overall efficiency of electrolysers. The following graph shows measurement of electrolyser voltage in time for various membranes.

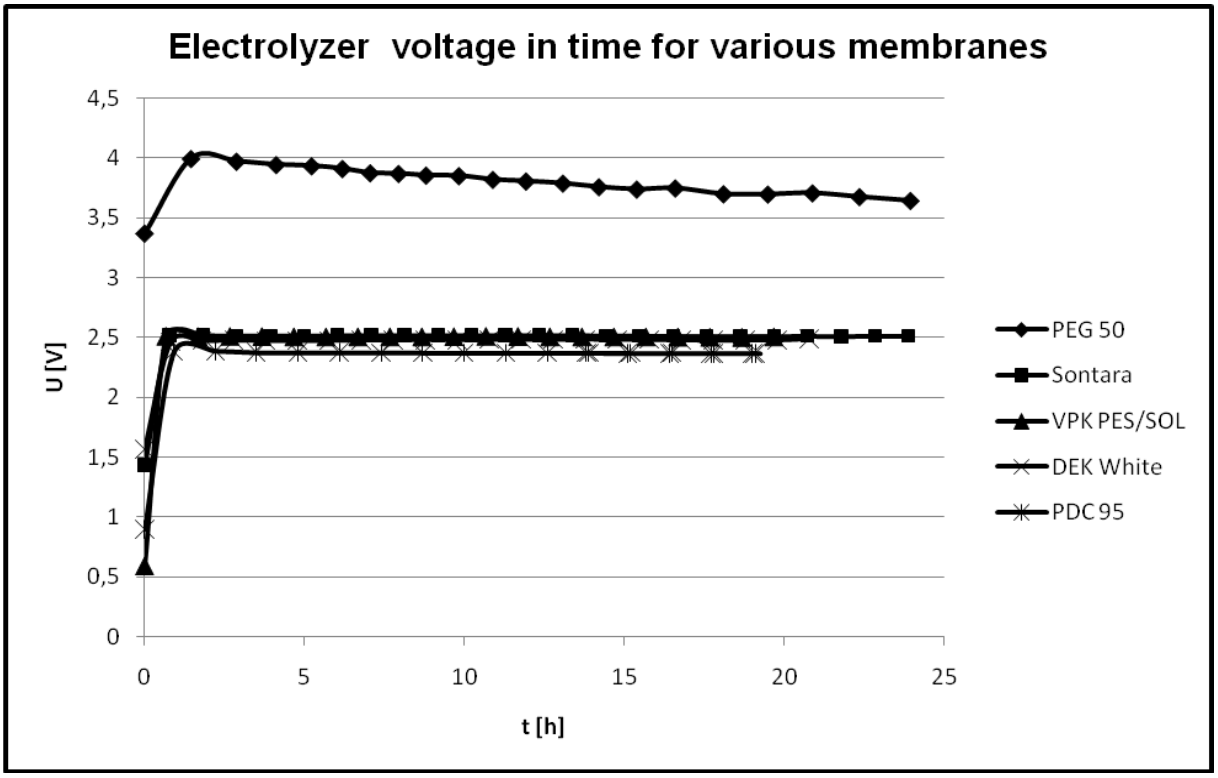

Fig. 6: *Electrolyser voltage in time for various membranes*

Before measurement, each membrane was dipped for 2 hours in the electrolyte to result in a perfect dipping. As the graph shows, the voltage waveform on electrolyser is at approximately the same for all membranes except membrane PEG 50. This membrane probably contains a certain proportion of conductive additives, which are behaving as another electrode in electrolyser. This fact causes higher electrolyser voltage when this membrane is used and the creation of gas bubbles in the surrounding membrane, which was verified visually during the measurements. Gas bubbles also cause a slight nonlinearity of electrolyser voltage in time, because their layer on the membrane restricts the passage of current and this creates a higher voltage drop on electrolyser. Electrolyser voltage with other membranes is linear and constant in time. The lowest voltage 2,38V was achieved by using membrane PDC 95 by the company BTP. For other membrane voltage was around 2.5 V.

Conclusions

Using measurement we ascertained, if it is possible to use non-woven fabrics as membranes for electrolyser. Most of the tested membranes proved to be suitable for this usage. The best results were achieved with the membrane PDC 95. By using this membrane electrolyser voltage was only 2,38V. Subject of further research will be hydrodynamic properties of membranes, especially for the throughput for generated gases.

The advantage of non-woven fabrics is their low price compared to commercial membranes. Using a non-woven fabrics as membranes for electrolyser would mean significant saving in design and manufacture of electrolysers. So, this equipment has become more affordable than using commercial membranes.

Acknowledgements

This article was supported by the Ministry of Education, Youth and Sports, Czech Republic (project MSMT 0021630516) and project FEKT-S-10-14

References

[1] VONDRÁK, J., SEDLAŘÍKOVÁ, M., BARATH, P.: Optimalizace a vývoj nového elektrolyzéru vody, Brno: Vysoké učení technické v Brně, zpráva grantu VaV SN/171/05 – příloha č. 4

[2] KUNOVJÁNEK, M. *Elektrolyzér pro výrobu vodíku.* Brno: Vysoké učení technické v Brně, Fakulta elektrotechniky a komunikačních technologií, 2008. 52 s. Vedoucí diplomové práce doc. Ing. Marie Sedlaříková, CSc.

THE INFLUENCE OF PURINES ON REDOX PROPERTIES OF COPPER

P. Barath[1], L. Trnkova[1], F. Jelen[2]

[1] Department of Chemistry, Faculty of Science, Masaryk University, Kotlarska 2, CZ-611 37 Brno and Metrohm Czech Republic s.r.o. Na Harfe 935/5c, 190 00 Praha 9, Czech Republic
[2] Laboratory of Biophysical Chemistry and Molecular Oncology, Institute of Biophysics, Academy of Sciences of the Czech Republic, v.v.i., Kralovopolska 135, CZ-612 65 Brno, Czech Republic

Corresponding author: Libuse Trnkova (libuse@chemi.muni.cz)
Phone: +420 549497754, Fax: +420 549492443

Introduction

Under suitable experimental conditions purines react with copper ions resulting in the formation of a copper-purine complex [1-2]. This complex requires monovalent copper ions which can be generated electrochemically in the vicinity of the electrode surface. Obtained complex is adsorbed on the electrode surface and following stripping step can be used for the sensitive detection of purines [3]. The stripping process resulted in a new voltammetric peak and in an enhancement of redox signals of the corresponding compound. Our contribution is aimed at study of the effect of some purines on copper redox system in aqueous solutions. The combination of two techniques, i.e. adsorptive stripping (AdS) and elimination voltammetry (EVLS), are presented.

Experimental

Voltammetric measurements were performed with an AUTOLAB analyzer (EcoChemie, The Netherlands). A standard cell with three electrodes was used. The working electrode was a pencil graphite electrode (PeGE) with a surface area of 1.67 mm^2 (Tombo 05 HB, Japan). The electrode Ag/AgCl/KCl (3 M) as a reference electrode and platinum wire as an auxiliary electrode were used. All experiments were carried out at room temperature. We used the accumulation potential -0.15 V and accumulation time 120s. For EVLS procedure total voltammetric currents were recorded at scan rates 200, 400, and 800 mV/s.

Results and Discussion

In the presence of copper(II) ions purines provided two separate anodic signals on PeGE. The first anodic signal is due to the oxidation of the metal complex and the second to the oxidation of the corresponding purine. It was found that the metal complex (copper(I)-purine) has influence on the anodic purine signal which can be used for sensitive detection of purines [4]. EVLS function eliminating the kinetic and charging current components with conservation of the diffusion current component [5] confirmed that the adsorption plays substantial role in a redox process of copper(I) –purine complex. Results concerning aminopurines are summarized in Fig.1.

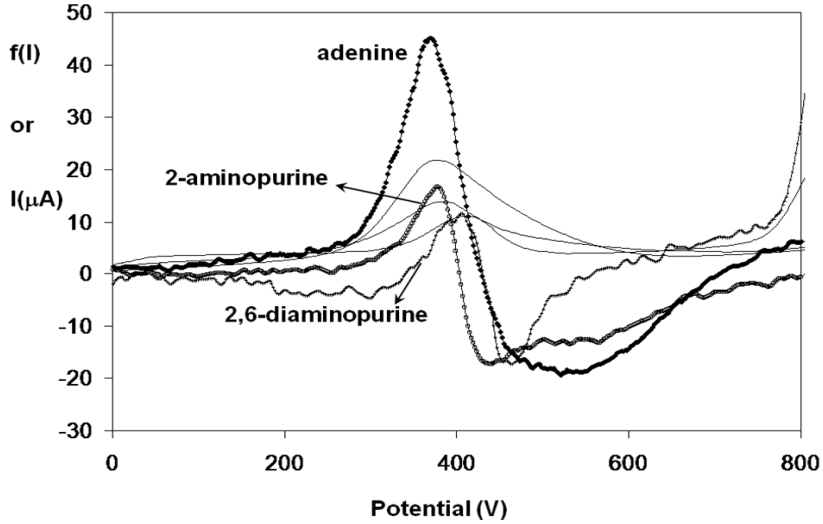

Fig.1: *Linear sweep (thin lines) and elimination voltammograms (thick lines) of Ade, 2-AP and 2,6-DAP (10 μM) with 20 μM Cu(II) on PeGE . Curves belong to anodic signals of copper(I)-purine complex; experimental parameters are: accumulation potential E_a -0.15 V, accumulation time t_a 120 s, reference scan rate 400 mV/s.*

Conclusions

Here it is presented the analysis of some purines in the presence of copper ions (II) by two voltammetric methods. We assume that corresponding steps are as follows:

a) Cu(II) + e = Cu(I) ; (b) Cu(I) + purine = [purine- Cu(I)] ;

b) [purine- Cu(I)= $[\text{purine- Cu(I)}]_{ads}$; (d) $[\text{purine- Cu(I)}]_{ads}$ = purine + Cu(II) + e

These steps can indicate the character of purine inhibition in the copper corrosion process. We assume that EVLS is a helpful tool for this project.

Acknowledgements

This work was supported by the Academy of Sciences of the Czech Republic (grants A400040804 and KAN200040651), the Ministry of Education, Youth and Sports of the Czech Republic (INCHEMBIOL MSM0021622412 and BIO-ANAL-MED LC06035), and institutional research plans (AV0Z50040507, AV0Z50040702).

References

[1] F. Jelen, A. Kourilova, P. Pecinka, and E. Palecek: Bioelectrochemistry **63** (2004) 249.
[2] L. Trnkova, L. Zerzankova, F. Dycka, R. Mikelova, and F. Jelen: Sensors **8,** (2008) 429.
[3] M. M. C. dosSantos, C. M. L. F. Lopes, and M. L. S. Goncalves: Bioelectrochem. Bioenerg. **39** (1996) 55.
[4] N. Aladag, L. Trnkova, A. Kourilova, M. Ozsoz, and F. Jelen: Electroanalysis **22** (2010) 1675.
[5] L. Trnkova: J. Electroanal. Chem. **582** (2005) 258.

11th ABAF

BRNO 2010

Advanced Batteries, Accumulators and Fuel Cells

Aqueous batteries

INFLUENCE OF DISCHARGING DEPTH AND OVERCHARGING ON PERFORMANCE OF ALPHA NICKEL HYDROXIDE

T.Máca[1, 2], L.Nezgoda[1], V. Špachman[1], J.Vondrák[3], M.Sedlaříková[2]

[1] Bochemie Inc., R&D Department
[2] Institute of Electrotechnology, Technical University of Brno, 602 00 Brno
[3] Institute of Inorganic Chemistry AS CR, 250 68 Řež near Prag

Corresponding author: Tomáš Máca (tomas.maca@bochemie.cz)

Introduction

Commercial alkaline accumulators with positive electrode based on nickel hydroxide generally comprise beta modification of the active material at present due to its excellent stabilization of performance during electrochemical cycling. The paper refers to a part of research work accomplished in R&D Department of the company Bochemie Inc., which has been aimed to utilization of alpha nickel hydroxide in alkaline batteries including exploration of possibilities to attain its stability in strong alkali medium of the electrolyte. We have focused our effort to elucidate reasons for its transformation tendency and to find way of their suppression. Based on previously obtained empirical evidence, introduction of appropriate variations in depth of discharge seems to be potentially proper solution for us, which led us to verify that.

Shallow discharge of Al-doped alpha nickel hydroxide

Discharge curves of Al-doped alpha nickel hydroxide are characterized by higher situated potentials in comparison with common beta phase and further by sharp breaks of progression when discharge is being finished i.e. abrupt potential falling in region of voltage for NiCd cell at 1,1 V. This featured property determines negligible charge retention and useless capacity below mentioned level of the cell voltage. Furthermore, major portion of charge corresponding to main working part of curve should be delivered in region of higher voltage bigger than about 30 up to 50 mV compared to beta phase of nickel hydroxide. Such behavior theoretically appears to be very advantageous and that´s why we have decided to do shallow discharge of these materials.

Deep discharge of Mn-doped alpha hydroxide

After being discharged to 1V Mn-doped alpha hydroxides retain still significant portion of capacity below this voltage level. The capacity retention results from lower discharge potentials of Mn-doped alpha hydroxides which have been observed in the discharge curves and that´s why it is necessary to consider those discharging processes as insufficient and prematurely terminated. The share of discharge capacity with the discharge voltage lower than 1 V is relatively high which indicates certain weakness of useful capacity. The retained capacity is delivered only after discharge was adjusted to cut off voltage equal to 0,8V. Described behavior well corresponds to content of manganese – this effect becomes more apparent with increasing amount of manganese in alpha nickel hydroxide.

Verify of the tolerance against irreversible structural changes during overcharging of alpha nickel hydroxide

Regularly arranged crystal lattice of alpha phase does not obviously become damaged when it is being overcharged. The only evolution of oxygen on positive and hydrogen on negative electrodes takes place. Following generation of gas microbubles causes rise of pressure inside both electrodes and cell with consequent elutriation of accumulator mass from carrier/current collector and structural degradation of pressed electrode and thereby enhancement of internal resistance. Gradual transition part of alpha phase to beta phase also proceeds with increasing cycle number and overcharging of this manner created beta modification to gamma phase leads to volumetric changes of active material joined by swelling and mechanical stress which can induce conductivity loss. Meanwhile formation of electrode for about first 5 cycles, involving gradual stabilizing and hydration of structure together with irreversible transition of secondary cobalt to conductive part of surface, is running a moderate slow overcharging of accumulator mass appears to be favourable for complete utilization of its entire volume. Further overcharging does not yield any benefit to working of electrode.

Experimental

Typical features of our electrochemical tests of positive electrodes based on $Ni(OH)_2$:

The active material and construction of electrodes

The electrochemical behavior of the substituted alpha nickel hydroxides was studied in Ni-Cd cells with 6M KOH electrolyte. There were pressed electrodes used in pocket version for the investigations on all of nickel hydroxide samples. The electrodes were constituted of an activated mixture of nickel hydroxide and graphite which gives improved electronic conductivity. The active material using β_{bc}-$Ni(OH)_2$ has served as a comparative mass/reference sample in carried out tests.

Measuring conditions

All measurements were performed using non-commercial equipment of Bochemie Inc. The cycling process at the 0,17 C rate is typically used in our laboratory for testing of the type of accumulator mass. It consists in continuous, galvanostatically led charging and discharging of the cell with short relaxation between the various steps. Four "forming" cycles of these electrodes are performed at the same rate (0,17 C) at the very beginning of the cycling, including strong overcharging of the cell in the first cycle (20 h successfully). The overcharging corresponds to 200% of the theoretical capacity for common accumulator mass based on beta nickel hydroxide.

Results and Discussion

Electrochemical measurements of discharge capacity

Testing of shallow discharge for Al-doped alpha nickel hydroxide

We have focused on the verification of the fact of assumed beneficial influence of such discharge regime on cyclic stability for Al-doped alpha nickel hydroxide. Levels of 1,15 V, 1,1V and 1V (common value) were chosen as final discharge voltage. A slow down effect for rapidly dropping performance through higher final discharging voltage really occurs on

first charge/discharge cycles. However, the performance decline systematically continues, unless it is being stopped. Experimental results in the case of the highest final discharge voltage seems to be a little bit unusual with regard to least steady continuance discharge capacity with increasing number of cycles. On the contrary performance falling accelerates (between 3rd and 4th cycle and between 6th and 7th cycle) in comparison to common discharge to 1V. Lower delivered charge corresponds with it. Comparison of discharge to 1V and 1,1 V can be evaluated more clearly. Discharge capacity declension of initial 10 cycles really slows down and moreover the capacity falls from higher achieved values. However, rates (sharpness) of the performance declension for both discharge ways equilibrate after achievement of 10th cycle. It is surprising, that delivered capacity for final voltage of 1,1 V in comparison with 1 V. This discrepancy could be better explained by different insulating range of the active material in charge state in particular cases. This insulation occurs to be very fast in case of Al-doped alpha nickel hydroxide after the beginning of electrochemical cycling.

It can be concluded that shallow discharge has not proved ability to restrain the active material from being insulated or transformed.

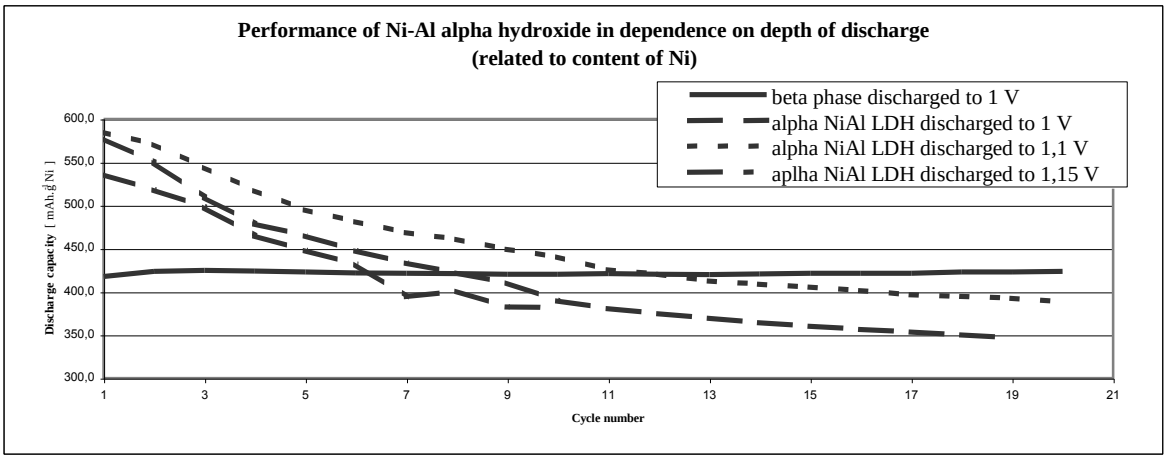

Fig.1: *Different depth of discharge for Ni-Al alpha nickel hydroxide*

Testing of deep discharge for Mn-doped alpha nickel hydroxide

Range of capacity retention was experimentally investigated by galvanostatic measuring of samples with molar ratio Ni:Mn = 9 synthesized by continually led precipitation in a flow reaction vessel for two different flowing-through period 1 hour and 3 hours. In order to do more precious expression long-term deep discharging was discontinued and further accomplished till cut off voltage was equal to 1V for several more cycles. Degree of charge retention for sample NiMn (9:1)/3h in 228th cycle means 21,3 % of discharge capacity delivered by deeper discharging to final cell voltage which equals to 0,8 V in previous cycle and in case of sample NiMn (9:1)/1h loss of capacity represents 19,9 % in 229th cycle.

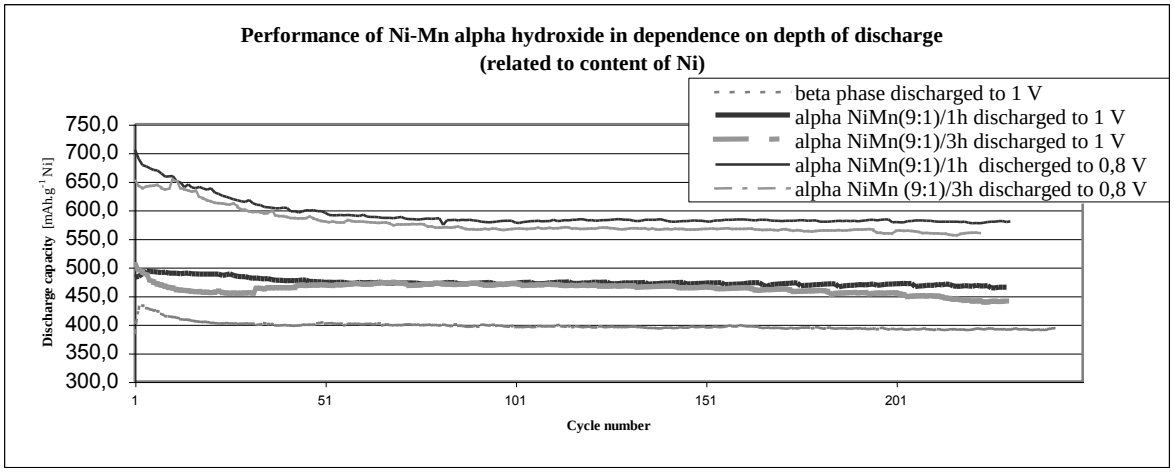

Fig.2: *Different depth of discharge for Ni-Mn alpha nickel hydroxide*

Overcharging of Al-doped alpha nickel hydroxide

Influence of overcharging on properties deterioration has not been confirmed yet. Two series of measurements have been accomplished – the first with vigorous overcharging in excess of 1,7 V and the second with charging of the same accumulator mass by commonly used algorithm till the cell voltage equals to 1,47V. Almost identical capacity continuance and rate of phase transformation (from alpha toward beta modification) have been exhibited for both methods and no deviations have been found. Slightly higher capacity can be delivered from the sample of overcharged active material in comparison with the sample that was charged to standard voltage. However such enhancing of discharge capacity occurs to be the detriment of considerable energy losses at charging (decreasing of charge efficiency) and possibility of construction´ s damage during short period if the active material is regularly overcharged.

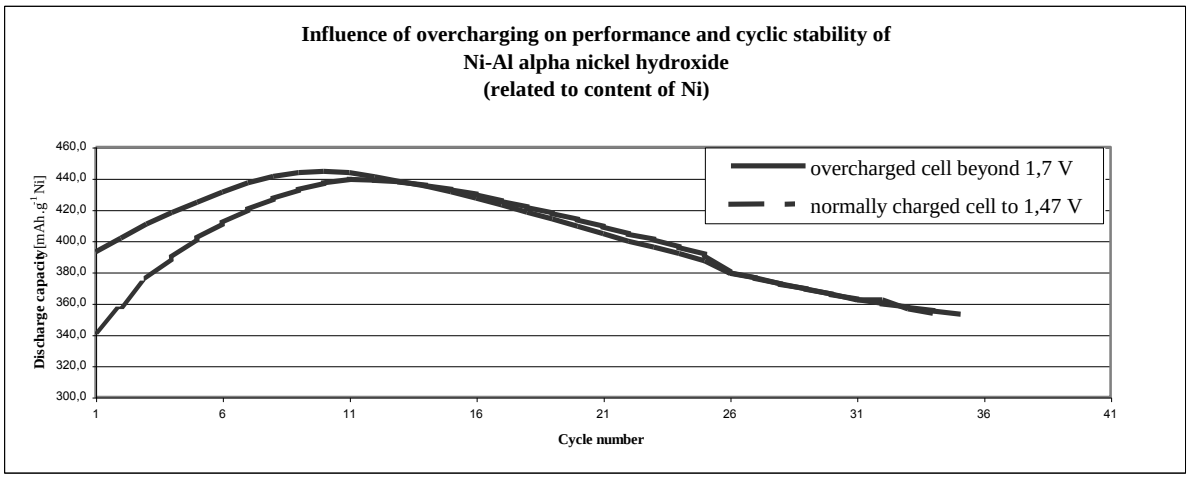

Fig.3: *Overcharging tests for Ni-Al alpha nickel hydroxide*

Conclusion

We have evaluated influence of deep discharging on electrochemical behavior of alpha nickel hydroxide with aluminium or manganese as doping agents. Our measurements were carried out to check slowing downs in performance declension through shallow discharge regimes. With the shalower discharge ,we have not found out any significant

effect on improvement in electrochemical properties such as performance and efficiency characteristics by shallower discharge which means that there is no capability to attain prolonged cyclic life of accumulator masses based on Al-doped alpha nickel hydroxide by adjusted operating conditions in this manner.

On the other hand, deeper discharge has clearly proved, that for Mn-substituted alpha nickel hydroxide it is necessary to gain retained portion of capacity.

The tolerance of alpha nickel hydroxide toward irreversible structural changes in conditions of intensive overcharging has been studied. There hasnot been found out any difference between electrochemical behavior of charged alpha nickel hydroxide to standard voltage and intensive overcharged state, which means that overcharging does not reduce cyclic life of positive accumulator masses based on alpha nickel hydroxide.

References

[1] Y.L. Zhao et al., International Journal of Hydrogen Energy 29 (2004) 889 – 896
[2] Mufit Akinc et al., Journal of the European Ceramic Society 18 (1998) I559- I564
[3] R. Acharyaet et al., Materials Chemistry and Physics 81 (2003) 45–49
[4] V. Ganesh Kumar et al., Journal of Power Sources 56. (1995) 1 I l-l 14

CHEMICAL AND ELECTROCHEMICAL SYNTHESIS OF NICKEL HYDROXIDE

D. Becker[1], G. Garaventta[1], F. Rodríguez Nieto[1], A. Visintin[1], P. Barath[2], M. Sedlaříková[2], J. Vondrak[2]

[1] Instituto de Investigaciones Fisicoquímicas Teóricas y Aplicadas (INIFTA), Facultad de Ciencias Exactas, UNLP, CCT La Plata - CONICET, C.C. 16, Suc. 4 – 1900 La Plata Argentina.

[2] Department of Electrotechnology, Faculty of Electrical Engineering and Communications, Udolni 53, 602 01 Brno, Czech Republic.

Introduction

Nickel hydroxide is still widely used as electrode material in different types of rechargeable batteries, such as Ni-Cd, Ni-H_2, Ni-Fe, and Ni-MH batteries [1], especially in those with high specific energy that are employed in a range of portable electronic devices and electric cars. Nickel hydroxide is also used as a precursor in various catalytic processes [2]. Currently, the development of Ni-MH batteries allows for the production of devices with high specific energy [3,4].

Nickel hydroxide is a complex crystalline material having a structure that generally depends on the preparation method. It occurs in polymorphic forms such as α-$Ni(OH)_2$ and β- $Ni(OH)_2$, which are transformed into γ-NiOOH and β-NiOOH during the electrode charging process. The electrochemical behavior of these phases differs from one to another due to changes in their structure, composition and morphological characteristics that modify the different processes occurring during charge and discharge cycles. Therefore, the electrode manufacturing process plays a key role in the electrochemical behavior of nickel hydroxide.

There are several methods for preparing $Ni(OH)_2$ as the active material of the positive electrodes of rechargeable alkaline batteries [5,6], which can also contain multiple modifier elements [7]. The addition of cobalt has been widely studied and shows beneficial results in the long-time stability of the electrodes [8,9].

For batteries for space applications, flat electrodes are needed. They are a few millimeters thick and have a high surface area, which requires the use of the electrochemical impregnation method [10,11].

The electrodes in alkaline batteries for ground applications are pressed onto a current collector mesh. So the indirect precipitation method is employed for the hydroxide, which is then pressed onto a metal nickel mesh.

The results show differences in the different methods for obtaining nickel hydroxide electrodes using chemical and electrochemical synthesis.

Experimental

Nickel hydroxide with cobalt modifier has been obtained by three different methods: (a) electrochemical impregnation with pulse-train perturbation (b) chemical precipitation, and (c) indirect electrochemical precipitation at constant current.

(a) Synthesis by electrochemical impregnation with pulse-train perturbation

The electrodes were made in a beaker-type cell (750 cm^3) and held in place by a Teflon fixture, maintaining a constant separation between them. A mixed 0.5 M nickel nitrate and 0.5 M cobalt nitrate solution in a 10:1 ratio used as electrolyte was magnetically stirred and heated on a hotplate, achieving a homogeneous concentration throughout the cell volume. The active material was impregnated by cathodic galvanostatic electrodeposition using an intermittent train of pulses with an amplitude of 400 mA applied to a 6.25 cm^2 electrode geometric area.

(b)Synthesis by chemical precipitation

A mixed metal–nitrate solution containing 0.5 M nickel and cobalt nitrate in a 10:1 ratio was added dropwise to a 20% w/w KOH solution with constant stirring at 30ºC and at constant pH 10. The precipitate was filtered and rinsed with milli-Q water until neutral pH. The green powder obtained was dried at 60ºC for 24 h.

(c) Synthesis by indirect electrochemical precipitation at constant current

Electrolysis was performed in an electrochemical cell using a cylindrical platinum mesh of 3 cm diameter and 5 cm height as working electrode; and two sintered porous plaques containing hollow nickel fiber, arranged symmetrically around the working electrode, as counter-electrode. The experiment was made in 400 ml of 0.5 M nickel nitrate and 0.05 M cobalt nitrate solutions at 30 $mA.cm^{-2}$ current density with constant stirring for 4 h in a bath at 70^oC. The precipitate was obtained in two portions: one part as impregnated material at the platinum mesh, and the second part as the dispersed particles in the solution. The precipitate material was thoroughly separated from the Pt mesh with a spatula and mixed with the material obtained by filtration. Then the powder was washed with milli-Q water until neutral pH in order to remove the excess of K^+, NO_3^- and OH^- ions. Finally, the material was dried at 60^oC for 24 h. The powders have been characterized by X-ray diffraction.

Electrochemical Characterization

In order to study the electrochemical behavior, the nickel hydroxide electrodes were prepared by mixing 80% w/w active material (samples “b” and “c”) with 10% w/w carbon and 10% Teflon (PTFE Grade 30) aqueous dispersion (DuPont). The mixture was then pressed onto a nickel mesh under a pressure of 0.5 Ton/cm^2. The resulting electrode was dried at 30º C for 24 h. Sample “a” contains 100% active material. A three-electrode cell containing 6M KOH at 298 K was used to determine the electrochemical characteristics. The working electrode was placed between two counter-electrodes of large surface area made of nickel mesh. The potentials were measured against a Hg/HgO reference electrode. The discharge capacity was determined as a function of the charge-discharge cycling number. To do this, a fixed cathodic current of 2 mA was applied for 9000 s in order to ensure the full charge of the electrode. The discharge was conducted at 2 mA

until the cut-off potential (0.2 V versus Hg/HgO) was reached. The proportions of each electrode element were changed in order to find the appropriate proportion for a good electrochemical performance. Then the above-mentioned composition was obtained.

Results and Discussion

X-Ray Diffraction

X-ray diffraction patterns of the synthesized samples are shown in figure 1. When compared with JCPDS cards [12], the three samples exhibit the typical reflections of polymorphic α and β–$Ni(OH)_2$ with different proportions in each sample. In sample "b" the intensity of peaks at 19, 33 and 38 degrees indicates a greater proportion of β–phase than in the other samples. In this case the very wide and asymmetric peak at 19 degrees could indicate the presence of co-precipitated cobalt hydroxide. Samples "a" and "c" show a sharp 001 reflection with high intensity compared with the other reflections, indicating a greater proportion of α phase; likewise, the broad and asymmetric peaks at 2θ = 30-40 indicate a turbostratic and interstratificate structure. In general, and considering reflections with $2\theta \geq 25$, the low intensity, the full width at half-maximum (fwhm) broad peak and the distortion of the representative reflections in the patterns indicate a quasi-amorphous structure with different forms of stacking fault.

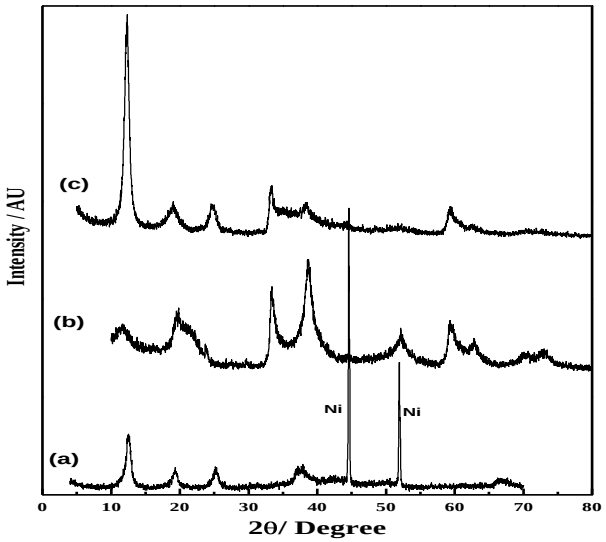

Fig. 1: *XRD patterns of nickel hydroxide with Co modifier powder synthesized by: (a) electrochemical impregnation with pulse-train perturbation, (b) Chemical precipitation, and (c) indirect electrochemical precipitation at constant current*

Electrochemical Performance

Figure 2 shows the variations in discharge capacities as a function of life cycles. Samples "b" and "c" need an activation period until the capacity stabilizes, while sample "a" goes directly to the maximum capacity. The electrochemical impregnation method produces a high active surface and allows the use of 100% of the powder in the electrode as compared to "b" and "c" methods.

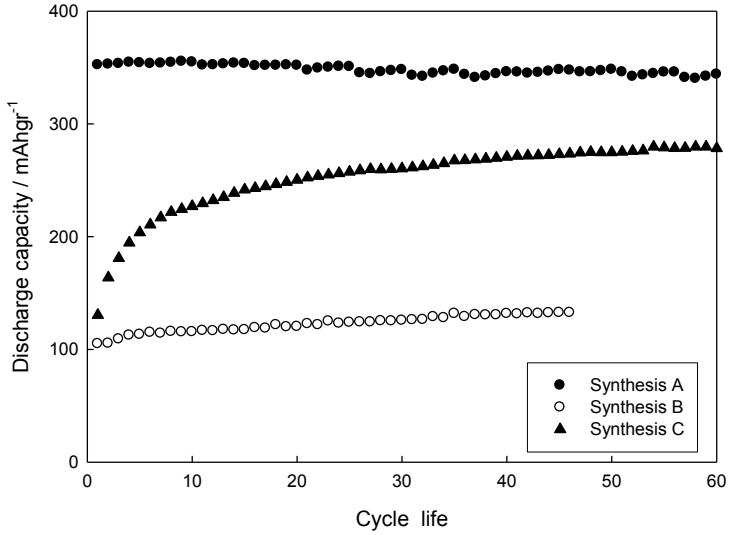

Fig. 2: *Discharge capacity vs. number of cycling number, Ic=C/2, Id=C/2, KOH 6M, T= 28 ºC.*

Figure 3 shows a typical constant current discharge for electrodes at discharge Id= *C/2*. In the case of synthesis "a", discharge curves are flat from the first cycle and exhibit a higher potential and an interesting discharge capacity value compared with theoretical values for alpha and beta phases. The impregnation technique gave encouraging results about the durability and specific capacity of the electrodes indicating that cobalt electrochemical addition improves the electrochemical performance.

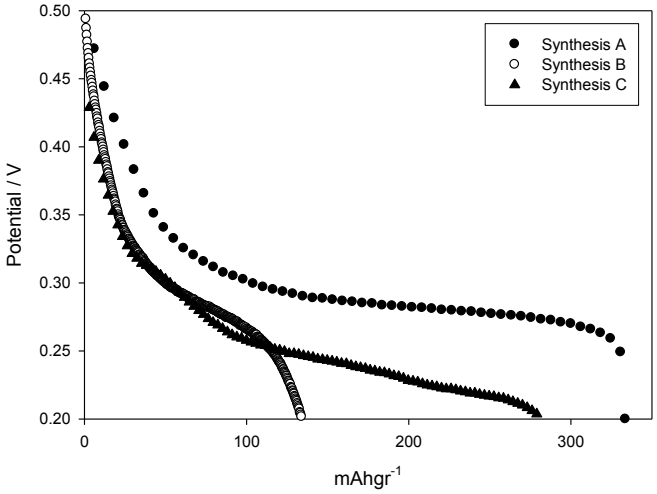

Fig. 3:*Typical constant current discharge curves, Id= C/2, KOH 6M, ---T= 28 ºC.*

Conclusions

Depending on the synthesis method, the powders obtained exhibit different degrees of disorder indicating a quasi-amorphous structure with different forms of stacking fault. The solid obtained by chemical synthesis shows a broad, asymmetric and distorted peak at 19º, which could indicate cobalt hydroxide segregation.

X-ray diffraction analysis shows the presence of the hexagonal crystal structure of nickel hydroxide with alpha phase predominance in electrochemical synthesis (samples “a” and “c”), while a predominance of beta phase is obtained with chemical precipitation.

When the material is deposited directly on the current collector, is obtained better stability in the cycling and the electrode exhibits a high discharge behavior of 350 $mAhg^{-1}$. This technique is interesting for electrode applications in high-performance batteries.

Acknowledgements

This work was supported by Consejo Nacional de Investigaciones Científicas y Técnicas of Argentina (CONICET), the Agencia Nacional de Promoción Científica, Tecnológica, the Comisión de Investigaciones Científicas (CIC), the Czech Academy of Sciences (Research Plan AV0Z40320502), Ministry of Education (project MSM 0021630516), and by the Cooperation program between the Czech Academy of Sciences and CONICET.

References

[1] Mc Breen, J. 0. Besenhard, Editor and VCH, (1997)
[2] Nathira Begum, V.S. Muralidharan, C. Ahmed Basha. International Journal of Hydrogen Energy 34 (2009)1548
[3] Delia M. Constantin, Eleonora Maria Rus, L. Oniciu, L. Ghergari, Journal of Power Sources. 74 (1998)188-197
[4] Chun-Chen, Yang,. Int. J. Hydrogen Energy 27, (2002) 1071–1081
[5] T. Takamura,Shirogami, Nakamura, Denki Kagaku 42, (1974) 582
[6] W. B. Zhang. Fudan University Journal (Natural Science) 17(1978), 3, 112
[7] C. Fierro, A. Zallen, J. Koch, and M.A. Fetcenko. Journal of Electrochem. Soc. 153 3 (2006) A492
[8] Z. Chang, Y. Zhao, Y. Ding. Journal of Power Sources. 77 (1999) 69
[9] A.B. Yuan and N.X. Xu. Journal of Applied Electrochemistry. 31 (2001) 245
[10] T. Takamura,Shirogami, Nakamura, Denki Kagaku 42, (1974) 582
[11] W. B. Zhang. Fudan University Journal (Natural Science) 17(1978), 3, 112
[12] Joint Committee on Power Diffraction Standards(JCPDS) Card No.22-0444 and 14-0117

THE INFLUENCE OF SURFACTANTS ON ALPHA NICKEL HYDROXIDE

J.Vrbický[1], J. Vondrák[2], M. Sedlaříková[1]

[1] Institute of Electrotechnology, Technical University of Brno, 602 00 Brno
[2] Institute of Inorganic Chemistry AS CR, 250 68 Řež, Prague

Corresponding: Jiří Vrbický (xvrbic00@stud.feec.vutbr.cz)
Phone: +420541146112, Fax Number: +420541146147

Introduction

Nickel hydroxide is the basic material for positive electrode of alkaline accumulators as Ni-Cd, Ni-MH and Ni-Fe. The three modifications of nickel hydroxide are known, these are alpha, beta and gama.

Alpha nickel hydroxide is stable under normal conditions, but in alkaline electrolytes it is unstable and turns into β- $Ni(OH)_2$. The β- $Ni(OH)_2$ has half capacity than beginning alpha electrode, and when β- $Ni(OH)_2$ is charged to β- NiOOH, the volume expansion is increasing so it shows many construction and durability problems, it also solves the electrode made of α- $Ni(OH)_2$.

Some additives can stabilize α- $Ni(OH)_2$. Stable forms of alpha modification have very high resistance, due to that charged material can not be discharged. The resistivity is caused by recrystallization of the nickel hydroxide. The surfactants can slow down or stop the recrystalisation.

Experimental

The samples for cyclic voltammetry were deposited on nickel substrate from 0,05M solution of $Ni(NO_3)_2$ with various amount of $Al(NO_3)_2$. The deposition proceeded for 300s with current of 1mA.

The samples were measured in 6M KOH solution with anionactive surfactant aditive by cyclic voltammetry for 150 cycles. Scan rate 10mV/s, potential window 0-600mV to Hg/HgO reference electrode.

Results and Discussion

The best results are in low concentrations of the aluminium in nickel hydroxide structure.

Pure nickel hydroxide has better properties in pure KOH solution. The 9:1 nickel/aluminium hydroxide has very good results in anionactive surfactant (Fig.2). Concentration of aluminium over 6:1 has low capacity. In electrolyte with surfactant the capacity of nickel/aluminium hydroxide is about 30% higher, than in electrolyte without surfactant.

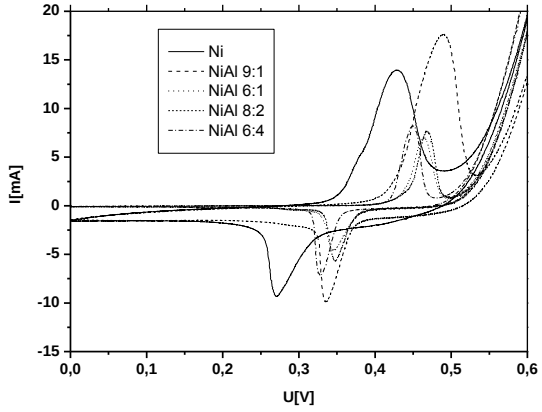

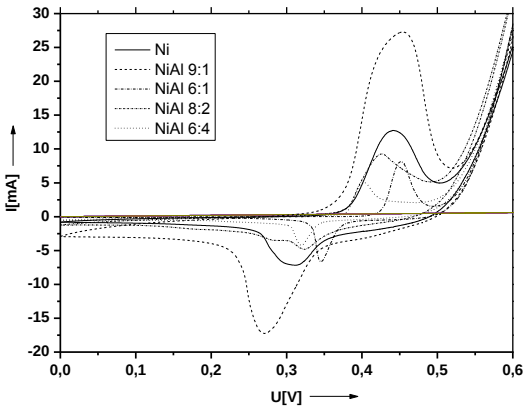

Fig. 1: (left) *Cyclic voltammogram of nickel/aluminium hydroxide in 6M*

Fig. 2: (right) *Cyclic voltammogram of nickel/aluminium hydroxide in 6M KOH with surfactant.*

Conclusions

Aluminium additive in nickel hydroxide makes it possible to produce stable alpha modification of nickel hydroxide. This modification with aluminium has very high resistance that makes it impossible to discharge. Surfactant additives influence useful capacity of this material in low concentration of aluminium is the capacity is higher than in pure KOH solution.

Acknowledgment

The investigations were supported by:
Ministry of Education of Czech Republic, Project MSM0021630516,

References

[1] M.A. Fetcenko , S.R. Ovshinsky, B. Reichman, K. Young, C. Fierro, J. Koch, A. Zallen, W. Mays, T. Ouch: *Recent advances in NiMH battery technology,* Journal of Power Sources *165 (2007) 544–551*

[2] Rand, D.A.J., Woods, R, Dell, R.M.: *Batteries for electric vehicles* – Tauton, Somerset, England, Research studies press, 1998

[3] Falk, S.U., Salkind, A.J.: *Alkaline storage Batteries* - New York, The electrochemical society INC., 1969

[4] Zhao, Y.L., Wang, J.M., Chen, H., Pan,T., Zhang, J. Q., Cao, C.N.: *Al-substituted α-nickel hydroxide prepared by homogenous precipitation method with urea*, International Journal of Hydrogen Energy, 2004

[5] Wang, C.Y., Zhong, S., Konstantinov, K., Walter, G., Liu, H.K.: *Strucural Study of Al-substituted nickel hydroxide*

[6] GANESH-KUMAR, V., BAET,S. W., LEE, J. S., NAM, K. W., KIM, K. B., Contraction of Alpha-nickel hydroxide Layers by Excess Coulombic Attraction of Anions

DETERMINATION OF LEAD ACID BATTERY STATE OF CHARGE (SOC) II

P. Křivík

Department of Electrotechnology, Faculty of Electrical Engineering and Communication Technologies, Technical University of Brno, Czech republic

Corresponding author: Petr Křivík (krivak@feec.vutbr.cz)

Introduction

Advanced method for determination of lead acid battery state of charge described in last work [1] proved to be the method of voltage change measurement after a short-term current loading (for both the charging and the discharging current). An accumulator at a high degree of charge should exhibit, after charging current application, a more substantial change of voltage than a battery at a lower degree of charge. Similarly, discharging current pulses would more accurately determine the state of batteries with a lower state of charge.

At the same time the changes of battery voltage after curent pulse application reflect the reaction processes in the electrode double layer at the boundary active substance-electrolyte, and also the diffusion processes inside the battery. All these reactions indicate the current state of charge of the lead acid accumulator.

Results and Discussion

For testing and investigation of charging and discharging characteristics an experimental cell was created (see fig. 1). Cell is composed from one's positive electrode about proportions 40 × 40 mm and one's negative electrode about proportions 40 × 40 mm. Electrodes are connected with two bars of lead plate about thickness 1 mm and proportions 70 × 10 mm. Two connectors are at the ends of these lead bars. Both electrodes are separate by PE separator and placed in plastic vessel about proportions 50 × 50 × 50 mm and immersed in H_2SO_4 solution about density 1,28 g/cm^3. After formation of cell and recharge, capacity was measured approximately 0,5 Ah [2].

Fig. 1: *Tested cell*

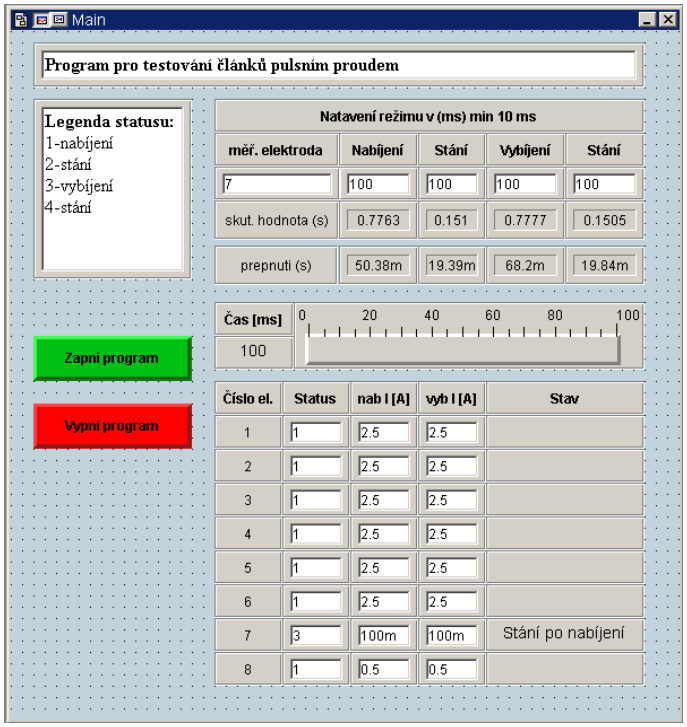

Fig. 2a: *Testing apparatus,* ***Fig. 2b:*** *Testing software*

Arrangement for application of current pulses – see fig. 2a. It is central measuring station AGILENT 34980A with relay MUX and SWITCH cards that is interconnected with set of sources. Mutual communication mentioned arrangement is possible by PC with software AGILENT Vee Pro 8.0. For generation of current pulses software was programmed – see fig. 2b.

Resulting graphs represents comparison of voltage dependencies on cell state of charge for 0, 25, 50, 75 and 100 % of charge. For testing constant charging and discharging time was set to 750 ms. Time of standing was set to 250 ms and current 100 mA.

Voltage dependence starting with charging pulse - see fig. 3, where is shown growth of voltage courses with raising of cell state of charge. Voltage dependence starting with discharging pulse - see fig. 4, where is shown growth of voltage courses with raising of cell state of charge too.

Voltage dependencies reflect, that the voltage level also depend on sequence of single pulses. If charging pulse is first, level of voltage is higher then in the event of discharging pulse is first. It is in accordance with theory.

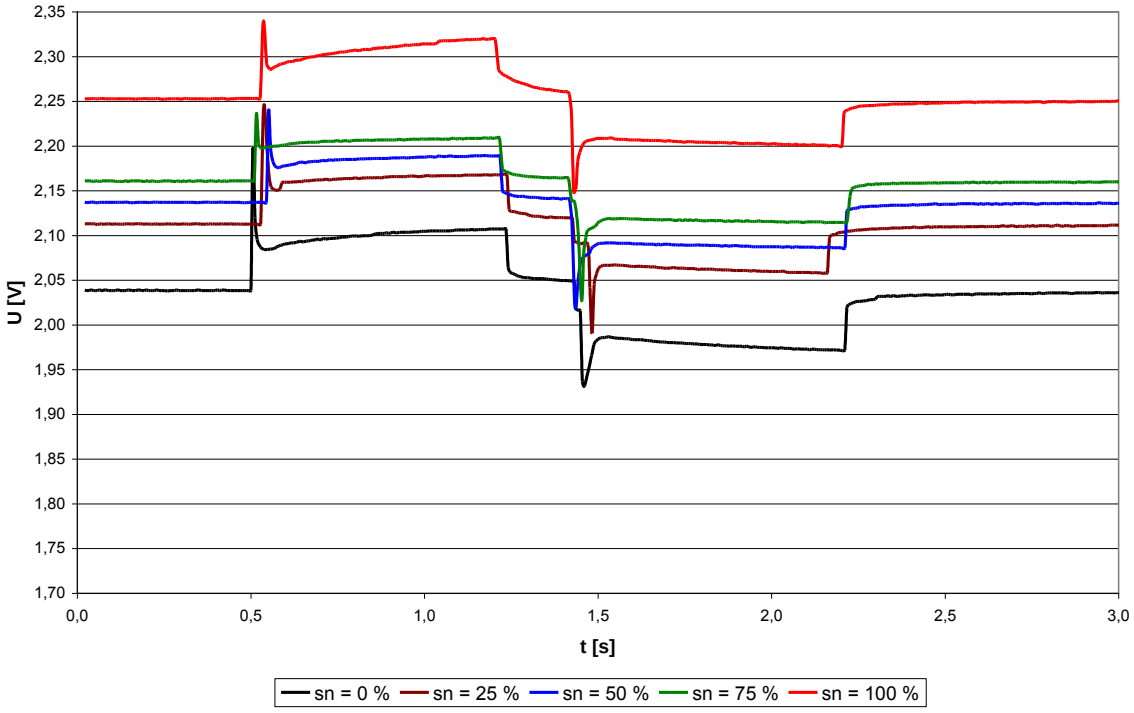

Fig. 3: *Time courses of cell voltage for various state of charge ; charge and discharge time 750 ms; standing 250 ms; I=100 mA;*

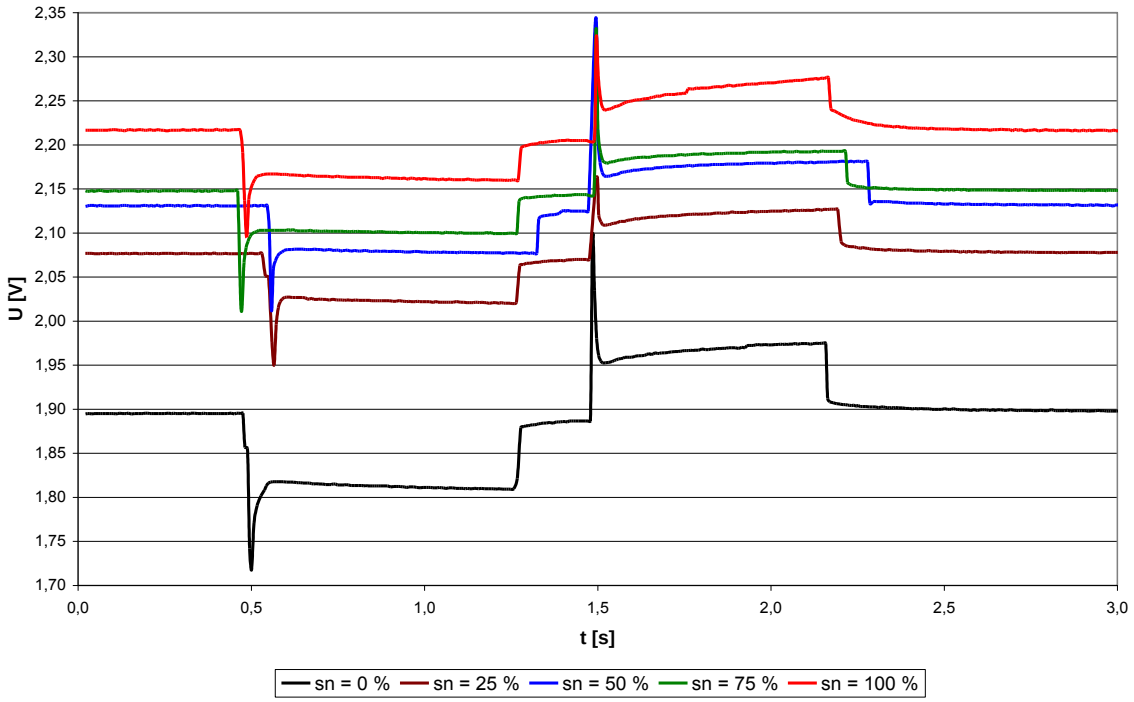

Fig. 4: *Time courses of cell voltage for various state of charge ; charge and discharge time 750 ms; standing 250 ms; I=100 mA;*

Voltage dependence for state of charge 100% represents dependence of voltage characteristics on magnitude of charging and discharging current. For testing constant charging and discharging time was set to 750 ms. Time of standing was set to 250 ms.

Voltage dependence starting with charging pulse - see fig. 5. It is evident that using of too high current pulses can cause too high voltage (gassing), that is undesirable. Therefore is necessary to set current pulse depending on battery capacity.

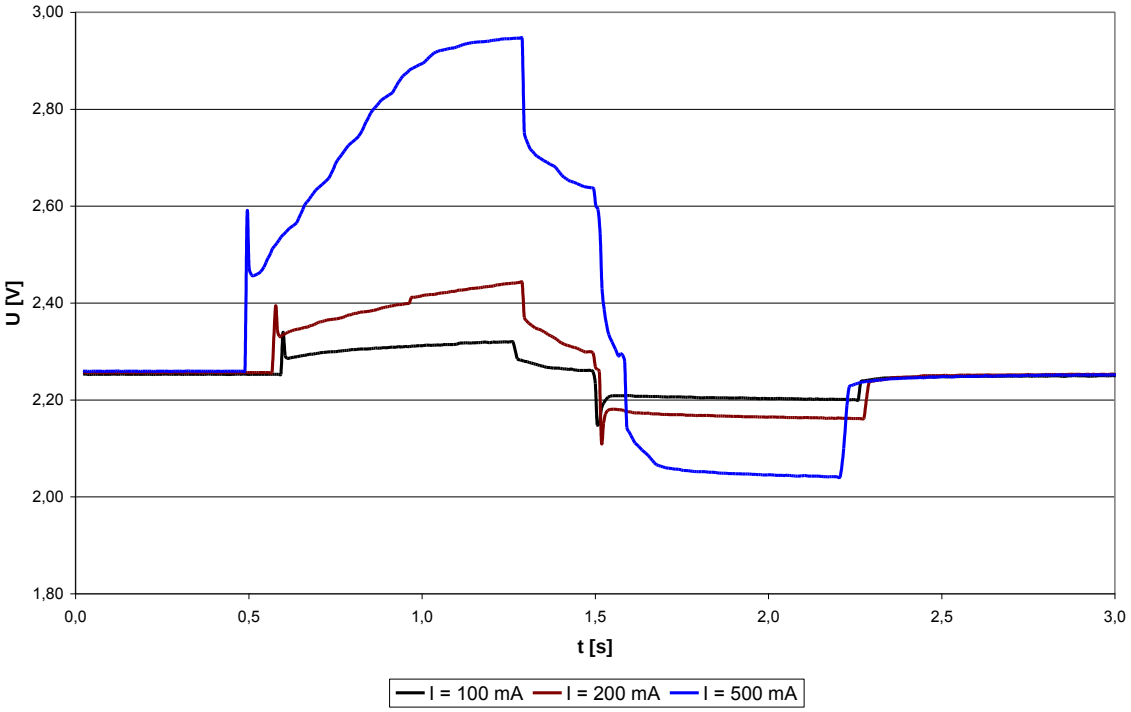

Fig. 5: *Time courses of cell voltage for various currents, state of charge = 100 %; charge and discharge time 750 ms; standing 250 ms;*

Conclusions

Changes in voltage courses during voltage measurements in current pulse regime reflect state of charge of lead acid battery cells. There plays an important role especially magnitude of current during charge and discharge pulses.

For correct determination of battery state of charge it is necessary to determine sequence of pulses, magnitude of current and length of pulse. Since various types of batteries have different characteristics, it is necessary to make measurements for every type of battery and create conversion table values of voltages depending on state of charge.

Acknowledgements

This work was sponsored by grant No. MSM0021630516.

References

[1] P. Křivík, Predikce stavu nabití olověných akumulátorů, sborník Jubilejní 30. NZEE, s. 76 – 79, Býkovice 2010.

[2] Ondřej Chochola, Predikce stavu olověných akumulátorů, diplomová práce, FEKT VUT v Brně, Brno 2010.

THERMAL PHENOMENA IN LEAD ACID BATTERIES, INFLUENCE OF DIFFERENT SEPARATORS

J. Neoral, P.Bača, P. Abraham

Department of Electrotechnology, Brno University of Technology, 602 00 Brno, Czech Republic

Corresponding author: Jiří Neoral (jiri.neoral@phd.feec.vutbr.cz)

Introduction

Following article introduces you into thermal phenomena connected with lead acid batteries and also describes experiments made in Department of Electrotechnology of Brno University of Technology.

VRLA batteries (Valve Regulated Lead Acid) have some significant problems which need to be solved before they could be used in hybrid electrical vehicles or electrical vehicles.

One of known problems which cause VRLA batteries to fail is effect called Thermal Runaway. It is usually defined as increase of batteries temperature while charging with constant potential. If internal heat isn't carried away, currents can rise to high levels and lead to batteries destruction. It is caused by positive feedback of current and temperature. Initial current which goes through cells cause temperature increase, this cause current increase, which cause additional temperature increase until temperature and current reaches to critical limit. [1]

VRLA accumulators also are subjects of degradation mechanisms connected with battery charging called PCL effects (Preliminary capacity loss) where third PCL effect is connected with insufficient charging of negative electrode. During charging current is converted into heat. This supports negative electrodes sulphating and makes charging even more uneasy. [2]

Therefore thermal phenomena in VRLA batteries are interesting subject of research.

Experimental

For our experiments we used experimental electrodes with system of non-continuous parallel ribs fixed in epoxy resin. Each rib was connected to one current and one voltage wire except of one where we used platinum thermal sensor of Jumo Měření a regulace s.r.o. according to standard DIN EN 60 751.

Electrodes with active mass with different additives were made as described in tab 1.

Additive	*Manufacturer*	*Additive grain size*
Carbon CR 2996	Graphite AG	4 um
Carbon 636843	Sigma-Aldrich	5-10 nm
SiO_2 637238	Sigma-Aldrich	10-20 nm
TiO_2 30444	Lachema a.s.Neratovice	2-8 um
Without additive		

Electrodes were formatted in 23 cycles by current 0,2 A. 4 hours charging, 2 hours standing.

Then electrodes were charged and discharged in deep cycles with different currents (1.2 A, 0.7 A and 2.5A) for different types of separators.

As separators were used:

Separator made of cellulose paper, separator made of glass fibbers in flooded construction and also separator made of glass fibbers in hermetic construction.

Then we started with PSOC (partial state of charge) cycling with current of 2.5 A.

Following figures are for separator made of glass fibbers in flooded construction and current of 0.7 A.

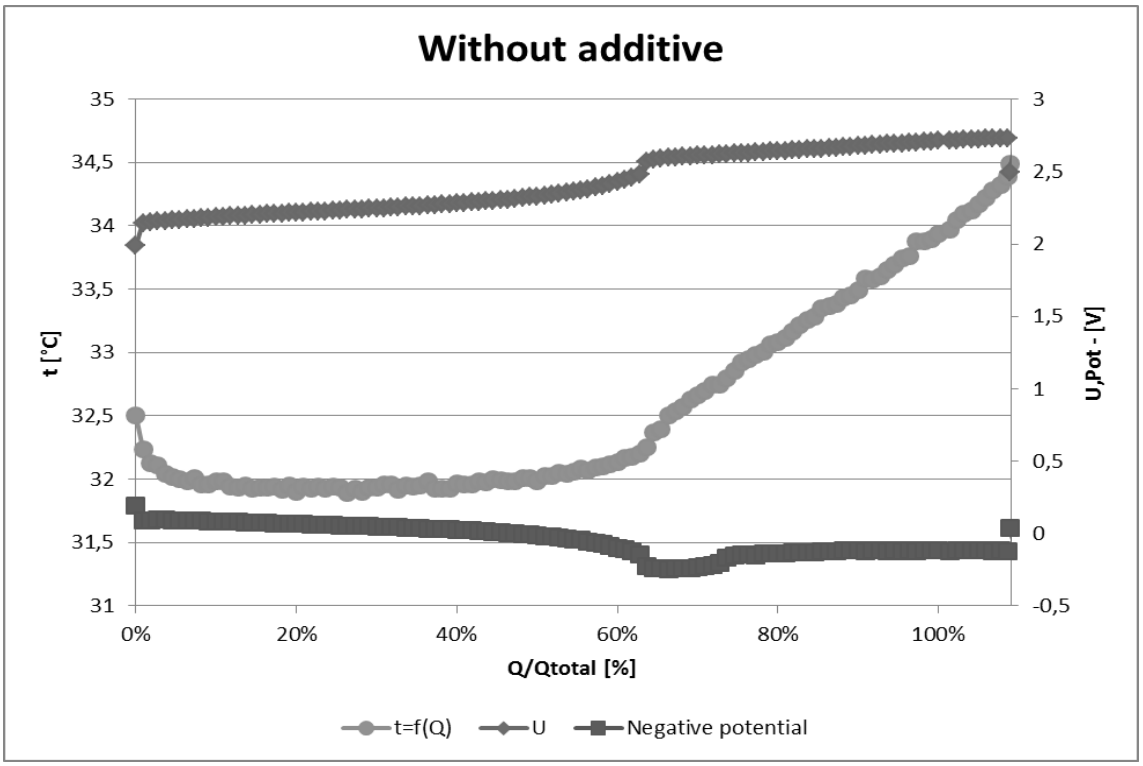

Fig. 1: *Negative electrode without additive charging with current of 0.7 A*

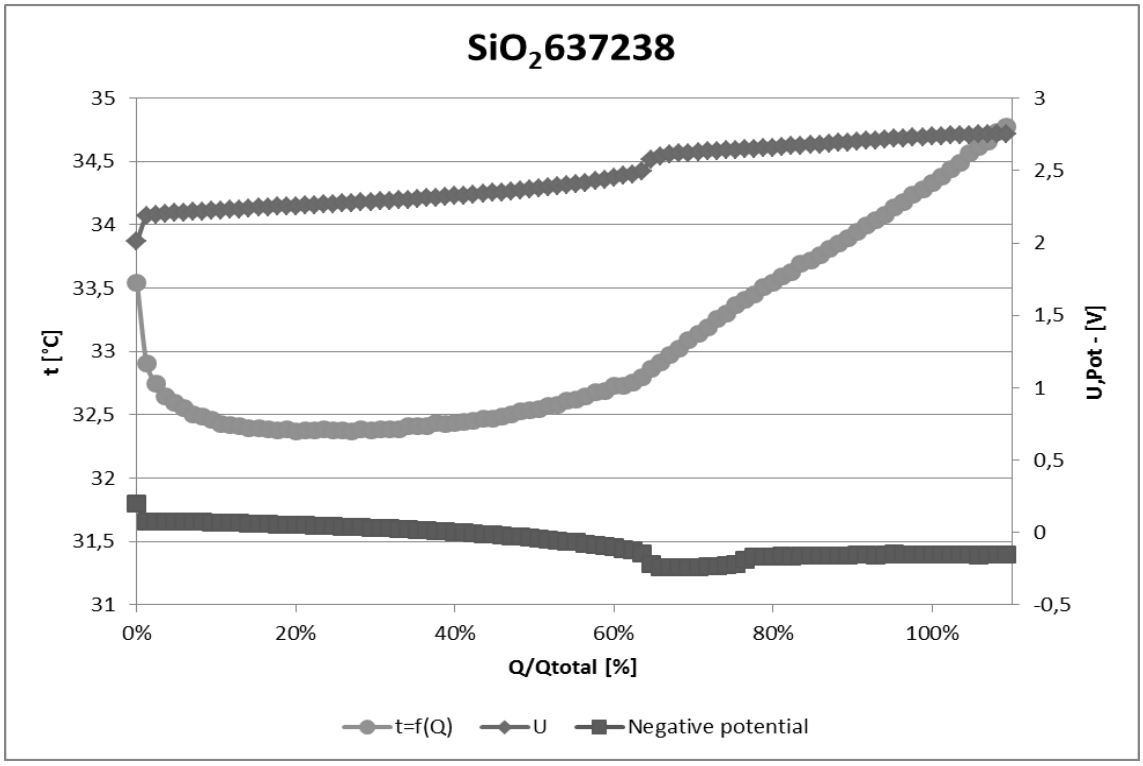

Fig. 2: *Negative electrode with additive of SiO_2 charging with current of 0.7 A*

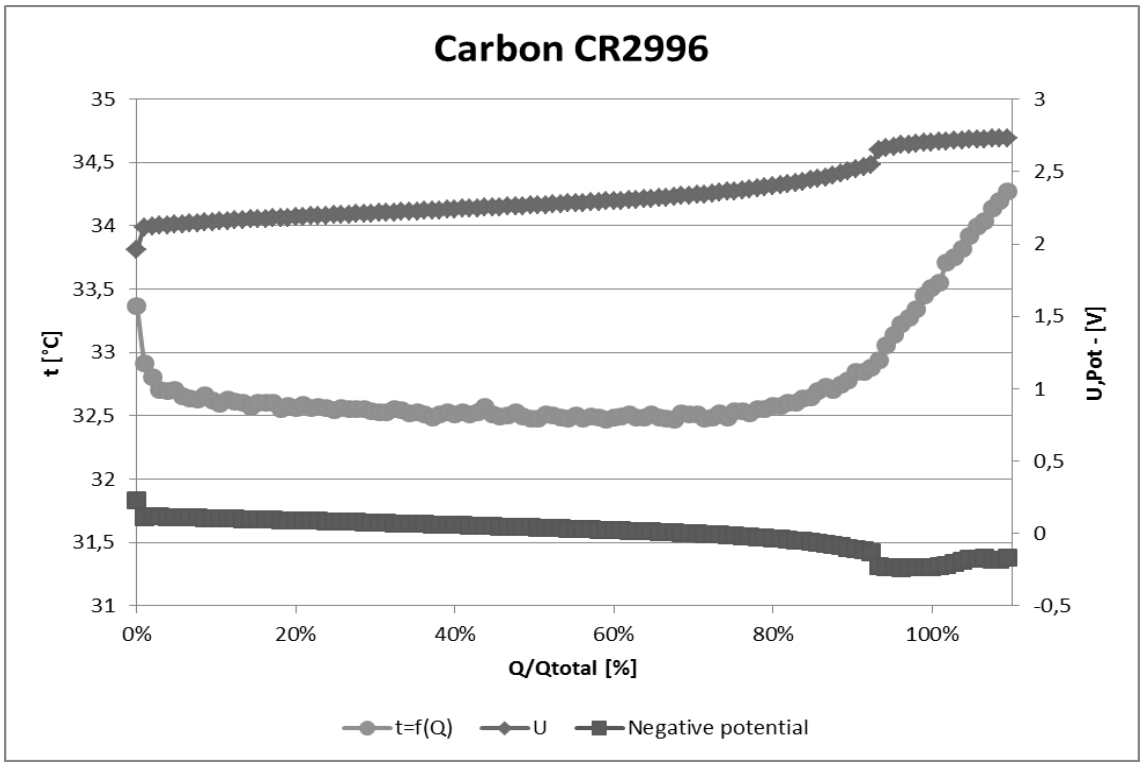

Fig. 3: *Negative electrode with additive of carbon charging with current of 0.7 A*

Results and Discussion

On figures 1-3 we can find, that both carbon delays temperature increase in comparison with electrode without additive. For electrode without additive it was close to 60% of charge. For carbon it was after 90%. SiO_2 behave similarly as electrode without additive this case.

Conclusions

Several experiments were made and there was found positive influence of carbon additive in active mass of lead acid battery on its thermal behaviour. Meanwhile further experiments are made which need to be evaluated.

Acknowledgements

Thanks to BUT Brno nr. FEKT-S-10-14 and VZ MŠMT MSM0021630516.

References

[1] D. Valkovska∗, M. Dimitrov, T. Todorov, D. Pavlov, Thermal behavior of VRLA battery during closed oxygen cycle operation, Journal of Power Sources 191 (2009) 119–126

[2] Ing. Vaněk J., Ph.D. Ing. Křivák P., Ph.D. Ing Novák V., Ph.D. Alternativní zdroje energie, 2006, skripta VUT

11th ABAF

BRNO 2010

Advanced Batteries, Accumulators and Fuel Cells

Solar Cells

ANALYSIS BACKSIDES OF SOLAR CELLS

J. Dolenský[1], J. Vaněk[1], A. Veselý[1], L. Winkler[1]

[1] Faculty of Electrical Engineering and Communication, Department of Electrotechnology, Údolní 53, 602 00 Brno, Czech Republic

Corresponding author: Jan Dolenský (jan.dolensky@phd.feec.vutbr.cz)
Phone Number: +420 541 146 168

Introduction

This paper describes a structure silicon solar cell. There are used several methods used for an analysis of solar cells. These methods have been applied so far to the front side of the solar cells. This paper tries to present an experimental analysis of the back side solar cell using a electroluminescence method.

Photovoltaic can be understood as a technology with unlimited growth potential and an unlimited possibility of electricity production. But it is not just an interesting technology, but also for advanced (high-tech) industry that the world is experiencing an unusual development, and positively affects not only business, but as well as jobs and skills of researchers. This fact is already understood by many advanced countries in the world, including countries of the European Union, seeks to promote photovoltaic and in the longer term, it implies the unique place in the energy "mix". This aspect becomes particularly relevant in view of growing energy dependence of many countries.

Possibilities back sides of solar cells

Today, in research and development of solar cells go considerable investment. The aim is to develop new structures which will require the maximum efficiency of converting solar energy into electrical energy. One of the problems of low efficiency of solar cells is the shading of the front contact grid of solar cells. In Figures 1-4, one can watch a graphical representation of the development of solar cells. Point of this research is to move both contact grids on the back of solar cells.

Figure 1 shows the structure of conventional monocrystalline silicon solar cell. Base material, silicon, (base) is of type P and subsidized layer (emitter) is of type N. The emitter is placed a metal grill (front surface). Serves to connect and contact article. The rear surface is often completely coated with a thin layer.

Figure 2 is seen structures MWT. It is a concept where the emitter is located on the front surface. It is also possible to monitor the transfer of the front contact on the back, which is ensured through the holes through the plate. This will expose the front surface and a strong buss bar moves to the back of the article.

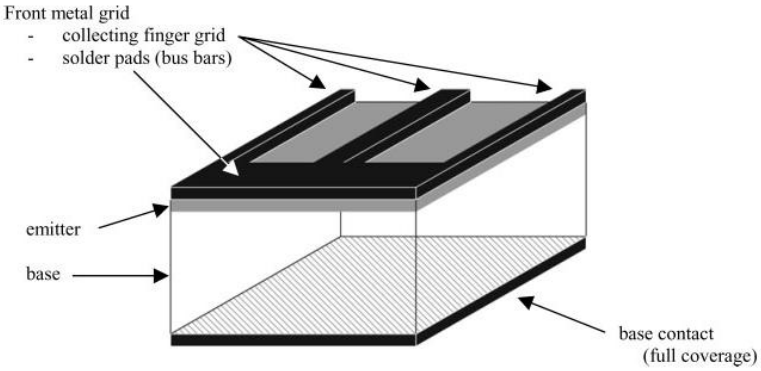

Fig. 1: *Schematic representation of convectional solar cell*

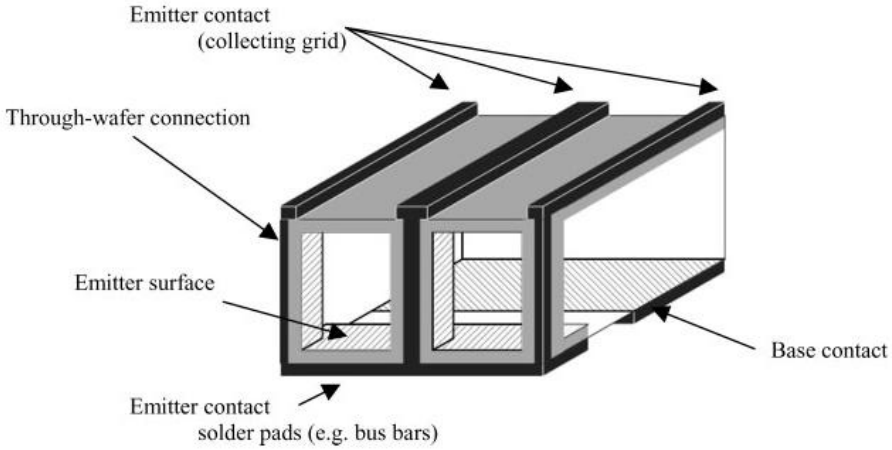

Fig. 2: *Schematic representation of a metallisation wrap-trough solar cell*

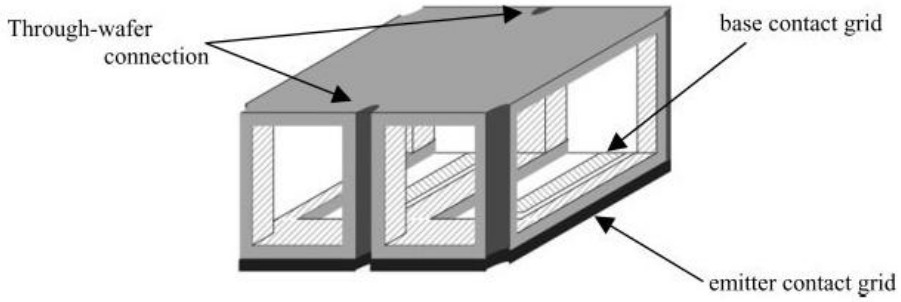

Fig. 3 *Schematic representation of an emitter wrap-trough solar cell*

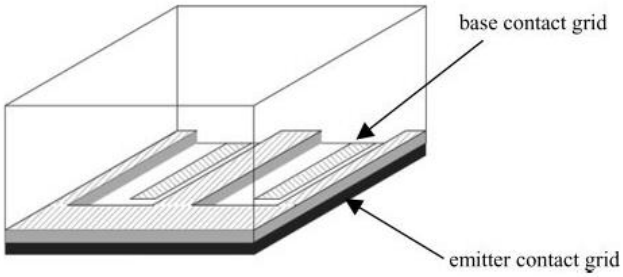

Fig. 4 *Schematic representation of a back-junction solar cell*

In the EWT concept is still maintained an emitter layer on the front of cells, however, has no metal (shielding). All contacts are located on the back surface of cells. Figure 3 shows how it is connected to the emitter contact and move to the rear through holes in the substrate coated with a layer of the emitter. The last concept is the BJ, which has the

emitter is not in the vicinity of the front surface, but is moved along with the contacts on the back surface (Fig. 4).

Analysis backside of solar cells

There is used the electroluminescence method for analyzing current distribution in the structure of solar cell. Analyzed article is connected in the forward direction for the rear side of the cell (reverse direction to the front). This makes it possible to observe the distribution of current density in the solar cell from the back and thus discover its defects. Possible damaged is due to breakdown in the PN junction. It is shows as a dark place on a slide and the area of the cell is faulty. In contrast, where the current density is higher (lighter), have better conductivity and less defects in the material structure.

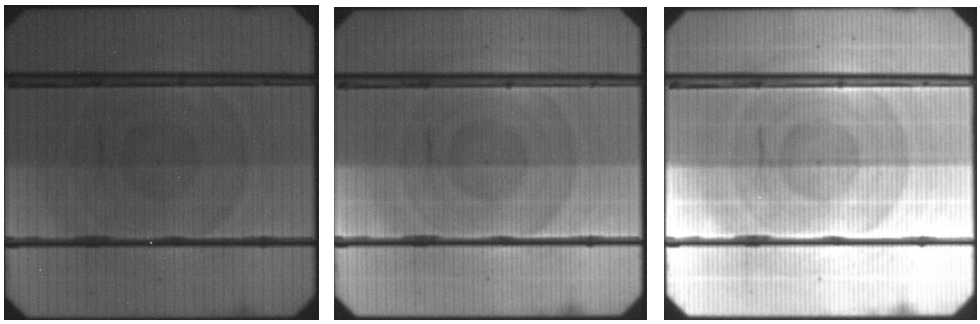

Fig. 5: *(left) cell 28 front (U=0,8 V; I=1,09 A)*
Fig. 6: *(middle) cell 28 front (U=0,9 V; I=1,55 A)*
Fig. 7: *(right) cell 28 front (U=1,2 V; I=2,53 A)*

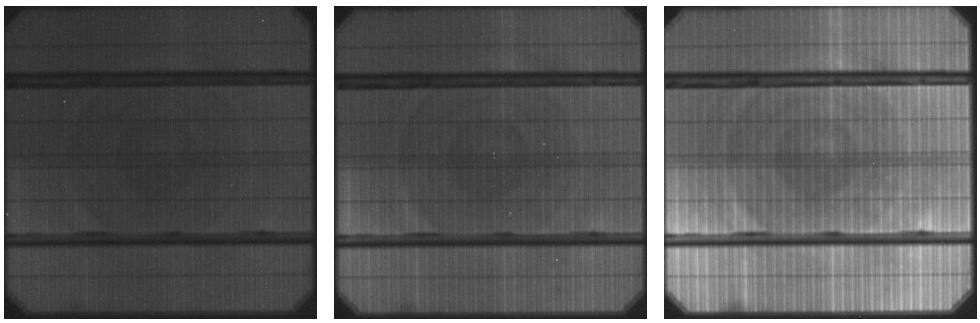

Fig. 8: *(left) cell 28 back (U=0,8 V; I=1,09 A)*
Fig. 9: *(middle) cell 28 back (U=0,9 V; I=1,55 A)*
Fig. 10: *(right) cell 28 back (U=1,2 V; I=2,53 A)*

Next Figures 5-10 were recorded using electroluminescence method, the filter in CCD camera is set to Clear, and shutter the camera at 200 sec. In the following matrix, composed of images of one cell, there is possible to see an evolution of current density in response to the change of voltage and current. It is also possible to compare how the defects and the distribution of current density are reflected, showing the front and back side of the solar cell with the same values of voltage and current. The first column is always turned the front part of the CCD camera and the second column is turned back of the CCD camera.

Conclusions

In the figures it is possible to observe swirl defect, which is usually caused by inhomogeneity of the substrate (manufacturing errors). On the front and back sides are visible exactly the same defects. Furthermore,on the back side seems to be more contrast to detect the instability current density compared to the front side of the cell. Theoretically the cell should have the same current density throughout the area. On the back side can also be reveal a smaller inhomogeneity current density (Fig. 9), which is from the front side almost invisible. This was confirmed by increasing the input voltage (Fig. 10). While on the front side at the same settings all coincided in one illuminating surface.

The concept uses the back side of the silicon solar cells definitely offers more potential for increasing their efficiency with the use of appropriate diagnostic methods.

Acknowledgements

This paper is based on the research supported by the Grant Agency of the Czech Republic, grant No. 102/09/0859 and the project VZ MSM0021630516.

References

[1] E. VAN KERSCHAVER, G. BEAUCARNE, Progress in photovoltaic: research and application, [Online]. 2009 [3.4.2009],
[2] URL: www.iee.ac.cn/fckeditor/UserFiles/File/tyndc/reference/19938777865185.pdf.
[3] [2] A. GOETZBERGER, J. KNOBLOCH, B. VOSS, Crystalline silicon solar cells, 1.vyd., 528 s. ISBN 0-471-97144-8

ACTIVE LOAD FOR THE TESTING OF SOLAR MODULES

J. Hofman[1], J. Vanek[1]

[1] Brno University of Technology, Department of Electrical and Electronic technology
Udolni 53, 602 00 Brno, Czech Republic

Corresponding author: Jiri Vanek (vanekji@feec.vutbr.cz)
Phone: +420 54114 6122, Fax: +420 54114 6147

Introduction

During the system design phase of the photovoltaic modules efficiency measurement system there were defined the requirements for stand-alone measurement unit which would be able to provide:

- **Very fast continuous measurement of the I-V characteristic** (fast measurement is necessary for minimization of influence caused by environmental condition changes and variation of intensity of incident light during the sampling period).
- **Direct measurement of Maximal Power Point (MMP)** of photovoltaic module using power controller with continual support of optimum panel load.
- **Open circuit voltage and short-circuit current measurement** of photovoltaic module (PVM)

This unit was called the Maximum Power Point Load (MPPL) and should be designed for a single module. Wattage range of actual PV modules (max. power up to 270 Wp, voltage 70 V, current 10 A) shall be supported.

Hardware

The solution of MPPL electronic design is coming out from selected concept of power measurement. PV module is loaded by an analog active load which is driven by DA converter. Output voltage of PV module is measured by AD converter. The control of unit and digital MPP tracker function are provided by the microcontroller which is connected with master computer via serial port using galvanic isolation (power is also isolated via transformers in power supply - potential ground loops are suppressed). Block diagram of the unit is on the Figure 1.

Active load

Active load circuit is based on a classical circuit design of the analog constant current controller. Current is measured by the precise shunt resistor network with very low temperature drift and active cooling. The power part of load consists of a single MOSFET transistor which is cooled by a heat sink with fans controlled by a solid-state relay. The configuration of transistor and cooler is designed for the absolute power dissipation of 270 W at ambient temperature 23°C. Current controller is driven by a high accurate Sigma–Delta DA converter whose input data word could be directly calibrated for current through the load (there is no need to measure the true value of current). This significantly accelerates the I-V characteristics measurement. The load is capable to regulate the

current only for input voltage higher than value Umin which is based on the value of the shunt resistance and the RDS(ON) resistance of power transistor channel. In operation Umin is function of current.

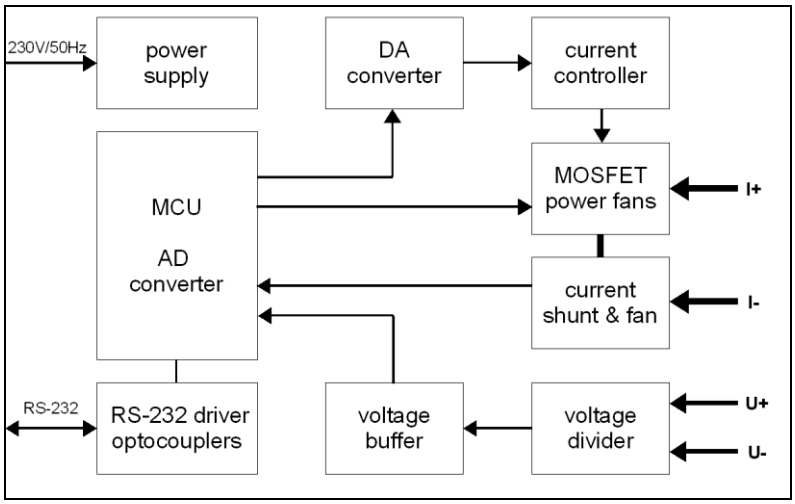

Fig. 1: *Block diagram of MPPL module*

In the case of short current measurement there is input voltage lower than Umin and calibration curve of DA converter is not valid. In this measurement mode the differential voltage across the shunt resistor is measured by the AD converter so the true value of short current is being captured.

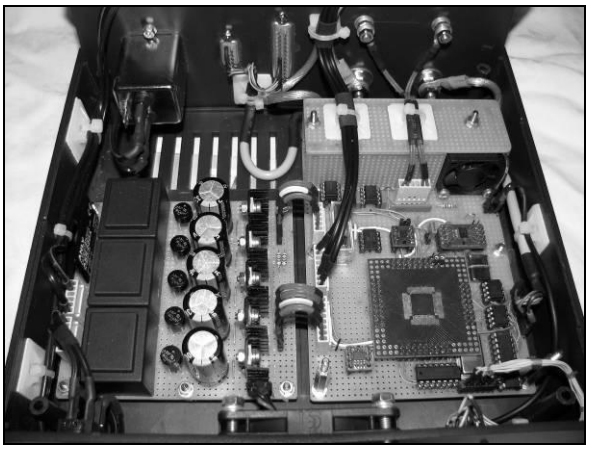

Fig. 2: *Hardware of the unit*

Voltage measurement of PVM

The measurement of output voltage of PV module is provided by an input voltage divider with very low thermal drift which is connected to the differential input of AD converter through a voltage buffer (precise operational amplifier). This allows using four-wire connection technique to eliminate measurement errors caused by cable voltage drops. This pseudo-differential input stage has high input resistance so there is no significant influence of PV module voltage. The AD converter is integrated within the microcontroller and it is using Sigma-Delta modulation. AD converter reference voltage is defined by precise external reference which is shared for the DA converter.

Fig. 3: *Whole view of active load and PPML*

Digital filter of AD converter is set for sampling frequency of 50 Hz which is a compromise between request for fast measurement and adequate suppression of main industrial frequency noise.

Software

Software of microcontroller is responsible for both the unit system related functions (control of cooling, etc.) and measurement functions (controlled by master computer via commands).

The first step of I-V characteristics procedure is the short circuit current measurement which defines the range of load current sweep used in the following loop, where the PV module is gradually loaded and its output voltage is measured.

During initialization of MPP measurement the I-V characteristic procedure is used to determine the starting value of MPP tracker load current. The MPP tracker software is based on the algorithm of 3 point weighting [3] whose goal is minimal oscillation of controlled output power and fast response on the changes of PV module lighting. The measurements of open circuit voltage and short circuit current are the special cases of measurement of I-V characteristics.

Calibration, testing

Calibration of MPPL unit is established by the set of high precision (calibrated) devices: by the stable linear DC voltage power source and by two precise 6.5 digits multimeters (the measurement of voltage and current). The whole calibration setup is fully automated using the LXI and GPIB buses.

The tests of MPPL already started during design phase by the simulation of its analog part. The tests of AD and DA converters and full analog part followed. The initial integration tests with PV module were made on 5Wp module. It was illuminated by the halogen lamp 500 W and also by the direct Sun. The final tests were made using the designed and realized lamp 2.2 kW which was designed for homogenous exposure of 50 Wp module Solartec [4] which will be used for long term measurement and research of photovoltaic panel efficiency. The distance between the lamp and the PV module can be smoothly changed so the output power of PW module can be set for any value within its operational range. This lab setup is especially used for MPP tracker software development. See Fig. 2

for an example of captured I-V curve of 50 Wp module illuminated by the Sun. This chart was automatically generated by the software UMS (Universal Measurement Software) which is a PC utility for data acquisition developed by the author of this paper.

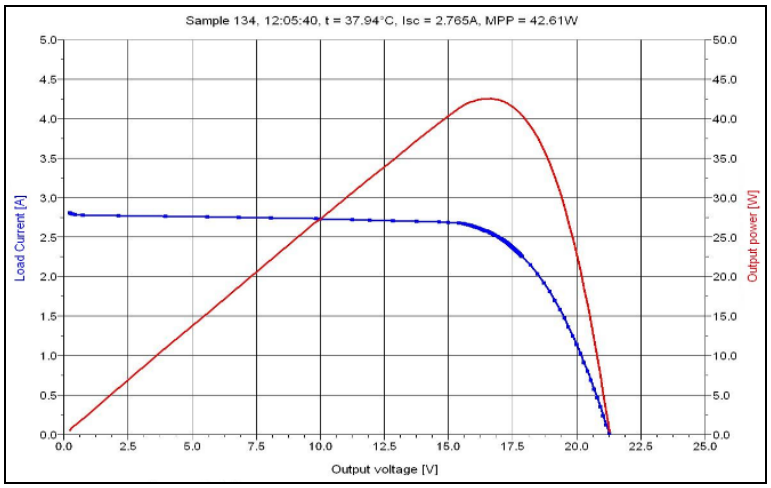

Fig. 4: *Example of measured I-V curve*

Conclusion

At the time of this paper release the prototype of MPPL unit was built and fully tested including its calibration and accuracy checks. The only remaining part to be finished is the software for MPP tracker, which is currently under development. The other parts of the complex measurement system are also about to be finalized. The intention is to launch first measurement campaign in August 2010.

The developed load unit could be also used for other purposes in the field of the test and measurement applications – with particular software modification the unit could be for example used for power supply Ripple and Noise tests.

Acknowledgments

This research has been subsidized by VZ MSM 21630516 Project and by the Grant Agency of the Czech Republic, grant No. 102/09/0859

References

[1] Murtinger, Beranovský, Tomeš.: Fotovoltaika. Energie ze slunce, ERA group, 2008
[2] Prof. Ing. Vitězslav Benda, CSc.: Solární články z krystalického křemíku – základní technologie současné fotovoltaiky, sborník z české fotovoltaické konference, Brno, 2006
[3] Jiang, Huang, Hsiao.: Maximum Power Tracking for Photovoltaic Power Systems. In: Tamkang Journal of Science and Engineering, Vol. 8, No 2, 2005, s. 147-153
[4] Solartec.: Katalogový list fotovoltaického panelu STR36-50/12 URL:< http://www.solartec.cz/files/docs/str_36-50_12_cs.pdf> [cit. 19.02.2010]

SYSTEM OF VERY LOW TEMPERATURE CONTROLLING DURING THE DEFECT DETECTION OF SOLAR CELLS

R. Stojan[1], J. Vanek[1]

[1] Brno University of Technology, Department of Electrical and Electronic technology
Udolni 53, 602 00 Brno, Czech Republic

Corresponding author: Jiri Vanek (vanekji@feec.vutbr.cz)
Phone: +420 54114 6122, Fax: +420 54114 6147

Introduction

Photoluminescence is a kind of luminescence evoked by energy of incident electromagnetic radiation. According to Stoke's law an excited radiation of light always has higher value of wave length (lower energy value) than exciting radiation. In material with indirect energy gap structure the third particle is joining the generation recombination process. Therefore not only photon in the silicon crystal is taking part of recombination but during the process of photoluminescence we need also the thermal energy deforming the crystalline structure and then we speak about interacting with phonon.

Photoluminescence spectroscopy is being used to investigate defects and localized band tail states within the band gap of silicon wafers. From the comparison of band-edge photoluminescence intensity and minority carrier lifetime, we confirmed that low photoluminescence intensity regions corresponded to short lifetime regions.

Electroluminescence (EL) surveying is a fast characterisation tool providing spatially resolved information about electrical, optical and material properties of solar cells.

The imaging techniques are much faster than use a CCD camera to obtain the spatial information simultaneously.

The EL emission due to radiative band-to-band recombination at room temperature of forward-biased crystalline silicon solar cells is surveyed with a CCD greyscale camera. Neglecting photonrecycling, the measured photon current is directly related to the local quasi Fermi-level splitting EFn-EFp according to

$$\Phi_{EL} \propto \int_0^w U_{rad}\,dz = \int_0^w Bpn\_\,dz = n_i^2 \int_0^w B \exp\left(\frac{E_{Fn} - E_{Fp}}{k_B T}\right) dz$$

Where w is the cell thickness. When analysing EL images it is important to know the contributions of the emitter, the base and the BSF to the electroluminescence signal. Due to band-gap narrowing the pn-product in the highly doped emitter and BSF regions is considerably enhanced compared to the base. Thus, despite the small thickness of these regions one might expect a large contribution to the EL signal. However, the radiative recombination coefficient B strongly depends on the free-carrier concentration and decreases considerably with increasing doping concentration.

This technique has recently been introduced by T. Fuyuki et al. as a tool for investigating the minority-carrier diffusion length for analysing the rear surface passivation quality of silicon solar cells. [2]

Both detection techniques declare the temperature dependence which we would like to explain more. For this we need equipment which enables testing the luminescence technique during large scale of temperature starting in cryo area and continuing to the temperature near the semiconductor function destruction temperature. For the low area of temperature the measuring system was designed on fig.1 which is enabling the measuring near the temperature of liquid nitrogen.

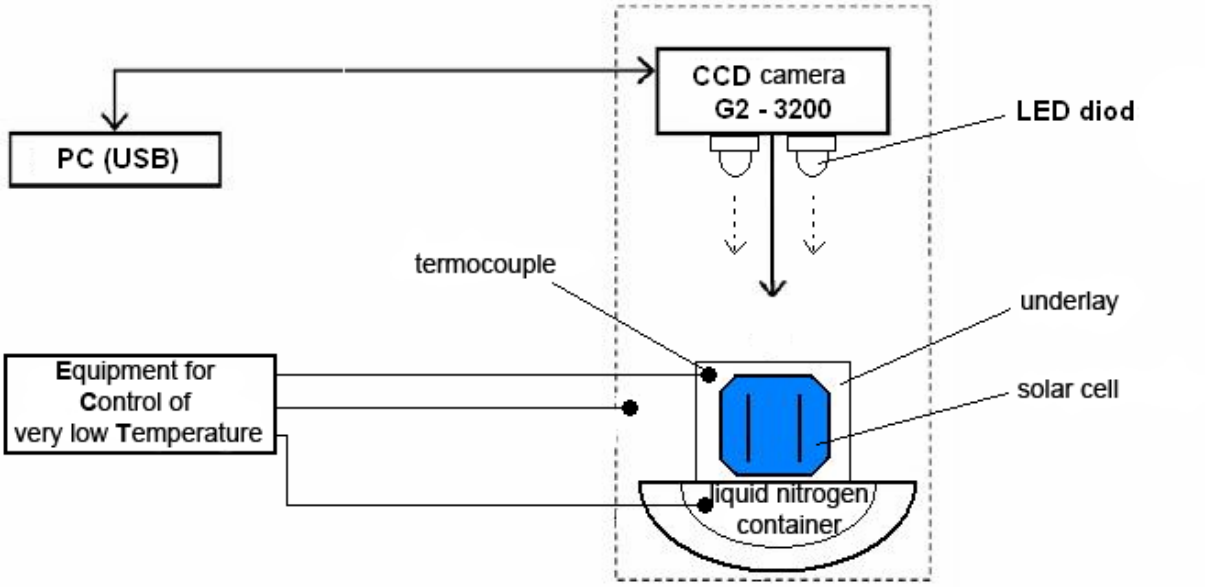

Fig. 1: *Workplace for photoluminescence testing method of solar cells in a very low temperature area.*

It is possible to modify this workplace for using the electroluminescence method and then we can also investigate the problematic of electroluminescence while measuring in cryo temperature area.

The main part of this workplace is equipment for controlling the temperature and also for protection of service staff from the frost-bite scorches.

For this reason the design for measurement equipment with thermocouples measuring temperature in three places in workplace was made:

In the container of liquid nitrogen and signal system - the caution of service staff of lack of liquid nitrogen in container.

On the solar cell surface – research data source

On the surface of chamber and on the surface of the door and the warning system – warning of the frost-bite scorches.

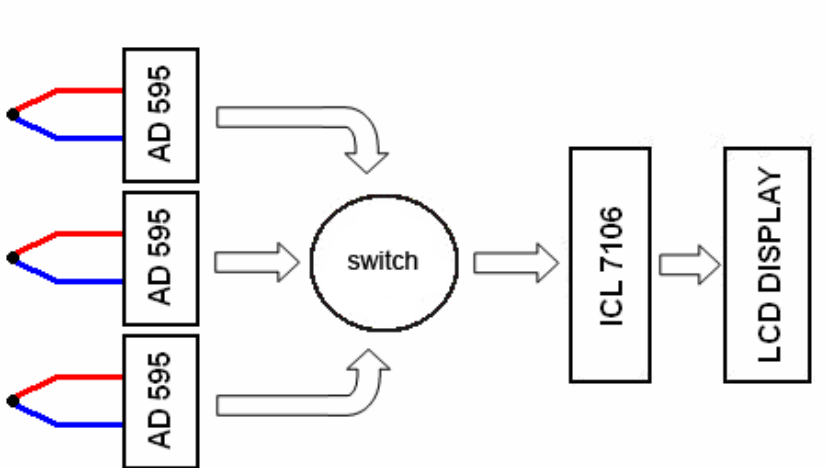

Fig. 2: *Block design of Equipment for control very low temperatures*

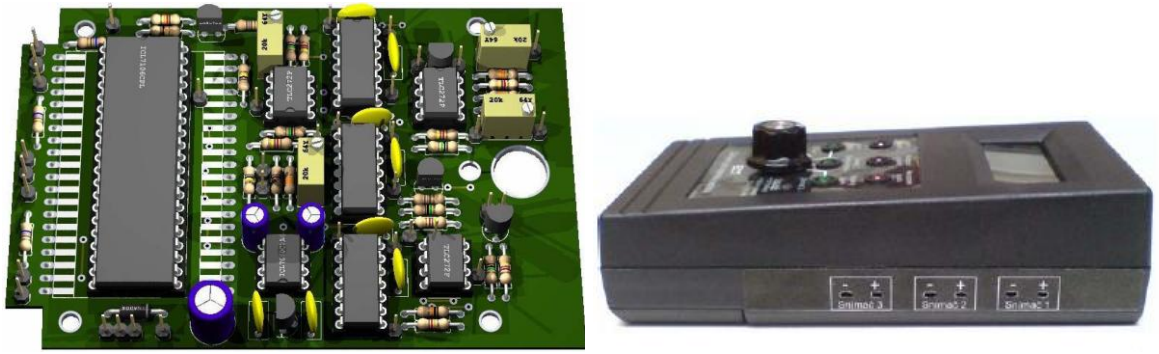

Fig. 3: *Mounted desk of Equipment and whole equipment designate for placing on the side of testing chamber*

Tab. 1: *Parameters of used thermocouples.*

Temperature [°C]	Voltage thermocouple type T [mV]	Uo AD595 [mV]	IDEÁL Uo AD595 [mV]
-200	-5,603	-1385,6	-2000
-180	-5,261	-1301	-1800
-160	-4,865	-1203,1	-1600
-140	-4,419	-1092,8	-1400
-120	-3,923	-970,2	-1200
-100	-3,379	-835,6	-1000
-80	-2,788	-689,5	-800
-60	-2,153	-532,4	-600
-40	-1,475	-364,8	-400
-20	-0,757	-187,2	-200
-10	-0,3383	-83,7	-100
0	0	0,0027	0

The thermocouples chosen were of the type T (parameters are in the tab 1) from manufacturer Omega Engineering and were encapsulated to aluminum tube of diameter 6 mm. The connection with the ceramic protection was placed inside and the whole space of tube was filled by the silicone gel.

Testing and results

There was the test made measuring with container of 10 liter of liquid nitrogen and testing process continued till full evaporating of all nitrogen. The equipment was set up to signalize the -140°C and to refill the nitrogen to container which contains 1.4 liter of liquid nitrogen. The refilling of nitrogen takes about 2 min. Opening of chamber made little increase of solar cell temperature and of the temperature on the surface of chamber. After the icing of chamber the equipment starts signalizing the danger of frost-bite scorches. With the starting temperature on solar cell 25°C we were able to cool it to the -72,8°C.

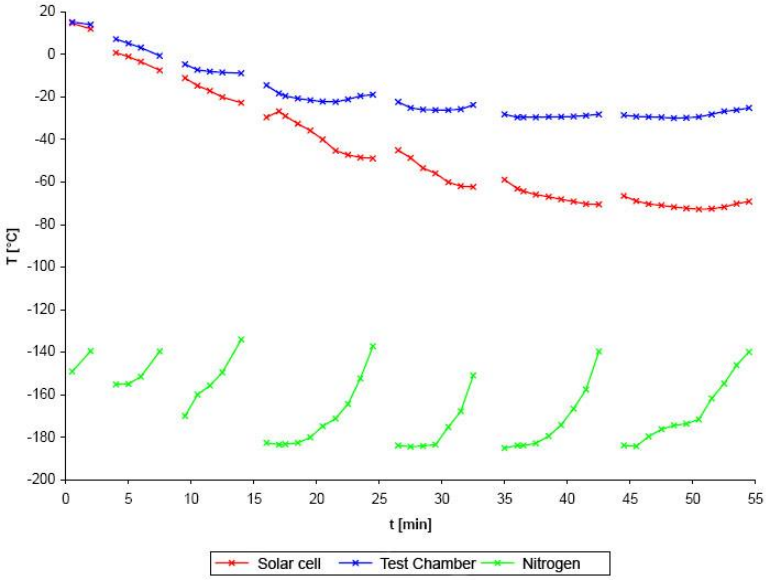

Fig. 5: *Temperature control results in the test chamber*

Acknowledgments

This research has been subsidized by VZ MSM 21630516 Project and by the Grant Agency of the Czech Republic, grant No. 102/09/0859

References

[1] TRUE, Bruce. Photoluminescence and Electroluminescence for Silicon Solar Cell Inspection [online]. Niederlassungen Deutschland : 2010 [cit. 2010-01-14]. Laser 2000,
[2] The future of Photonics. Enable from WWW:
[3] <http://www.laser2000.de/fileadmin/kataloge/INTEVAC_SolarCellWhitePaper_Bruce True.pdf>.
[4] Fangsuwannarak T., Cho E.C., Conibeer G., Huang Y, Trupke T., Green M.A.: Analysis of the effect of silicon quantum dot density on the photoluminiscence spectra of silicon dot/silicon dioxide superlattices, 21 EU PVSEC 2006, Dresden

NEW CONTROL SOFTWARE FOR LBIC WORKPLACE

A. Vesely[1], J. Vanek[1], J. Dolenský[1], F. Kucera[1]

[1] Brno University of Technology, Department of Electrical and Electronic technology
Udolni 53, 602 00 Brno, Czech Republic

Corresponding author: Ales Vesely (ales.vesely@phd.feec.vutbr.cz)
Phone: +420 54114 6168, Fax: +420 54114 6147

Introduction

A basic the LBIC measuring workplace is the plotter Mutoh IP-210, which has modified writing part. In place of the writing pen is a LED diode (LASER diode), which illumines solar cell. LED diode is moving just above the surface of solar cell so that light beam from the diode is focused on the sample and thanks to local response from the solar cell we can take an X-Y scan of the local variations. From these values we can create greyscale image of the solar cell from which it is possible to find most types of defects. Our modified plotter is connected to the PC via the LPT port from which this plotter is operated. Minimal step value of the plotter is 25μm. In the PC there is measuring card Tedia PCA-1208, which has still old ISA slot, and which measures voltage on the solar cell. It is necessary to implement this measuring in the darkness to prevent measuring from the influence of the daylight. On that ground this plotter is placed in the dark case. This case is manufactured from the aluminium plate which makes it easier for manipulating. The inside of the case is covered with black fabric texture which prevents the light from penetrating and reflecting in the case.

Current measuring method is based on scanning dot by dot. Light source placed on the moving part moves in location at one step every time. This step is set up beforehand on the PC. After transfer of the light source (e.g. from the point X11 to the point X12) will to enlightenment of the actual point and measure voltage value on the photovoltaic cell. Measured value is then saved to the memory and there is a shift of the light source one step backwards. The whole procedure is thus repeated until the entire measurement area of the solar cell. This method uniquely identifies a location of measured point.

This method may be capable of providing a relatively good picture, but it is dependent on the size of the measuring step. Disadvantages of this method include a relatively long scan time, solar cell. Cause lengthy of measuring is in constant stop-and-slide mechanism of the subsequent divergence plotter. This principle of mechanical movement of the plotter increases greatly the time required to run over plotter from one side of a photovoltaic cell to another. The newly proposed method for measuring workplace LBIC is almost wholly based on a new hardware, an original hardware is maintained and the only way the plotter is modified is technically and economically.

Innovative workplace

The newly developed software will run on the new desktop hardware. To measure the voltage solar cell the Agilent 34411A multimeter is used, this multimeter will be connected to a PC via LAN interface. Demonstration of the usage of the newly designed measuring workplace is provided in the figure Fig. 1. Usage of the LAN interface for measurement

was chosen on the grounds that the greatest attainable speed of the interfaces described above, does not need any special hardware to interconnect the meter and the PC. Network interface is now available at every new desktop PC. Connections between the current adjusted plotter and the desktop PC via LPT interface remain the same.

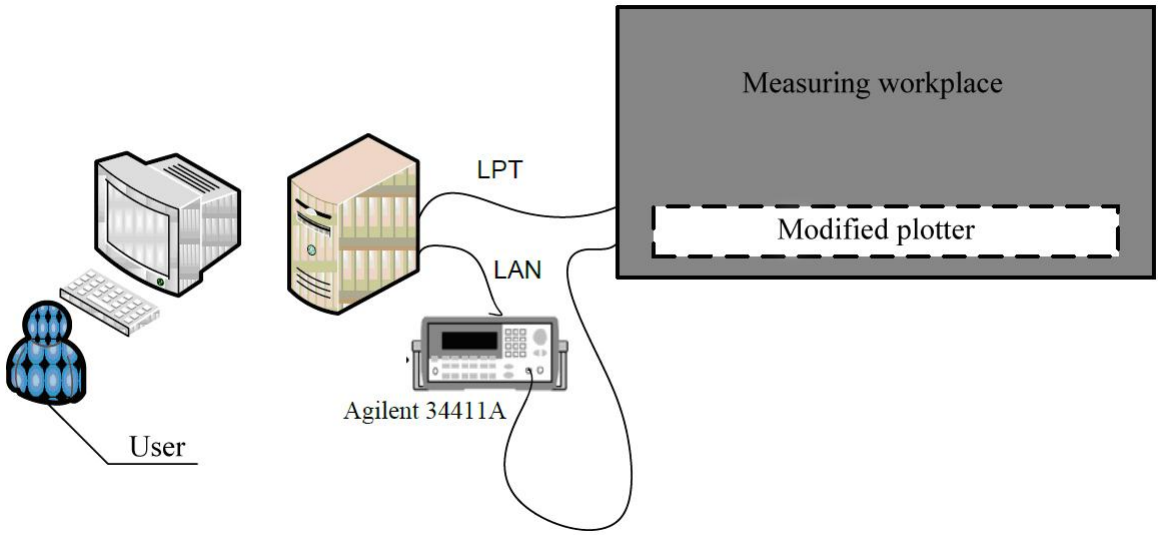

Fig. 1: *Chart showing a new measuring workplace for LBIC method*

Remote control plotter

The newly proposed workplace will use an existing modified plotter, which perfectly corresponds with our purpose. Originally it was a personal plotter A3 with eight pens that could have been operated manually, remotely. For our purposes the plotter was modified so that all the pens were removed and replaced by a special holder for the LED. Minimal movement of the plotter is 25 μm and corresponds to one plotter unit.

For remote control plotter should be before the actual measurements put a plotter into remote mode. This is done by pressing the Remote, which is located below the LCD display. The plotter can be controlled by up to 56 commands of the BASIC programming language, or using commands Mutoh 7475A Hewlett-Packard Graphic Language with which the plotter is fully compatible. For our purposes it is sufficient to use a few basic commands.

PU - PEN UP (lifting Paint pens)
PD - PEN DOWN (start Paint pens)
PA - PLOT ABSOLUTE (pen movement to a defined position XY)
PR – PLOT RELATIVE (movement of the stylus to the position defined by an absolute ΔXΔY)
VS – VELOCITY SELECT (speed settings of the movements of the pen)

For a correct entry of commands it is a necessary to consult the manual of the plotter[1]. The plotter allows the user to set several speeds, which serve to set the quality of drawing.

Tab. 1: *Movement speed of the pen plotters Mutoh iP-210*

PV1	50 mm·s^{-1}	PV5	250 mm·s^{-1}
PV2	100 mm·s^{-1}	PV6	300 mm·s^{-1}
PV3	150 mm·s^{-1}	PV7	400 mm·s^{-1}
PV4	200 mm·s^{-1}	PV8	500 mm·s^{-1}

The commands are sent to the plotter in the form of strings. There is an example of character strings for controlling the plotter provided:

InitPlotr = "PU;VS50;PA5200,4500;PD;";

A string called "InitPlotr" contains several commands, first lifts the Paint pen, the second sets the moving speed of the pen plotter to the speed 500 mm·s^{-1}, the third statement includes all the data connected with the directions of the pen, and the fourth command starts the paint pen on the drawing area .

Development and implementation of a new algorithm for LBIC

A new measurement method is based on measurement of the photovoltaic moving light source from the initial position X to the final position X (see Fig. 2). The light source is attached to the moving parts plotter which moves over photovoltaic defined speed (e.g. 50 mm·s^{-1}) during which the meter Agilent 34411A can measure out a sufficient number of samples. Samples are moved over the light source stored in the memory of the meter and at the end of each line, all data from an entire row is sent to the PC.

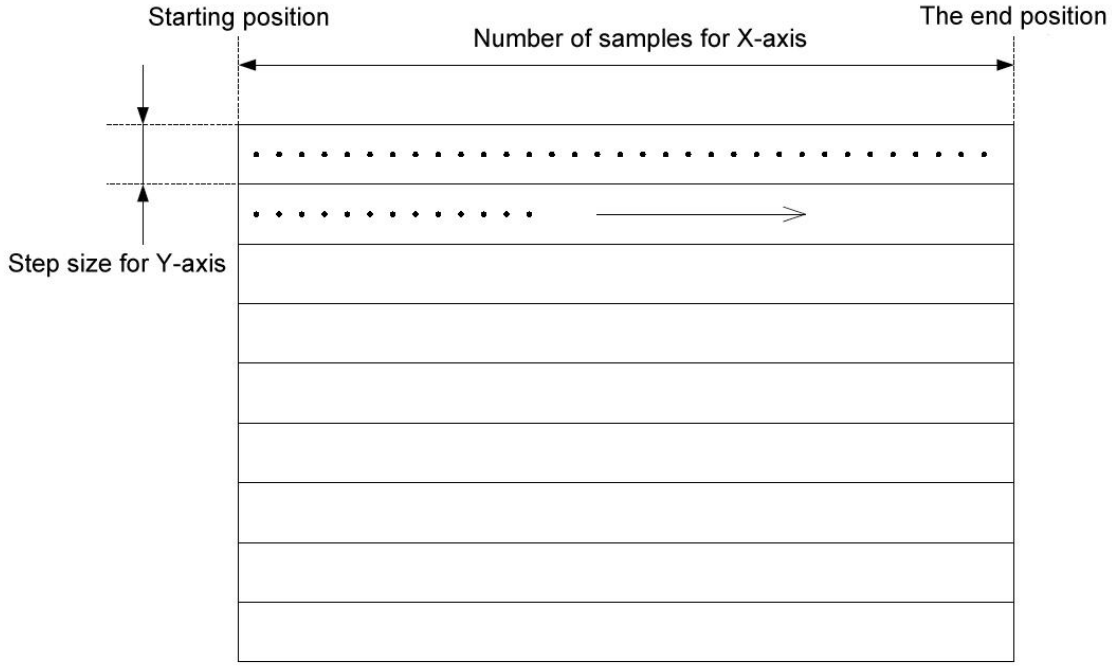

Fig. 2: *New measuring method*

Implementation of a new measurement algorithm

After starting the program *LBIC_verze2.exe* will initiate the necessary values for the measurements. The default setting parameters for measurement can be changed before

running a scan. After pressing the SCAN first check that the meter is connected to the PC, if connected, it will retrieve the specified values for the measurements. Following by two calls of functions *InicializaceObrazku()* function sets the required size of the image in which the for storing the measured values needed to plot. Using *InicializaceMericihoPristroje()* the multimeter will be reset, the meter settings range of 10V DC, to set a high input impedance measurements to adjust the number of samples after and to start to set the measurement period. Then check that the method of measurement is selected, if the set method of measuring left to right will set the starting coordinate's plotter in the upper right corner of the photovoltaic cell. For other methods of measurement there are coordinates plotter default settings in the upper left corner of the photovoltaic article.

Succeed scanning of solar cell according to choose methods of measurement. If the method is selected from right to left, there is a shift to the left 50 $mm \cdot s^{-1}$ and speed while moving through the wilderness with measurement values. After the measurement of a line waiting to receive data from previous measurements, followed by transfer to the starting position plotter X speed 500 $mm \cdot s^{-1}$. LBIC program receives measured data from the meter in the form of a text string, followed by a text string of data sharing and transfer of values in numerical form. Succeed the plot and save the values in each field. The whole cycle is repeated until the processing of measured data from one row. After processing all the data is moved to a new line speed 500 $mm \cdot s^{-1}$ and the whole cycle is repeated until the measurement of the whole cell. For this method of measuring make scanning from one side due to location of sync measurement points, because we have no other hardware feedback to identify the location of measurement points.

Conclusions

New control software for the workplace LBIC is very fast, of the previous 25 hours that this measurement method can handle in the tens of minutes up to few hours depending on the level of accuracy. Unfortunately, this type of measurement, struggles with a low contrast in the final image due to the weak response of a small solar cell in the rapid transit light sources. This disadvantage will need to be solved in future. So far, the best solution appears to be a much more intense source of light.

Acknowledgements

This research has been subsidized by the Grant Agency of the Czech Republic, grant No. 102/09/0859, MSMT FRVS project No. 2503/G1 year 2010 and by VZ MSM 21630516 Project.

References

[1] MUTOH, Personal plotter IP-210 – User Guide, [online] [cit. 2010-05-20]. URL:
[2] < http://www.mutoh.be/binarydata.aspx?type=doc/ip-210_ug_en.pdf>.
[3] AGILENT TECHNOLOGIES, Agilent 34410A/11A 6 ½ Digit Multimetr – Programmer's Reference, [online] [cit. 2010-03-25]. URL:
[4] http://www.home.agilent.com/agilent/techSupport.jspx?pid=692834&cc=CZ&lc=eng&t=80039.k.1&guid=171821

11th ABAF

BRNO 2010

Advanced Batteries, Accumulators and Fuel Cells

Electric Vehicles

E-CAR ENERGY MANAGEMENT SIMULATION

M. Patočka[1], P. Huták[1], D. Červinka[1], P. Vorel[1]

[1] UVEE FEKT, Brno University of Technology, Technická 8, 616 00 Brno, Czech republic

Corresponding author: Miroslav Patočka (patocka@feec.vutbr.cz)
Phone: +420 5 4114 2690, Fax: +420 5 4114 2464

Introduction

The global simulation of the E-car energy balance was done. This is necessary for the accumulator capacity and peak power dimensioning. The simulation results are also used to qualify the power (speed - torque) dimensioning of the traction drive. The standard vehicle speed profile EURO EC15 was taken into consideration in this simulation.

The main simulation schema is in Fig.1. All simulations were created in MATLAB - Simulink.

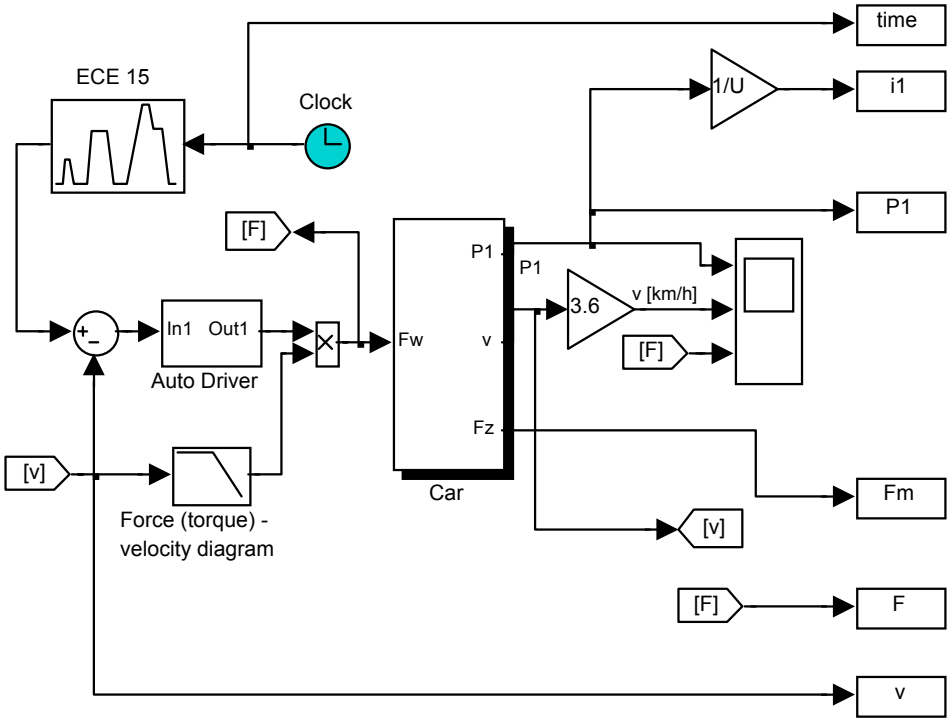

Fig. 1: *Energy management simulation block diagram*

A defined fixed dependence of vehicle speed on time creates the input variable of the simulation. A speed control loop is used in the simulation. The outputs of this simulation block are:

traction force as a function of time $F = F(t)$
electrical source power as a function of time $P_1 = P_1(t)$
electrical source actual current $i_1 = i_1(t)$
The inside blocks of the schema shown in Fig.1 are described in following text.

E-car dynamic model (block “CAR”)

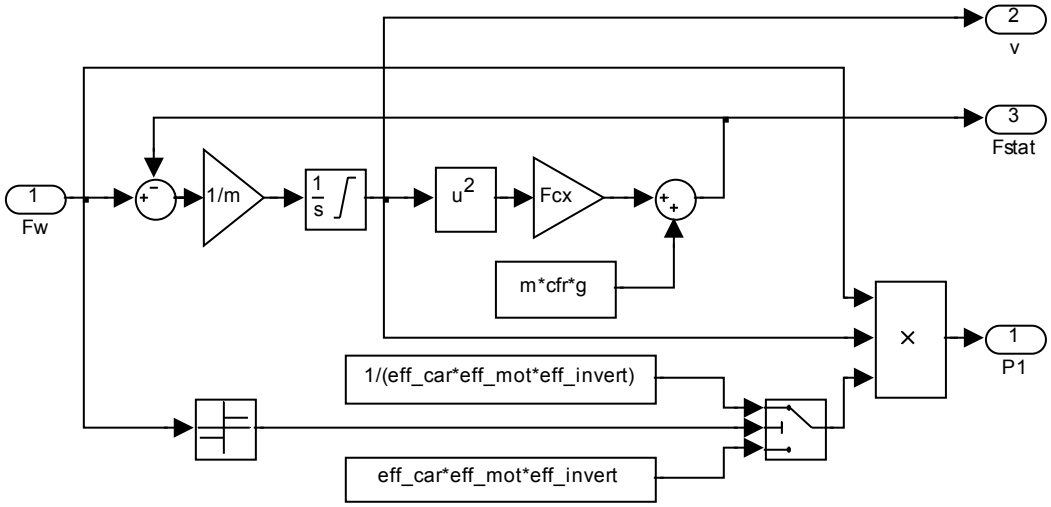

Fig. 2: *Inside structure of the block “CAR”*

This simulation block represents following motion equation (1):

$$F = m\frac{dv(t)}{dt} + mg\sin\alpha + c_{fr}mg + k_v v(t) + \frac{1}{2}c_x A_f \rho v^2(t) \qquad (1)$$

A zero road declination is assumed. Therefore the element $mg.\sin\alpha$ is zero. Further no viscous friction is taken into consideration so the element $k_v v(t)$ is zero too.

Other parameters are chosen as a typical example for a medium-size class vehicle:

mass: m = 1150 kg

aerodynamic coefficient: $c_x A_f$ = 0,8

rolling coefficient: $c_{f\,r}$ = 0,0120

tyre rolling radius: r = 0.286 m

Traction characteristics of the drive

The proposed traction characteristics is in Fig. 3. The linear decrease of the traction force was chosen in the de-excitation area for simulation.

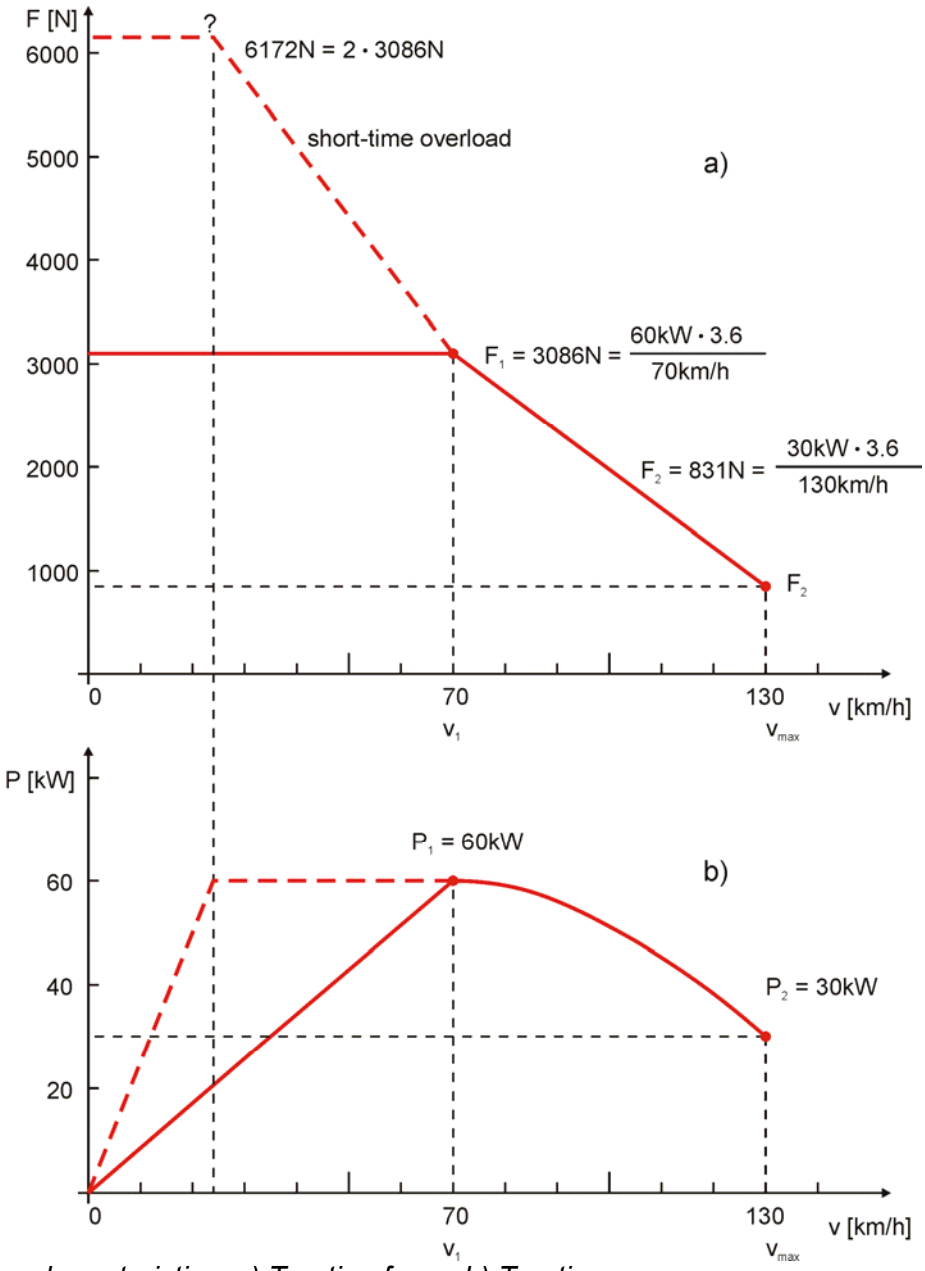

Fig. 3: *Traction characteristics. a) Traction force. b) Traction power.*

Two significant points v_1, v_{max} in Fig.3 were determined from following chosen data (typical E-car values):

Rated torque continuous service (S_1, 1h) [Nm]:	100
Transient maximum torque (S_3, 3min) [Nm]:	200
Rated power P_2 (from base to max speed) [kW]:	30
Maximum transient power P_1 [kW]:	60
Maximum speed v_{max} [km/h]:	130
Maximum motor operative speed ω_{max} [rpm]:	11000

Motor speed in the nominal point:

$$\omega_1 = \frac{P_1}{T_1} = \frac{60\text{kW}}{100\text{Nm}} = 600\text{rad/s} = 5730\text{rpm} \tag{2}$$

Car velocity in nominal point (beginning of de-excitation area):

$$v_1 = \frac{\omega_1}{\omega_{\max}} v_{\max} = \frac{5730\text{rpm}}{11000\text{rpm}}\ 130\text{km/h} = 70\text{km/h} \tag{3}$$

Nominal traction force:

$$F_1 = \frac{3.6P_1}{v_1[\text{km/h}]} = \frac{3.6 \cdot 60\text{kW}}{70\text{km/h}} = 3086\text{N} \tag{4}$$

Traction force at maximal speed:

$$F_2 = \frac{3.6 \cdot P_2}{v_{\max}[\text{km/h}]} = \frac{3.6 \cdot 30\text{kW}}{130\text{km/h}} = 831\text{N} \tag{5}$$

Simulation results

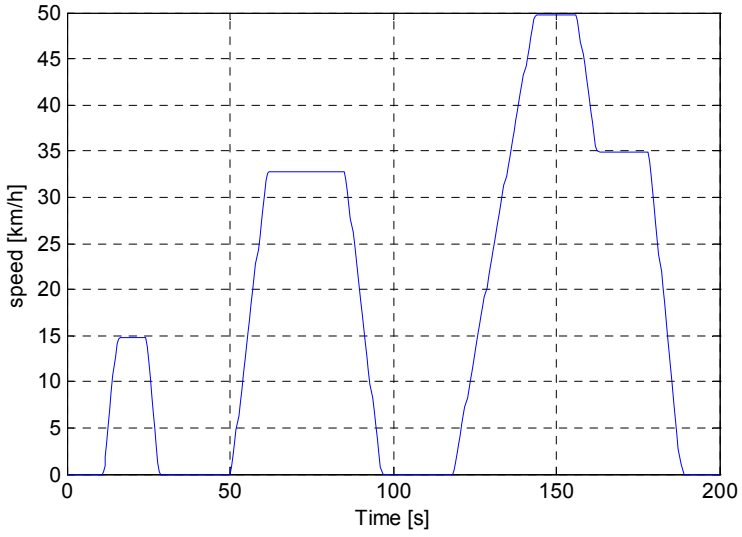

Fig. 4: *Standard EC15 vehicle speed profile.*

The simulated traction force using the mentioned EC15 velocity profile is in Fig.5. Then the energy source power and actual current are in Fig.6 and 7. The shapes displayed in Fig.6 and 7 are the same because the battery voltage is assumed to be constant and therefore following must be true:

$$i(t) = \frac{P(t)}{U_{bat}} \tag{6}$$

The battery voltage Ubat = 600V.

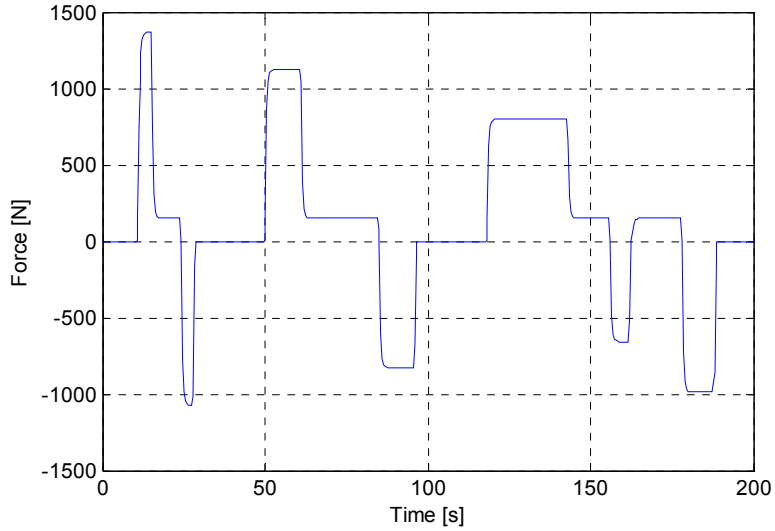

Fig. 5: *Simulated traction force on EC15 speed profile*

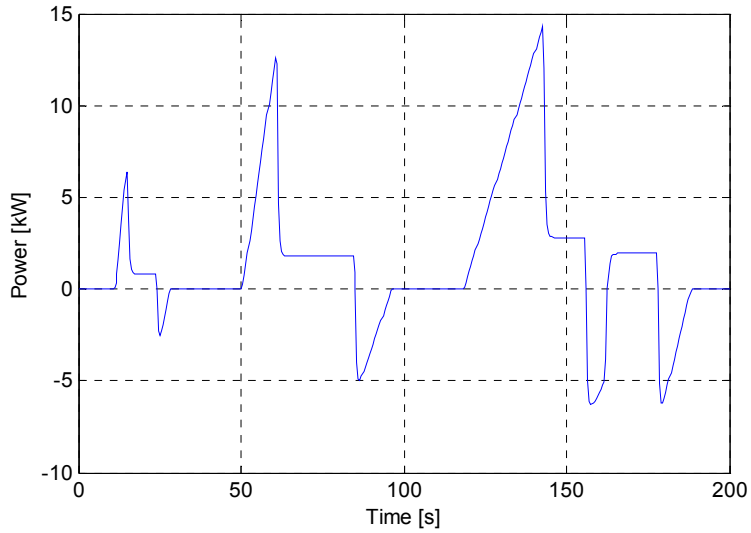

Fig. 6: *Battery power on EC15 speed profile*

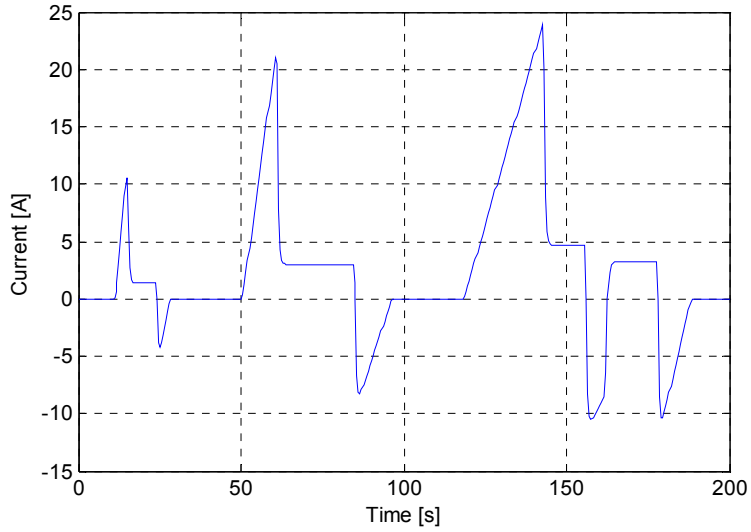

Fig. 7: *Battery current on EC15 speed profile*

Conclusions

Finally following useful results can be found out from Fig. 6 and 7:

Total energy consumption E_{bat} on EC15 speed profile:	281 kJ*
Mean power $P_{traction}$ on EC15 speed profile:	1.4 kW
Energy taken form battery E_{taken} on EC15 speed profile:	388 kJ*
Energy putted back to battery E_{back} on EC15 speed profile:	107 kJ*
Mean value of battery current I_{batAV} on EC15 speed profile:	2.3A
RMS value of battery current I_{batRMS} on EC15 speed profile:	6.7A

$$* \; E_{\text{bat}} = E_{\text{taken}} - E_{\text{back}}$$

Definition of the recuperation efficiency on EC15 speed profile:

$$\eta_{recuper} = \frac{E_{back}}{E_{taken}} = \frac{107}{388} = 0{,}28 \qquad (7)$$

This optimistic result is valid only if no electro-chemical time constant is assumed what need not be true.

The proposed simulation mechanism represents a useful tool for battery-supplied electric vehicles designing.

Acknowledgements

This research has been supported by the European Commission under the ENIAC CA-E3Car-2008-120001 E3CAR - Nanoelectronics for an Energy Efficient Electrical Car project. Further this was supported by the project MSM0021630516 “Zdroje, akumulace a optimalizace využití energie v podmínkách trvale udržitelného rozvoje”.

References

[1] PROCHÁZKA, P.; VOREL, P.; KLÍMA, B.; HUTÁK, P.; ČERVINKA, D.; PATOČKA, M. Pohon automobilu s vodíkovým palivovým článkem. In XXXI. celostátní konference o elektrických pohonech. Plzeň: Česká elektrotechnická společnost, 2009. s. 79-82. ISBN: 978-80-02-02151- 3.

[2] PATOČKA, M.; VOREL, P.; ČERVINKA, D.; ŠTĚPANČÍK, F. Trakční pohon s vodíkovým článkem a ultrakapacitorem. In Workshop hydrogen technologies, fuell cells and applications HT-FCA 2006. Ostrava: VŠB-TUO, 2006. s. 36-40. ISBN: 80-248-1179-0.

ULTRACAPACITORS IN E-CARS, YES OR NOT?

M. Patočka[1], D. Červinka[1], P. Huták[1], P. Vorel[1]

UVEE FEKT, Brno University of Technology, Technická 8, 616 00 Brno, Czech republic

Corresponding: Dalibor Červinka (cervinka@feec.vutbr.cz)
Phone: +420 5 4114 2438, fax: +420 5 4114 2464

Introduction

Some types of traction accumulators for electric vehicles, especially lead-acid, are not able to absorb the energy of regenerative braking if the braking starts immediately after the state when the battery was discharged (the current flew from the battery - driving regime). This is caused by the time constant of the chemical reactions in the accumulator. In this case a significant part of the energy will not be stored to the battery.

Using the ultracapacitor the battery current can be filtered to its long term average value without braking and accelerating peaks. Then the previously described negative effect is strongly eliminated. Moreover the long term RMS value of the current decreases in this way and so the power loss on the internal resistance of the accumulator decreases too. So the trailing throttle of the vehicle and the life time of the accumulators can be increased.

Both negative effects (time constant of chemical reactions and high internal resistance) are typical for older types of batteries. Using new types of batteries (like LiFePO) these effects are not so significant and then the usage of ultracapacitors looses its importance.

This contribution presents an analysis of a typical concrete E-car energy balance and it gives a decision whether the ultracapacitor should be used or not.

Ultracapacitor connection and dimensioning

A direct parallel connection of the ultracapacitor to the battery is not suitable because the voltage of the ultracapacitor has to be changed in a wider range so that a large amount of energy of the ultracapacitor can be used. That is why a solution in Fig.1 was designed. The 2-quadrant converter is able to transfer the energy in both directions between the accumulator (DC link of the traction inverter) and the ultracapacitor C_U.

The ultracapacitor is able to absorb or give out the same amount of energy ΔW. Due to the converter proper operation the ultracapacitor voltage must not drop under approx. one half of the battery voltage. Then the ΔW can be calculated by following relation (deduced in [1]):

$$\Delta W = \frac{3}{16} C_U U_B^2 \qquad (1)$$

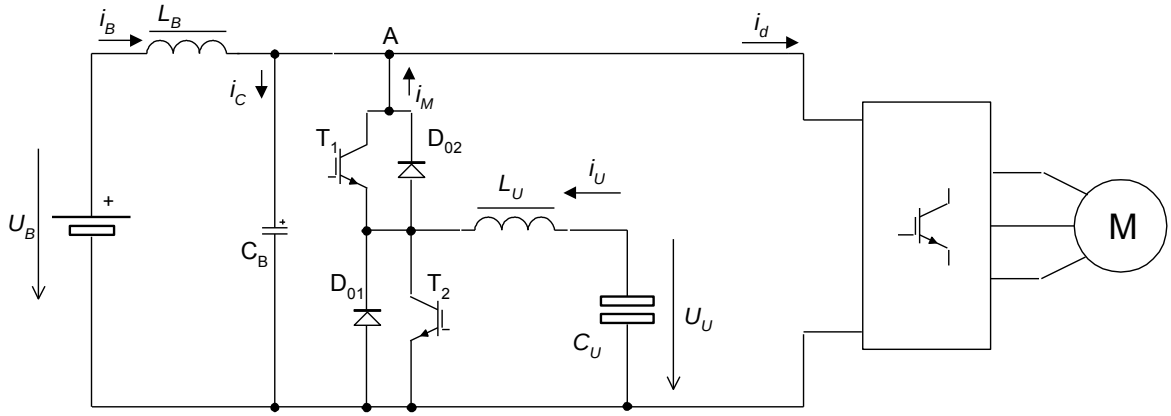

Fig. 1: *Connection of the ultracapacitor to the DC link.*

Example:

Values C_U = 10F and U_B = 550V were used in an electric bus constructed in our department before. Then ΔW = 567 kJ. This represents a peak power of 100kW during 5,67s (acceleration or regenerative braking).

In our present system (medium-size E-car) we suppose C_U = 2,6F and U_B = 600V what represents ΔW = 175,5kJ. This is a suitable value according to the maximum power of car 60kW and to its weight 1150kg and maximum speed 130km/h.

We can use 250 cells 650F/2,7V (type BCAP0650 fy MAXWELL) in serial connection. So we have a battery 2,6F/675V. The nominal voltage of the used traction accumulator is 600V. Then its maximum voltage can be higher if it is fully charged and the regenerative breaking comes. This battery voltage increasing caused by the regenerative braking is electronically limited in the main traction inverter of the car to max. 650V (for example). The internal resistance of complete capacitor battery is 0,2Ω.

Control algorithm

The control circuit has to guarantee an elimination of the battery current peaks setting the voltage of the ultracapacitor onto a demanded value in dependence on the actual speed. The voltage of the ultracapacitor is controlled only “long – termed”. The detailed description of the control structure was presented in [1].

The fast slave current loop controls the current of the ultracapacitor in such a way to smooth the battery current. In fact there is a proportional controller of the battery current changes to a demanded zero value.

The slow master loop keeps the voltage of the ultracapacitor inverse proportional to the speed of the vehicle (with respect to the condition of minimum value of $U_B/2$). So if the vehicle is standing then the capacitor will be charged onto the full voltage in order to have the maximum energy (ΔW usable for acceleration). At the maximum speed the voltage will be suitably decreased so the ultracapacitor can absorb also the maximum energy ΔW when the expected breaking comes.

Mathematical model of the E-car using the ultracapacitor

The whole simulation schema is in Fig. 2. The base of the simulation schema is the block "System" which represents the mechanical dynamics of the E-car. A detailed description of this block is present in another contribution in this proceedings named "E-car energy management simulation". The block "Control of ultracapacitor" contains the mentioned control structure of the converter described in Fig.1. A more concrete simulation diagram of this block is in Fig.3.

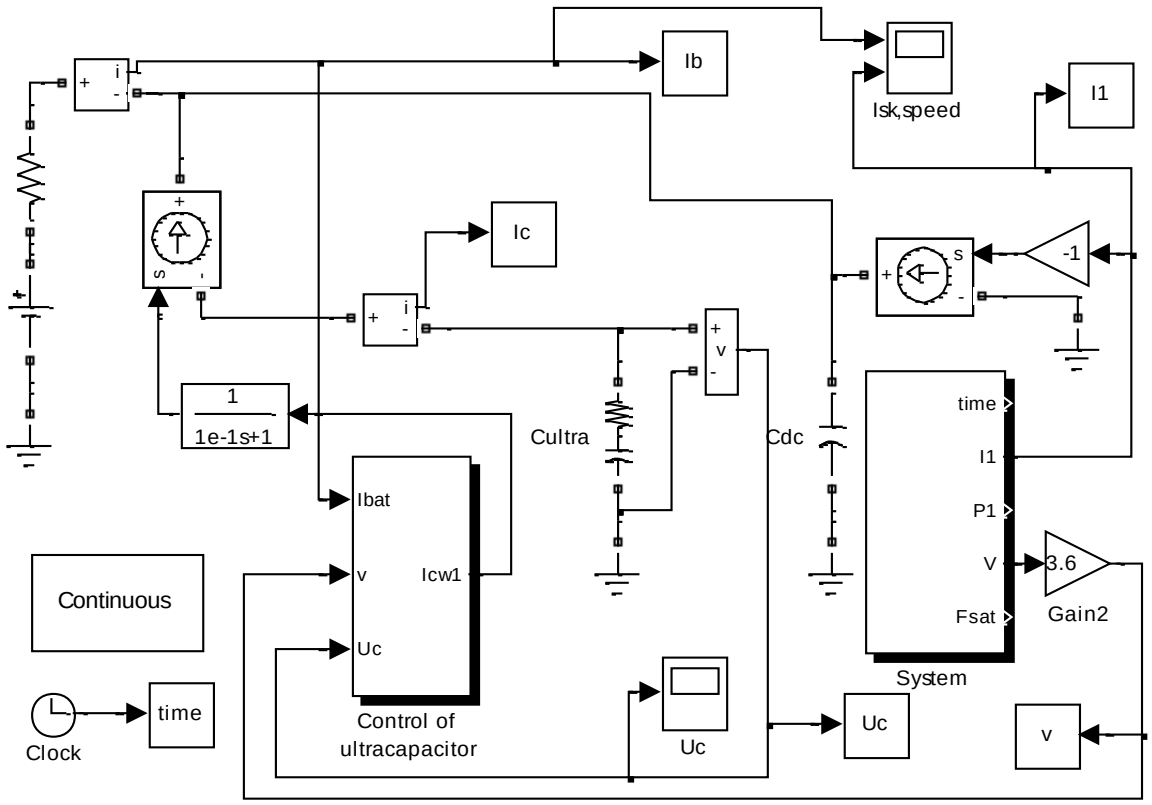

Fig. 2: *Simulation schema.*

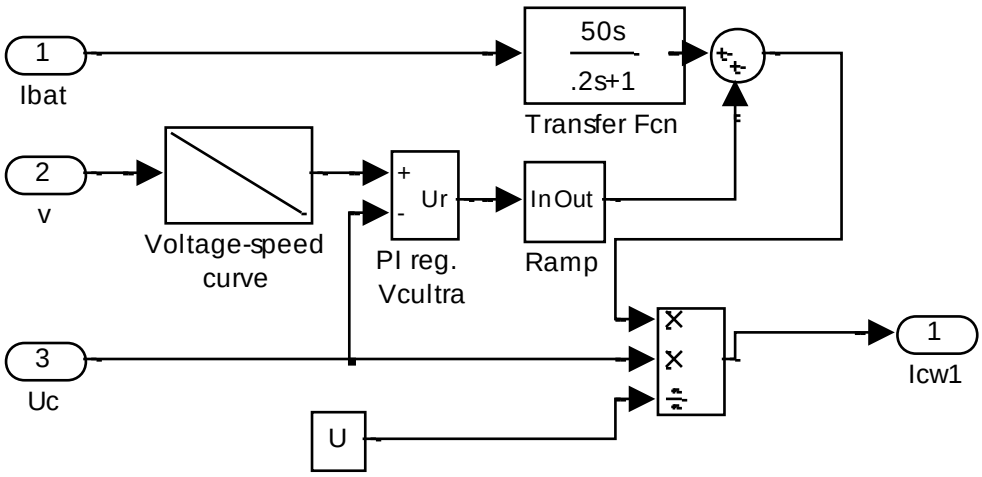

Fig. 3: *Block "Control of the ultracapacitor" internal structure.*

Simulation results

The simulation results are in Fig.4. This figure contains the battery current i_b, ultracapacitor current i_c and input current i_{conv} of the traction DC/AC converter.

Note:

The balance $i_{conv} = i_c + i_b$ is not true because a DC/DC converter (with varying duty cycle) is placed between the ultracapacitor and the DC link.

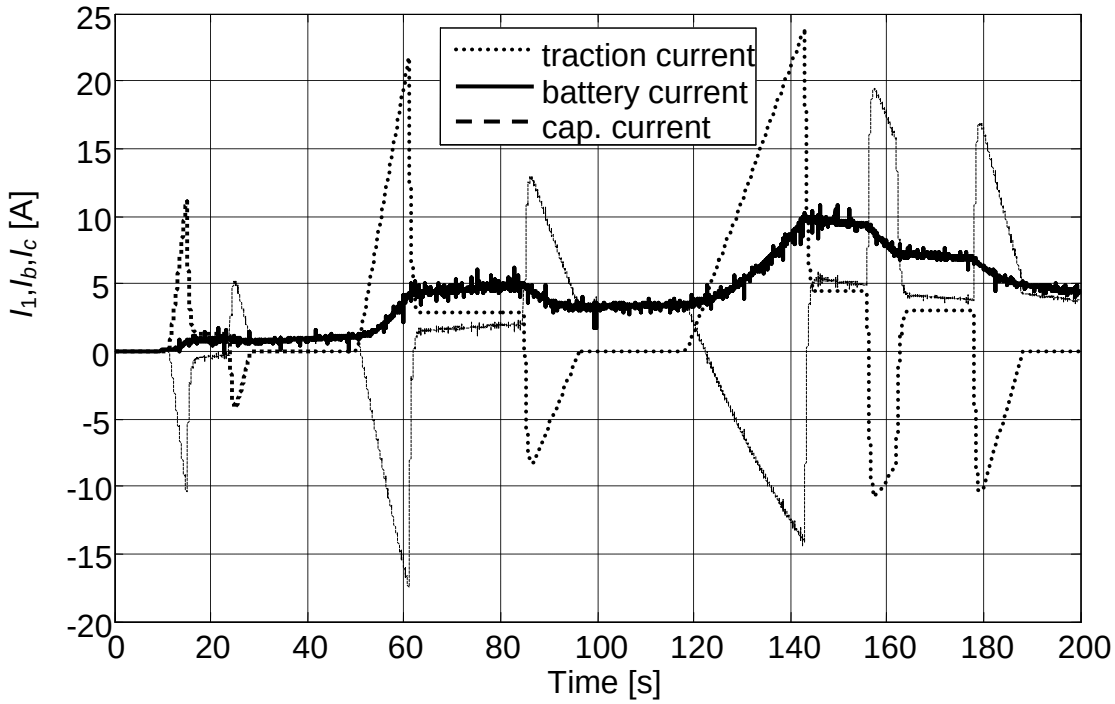

Fig. 4: *Simulation results*

Following calculations were done using Fig.4:
RMS value of traction inverter input current $I_{RMS,conv}$, on EC15 speed profile: 6.7A
RMS value of battery current $I_{RMS,bat,2}$ on EC15 speed profile: 4.9A
RMS value of ultracapacitor current $I_{RMS,cap}$ on EC15 speed profile: 6.5A
These values are used for loss analysis presented in the following chapter.

Result discussion

An ultracapacitor application with the above mentioned control structure in an electric scooter can be shown as an example. This scooter was constructed at the Department of Power electrical and Electronic Engineering, Brno Technical University, Faculty of Electrical Engineering in year 2002. It is supplied from a lead-acid accumulator 4×12V / 44Ah. An induction traction motor 1,8kW is used. The action radius was increased about 20% using the ultracapacitor 20F in the city traffic.

In a case of modern accumulators Li-Ion, Li-Fe-PO it´s necessary to find out the electro-chemical time constant. If it is high then the ultracapacitor usage is explicitly useful. If it is

low then following losses analysis decides whether the ultracapacitor usage is useful or not:

If no ultracapacitor is used then the average i.e. active battery power (at the time interval EC15) is given by this equation:

$$P_{loss,bat,1} = I^2_{RMS,bat,1} R_{i,bat} = (6.7\text{A})^2 R_{i,bat} \quad (2)$$

The RMS battery current $I_{RMS,bat,1}$ is in this case equal to the $I_{RMS,conv}$.

If the ultracapacitor is used then the average i.e. active battery power (at the time interval EC15) is given by this equation:

$$P_{loss,bat,2} = I^2_{RMS,bat,2} R_{i,bat} = (4.9\text{A})^2 R_{i,bat} \quad (3)$$

The ultracapacitor average loss power is given by equation:

$$P_{loss,cap,2} = I^2_{RMS,cap,2} R_{i,cap} = (6.5\text{A})^2 \cdot 0.2\Omega \quad (4)$$

Let ´s define the average loss power of the ultracapacitor 2-quadrant DC/DC converter as $P_{conv,2}$. This power can be calculated simply however it depends on actual used parameters.

Conclusion

The ultracapacitor presence is explicitly useful if the electro-chemical time constant of the traction accumulator is high (i.e. it is not able to change suddenly the regime from discharging to charging). This is a typical property of lead-acid accumulators - their electro-chemical time constant may be several seconds.

If the electro-chemical time constant of the traction accumulator is low (LiFePO etc.) then the ultracapacitor presence is useful only if following inequality is true:

$$P_{loss,bat,2} + P_{loss,cap,2} + P_{conv,2} < P_{loss,bat,1} \quad (5)$$

From the text above it is clear the result depends on the internal resistance of the ultracapacitor and of the battery.

The price, dimensions and mass of the ultracapacitors are next deciding criterions.

Following ultracapacitor set was taken into consideration in the above presented simulations of the E-car:

type:	BCAP0650 fy MAXWELL
number of cells:	250pc
total mass:	40kg
total volume:	75dm^3
total serial resistance:	0,2Ω
nominal voltage:	250 × 2.7V = 675V

Acknowledgements

This research has been supported by the European Commission under the ENIAC CA-E3Car-2008-120001 E3CAR - Nanoelectronics for an Energy Efficient Electrical Car project. Further this was supported by the project MSM0021630516 “Zdroje, akumulace a optimalizace využití energie v podmínkách trvale udržitelného rozvoje”.

References

[1] VOREL, P., HUTÁK, P. A traction drive with a battery and ultracapacitor. In Advanced Batteries and Accumulators - 4rd. Brno: VUT Brno, 2003. s. 78-80. ISBN: 80-214-2083-1.

[2] VOREL, P., HUTÁK, P. Traction drive of an electric vehicle using an ultracapacitor. In National conference with international participation Engineering mechanics. Praha: Akademie věd České republiky, 2003. s. 120-121. ISBN: 80-86246-18-3.

[3] VOREL, P., HUTÁK, P. Ultracapacitors in electric vehicles. In Telecommunications and signal processing TSP - 2003. Brno: VUT Brno, 2003. s. 263-266. ISBN: 80-214-2433-8.

BATTERY ELECTRIC CAR CONVERSION OF SKODA SUPERB

J. Marušinec[1]

[1] *Brno University of Technology, Antonínská 548/1 Brno, Czech Republic*

Corresponding author: Jaromír Marušinec (marusinec@ro.vutbr.cz)
Phone: +420 603 231 785

Introduction

Accumulators are the most important parts of electric vehicles. Although many promising types of accumulators already exist, however for the production of EV only a few types are available. Limitation is caused by safety, weight, size and mainly by price. In these days the price is about 1000 CZK/1 km autonomy.

Experimental

Three methods of building electric car existing:

1) **Conversions of combusting cars:** In Czech Republic converts cars company EVC Group, in Italy MicroWett company, in UK Smith company, Tesla in USA.
2) **Powertrain changes by vehicle manufacturer:** In Czech Republic SOR company creates electro busses, AVIA electro truck. In France Renault, PSA Peugeot Citroen, in Germany VW, BMW Mini preparing their own electric cars on standard chassis.
3) **Cars designed from the beginning as the electric:** For example TH!NK from Norway, Smart, Pininfarina BlueCar from Italy, Mercedes B-zero from Germany.

For demonstration project of student electric car was determined model Skoda Superb. Price of this car is higher, but future customers car better car if may pay for accumulators.

The car was converted to EV in company EVG Group by Ph.D. student of Faculty mechanical engineering Ing. Martin Solař and a student from Faculty information technology BUT Bc. Miroslav Svačina.

Students and researcher from Faculty of Electrical Engineering and Communication BUT doc. Pavel Vorel, Ing. Dalibor Červinka, Ing. Jan Kuzdas, Ivo Pazdera a Jan Knobloch are working on a speed charger 40kW for this EV. The charger would be able to charge the vehicle within 30 minutes for 180 km autonomy.

Fig.1: *EV Superbel on Autosalon Brno 2010*

Modern methods of charging batteries

Charging speed is measured, like speed of move in km per hour. For medium-fast charging speed is considered to be over 300 km/h, ie a charge more than 20 minutes for the next 100km. This speed of charge becomes from 16kWh per 100 km energy consuptions and 44kW electrical power from three-phase 3x63A source.

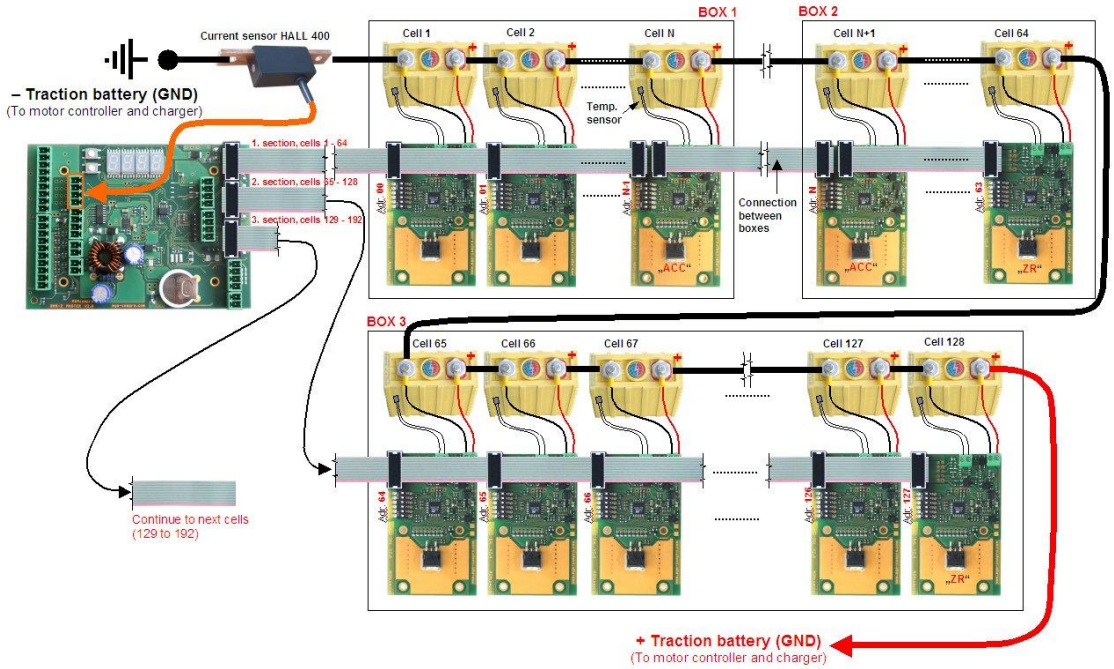

Fig.2: *Diagram of the Czech BMS and balancers (MGM Compro)*

Charge consists of two stages. First, it is almost a constant charging current, which can be limited when rapidly charging the battery construction. During this phase, tension mounts on the article to set the maximum voltage. After reaching 80% of battery capacity reaches

the maximum voltage that maintains constant and direct current to drop to zero. If you respect the restrictions given by the manufacturer, should fast charging significantly shorten battery life.

The absence of BMS (Battery management system) in the past was an important factor for the limited applicability of electric vehicles. With the falling prices of electronics and computer chip came a new generation of sophisticated BMS.

BMS task is to intelligently reduce undercharging and overcharging each battery cell separately. The first generation of BMS protects battery cells as one accumulator with high voltage. A new generation of BMS, each governed by article basis.

The basic function car BMS and balancers

- Restrictions charging current when reaching the upper voltage. If the logic is at the battery cells, to react to achieve the upper voltage on any cell.
- Restrictions on Discharge Current in achieving lower voltage levels. If the logic is at the battery cells, to react to achieve the lower voltage on any of the cell. In practice, it is realised by restrictions on the power control of electric motors, on AC drives with frequency converters. When the voltage on any cell is below the minimum voltage is cut off travel. Usually the final disconnection done before achieving critical voltage drop during the stop by the driver. It is assumed that the driver stops at a safer place than it would halt the vehicle itself.
- Restriction of high temperature measured on each cell by safety reason.

Car charging connectors

The european standard three-pins plugs and sockets 230V 16A are the most frequently used for slow charging. Currently, the fast charging are use DIN standardized three-phase 5-pins plug and socket 3x24A, 3x32A or 3x 63A.

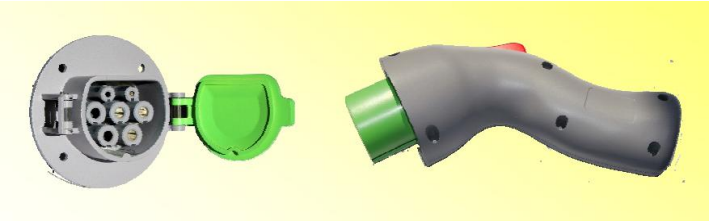

Fig.3: *New 7-pins connector for EV (REMA)*

A new 7pins electric car plug and socket is prepared under the forthcoming European (German) standard IEC 62196-2, which should be completed by the end of 2010. The advantage of this standard is ability to detect active connection to prevent departure of the connected vehicles and allow easy connections effortlessly less skilled users and the possible detection of charging power by pin rezistors.

The upcoming standard for electric cars approved October 27, 2009 in Brussels with representatives of energy companies and Eurelectric.org automakers ALLIANDER - Think City, CEZ - Fiat, EDF - Toyota, ENEL - Piaggio, ENEXIS - Volkswagen, E. ON AG - Mini ESB - Smith Edison, Essent - Volkswagen, RWE - Tesla, Vattenfall - Volvo.

Charging infrastructure

With preparations for billions in infrastructure investments CEZ for electric vehicles is shaping the structure of suppliers charging stations and stands. Suppliers are beginning to specialize in different customers.

- Service station network is available docking station that allows full integration with the established payment and information system petrol station. For many service stations no longer sell fuel the main source of income. This makes the sale of goods in shop and other restaurant services. Therefore, it is advantageous to sell cheap electricity, for which the customer more and longer stay and spend money. Customers are able to pay more per kWh than its own connection at home or work.
- Shopping centres, restaurants, museums, parkings, camps, buy universal stations, which are either free of charge (on the car parking in the hypermarket) or accept coins, cards or special contactless cards.

Since 2008 we create a European map of the charging infrastructure (www.pluginmap.eu), which currently contains 136 charge sites in the Czech Republic. The charging points can be stored in navigation software. In the future, will be complemented a European charge map and will be online to communicate with modern fast charging sites.

Fig.4: *Czech charging infrastructure map (www.pluinmap.eu)*

Czech EV Industry Association

EV and charging infrastructure companies founded in 2010 in Brno, Autosalon new Czech EV Industry Association (www.asep.cz). Association members are in addition to 75 individuals and 21 small and medium-sized companies in the Czech Republic and Slovakia, focusing not only on electric vehicles and charging infrastructure, but also to electric buses, boats, electric planes and electricity production from renewable sources.

INFORMATION ABOUT THE ELECTROCHEMICAL SOCIETY

Introduction

ABAF 2010 is co-sponsored by the Electrochemical Society, Inc (ECS). ECS was founded in 1902 as an international nonprofit, educational organization concerned with a broad range of phenomena relating to electrochemical and solid state science and technology. The Electrochemical Society has about 8,000 scientists and engineers in over 75 countries worldwide, who hold individual membership, as well as roughly 100 corporations and laboratories, that hold corporate membership. ECS objectives are:

- to advance the theory and practice of electrochemistry, solid-state science, and allied subjects;
- to encourage research and dissemination of knowledge in these fields; and
- to assure the availability of adequate training and education of fundamental and applied scientists and engineers in these fields.

First founded as the American Electrochemical Society in 1902, the name of the Society was changed to The Electrochemical Society already in 1930 to more accurately reflect its international activities and membership. Presently, more than 50 % of members reside outside USA. ECS has grown and continued to respond to the changing technical needs and interests of its members; and in 2000, adopted the official acronym of ECS, to encompass long tradition of advancing the theory and practice of both solid-state and electrochemical science and technology. ECS continues to disseminate information through individual membership, corporate membership, student services, technical journals, a quarterly news magazine, books, technical meetings, and awards; and to provide networking contacts through ECS's thirteen Divisions. Geographically, members can also associate with Sections. For example, most members in Europe will be members of the European Section.

ECS bridges the gaps among academia, research, and engineering—bringing together scientists from around the world for the exchange of technical information. This unique blend provides an unparalleled forum for the integration of these areas of science and technology. The ECS staff can provide support to you in learning more about ECS and its many activities.

The Society actively recruits students and gives them the opportunity to get organized in student chapters. One of the active chapters is also in Brno, the site of this year's ABAF meeting. Student membership can be obtained at a discount.

ECS maintains digital library of its collection of publication. Access to the library, with certain number of downloads, is part of the membership package.

Full information can be obtained at www.electrochem.org.

(contributed by Petr Vanýsek, pvanysek@niu.edu)

Bochemie Group is a leading Central European manufacturer of branded household products and owner of SAVO label and other brand labels. On a global scale it is a successful manufacturer of specialty chemicals for market niches.

Bochemie has been developing its know-how for more than 100 years. Management team privatized the company in 1994 and in mid-1990´s created Bochemie Group which was sold to Benson Oak Capital. At the end of 2007 Bochemie s.r.o. mergered with acquisition vehicle Bochemie a.s. The group headquarter is located in the Czech Republic, the branches are in the Slovak Republic, Poland, Hungary, Bulgaria, Romania and Russia.

Bochemie performs its business activities in six strategic business units:

SBU SAVO – range of liquid cleaning/sanitation products for households and professional market with highly recognized traditional brands – SAVO and ULTRA

SBU DEZI – range of disinfection products primarily for healthcare market as well as agriculture

SBU FUNGI – range of fungicidal and insecticidal products for wood protection and masonry

SBU ACCU – various products for Ni-Cd and Ni-Fe accumulators, perforated bands, accumulator massses and electrodes

SBU Feropur – production of Feropur, a unique chemical for pre-pickling of the stainless steel long products (wire rod, bars)

Our commitment to future

SBU Green projects – developing new strategic competences in the area of green economy and focusing on: recycling, new materials and new technology.

Bochemie is seeking projects in diverse areas of „GREEN ECONOMY“

- Green buildings
- Green transportation
- Green energy
- Agriculture, Forestry, Water Management, Air pollution and others

www.bochemie.cz
www.savo.eu

Bochemie a.s., Lidická 326, 735 95 Bohumín
Tel: 596 091 111, e-mail: bochemie@bochemie.cz

ENVINET a.s.

jaderná energetika a průmysl I kvalita a znalosti



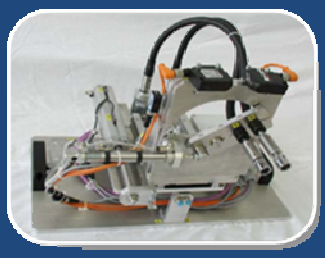

… inženýrsko-dodavatelská společnost zajišťující komplexní dodávky a služby pro zákazníky v České republice i v zahraničí

… tradiční dodavatel zařízení a služeb pro jadernou energetiku a průmysl, laboratorních technologií, zákaznických softwarů, průmyslové automatizace a systémů pro detekci ionizujícího záření

… společnost certifikovaná podle mezinárodních standardů ISO 9001 a ISO 14001, s registračním osvědčením Českého metrologického institutu pro opravy a montáž měřidel a oprávněním k výkonu úředního měření ionizujícího záření

… společnost nabízející komplexní řešení, vysokou profesionalitu služeb a zajištění trvalé systémové i odborné podpory zákazníka

Založeno:	**1995**
Sídlo:	**Třebíč, Česká republika**
Pobočky:	**JE Dukovany, JE Temelín, Praha, Kralupy nad Vltavou, Brno**
Dceřiné společnosti:	**Praha, Trnava (Slovensko)**
Základní kapitál:	**50 mil CZK**
Obrat 2009:	**330 mil. CZK**
Počet zaměstnanců:	**190**
Adresa:	**Modřínová 1094 674 01 Třebíč, CZ**
Tel:	**+420 568 409 811**
Fax:	**+420 568 409 875**
E-mail:	**info@envinet.cz**

www.envinet.cz

Rastrovací hrotové mikroskopy Agilent Technologies

Společnost H TEST a.s. rozšířila svoji nabídku testovacích systémů i o produkty divize Agilent Materials Sciences Solutions tj. AFM (Atomic Force Microscopy)/SPM (Scanning Probe Microscopy) rastrovací mikroskopy.
Zásadní výhodou technologie AFM oproti elektronovým mikroskopům je, že měřené vzorky nemusí být vodivé! S technologií AFM lze dosáhnout rozlišení až v řádu jednotek nanometrů.

Systémy Agilent se uplatní v:

- **elektrochemii**
- **nanolitografii**
- **aplikacích s polymery**
- **biotechnologiích**
- **medicíně**

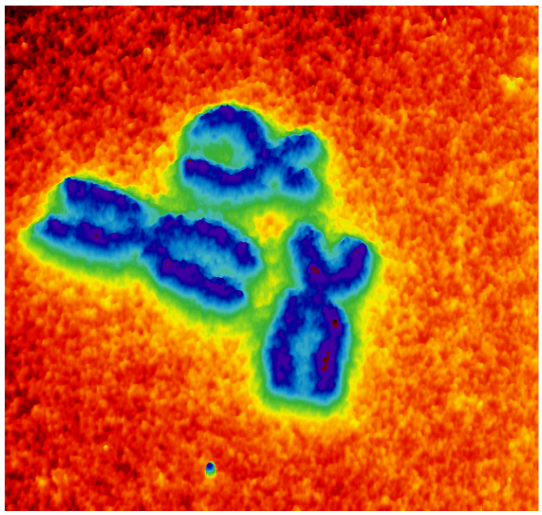

Série 5500 AFM/SPM
AFM mikroskop Agilent 5500 je vrcholný víceúčelový výzkumný mikroskopický systém pro AFM a SPM. Modulární koncepce této série dovoluje jednoduchou integraci stojanu pro velké vzorky až 150 x 200 mm (LS), invertovaného mikroskopu (ILM), scannerů pro malé i velké zobrazované plochy, adaptérů pro uchycení vzorků, soupravy pro elektrochemii nebo video mikroskopu.

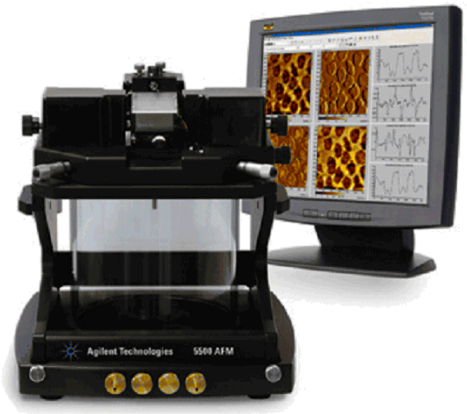

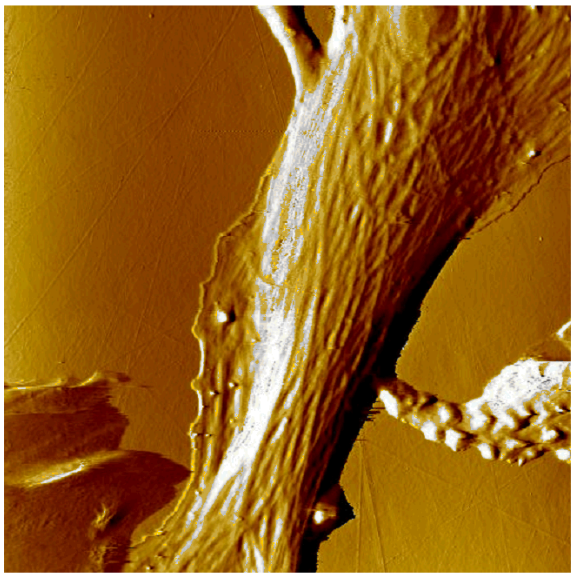

Série 5100 AFM/SPM
AFM mikroskop Agilent 5100 je vhodný pro uživatele, kteří nepotřebují plnou funkčnost vrcholného modelu Agilent 5500, a přesto vyžadují možnost plné kontroly prostředí, ve kterém se nachází měřený vzorek. Pro plnou kontrolu prostředí, ve kterém se nachází měřený vzorek, je k dispozici volitelná hermeticky uzavřená komora a teplotně regulovaný adaptér pro uchycení vzorků.

- Velikost vzorku 20 mm x 20 mm
- Kontrola teploty a prostředí

Série 5400 AFM/SPM
Nový AFM mikroskop Agilent 5400 AFM/SPM je velmi přesný, univerzální přístroj za dostupnou cenu, určený zejména pro oblast vzdělávání a výzkumu a představuje tak ideální možnost zpřístupnění AFM technologie širokému spektru potenciálních uživatelů. Mikroskop je dodáván s podklady pro výuku AFM včetně vzorků pro experimenty.

- Velikost vzorku 20 mm x 20 mm
- Kontrola teploty

Kontaktní informace:

H TEST a.s.
Na okraji 44B
16200 Praha 6
Tel: 235 365 207, 204
Fax: 235 363 893
E-mail: info@htest.cz

www.htest.cz
www.agilent.com/find/nanotech

Agilent Technologies
Authorized Distributor

SIGMA-ALDRICH™

sponzor 11. mezinárodní konference

„ Moderní baterie, akumulátory a palivové články"

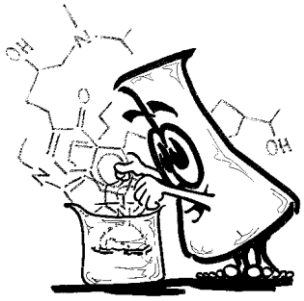

navštivte naše internetové stránky

http://www.sigmaaldrich.com/materials-science.html

- **naleznete zde více než 4000 produktů z oblasti Material Science a brožury CHEMFILES zaměřené na konkrétní oblasti materiálových věd a polymerů jako např.:**

- **Biocompatible/ Biodegradable Polymers, Engineering Polymers, Organic Electronics (Charge Transport, Liquid Crystal Materials, Photolum. Polymers, Photoluminescent Small Molecules,.)**

- **Polymerization Tools (Monomers, Initiators, Additives, Functional Polymers, Free Radical Initiators,..),CVD/ALD, Sol/Gel, Nanopattering, Electronic Materials and Chemicals, Ceramics, Energy Generation, Catalysts for Fuel Cells**

a mnoho dalšího

SIGMA-ALDRICH™

SPECION s.r.o.

Budějovická 1998/55, 140 00 Praha 4, tel. +420-244 402 091, fax. +420-244 460 379
E-mail : info@specion.biz, Internet: **www.specion.biz**

(ex LABIMEX s.r.o.)

DOVOZCE ZKUŠEBNÍCH A TESTOVACÍCH PŘÍSTROJŮ

CTS klimatické, teplotní a šokové komory. Komory pro zkoušky airbagových modulů, komory pro vibrační zkoušky

IMTECH Walk-in testovací celky pro sluneční, teplotní, klimatickou simulaci. Aerodynamické tunely, test benche pro převodovky, motory, kalorimetry pro zkoušky tepelných výměníků a klimatizačních jednotek

KÖHLER korozní komory pro kondenzační zkoušky a zkoušky korozními plyny

HGH SYSTEMES INFRAROUGES specialista v oboru elektro-optiky a infračervené detekce, produkty pro bezpečnostní a obranné aplikace, ale i pro laboratoře, monitorování výrobních procesů v průmyslu

CAMECA elektronové mikrosondy a SIMS

HITACHI elektronové mikroskopy, EDS, WDS

HIROX high-end videomikroskopy pro optickou inspekci, analytický software, 3D morfologie, 360°zobrazení objektu atd.

SCALAR ruční videomikroskopy

HORIBA SCIENTIFIC optické komponenty, monochromátory, RAMAN spetrometry, spektroskopická elipsometrie, spektrofluorometrie, rentgenfluorescenční analyzátory prvkového složení – vč. WEEE + RoHS, UV stanovení obsahu síry v palivech a olejích, GD – optická emisní spektrometrie, Imaging SPR Laserové analyzátory velikosti částic, statický i dynamický rozptyl, Zeta potenciál

SETARAM termická analýza, termogravimetrie, dilatometrie, kalorimetrie, DTA,DSC, micro DSC,

MICROCAL (GE HEALTHCARE) ultracitlivé kalorimetry ITC a DSC pro biovýzkum a farmacii, VP- DSC, ITC 200

JPK INSTRUMENTS Scanning probe BioAFM NanoWizard II a Optické tweezery Nanotracker

IMPEDANCE PROPERTIES OF ELECTRODES WITH DIFFERENT ADDITIVES IN LEAD-ACID ACCUMULATOR

P. Abraham, P. Bača, J. Neoral

Department of Electrotechnology, Brno University of Technology, 602 00 Brno, Czech Republic

Corresponding author: P.Abraham (xabrah02@stud.feec.vutbr.cz)

Introduction

This paper deals with measurement of negative electrodes with different additives in electrode active mass. The main aim of experiment was to find out if additives will have significant effect to imaginary part of impedance. Three electrodes were compared. The first electrode (nr.2) had titan dioxide additive, the second electrode (nr.3) had nano-size titan dioxide additive and the third electrode (nr.5) had the carbon type CR2996 additive.

Measurement method used was slightly modified electrochemical impedance spectroscopy. New method evolved from older one developed at our department of electrotechnology twenty years ago.

This method required us to create our own electrodes with non-continuous system of parallel ribs, because to each rib two (voltage and current) wires are connected. So we can select ribs of electrode we wanted to measure. [1,2]

Experimental

As it was told above, experimental electrodes with system of non-continuous parallel ribs (Fig. 1) were used. Ribs were fixed by epoxy resin. To each rib one voltage and one current wire were connected.

Equivalent diagram of experimental electrode is at fig. 2. Rp means wire resistance that was measured before the experiment begins, Zk means corrosion impedance of interphase electrode/electrolyte, Zm means impedance of active mass.

Measurement procedure is similar as one used in our experiments published lately [1]. Measurement is composed of two steps, frequency dependency is measured between ribs 2-3. During first step current flows between ribs 1-4 and in second step the current flows between ribs 2-4. In first step we theoretically measure impedance of active mass Zm and in second step we measure compounded impedance Zm+Zk. When we substract these two values for each frequency we get impedance curve of corrosion layer.

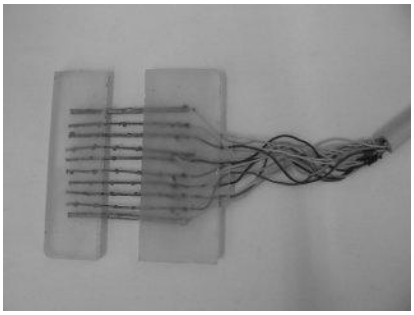

Fig. 1: *Electrode with system of non-continuous parallel ribs (yet without active mass)*

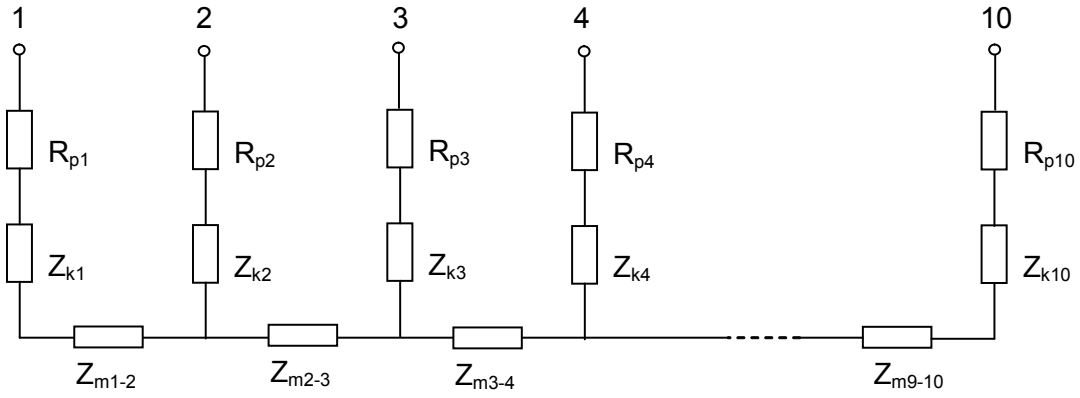

Fig. 2: *Equivalent diagram of electrode*

Results and discussion

The ribs of experimental electrode were made of standard lead alloy Pb Sb1.68 Sn0.05 (wt%) used in commercial lead-acid accumulators. Individual ribs of electrode had dimensions 20x1 mm. Distance between ribs was 5.5 mm. Active mass was made by standard procedure at laboratory conditions. One percent of carbon was used as additivim. Measurement was done at fully charged state.

As measure device we used poteciostat BioLogic VSP in galvanostatic mode. Measurement was done at frequencies from 100 kHZ to units of Hertz. Maximal current was limited to 25 mA.

Results of Zk impedance for each additive are presented at figs 3 to 5. You can see how negative values of imaginary part of impedance are rising at higher frequencies.

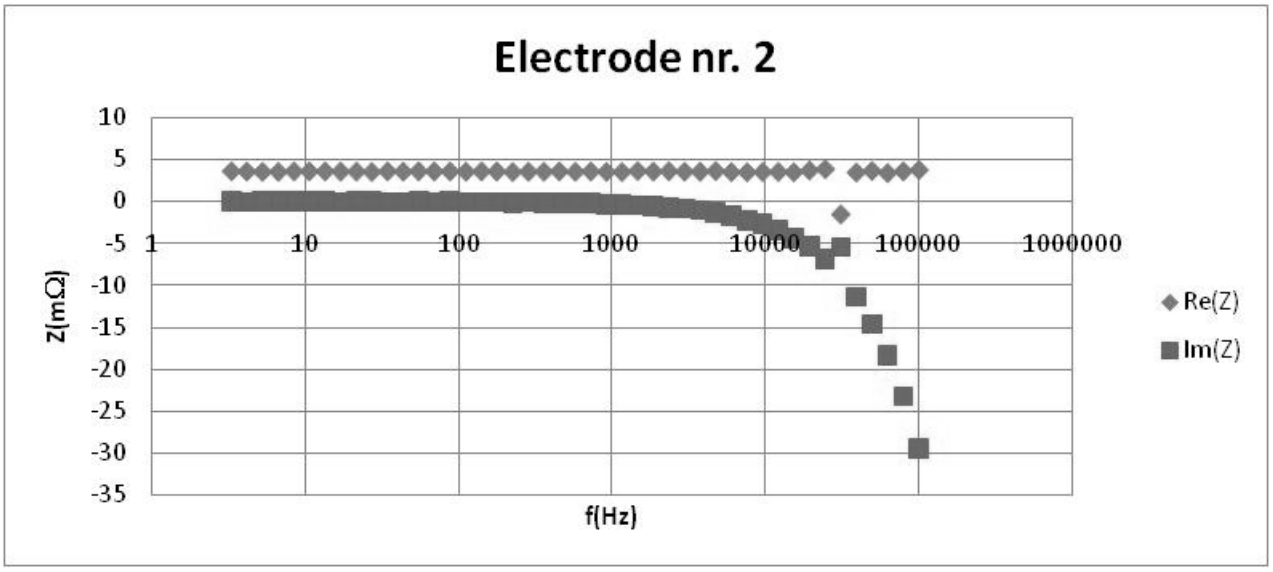

Fig. 3: *Zk Additive TiO_2*

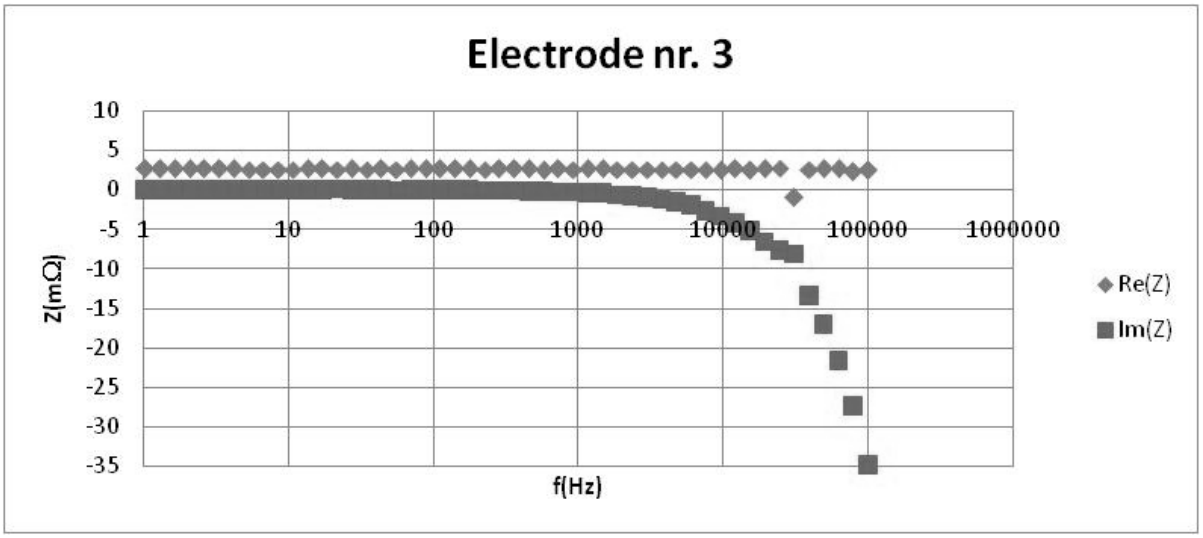

Fig. 4: *Zk additive TiO_2 (nano)*

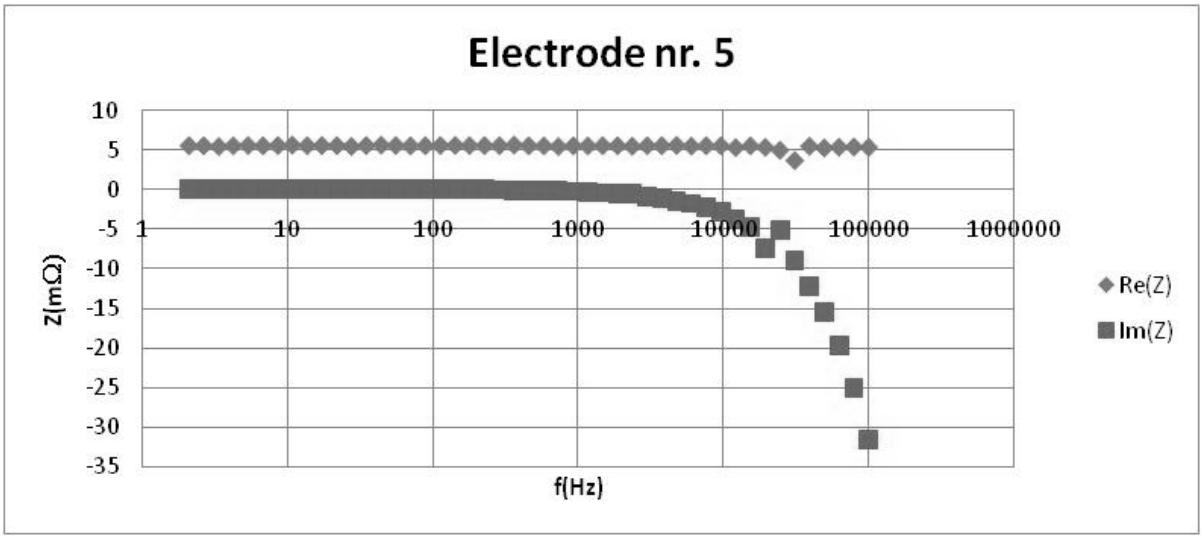

Fig. 5: *Zk additive carbon type CR2996*

Conclusions

Three additives to active mass of electrodes were compared in this experiment. As we can see in charts the curves are very similar. So additives do not have significant effect on shape or size of curves. That is not exactly what we expected, but it is important piece of knowledge for our future experiments. We can also see an error at frequency of about 75 kHz that occurs at all three measurements. Origin of that error is yet unknown to us, we can only assume that it has something to do with resonance frequency of whole system.

Acknowledgements

Thanks to BUT Brno nr. FEKT-S-10-14 and VZ MŠMT MSM0021630516.

References

[1] BAČA, P. Modified Conductometric Method. In Advanced Batteries and Accumulators - 9th ABA. Brno: TIMEART agency, 2008. s. 153-155. ISBN: 978-80-214-3659-6
[2] Prof. RNDr. František Opekar, CSc. Učební texty na Př.f. UK

Title:	Advanced Batteries Accumulators and Fuel Cells – 11th ABAF
Edited:	Jiří Vondrák Vítězslav Novák Petr Bača
Publishing Office:	Vítězslav Novák Petr Bača
Deadline:	August 15th 2010
Publisher:	Brno University of Technology Faculty of Electrical Engineering and Communication Department of Electrotechnology
Press:	Tribun EU s.r.o., Gorkého 41, 602 00 Brno
Year:	2010
Number of Copies:	70

The autors are fully responsible for the content and language of their contribution

ISBN 978-80-214-4148-4